Precipitation of calcium carbonate and its impact on heat exchangers of cooling water systems

Author:
Kuo, Cheng Hoong

Publication Date:
1984

DOI:

License:

PRECIPITATION OF CALCIUM CARBONATE

AND ITS IMPACT ON

HEAT EXCHANGERS OF COOLING WATER SYSTEMS

BY

CHENG HOONG KUO

B.Sc. (Hons), Singapore, M.App.Sc., Australia

A thesis submitted to the University of New South Wales

for the degree of

Doctor of Philosophy

November, 1984

SR.P.T10

CERTIFICATE OF ORIGINALITY

I hereby declare that this thesis is my own work and
that, to the best of my knowledge and belief, it contains
no material previously published or written by another
person nor material which to a substantial extent has
been accepted for the award of any other degree or
diploma of a university or other institute of higher
learning, except where due acknowledgement is made in
the text of the thesis.

This thesis has not been previously presented
in whole or part, to any University or Instituition for a
higher degree.

CHENG HOONG KUO

November, 1984

Dedicated to

MY WIFE

Revised & shortened

ABSTRACT

The solubility of calcium carbonate decreases with increasing temperature. It can therefore precipitate in cooling water systems, causing a loss of thermal efficiency. In order to be relevant to cooling water systems, the calcium carbonate precipitation was studied in an unseeded batch stirred reactor. All three crystallographic forms of calcium carbonate (calcite, aragonite and vaterite) were observed in the experiments covering a wide range of degrees of supersaturation, stirring speeds and temperatures. The interfacial energies of calcite and vaterite were calculated. An empirical expression for secondary nucleation incorporating power was derived. The mechanism of crystallization was established as surface-reaction controlled and the kinetics expressed by the Davies and Jones equation. This led to the calculation of overall growth rate constants of calcite and vaterite.

Scaling in the heat exchangers was studied at pilot plant scale by a test rig constructed to model the Lake Liddell power station cooling water system. The threshold Langelier Index for scaling to occur was found to be 1.40 and 1.25 with ion pair consideration. This indicates that the traditional +1.0 Langelier Index recommended for power station cooling water practice is justified. The threshold Langelier Index calculated at the heat transfer surface temperature was 1.69 and 1.52 with ion pair consideration. This successfully correlated with literature data and that generated at Wallerawang power station.

Scaling was found to be completely prevented due to high velocity shear stress especially when the threshold Langelier Index based on surface temperature was moderately exceeded. From the precipitation study, the formation of discrete aragonite at 35°C and beyond also explained the fact that higher threshold Langelier Indexes were tolerable. The overall growth rate model based on the concept of the surface-controlled mechanism used to derive crystallization kinetics in the precipitation study was developed to predict the scaling rate. When combined with the Hasson's diffusion model, the former overestimated the scaling rate whereas the latter underestimated the scaling rate. The failure to incorporate the actual reaction/mass transfer surface area in both models was considered to be critical.

ABSTRACT

The solubility of calcium carbonate decreases with increasing temperature. It can therefore precipitate in cooling water systems, causing a loss of thermal efficiency. It is important to gain an insight into the processes of calcium carbonate precipitation in order to reduce scaling in the heat exchangers of cooling water systems. This thesis reports investigations into both calcium carbonate precipitation and scaling in heat exchangers. An attempt is made to derive guidelines for scaling control.

In order to be relavant to cooling water systems, the calcium carbonate precipitation was studied in an unseeded batch stirred reactor. The spontaneous precipitation generated enabled the processes of nucleation and crystallization to be studied in a single experiment. Microscopes - both light transmitting and scanning electron were used to evaluate the formation and microstructure of different crystal habits. All three crystallographic forms of calcium carbonate (calcite, aragonite and vaterite) were observed in the experiments covering a wide range of degrees of supersaturation, stirring speeds and temperatures. The interfacial energies of calcite and vaterite were calculated as 101-110 mJ/m^2 and 114-118 mJ/m^2 respectively. An empirical expression for secondary nucleation incorporating power was derived. The mechanism of crystallization was established as surface-reaction controlled and the kinetics expressed by the Davies and Jones equation. The overall growth rate constants of calcite and vaterite were calculated as $11.5 \pm 1.0 \times 10^3$ $L^2/mole$ min m^2 and $20.5 \pm 2.3 \times 10^3$ $L^2/mole$ min m^2 respectively assuming a mono-sized precipitate. If a multi-sized system were adopted, the results were 17.2 -

25.2×10^3 L^2/mole min m^2 and $28.3 - 40.2 \times 10^3$ L^2/mole min m^2 respectively. The presence of magnesium at 1:1 Mg/Ca molar concentration had no significant effect on the rate of crystallization. However, it encouraged the formation of discrete acicular aragonite when the power input was 0.24 to 0.48 watts per litre.

Scaling in the heat exchangers was studied at pilot plant scale by a test rig constructed to model the Lake Liddell power station cooling water system. The actual lake water was used as the cooling water. The effects of total alkalinity and calcium concentration were investigated. The reduction in overall heat transfer coefficient of the system was used as the indication of scaling. The threshold Langelier Index for scaling to occur was found to be 1.40 and 1.25 with ion pair consideration. This indicates that the traditional +1.0 Langelier Index recommended for power station cooling water practice is justified. The heat transfer surface temperature was found to be a critical factor. This was determined as 1.69 and 1.52 with ion pair consideration. The Langelier Index calculated at the heat transfer surface temperature successfully correlated with literature data and that generated at Wallerawang power station.

The velocity shear stress was found to be important in scaling. Scaling was found to be completely prevented due to high velocity shear stress especially when the threshold Langelier Index based on surface temperature was moderately exceeded. From the precipitation study, the formation of discrete aragonite at 35°C and beyond also explained the fact that higher threshold Langelier Indexes were tolerable, possibly due to the weaker scale formed by the aragonite which was easily swept away by the flows.

The overall growth rate model based on the concept of the surface-controlled mechanism used to derive crystallization kinetics in the precipitation study was developed to predict the scaling rate. When combined with the Hasson's diffusion model, the former overestimated the scaling rate whereas the latter underestimated the scaling rate. The failure to incorporate the actual reaction/mass transfer surface area in both models was considered to be critical.

ACKNOWLEDGEMENTS

TABLE OF CONTENTS

LIST OF FIGURES

LIST OF TABLES

CHAPTER 1

INTRODUCTION

1.1 GENERAL

Calcium carbonate is the major constituent of limestones, marbles, chalks, oyster shells, and corals. It is a white powder that is insoluble in water but becomes soluble in the presence of carbon dioxide. Natural water containing dissolved calcium carbonate is called 'hard' water. Calcium carbonate obtained from natural sources is used as a filler for various products, such as ceramics and glass, and as starting material for the production of calcium oxide.

Calcium carbonate is also prepared synthetically by passing carbon dioxide gas through milk of lime (calcium hydroxide) or by combining solutions of calcium chloride and sodium carbonate. The product is called 'precipitated' calcium carbonate and is used when high purity is required. For example in medicine (antacid and dietary calcium supplement), in food (baking powder), and in laboratory chemical synthesis. Pure calcium carbonate has a specific gravity ranging from 2.70 to 2.93 and decomposes when heated to about 825°C.

There are five known polymorphs of calcium carbonate (Encyclopedia Britannica, 1984), namely calcite, aragonite, vaterite, calcite II and calcite III. Calcite II and calcite III are only found in the laboratory under pressures of the order of 20,000 atm. at room

temperature. The commonest polymorph of calcium carbonate in nature is calcite, while aragonite is the next most common and vaterite is comparatively rare.

Calcium carbonate will precipitate out from solution if it exceeds its solubility product. The crystallographic forms of calcium carbonate are dependent on the condition of precipitation. Although calcium carbonate precipitates in nature to form stalactites and stalagmites in limestone caves, their precipitation in heat exchangers and water transmitting pipelines is an unwanted phenomenon. The precipitation of calcium carbonate in the heat exchangers also known as precipitation fouling or more commonly, scaling, will significantly reduce the design heat transfer capacity because of the poor heat conductivity of the calcium carbonate deposit on the heat transfer surfaces.

Scaling of the heat exchangers is commonly encountered in the cooling water systems. There are three types of cooling water systems.

1. Once-through systems, in which the water is discharged, after use, usually to the source from which it was originally withdrawn.

2. Open recirculating systems, in which the water is used repeatedly. The heat picked up by the water during the passage through the heat exchangers is dissipitated by direct contact with atmospheric air in the evaporative cooling device such as a cooling pond, a spray pond, or a cooling tower.

3. Closed recirculating systems, in which the water is also used repeatedly but the heat which is picked up is removed by some

form of heat exchanger where there is no direct contact between the water and the coolent. The typical examples of such systems are the cooling systems of diesel and other internal combustion engines.

The closed recirculating systems are generally more susceptible to corrosion because they are often made up of a number of dissimilar metals in contact and consequently increase the risk of corrosion. Both once-through and open recirculating systems are widely used in the large scale practice. The heat exchangers of these systems are susceptible to both scaling as well as corrosion depending on the quality of the water. The indexes to indicate the corrosivity and scale-forming potential of the water will be discussed in Chapter 6. Calcium carbonate is a natural constituent of water. Unfortunately its solubility is inversely proportional to temperature. This makes the hot surfaces of the heat exchangers more susceptible to calcium carbonate precipitation due to local temperature gradients. The increase in concentration in the open recirculating systems due to evaporation also increases the risk of scaling. The current state of art to deal with calcium carbonate scaling in heat exchangers consists of two areas of management. Firstly, the heat exchangers are designed to incorporate a safety factor called a fouling factor caused by the calcium carbonate deposit. Secondly, the cooling water system will be operating with some forms of treatment and monitoring programme to avoid calcium carbonate precipitation in the heat exchangers. In the first instance, the capital installation cost is increased because of the fouling factor incorporated. It was estimated in United Kingdom that in 1977 the extra capital cost on heat exchangers attributed to all forms of fouling was approximately 40 million pounds (Thackery,

1979). If the ancilliary items such as boilers, water treatment plants etc. were included, the approximate total was 100 millions pounds. Obviously, the cooling water management has already generated on entire industry to keep the heat exchangers clean. The problem of heat exchangers fouling is a very real one. Because of the huge extra capital cost involved in catering for large heat transfer surface, the choice of fouling factor has to be realistic. However, this requires a better understanding of fouling mechanisms involved in each type of fouling. In the case of fouling in water cooling systems, the fouling due to calcium carbonate precipitation is the most widely reported.

The precipitation of calcium carbonate is the obvious starting point to achieve a better understanding of calcium carbonate scaling in heat exchangers. The detailed study of such a process falls into the areas of chemical nucleation and crystallization of inorganic salts from the solution.

1.2 SCOPE OF THIS RESEARCH

This study was initiated to provide information on the mechanism of calcium carbonate precipitation and the control of the precipitation in full scale plants. The following are the areas of this research:

1. To investigate the bulk nucleation of calcium carbonate in the solution.

2. To investigate the bulk nucleation of calcium carbonate in the presence of magnesium.

3. To investigate the effect of mechanical power absorbed by the

solution to the precipitation of calcium carbonate.

4. To investigate the kinetics of calcium carbonate bulk crystallization in pure calcium system as well as in the presence of magnesium.

5. To investigate the scale-forming potential of Lake Liddell water used for Liddell power station cooling water system.

6. To establish a threshold of scaling for Liddell power station cooling water system as indicated by Langelier Index and controlled by dosing sulphuric acid into the cooling pond (Lake Liddell).

7. To test the general applicability of such a scaling threshold represented by the Langelier Index on cooling water systems.

8. To apply the kinetics of calcium carbonate bulk precipitation in explaining and predicting the rate of scaling in the heat exchangers of the cooling water systems.

CHAPTER 2

THEORIES OF NUCLEATION AND CRYSTALLIZATION FROM SOLUTION

2.1 INTRODUCTION

Although crystallization is a common phenomenon observed, a detailed understanding of the mechanism is still limited. In the chemical industry where crystallization processes are exploited to produce chemicals, it is still as much an art as a science. Crystallization is generally considered to take place in three stages: nucleation, growth and recrystallization (Buckley, 1951; Van Hook, 1961; Nielsen, 1964; Strickland-Constable, 1968; Mullin, 1972). Recrystallization is sometimes further classified into ripening and recrystallization (ageing) (Lieser, 1969). Nevertheless, the above classification of crystallization is only a convenient description of the process because the various steps overlap during the crystallization process.

2.2 NUCLEATION

In order for crystallization to occur, firstly the dissolved substance in the solution must be supersaturated. Secondly there must be centres of crystallization, seeds, embryos or nuclei present in the solution. Nucleation is the process of phase transformation of dissolved substances (ions or molecules) into submicroscopic particles. Nucleation can be either homogeneous (spontaneous) or heterogeneous.

Homogeneous nucleation can only occur due to the availability of sufficient chemical potential, namely supersaturation. The dissolved ions or molecules combine together to form clusters. Heterogeneous nucleation takes place on small particles of foreign matter (seeds) on which ions or molecules are deposited (eg. by adsorption) until a nucleus has been formed. These types of nucleation are also known as primary nucleation. On the other hand, nuclei are always generated in the vicinity of crystals present in a supersaturated system. This phenomenon is known as secondary nucleation.

2.2.1 **Homogeneous Nucleation**

The formation of crystlal nuclei is the processes by which ions and molecules coagulate together, resist the tendency to redissolve, and also arrange themselves into crystal lattice. The number of molecules in a stable crystal nucleus can vary from about ten to several thousand. Therefore, the formation of a stable crystal nucleus produced from the simultaneous collision of the required number of molecules is extremely unlikely. The most probable mechanism of nucleation is a bimolecular addition process as shown in the following scheme:

$$A + A \quad A_2$$
$$A_2 + A \quad A_3$$
$$\cdot \qquad \cdot \qquad \cdot$$
$$\cdot \qquad \cdot \qquad \cdot$$
$$\cdot \qquad \cdot \qquad \cdot$$
$$A_{n-1} + A \quad A_n \quad \text{(critical cluster)}$$
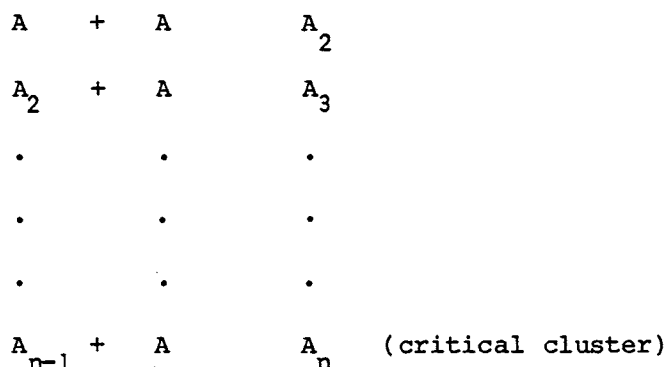
where A is the molecule and the growing nucleus collides with an additional molecule.

The nature of the critical cluster (nucleus) is still not certain. They could be miniature crystals or could be a structure without a clearly defined surface (Christiansen, 1954; Khamskii, 1969; Mullin, 1972). The size of nuclei and the short existence of nuclei in the crystallization process present both theoretical and practical difficulties to the study of this phenomenon. Nevertheless, some attempts have been made to describe this phenomenon using both thermodynamic and kinetic approaches.

2.2.1.1 Thermodynamic Theory of Nucleation

The classical theory of nucleation is derived from the work of Gibbs (1928), Volmer (1939), Becker and Döring (1935) and is based on thermodynamic consideration. The formation of a stable nucleus in a supersaturated solution is accompanied by the work done, W. This is equal to the sum of the work required to form the surface, W_s (a positive quantity), and the work required to form the bulk of the particle, W_v (a negative quantity); $W = W_s + W_v$. If this is expressed as free energy:

$$\Delta G = \Delta G \text{ (surface)} + \Delta G \text{ (bulk)} = \sigma A - n'(\mu_1 - \mu_2) \qquad (2-1)$$

where σ is the solid-liquid surface energy

A is the surface area

n' is the number of molecules in a nucleus

μ_1 is the chemical potentials of the substance per molecules in the dissolved state

μ_2 is the chemical potentials of the substance per molecule in the solid state

Assuming spherical nuclei,

$$\Delta G = 4\pi r^2 \sigma - (\frac{4}{3}\pi r^3 / V_m)(\mu_1 - \mu_2) \qquad (2-2)$$

where V_m is the molecular volume of the crystal and the radius of the nucleus.

$$\mu_1 - \mu_2 = KT\ln(a_{sol}/a_{sod}) \qquad (2-3)$$

where a_{sol} and a_{sod} are activities of the solution and the solid res-
pectively

   K is the Boltzman constant

   T is the absolute temperature

If the concentration and saturation concentration are used as approxi-
mation for the activities,

$$\mu_1 - \mu_2 = KT\ln(c_{sol}/c_{sod}) \qquad (2-4)$$

Therefore Equation (2-2) becomes

$$\Delta G = 4\pi r^2 \sigma - (\frac{4}{3}\pi r^3 / V_m)KT\ln(c_{sol}/c_{sod}) \qquad (2-5)$$

When c_{sol}/c_{sod} is less than 1, the solution is not supersaturated, ΔG is always positive or zero. This implies that all of the nuclei will dissolve. Alternately, if r is sufficiently large, ΔG will tend to become negative and nucleation will occur. Therefore there is a crit-
ical ΔG^* which represents an energy barrier for nucleation.

Information about the radius of a critical nucleus and the number of molecules that it contains can be estimated by differentiating Equation (2-5):

$$\frac{d\Delta G}{dr} = 8\pi r\sigma - \frac{4\pi r^2 KT\ln(\frac{c_{sol}}{c_{sod}})}{V_m}$$

Setting $\frac{d\Delta G}{dr} = 0$,

$$r^* = \frac{2V_m\sigma}{KT\ln(\frac{c_{sol}}{c_{sod}})} \tag{2-6}$$

The particles of size less than r^* will dissolve, those particle greater than r^* will grow. The number of molecules in a critical nucleus is

$$n^* = \frac{V^*}{V_m} = (\frac{r^* F^*}{3}) \times (\frac{1}{V_m}) \tag{2-7}$$

where $F = \frac{3V}{r}$

Therefore

$$n^* = \frac{F^*}{3} \times \frac{2V_m\sigma}{KT\ln(\frac{c_{sol}}{c_{sod}})} \times \frac{1}{V_m} = \frac{2\sigma F^*}{3KT\ln(\frac{c_{sol}}{c_{sod}})} \tag{2-8}$$

The critical free energy is therefore

$$\Delta G^* = -n^* KT\ln\left(\frac{c_{sol}}{c_{sod}}\right) + \sigma F^* = -\frac{2\sigma F^*}{3} + \sigma F^* = \frac{\sigma F^*}{3} \qquad (2-9)$$

with the aid of Equation (2-8)

$$F^* = 3\beta' \frac{\sigma^2 V_m^2}{[(KT\ln\left(\frac{c_{sol}}{c_{sod}}\right))]^2} \qquad (2-10)$$

where β' is a geometric shape factor

$$\beta' = \frac{4F^3}{27V^2} \qquad (2-11)$$

$[\beta' = 16.76$ (spheres), 2.22 (icosahedron), 22.30 (dodecahedron), 27.71 (octahedron), 32 (cube), 55.43 (tetrahedron)].

Therefore the number of molecules in a critical nucleus will be in the form

$$n^* = 2\beta' \frac{\sigma^3 V_m^2}{[KT\ln\left(\frac{c_{sol}}{c_{sod}}\right)]^3} \qquad (2-12)$$

The first equation for the rate of nucleation was described by Volmer and Weber (1922;1929) and subsequent work was by Becker and Doring (1935), also Nielsen (1964) and Kahlweit (1960). The rate of nucleation (number of nuclei formed, $cm^{-3}s^{-1}$) is estimated by calculating the rate at which the nucleus attains its critical size; ie.

$$J = A_1 \exp[-\Delta G^*/KT] = A_1 \exp[\frac{- \beta' \sigma^3 v_m^2}{(KT)^3 \ln(\frac{c_{sol}}{c_{sod}})^2}]$$
$$(2-13)$$

2.2.1.2 Kinetic Theory of Nucleation

This is a more empirical approach to nucleation than thermo-dynamic theory. It was proposed by Christiansen and Nielsen (1951). They developed the ideas of elementary processes proposed by Stranski and Kaishev (1939) and the classical nucleation theory of Becker and Döring (1935). The theory considered that the nucleation process is similar to the chemical reaction of polymerization. Therefore, the rate of nucleation is given by:

$$J = K_{(2-14)} c^{n^*}$$
$$(2-14)$$

where $K_{(2-14)}$ is a constant and n^* is the number of molecules in a critical nucleus. They also showed the relationship between the induction period, θ_{ind} (the time interval between mixing two reacting solution and the appearance of the precipitate) and the initial con-centration c_{in} of the supersaturated solution:

$$\theta_{ind} = K_{(2-15)} c_{in}^{1-n^*}$$
$$(2-15)$$

The induction period is considered as the time required for the assem-bly of a critical nucleus. Therefore this theory suggests that nucleus size is independent of supersaturation whereas thermodynamic

(classical) theory indicates a supersaturation-dependent nucleus size.

2.2.2 Heterogeneous Nucleation

Homogeneous nucleation only takes place when the solution is dust-free. This is virtually impossible to achieve in practice. Water that is prepared in the laboratory usualy contan 10^6 - 10^8 per cm^3 of dust particles and under careful filtration, the number can be reduced to less than 10^3 per cm^3. Nucleation from solution therefore takes place in the presence of dust particles. From the theory of homogeneous nucleation the rate of nucleation is governed by the overall free energy change associated with the formation of the critical nucleus. It has been noticed that many reported cases of spontaneous nucleation on further examination were found to be induced in some way (Melia, 1965). Since heterogeneous nucleation takes place at lower critical supersaturation than homogeneous nucleation, the overall free energy change is less than for homogeneous nucleation, ie.

$$\Delta G^{*'} = \phi \Delta G^{*} \qquad (2-16)$$

where $\Delta G^{*'}$ is the critical free energy change associated with
heterogeneous nucleation.

ϕ is a factor that is less than unity

Figure (2-1) shows the balance of interfacial energies between solution, nucleus and dust particles.
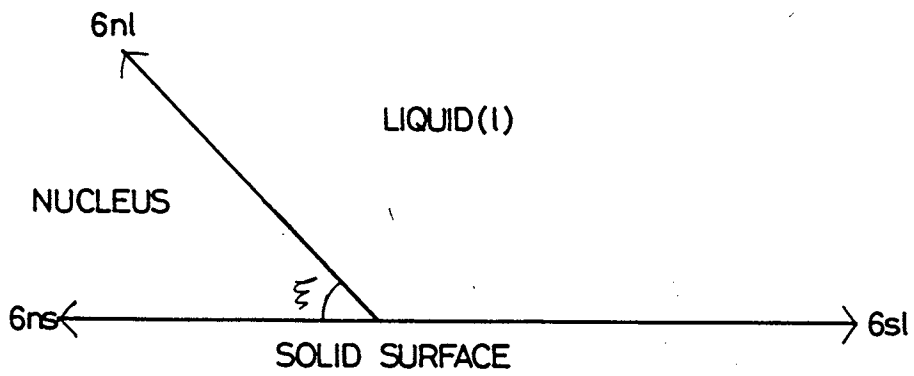
FIGURE 2-1 Surface Energies at the Boundaries Between
Three Phases (Two Solids, One Liquid)

σ_{nl}, σ_{sl} and σ_{ns} are the interfacial energies of nucleus-liquid, solid-liquid and nucleus-solid respectively. ξ is the contact angle. For $180° > \xi > 0°$

$$\sigma_{nl} = \sigma_{nl} + \sigma_{nl} \cos\xi \qquad (2-17)$$

Volmer (1945) derived the factor ϕ, where

$$\phi = \frac{(2 + \cos\xi)(1 - \cos\xi)^2}{4} \qquad (2-18)$$

if $\xi = 180°$, this is the case of complete non-wetting,

$$\xi = 1, \quad \Delta G^{*'} = \Delta G^{*}$$

This implies homogeneous nucleation.

If ξ lies between $0°$ and $180°, \phi < 1$; therefore

$$\Delta G^{*'} < \Delta G^{*}$$

This is the case of heterogeneous nucleation.

If $\xi = 0$, which implies complete wetting of the solid-liquid system. Therefore $\phi = 0$, nucleation takes place on the solid which in this case is a tiny crystal seed of the solution.

Turnbull and Vonnegut (1952) considered the catalytic potency of the solid particles to nucleation in the solution based on crystallographic theory. The basic postulate of this theory is that the interfacial energy between nucleus and the catalytic surface element is a minimum when the nucleus forms coherently. When the nucleus does not

match the solid particle, strain is induced in the crystal nucleus. In general the nucleus will not match the solid particles perfectly but are strained by an amount Σ,

$$\Sigma = (x - d_0)/d_0 \qquad (2-19)$$

where x and d_0, are the lattice parameters of the nucleus in the strained and strain-free condition respectively.

The lattice mismatch, δ' (disregistry), between the two solids is defined as

$$\delta' = \Delta d/d_0 \qquad (2-20)$$

where Δd is the difference in lattice parameter between solid and nucleus.

If $\delta > \Sigma$, the interface is said to be coherent. If $\delta > \Sigma > 0$, the nucleus is said to be incoherent with the catalytic solid. In general, the nuclei form coherently with the catalyst when the disregistry (δ) ~ 0.005 - 0.015. The boundary condition for epitaxis or oriented overgrowth is ~ 0.20. Nevertheless, Johnson (1951) had found oriented overgrowth for δ as large as 0.50.

2.2.3 Secondary Nucleation

Secondary nucleation is nucleation induced by crystals. It is a special case of heterogeneous nucleation where the nucleation sites are the crystal themselves. The fact that the supersaturated solution

nucleates much faster under crystal seeded condition is well known
(Mullin, 1972). This is sometimes called self-nucleation. Mason and
Strickland-Constable (1966) conducted extensive studies on secondary
nucleation and identified three types of crystal nucleation mechan-
isms.

1. Initial breeding - this was seeding due to microscopic particles.
    They were attached onto dry seed-crystals and then swept off to
    become new seeding sites.
2. Needle breeding - this was observed under very high supersatura-
    tions. The dentritic growth from the face of crystals broke off
    and formed new nuclei.
3. Collision breeding - new nuclei were generated due to collision
    of crystals with one another and also with the other solid parts
    such as impeller and surface of the crystallization vessel.

Strictly speaking, the first two mechanisms cannot be classified as
secondary nucleation. The third mechanism is often considered as the
major source of secondary nuclei. Lal et. al. (1969) were among the
first to demonstrate conclusively the existence of collision breeding.
They carried out studies on $MgSO_4 \cdot 7H_2O$, KCl and KBr crystals. The
following conclusions were drawn:

1. Fluid shear alone did not give rise to nucleation.
2. High rates of nucleation resulted when a crystal maintained con-
    tact with a surface while moving about in a stirred solution.
3. Nucleation occurred when a crystal touched a solid object.
4. The rate of nucleation was strongly dependent on the supersatur-
    tion.

Clontz and McCabe (1971) conducted a now classical experiment which gave an insight into collison breeding mechanism. With a single $MgSO_4 \cdot 7H_2O$ crystal which was allowed to collide with a metal rod or another single crystal with collision energy in a flowing stream of supersaturated solution, they counted the generated nuclei. It was shown that the number of nuclei produced per unit crystal area was approximately proportional to the impact energy and to the supersaturation. Crystal-crystal contacts produced two to five times as many nuclei as did crystal-rod contact. Their data can be represented in the following equation:

Crystal-rod collisions:

$$N/A = K_{(2-21)}[(c_b - c_s)/c_s]E_{imp}A^{-1/2} \qquad (2-21)$$

Crystal-crystal collisions:

$$N/A = K_{(2-22)}[(c_b - c_s)/c_s]E_{imp} \qquad (2-22)$$

where N is the number of nuclei generated by one collision

A is the contact area at a collision

c_b is the bulk concentration of solute

c_s is the saturation concentration

E_{imp} is the impact energy

$K_{(2-21)}$ and $K_{(2-22)}$ are constants

Johnson et. al. (1972) studied the effect of different contact surface by using rods made of different materials. They concluded that the surface roughness and the hardness of the

crystal as well as the rod affected collision breeding. Only materials as hard as or harder than the crystal surface were capable of causng contact nucleation. Secondary nucleation was referred to as "micro-attrition".

Cise and Randolph (1972a, 1972b) studied the effect of secondary nucleation of potassium sulphate crystals in a seeded backmixed magma (MSMPR) crystallizer. The nuclei were conducted in the 1.3 - 26 micron size range by a multi-channel coulter automatic particle counter. Nucleation increased with supersaturation, seed crystal mass and with the size and stirring rate. Nucleation also depended on crystal habit. They observed that under the same size and mass concentration condition, polycrystalline habit generated more secondary nuclei than the microcrystalline habit crystals. This indicated that secondary nucleation occurred on a favoured face. In addition, at a given mass concentration, larger crystals were noticed to be more effective than smaller crystals in generating secondary nuclei. The growth rates of crystals were size dependent, and decrease with decreasing size.

The experimental data were also used to correlate nucleation rate with the factors considered. Nucleation rate was expressed in terms of supersaturation, the fourth moment of the parent seed-crystal distribution and stirring rate.

$$B^o = \exp(-65.8)\exp(-5440/T)S'^{0.056} m_4^{1.126} (Re_s)^{5.78} \qquad (2-23)$$

where B^o is the nett apparent nucleation rate, no./cm^3 min, which

was obtained by extrapolating the measured CSD of macro-sized crystals back to zero size

S' is the solute supersaturation, g/L

m_4 is the 4th moment about zero of population distribution

T is the absolute temperature, °K

Re_s is the Reynolds number for stirring

Ottens et. al. (1972) also studied secondary nucleation in a stirred vessel cooling crystallizer. They derived an equation for nucleation rate analogous with the equations of Clontz and McCabe as:

$$dJ_{c-i} = K_{(2-24)}(\Delta c)^p \, w_{d_p} E_{imp} n^o d(d_p) \qquad (2-24)$$

where J_{c-i} is the contact nucleation rate due to collision of crystal with an object

Δc is supersaturation

w_{d_p} is collision frequency of crystal with size d_p

d_p is particle size

n^o is nuclei population density

$K_{(2-24)}$ is a constant

With Equation (2-21) they derived the equations for crystal-stirrer collision, crystal-stationary surface collision and crystal-crystal collision.

For crystal-stirrer collision and crystal-stationary surface collision

$$J_{c-ms} = K_{(2-25)}(\Delta c)^{P}\varepsilon M_{x} \qquad (2-25)$$

where $K_{(2-25)}$ and p are constants

ε is dissipated energy per unit mass of slurry by the

stirrer

M_{x} is total crystal mass above size, d_{x}

For crystal-crystal collision

$$J_{c-c} = K_{(2-26)}(\Delta c)^{P}\varepsilon M_{x}^{2} \qquad (2-26)$$

In the experiments it was concluded that the nucleation rate is determined by nucleation due to crystal-stirrer collisions.

Youngquist and Randolph (1972) studied the Ammonium-Sulphate-Water system by using an MSMPR crystallizer, and corre-lated the experimental data of nucleation by the equation:

$$B^{o} = 1.04 \times 10^{-18} (rev./min.)^{7.84} G^{1.22} (M_{T})^{0.98} \qquad (2-27)$$

where B^{o} is nucleation rate in no./cm^{3} min

G is the crystal growth rate in microns/min

M_{T} is the solids concentration in g/cm^{3}

The experiment was tested at low supersaturation and it was concluded that the nuclei were formed by micro-attrition of seed crystals 1.26 to 25.4 microns in size. Nucleation rate was determined from the birth distribution function B(L) as no./cm^{3} micron. B(L) was calculated from population density data gen-erated from Coulter counter data with the growth term suppressed

in the population balance linear dependence on solids concentration. This implies that secondary nuclei are generated by collisions of the seed crystals with the impeller blades. The growth rate of the nuclei was very small compared to that of large crystals.

Bauer, Larson and Dallons (1974) also studied contact nucleation of $MgSO_4.7H_2O$ in a continuous MSMPR crystallizer. They mounted a $MgSO_4.7H_2O$ crystal in a specialy designed crystal contactor and immersed the crystal and contactor into the crystallizer.

The concentration of the nuclei in the solution was measured with a Coulter counter. The number of nuclei generated due to the controlled energy and frequency of contact between a perspex rod and the mounted parent crystal were calculated from crystal size data (CSD). This was related back to supersaturation, residence time, contact energy and frequency of contact. The number of nuclei produced was found to increase with supersaturation. The nuclei production also increased with contact energy, but decreased at energy inputs in excess of 15,000 ergs. Lower nuclei production per contact was observed as frequency of the contact increased. It was noticed that size-dependent growth occurred as the number of nuclei increased with residence time and indicated that the small crystals grew much slower than the large crystals.

Sung et. al. (1973) demonstrated the effect of shear force of a flowing stream in creating nuclei. They found that nuclei were created from the parent crystal growing in a slightly saturated solution by high fluid shear rates across the surface of the crystal. The shear created nuclei were believed to be of the size of the critical nucleus. This experiment is interesting because it suggests the presence of the adsorption layer which is in agreement with the crystal growth theory.

Randolph and Sikdar (1976) investigated the formation of secondary nuclei of potassium sulphate in a MSMPR crystallizer. They investigated the observation by Randolph and Cise (1972) and Youngquist and Randolph (1972) of the very large population of small-sized crystals in a MSMPR. This portion of population disappeared in long-retention MSMPR experiments. In order to explain this phenomeon, they conducted experiments on:

1. Short residence time MSMPR.

2. Long residence time MSMPR.

3. Seed trap experiments to test the hypothesis that nuclei near 1 μm in size reattached on the parent macrocrystals, and

4. Ripener experiments by withdrawing a measured volume of nuclei-laden crystallizer effluent and allowing it to ripen for a period of time.

They concluded that only a fraction of originally formed secondary nuclei survived to populate the large size ranges. The fraction of surviving nuclei increased with supersaturation,

therefore the correlated nucleation kinetics was based on observable, not viable nuclei.

Garside and Larson (1978) observed secondary nucleation for potash alum and magnesium sulphate heptahydrate directly by microscope examination. A crystal, approximately 3 mm in size, was glued onto a support rod in the saturated solution contained in a cell. The temperature of the solution was controlled by thermostatically-controlled criculating water outside the cell. The contact nucleation was achieved by rotating a contacting rod. Photomicrographs were taken to record the crystals and nuclei generated. The data indicated:

1. Secondary nuclei were readily produced as a result of attrition of a crystal surface by a solid object, even at very low contact energies.

2. The nuclei were formed in both supersaturated and unsaturated solutions. But the nuclei dissolved rapidly in unsaturated solution.

3. Secondary nuclei produced in supersaturated solution were over the size range 1 to 50 μm. The number of large 'nuclei' was found to relate to the level of supersaturation.

4. Many of the nuclei smaller than about 10 μm seemed to grow very slowly or did not grow at all.

In a recent paper given by Larson (1982), he made a very interesting suggestion on the mechanism of secondary nucleation. Studies of sliding contact on the crystal produced more crystals

and nearly all appeared to have the characteristic habit immedi-
ately (Garside and Larson, 1979; Rusli et. al., 1980; Berglund
et. al., 1981), even sliding contact had less energy than direct
contact. This piece of information strongly suggests the
existence of a semi-order partially desolvated layer near the
surface of the growing crystal, which is the starting point for
many crystal growth theories and must be the prime source of
secondary nuclei.

In Larson's paper, he also listed the findings of secondary
nucleation works by all investigators in the past decade:

1. It occurs as a strong function of supersaturation, more spe-
    cially, as a function of the rate of growth of the contacted
    surface.

2. A variety of sizes are produced ranging from 2 μm to 40 μm.

3. Number and size distribution are dependent on contact
    energy, supersaturation , hardness of contactor. Sliding
    contacts produce more nuclei.

4. Most particles immediately exhibit a characteristic habit.

5. Number is an inverse function of temperature.

6. Certain highly charged anions as well as certain dyes and
    surface active agents inhibit nucleation.

7. Fluid shear causes nucleation.

Similarly for the growth of nuclei:

1. Very small nuclei tend not to grow unless the supersatura-
    tion is increased above that at which they were produced.

2. Intermediate size nuclei exhibit growth dispersion.

3. Growth is a strong function of initial size.

4. Impurities change the growth dispersion characteristics.

2.3 CRYSTAL GROWTH FROM SOLUTION

Phase change from solution to solid takes place in the supersaturated solution governed by the principles of thermodynamics. After the formation of a stable nucleus, they continue to grow into crystals. Crystal growth rate is dependent on supersaturation, but other factors such as relative velocity of crystal in the solution, crystal size and impurities are able to affect the crystal growth. The degree of dependence on these factors varies greatly between the molecular compound being formed because of the different crystal growth mechanism. The theories of crystal growth are numerous, but there is still no universal theory to explain crystal growth rate. All the theories are only applicable to certain aspects of crystal growth. Crystal growth is a complex process. The crystallization of ionic substances from aqueous solution can involve the following processes (Mullin, 1972):

1. Bulk diffusion of solvated ions through the diffusion boundary layer.

2. Bulk diffusion of solvated ions through the adsorption layer.

3. Surface diffusion of solvated or unsolvated ions.

4. Partial or total desolvation of ions.

5. Integration of ions into the lattice.

6. Counter-diffusion of released water through the adsorption layer.

7. Counter-diffusion of water through the boundary layer.

Theories of crystal growth can be broadly classified under surface energy theories, surface processes theories and diffusion theories. Surface energy theories have failed to gain general acceptance. The rest of the theories are still very popular and continue to improve and expand in order to explain the experimental crystal growth data.

2.3.1 Surface Energy Theories

In an isolated drop of liquid there is minimum free energy and area. Gibbs (1928) suggested that the growth of crystal could be treated as a special case of this principle. This means that the total free energy of a crystal in equilibrium with its surroundings at constant temperature and pressure would be a minimum for a given volume. Accordingly, the shape of such a crystal would be

$$\sum_{1}^{n} A_i G_i = minimum \qquad (2-28)$$

where A_i is the area of the ith face of a crystal bounded by n faces.

G_i is the surface free energy per unit area of the ith face.

In other words, the crystal would grow in such a manner to maintain a minimum surface free energy for a given volume developed into an 'equilibrium' shape.

This simple concept of crystal growth was developed by Wulff (1901). Mathematical proof was given by Hilton (1903), Liebman (1914), Von Lane (1943), Strickland-Constable (1968). However, the

analogy of liquid droplet for crystal is an over simplification. In a liquid atoms and molecules are randomly dispersed whereas crystal molecules have to incorporate into a crystal lattice structure. The presence of impurities, solvent molecules and solution flow condition always change the growth rate of the individual crystal face. In general this theory fails to explain the effects of supersaturation and solution movement on the crystal growth rate. As a result, it is not generally accepted.

2.3.2 Surface Processes Theories

2.3.2.1 Introduction - Surface Structure

The majority of the crystal growth theories have been derived from fundamental studies of the surface structure of crystals by Kossel (1934) and Stranski (1928, 1930, 1939). According to these discussions, there are various energetically favorable sites for the attachment of solute molecules or growth units. (Figure (2-2)).

The flat area of a crystal face is energetically unfavourable for molecule incorporation onto the crystal. This is position A in Figure (2-2). Position B is more energetically favourable where the molecule is attached and bonded onto the step face as well as to the surface. The most energetically favourable location is indicated by C, where three sides of the molecular cube are bonded. It is said to be kink-bonded because the molecule is bonded in a kink of a step. Growth molecules diffuse from the bulk of the solution onto the crystal surface and incorporate into kinks. The kinks move along the step and eventually cover the face. Based on Kossel-Stranski's view of surface
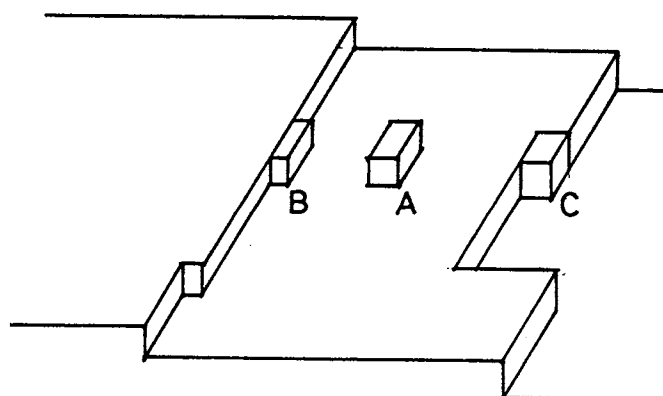
FIGURE 2-2 Surface Structure of Crystal

structure, Volmer (1939) used the Becker-Doring theory (1935) of nucleation to describe the growth of crystals by a surface-nucleation mechanism. This established the basis of surface processes for subsequent growth theories. The growth molecules arrive at the surface of the crystal, and migrate freely over the surface (surface diffusion). The molecules eventually incorporate into crystal lattice or desorb along the migration. Therefore, there will be a loosely adsorbed layer of growth molecules at the crystal interface.

2.3.2.2 Two-dimensional Nucleation Theories

The fresh step of crystal growth (centre of crystallization) is created by surface nucleation. The migration of surface adsorbed molecules undergo binary, ternary....collisions on the surface. These clusters are unstable and are easily broken up. However, when a 'critical-sized' two dimensional cluster is formed, it will be stable and become a fresh step for crystal growth. Ohara and Reid (1973) have derived the mathematical expression for the rate of formation of steps (two-dimensional nucleation rate) and the relevant equations are as follows:

$$r^* = \sigma V_m / KT\ln S \qquad (2-29)$$

where r^* is the radius of critical-size two-dimensional nucleus

σ is the interfacial free energy

V_m is the volume of the molecule

KT is the product of Boltzman's constant and absolute temperature

S is the degree of supersaturation

$$J' = K_{(2-31)} [\ln S]^{1/2} \exp[-K_{(2-32)}/T^2 \ln S] \qquad (2-30)$$

where J' is the two-dimensional nucleation rate.

$$K_{(2-31)} = (2/\pi)n_1^2 \bar{v}_s (V_m/n_m)^{1/2} \qquad (2-31)$$

$$K_{(2-32)} = \pi h\sigma^2 V_m/K^2 \qquad (2-32)$$

where n_m is the number of the monomer

$\bar{v}_s$ is the average speed of surface adsorbed

h is the step height

There are two extreme cases of crystal growth. The mononuclear growth takes place if the rate of growth is determined by two-dimensional nucleation. The step subsequently spreads at an extremely fast rate to cover the face of crystal. Subsequent growth is further initiated by nucleation. The crystal growth rate is simply

$$R_c = hAJ' \qquad (2-33)$$

where R_c is the crystal growth rate perpendicular to the surface

A is the total area of crystal face

On the other hand, the formation of surface nuclei (steps) is very fast. Therefore the crystal grows by accumulating sufficient number of surface nuclei to cover the entire surface.

$$R = J'(\pi r_c)^2 h = (K_{(2-35)}/T^3 [\ln S]^{3/2}) \exp[-K_{(2-32)}/T^2 \ln S] \quad (2-34)$$

$$K_{(2-35)} = 2\bar{v}_s (\sigma n_m/K)^2 h^{1/2} v_m^{5/2} \qquad (2-35)$$

Obviously there are intermediate rate models between these two extremes such as Nielsen's (1964) birth and spread model.

2.3.2.3 Screw Dislocation Theory of BCF

The two-dimensional nucleation theories predict the requirement of sufficient supersaturation in order for surface nucleation to take place. However, many crystal faces in solutions of relatively low supersaturation can grow at a rate much faster then surface nucleation mechanism can explain. Therefore it seems that the surface nucleation mechanism and Kossel's model are not a correct explanation of the crystal growth rate. Frank (1949) postulated that the role of crystal dislocations in crystal growth is important. These dislocations especially screw dislocations provide crystal growth sites. The step is produced on the face at a height equal to the Burger's vector. This step is perpetuated on the face 'up a spiral staircase' as the crystal grows by adsorption of molecules. Since the step is self-perpetuating, it by-passes the requirement of surface nucleation and provides an explanation for the crystal growth rate at relatively low supersaturation.

Subsequently Burton, Cabrera and Frank (1951) developed the well known BCF crystal growth kinetics based on Frank's spiral growth concept. In this model, if the surface is considered to contain multiple straight steps or islands, molecules are adsorbed onto the surface and then diffuse along the surface toward energetically favourable kink sites. Some molecules proceed directly toward the kinks, others impinge onto the step and diffuse along the step toward kinks (ledge

or edge diffusion). The velocity of a straight step in a group of parallel straight steps equally spaced by a dimension Y_o is:

$$v_\infty = (V_m/hX_x)(2D_s C_{SE} \beta_r \sigma' \gamma_0) \tanh(Y_o/2X_s) \qquad (2-36)$$

where X_s is the mean diffusion distance on the surface in time

D_s is the surface diffusion coefficient.

C_{SE} is the equilibrium concentration of surface adsorbed molecules at the given temperature

β_r is the rate of removal of molecules from a molecular cluster

$\sigma' = S-1$ where S is the degree of supersaturation

γ_o is the kink retardation factor

If screw dislocations exist on the surface, the growth rate perpendicular to the surface is calculated by the apparent angular velocity of the spiral, ω. The radius of curvature can be related to ω and also to the step spacing between spiral, Y_o. The final equations are:

$$R = v_\infty h/Y_o = K_{(2-38)} T \sigma'^2 \tanh(K_{(2-39)}/T\sigma') \qquad (2-37)$$

$$K_{(2-38)} = \frac{2D_s C_{SE} K \beta_r \gamma_o}{19X_s \sigma} \qquad (2-38)$$

where σ is the interfacial energy between crystal and solution.

$$K_{(2-39)} = 19\sigma V_m/2KX_s \qquad (2-39)$$

If σ' is very low, $\tanh(K_{(2-39)}/T\sigma) \sim 1$

$$\text{ie. } R = K_{(2-38)} T\sigma'^2 \tag{2-40}$$

which is a parabolic relationship. If σ' is very high, tanh $(K_{(2-39)}/T\sigma'^2) \sim (K_{(2-41)}/T\sigma')$

$$\text{ie. } R = K_{(2-38)} K_{(2-41)} \sigma' \tag{2-41}$$

which is a linear relationship.

2.3.3 Diffusion Theories

The concept of solute diffusion in the solution under a chemical driving force can be applied to crystal growth mechanisms. A growth unit is considered to diffuse and eventually deposit onto the crystal surface to cause crystal growth. The earliest work was done by Noyes and Whitney (1897a,1897b) and modified by Nernst (1904) by introducing the concept of the presence of this stagnant film of liquid surrounding the crystal. The film is the diffusion resistance commonly encountered in the mass transfer approach to chemical engineering problems.

$$\frac{dW}{d\theta} = \frac{D}{\delta}A(c_b - c_s) \tag{2-42}$$

where $dW/d\theta$ is the mass growth rate of the crystal

$\quad$ D is the diffusion coefficient of solute

$\quad$ A is the diffusion coefficient of solute

$\quad$ δ is the length of diffusion path

$\quad$ c_b is the bulk concentration

c_s is the equilibrium concentration

Unfortunately, Marc (1908) later found that such liquid film thickness in a vigorously stirred solution is virtually zero. This therefore implies a infinite growth rate which is impossible. This difficulty was resolved when Berthond (1912) and Valeton (1923,1924) further modified the above diffusion theory by considering the presence of two steps in the processes. Solute molecules diffused from the bulk of the solution to the crystal surface, and then incorporate themselves into crystal lattice by a first-order reaction. These two processes are under the influence of different concentration driving forces as represented by the following equations:

$$\frac{dW}{d\theta} = K_d A(c_b - c_i) \qquad (2\text{-}43)$$

$$\frac{dW}{d\theta} = K_r A(c_i - c_s)^Z \qquad (2\text{-}44)$$

where K_d is the coefficient of mass transfer by diffusion

K_r is the rate constant for the surface reaction

c_i is the solute concentration in the solution at the crystal-solution interface ($c > c_i > c_s$)

$Z = 1$

With the above reasoning, crystal growth meachanism can be visualized as diffusion-controlled, surface reaction-controlled or an intermediate reaction.

c_i is difficult to estimate. A general crystal growth equation can be written by avoiding the c_i term (Mullin, 1972):

$$\frac{dW}{d\theta} = K_G A(c_b - c_s)^n \qquad (2\text{-}45)$$

where K_G is the overall crystal growth coefficient

n is the so called 'order' of overall crystal growth process

This empirical equation is commonly used in interpreting crystal growth data.

Burton, Cabrera and Frank (1951) also carried out rigorous mathematical calculation to derive the rate of crystal growth by applying the concept of bulk diffusion to two-dimensional steps or dislocation steps. The molecules diffuse directly to the kinks without surface adsorption followed by surface diffusion and ledge diffusion, the final equation contains the concentration boundary layer thickness. Certain assumption used in the calculation were criticised by Ohara and Reid (1973). Chernov (1961) simplified BCF bulk diffusion model by assuming a step as a line sink, ie. neglecting kinks. Therefore the diffusion fields considered were only created by the bulk concentration and steps. Again the final crystal growth equation contains the concentration boundary layer thickness. These two theoretical approches deal with diffusion controlled growth mechanism. Other theoretical treatments were also published in the literature (Frisch and Collins, 1952,1953; Ham, 1958; Goldstein, 1968; Cable and Evans, 1967). For many sparingly soluble salts the controlled mechanism is not diffusion controlled because growth rate does not increase with stirring. Referring to the previous equations suggested by Berthond and Valeton, the first order surface reaction is questionable because this will render n in Equation (2-45) to be unity. In fact many inorganic salts growth data published in the literature require n=1.5 to 2 to fit Equation (2-45). Therefore, a more realistic model for surface reaction will have Z > 1. This also suggests the existence of intermediate rate controlled mechanisms

between the diffusion and surface reaction. A quantitative measure of the degree of diffusion or surface reaction control was proposed by Garside (1971) through the concept of effectiveness factors.

η_r = (measured over-all growth rate) / (growth rate expected when the crystal surface is exposed to conditions in the bulk solution)

$$= \frac{R_G}{K_r (c_b - c_s)^z} \qquad (2-46)$$

When $\eta_r \rightarrow 1$, the surface reaction mechanism is increasingly dominant.

2.3.4 Further Development of Surface Processes Theories

2.3.4.1 Introduction

Most sparingly soluble inorganic salts grow by surface reaction (processes) controlled mechanisms. The growth rate is controlled by the molecules or ions incorporate into the crystal lattice through dehydration and migration to the kinks. The following theories are a further development of surface processes theories mentioned in Section (2.3.2) concentrating on the role of growth unit incorporation into crystal lattice as the rate controlling step for crystal growth from solutions.

2.3.4.2 Surface Reaction Models of Doremus (1958, 1970)

Two models were proposed, based on the following mechanisms:

Model A

1. Adsorption of ions from solutions onto the surface.

2. Combinations of oppositely charged ions into "molecules" on the crystal face.

3. Incorporation of "molecules" into crystal lattice.

Model B

1. Adsorption into a surface layer as for model A.

2. Alternate incorporation of oppositely charged ions into the crystal lattice.

The rate equations based on Model A are

$$\frac{dW}{dt} = K_r (c_i - c_s)^3 \quad \text{(one-one electrolyte)} \quad (2\text{-}47)$$

$$\frac{dW}{dt} = K_r (c_i - c_s)^4 \quad \text{(two-one electrolyte)} \quad (2\text{-}48)$$

$$\frac{dW}{d\theta} = K_r (c_i - c_s)^2 \quad \text{(one-one electrolyte)} \quad (2\text{-}49)$$

$$\frac{dW}{d\theta} = K_r (c_i - c_s)^3 \quad \text{(two-one electrolyte)} \quad (2\text{-}50)$$

The coefficient K_r is therefore assumed to include factors such as frequency of collision of adsorbed ions with the kink and probability of incorporation due to collision. Both models do not explain why the growth rates are not governed by the order of individual concentration as occurs for the chemical rate equation, rather they are governed by some power of the concentration driving force.

2.3.4.3 Surface Adsorption Model of Walton (1920)

The rate of surface reaction is considered to be proportional to the concentration of the adsorbed ions on the surface. Based on the Temkin isotherm:

$$c_+' = K_1 \ln c_+ + \text{const}1 \qquad (2\text{-}51)$$

$$c_-' = K_2 \ln c_- + \text{const}2 \qquad (2\text{-}52)$$

where c_+' and c_-' are total concentration of adsorbed cations and anions of growth unit respectively

c_+ and c_- are concentrations of bulk cation and anions respectively

When $c_+ = c_{+s}$ where c_{+s} is the equilibrium concentration, c_+' is taken as zero. Therefore Equations (2-51) and (2-52) are written as:

$$c_+' = K_{(2\text{-}53)} \ln(c_+/c_{+s}) \qquad (2\text{-}53)$$

$$c_-' = K_{(2\text{-}54)} \ln(c_-/c_{-s}) \qquad (2\text{-}54)$$

Since

$$\frac{dW}{d\theta} = -K_{(2\text{-}55)} c_+' c_-' \qquad (2\text{-}55)$$

Therefore

$$\frac{dW}{d\theta} = -K_{(2\text{-}55)} K_{(2\text{-}53)} K_{(2\text{-}54)} \ln(c_+/c_{+s}) \ln(c_-/c_{-s}) \qquad (2\text{-}56)$$

If the supersaturations are low,

$$\ln(c_+/c_{+s}) = \frac{c_+ - c_{+s}}{c_{+s}} \qquad (2-57)$$

$$\ln(c_-/c_{-s}) = \frac{c_- - c_{-s}}{c_{-s}} \qquad (2-58)$$

Therefore

$$\frac{dW}{d\theta} = -\frac{K_{(2-55)}K_{(2-53)}K_{(2-54)}}{c_{+s}c_{-s}}(c_+ - c_{+s})(c_- - c_{-s}) \qquad (2-59)$$

which is a second order equation.

The theory still suffers shortcomings because the Temkin isotherm is not valid (Konak, 1974)). The zero concentration of adsorbed ions at equilibrium is also not acceptable to adsorption theories because there is always some adsorbed ions due to the opposite charges in the solution (Trapnell and Hayward, 1964).

2.3.4.4 Davies and Jones Double-layer Model (1955).

This model is one of the popular crystal growth model adopted for calcium carbonate crystal growth (see Section (4.1.3)). Davies and Jones postulated the presence of an adsorption layer and made the following assumptions:

1. A crystal in contact with an aqueous solution always tends to be covered with a monolayer of hydrated ions. Secondary adsorption on this monolayer is negligible.

2. Crystallization occurs through the simultaneous dehydration of pairs of cations and anions.

3. Every ion striking the surface from a saturated solution enters the mobile adsorbed monolayer.

A brief account of the derivation of the rate equation is given in Section (4.1.3). The final equation is in the form

$$- \frac{dc}{d\theta} = K_{DJ} N [(c_+ c_-)^{1/2} - c_s]^2 \qquad (2-60)$$

where C is the solute concentration at any instant

K_{DJ} is the constant for the Davies and Jones model

N is the number of particles per unit volume at any instant.

2.3.4.5 Surface Reaction Model of Konak (1971,1974)

Konak (1971) surveyed the crystal growth theories available and extracted the important aspects of these theories to formulate a new model for surface reaction - controlled growth of crystals from solution. He considered the crystallization process consisted of mass transfer followed by surface reaction, and then adsorption, dehydration and counter diffusion. He explained that the growth rate was proportional to $(c-c_s)$ instead of to the concentration of the solute because the free energy of the adsorbed layer at equilibrium concentration of crystal is a minimum. In order to maintain such a minimum, excess ions will have to be "rejected" by deposition on the crystal surface. Adsorption layer concentration can be expressed as (De Boer, 1968)

$$c'_+ = K_{(2-61)}(c_+ - c_{+s}) + c'_{+s} \qquad (2-61)$$

where c'_{+s} is the adsorbed equilibrium concentration of the cation.

A similar equation can be written for the anion. The growth rate is proportional to $(c'_+ - c'_{+s})$ at the adsorption layer, therefore it is proportional to the $K_{(2-61)}(c_+ - c_{+s})$ which implies that growth rate is proportional to $(c_b - c_s)$ rather than c_b.

Another major assumption he made was that the movement of steps was caused by vibration of steps and kinks due to thermal agitation of ions in the steps and consequently incorporated the adjacent adsorbed ions. Such vibration and incorporation caused the step to move as compared to surface diffusion of ions or molecules to the kinks. The velocity of straight step v_∞ is expresed as follows:

$$v_\infty = K_{(2-62)}(c_+ - c_{+s})^{z1}(c_- - c_{-s})^{z2} \qquad (2-62)$$

$$K_{(2-62)} = K_{(2-63)} v \exp\left(-\frac{2U_K}{KT}\right) \exp\left(-\frac{W_i + W_K}{KT}\right) \exp\left(-\frac{E}{KT}\right) \qquad (2-63)$$

where $K_{(2-62)}$, $K_{(2-63)}$ are constants

z_1, z_2 are the valencies of cation and anion respectively

v is the frequency of oscillations of the growth units in steps

U_K is the activation energy for formation of a kink

W_i is the dehydration energy of ions

W_K is the dehydration energy of kinks

E is the activation energy for incorporation

again when expressed in linear growth rate,

$$R = \frac{hv_\infty}{Y_0} = K_{(2-62)}\frac{h}{Y_0}(c_+ - c_{+s})^{z1}(c_- - c_{-s})^{z2} \qquad (2-64)$$

for equal ionic concentration in the bulk solutions,

$$R = K_r(c_b - c_s)^z \qquad (2-65)$$

where

$$z = z_1 + z_2 \qquad (2-66)$$

and

$$K_r = K_{(2-62)}\frac{h}{Y_0} \qquad (2-67)$$

2.3.4.6 <u>Nielsen Electrolyte Crystal Growth Theory</u> (<u>Nielsen, 1982</u>)

Recently Nielsen derived the theoretical explanation to apply BCF surface spiral mechanism to conventional surface reaction-controlled growth rate equation. Many sparingly soluble inorganic salts follow a parobolic rate law as indicated by the familiar equation

$$\frac{dL}{d\theta} = K_r(c_b - c_s)^2 \qquad (2-68)$$

where L is the size of the crystal

  θ is the time

According to Nielsen, Equation (2-68) can also be written as

$$\frac{dL}{d\theta} = K_{(2-69)}(S - 1)^2 \qquad\qquad (2\text{-}69)$$

where $K_{(2-69)}$ is the rate constant

This is similar to the parabolic law obtained from the BCF screw dislocation theory. A generalized version of Equation (2-68) for an $A_\alpha B_\beta$ electrolyte is:

$$\frac{dL}{d\theta} = K_{(2-70)}(\Pi^{1/\zeta} - K_{sp}^{1/\zeta})^2 \qquad\qquad (2\text{-}70)$$

where $\Pi = [A^{a+}]^\alpha [B^{b-}]^\beta$

$\zeta = \alpha + \beta$

K_{sp} is the solubility product

Similarly Equation (2-70) can be written as:

$$\frac{dL}{d\theta} = K_{(2-69)}(S - 1)^2 \qquad\qquad (2\text{-}71)$$

where S is defined as $(\Pi/K_{sp})^{1/\zeta}$

$K_{(2-69)}$ was derived by Nielsen assuming that the rate-determining step was the integration of ions into kinks in growth spirals. The ions entering from adsorption layer formed by ions in equivalent (electroneutral) ratio. The layer is in adsorption equilibrium with the solution. The final result of $K_{(2-69)}$ as a complex term which contains step height, interfacial energy, ion pair association constant, adsorption equilibrium constant and is temperature dependent.

2.4   CONCLUSIONS FOR CHAPTER 2

Crystallization is still not fully understood because of the complexities involved in the process. However important progress had been made in the past 20 years for both theoretical and experimental treatment of the subject. The role of secondary nucleation in industrial crystallization processes is already well recognized. This leads to new criteria in crystallizer design for crystal size distribution control. Factors such as the degree of supersaturation, hydrodynamic condition, impurities, power input, magma density are all treated with improved theoretical bases on nucleation and crystal growth. Recent works by Larson (1982) and Nielsen (1982) have brought out the significance of crystal surface processes. Kossel's surface concept in conjunction with BCF mechanism seems to be still the most important approach. When it combines with the adsorption desolvated ion layer concept it can offer a more accurate prediction for crystallization from solution. It is therefore important, as suggested by Larson (1982) that detailed studies of the crystal-liquid interface at the 100°A layer will provide useful information relavant to many unanswered questions.

CHAPTER 3

WATER CHEMISTRY OF CALCIUM CARBONATE/COMPUTER PROGRAMMES

FOR CHEMICAL COMPOSITION CALCULATIONS

3.1 BASIC CHEMISTRY OF CALCIUM CARBONATE IN AQUEOUS SYSTEM

3.1.1 Introduction

Calcium carbonate precipitation from aqueous solution has many implications to us. It may take the form of beautiful limestones in a cave or notorious hard scale in water piping systems and heat exchangers. Irrespective of the forms of calcium carbonate, the basic mechanism of these phenomena is the solubility of calcium carbonate in the aqueous solution. Calcium carbonate is only sparingly soluble in water. The quantity that can remain in water at equilibrium is determined by the solubility product of calcium carbonate:

$$K_{sp} = \{Ca^{2+}\}\{CO_3^{2-}\} \qquad (3-1)$$

where K_{sp} is the solubility product

$\{Ca^{2+}\}$ and $\{CO_3^{2-}\}$ are activities of calcium and carbonate ions respectively

However, the picture is far more complicated then just solubility product considerations. The aqueous system contains other cations and anions. They are all in dynamic equilibrium with each other according

to the temperature, pressure and ionic strength of the system. The carbonate ion, which is part of calcium carbonate solubility product , is further determined by the dynamic distribution of carbonic species in the water. Carbonic species distribution is the single most important factor to determine how much calcium carbonate can remain in water. There are two different systems for carbonic species distribution, those for solutions in contact and not in contact with a gas phase.

3.1.2 Carbonate Species Distribution in a Closed System (Stumm and Morgan, 1970; Loewenthall and Marais, 1976)

When water is not in contact with a gaseous phase, the equilibria of carbonic acid can be determined by the following equations:

$$CO_2 + H_2O \rightleftharpoons H_2CO_3 \tag{3-2}$$

$$H_2CO_3 \rightleftharpoons H^+ + HCO_3^- \tag{3-3}$$

$$HCO_3^- \rightleftharpoons H^+ + CO_3^{2-} \tag{3-4}$$

$$H_2O \rightleftharpoons H^+ + OH^- \tag{3-5}$$
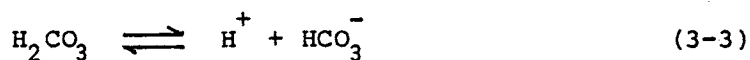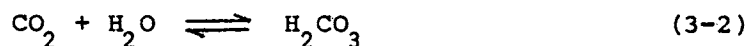
The respective equilibrium constants are Equations (3-6),(3-7) and (3-8).

$$\frac{\{H^+\}\{HCO_3^-\}}{(\{CO_2\}+\{H_2CO_3\})} = \frac{\{H^+\}\{HCO_3^-\}}{\{H_2CO_3^*\}} = K_1 \tag{3-6}$$

where $\{H_2CO_3^*\}$ is the sum of $\{H_2CO_3\}$ and molecularly dissolved CO_2 in solution $([CO_2] \gg [H_2CO_3^*])$.

$K_1 = 4.45 \times 10^{-7}$ at 25°C and unit activity. This corresponds to pH = 6.3 at which $\{HCO_3^-\} = \{H_2CO_3^*\}$

$$\frac{\{CO_3^{2-}\}\{H^+\}}{\{HCO_3^-\}} = K_2 \qquad (3-7)$$

where $K_2 = 4.69 \times 10^{-11}$ at 25°C and unit activity. This corresponds to pH = 10.3 at which $\{CO_3^{2-}\} = \{HCO_3^-\}$. The dissociation constant of water is:

$$\{H^+\}\{OH^-\} = K_w \qquad (3-8)$$

where $K_w = 10^{-14}$ at 25°C and unit activity.

The total carbonic species in molar concentration, C_T is expressed as:

$$C_T = [H_2CO_3^*] + [HCO_3^-] + [CO_3^{2-}] \qquad (3-9)$$

The distribution fractions of the carbon are evaluated in the following equations:

$$\alpha_0 = [H_2CO_3^*]/C_T \qquad (3-10)$$

$$\alpha_1 = [HCO_3^-]/C_T \qquad (3-11)$$

$$\alpha_2 = [CO_3^{2-}]/C_T \qquad (3-12)$$

$$\alpha_0 = \{1 + (K_1'/[H^+]) + (K_1'K_2'/[H^+]^2)\}^{-1} \qquad (3-13)$$

$$\alpha_1 = \{1 + ([H^+]/K_1') + K_2'/[H^+]\}^{-1} \qquad (3-14)$$

$$\alpha_2 = \{1 + ([H^+]/K_2') + ([H^+]^2/K_1'K_2')\}^{-1} \qquad (3-15)$$

where K_1' and K_2' are dissociation constants defined as above but also including activity coefficients of the ionic specis.

The distribution of carbonate species is primarily dependent on pH (Figure (3-1)), temperature and ionic strength also affect the distribution but the effect is only moderate. As pH increases, $[CO_3^{2-}]$ increases and consequently reduces the quantity of calcium carbonate that can remain in solution in water.

3.1.3 Carbonic Species Distribution in an Open System (Stumm and Morgan, 1970; Loewenthall and Marais, 1976)

When the water is in contact with a gaseous phase, carbonic dioxide can transfer between these two phases depending on the direction of driving force. The solubility concentration of carbon dioxide in a dilute solution is in equilibrium with the partial pressure of carbon dioxide in the gaseous phase expressed by Henry's law.

$$P_{CO_2} = K_H [CO_2] \qquad (3-16)$$

where P_{CO_2} is the partial pressure of carbon dioxide
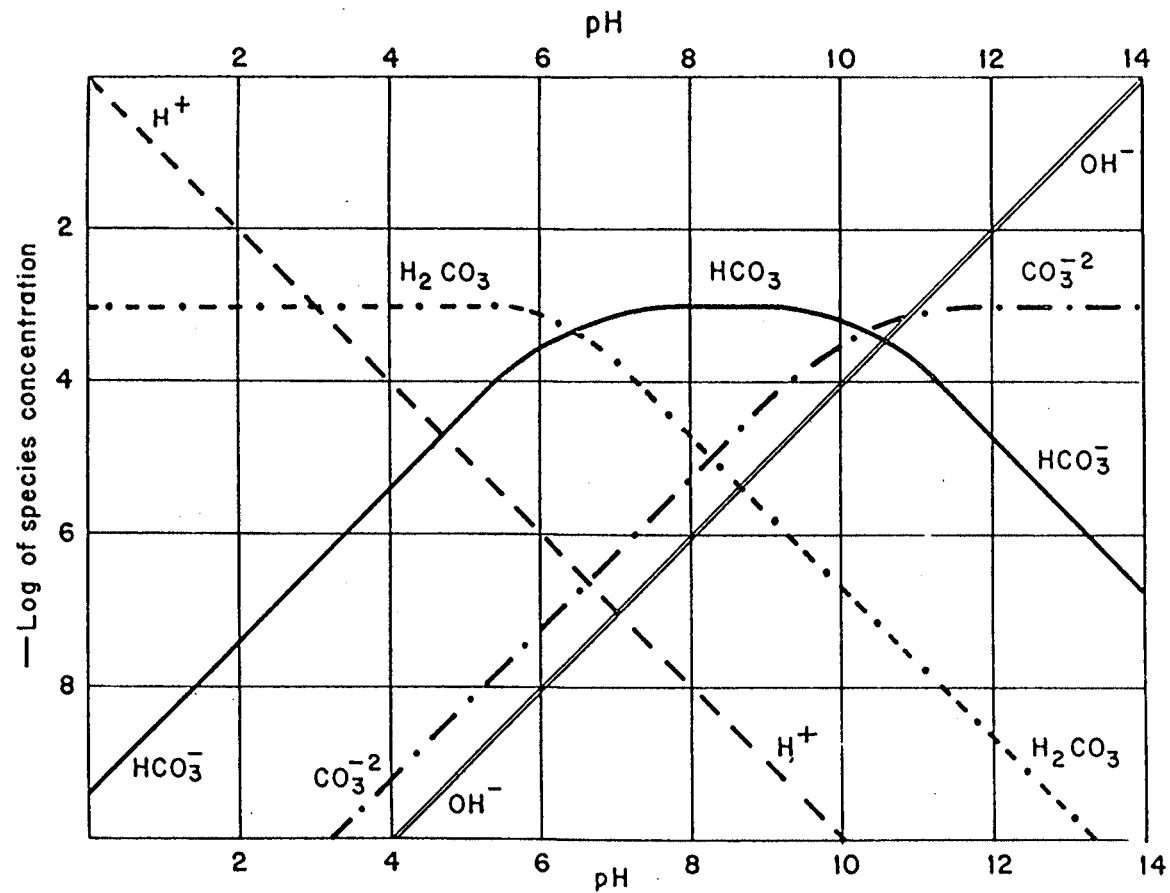
FIGURE 3-1 Distribution of Carbonic Species with pH for 1.0×10^{-3} M Total Carbonic Concentration

K_H is the Henry's constant

$[CO_2]$ is the concentration of dissolved CO_2

Because of this additional equilibrium equation, carbon dioxide transfer to achieve equilibrium therefore results in a different pH value of the water. If CO_2 is transferred out of the water, the pH will increase and consequently increase the carbonate ionization fraction. This will precipitate out some calcium carbonate. On the other hand, absorption of CO_2 from the gaseous phase will depress the pH of the water and tend to dissolve more calcium carbonate.

3.1.4 Ion Pairs Consideration

Natural water always contains a wide range of inorganic salts. Together with the carbonic species distribution, they form the matrix of the aqueous system. Apart from their free ionic form, these ions are able to complex among themselves to form ion pairs and a dynamic equilibrium exists in the solution. The following equations are some examples:

$$CaHCO_3^+ \rightleftharpoons Ca^{2+} + HCO_3^- \qquad (3-17)$$

$$CaOH^+ \rightleftharpoons Ca^{2+} + OH^- \qquad (3-18)$$

$$CaCO_3^0 \rightleftharpoons Ca^{2+} + CO_3^{2-} \qquad (3-19)$$

$$MgHCO_3^+ \rightleftharpoons Mg^{2+} + HCO_3^- \qquad (3-20)$$

$$MgOH^+ \rightleftharpoons Mg^{2+} + OH^- \tag{3-21}$$

$$MgCO_3^0 \rightleftharpoons Mg^{2+} + CO_3^{2-} \tag{3-22}$$

$$CaSO_4^0 \rightleftharpoons Ca^{2+} + SO_4^{2-} \tag{3-23}$$

$$MgSO_4^0 \rightleftharpoons Mg^{2+} + SO_4^{2-} \tag{3-24}$$
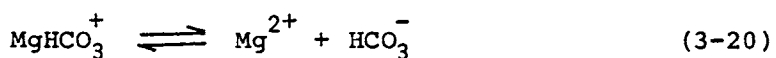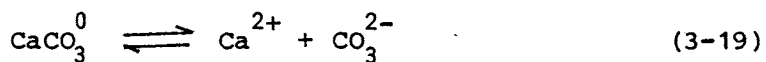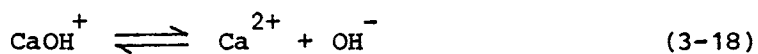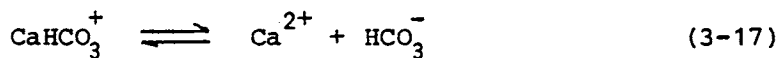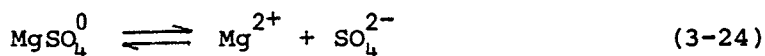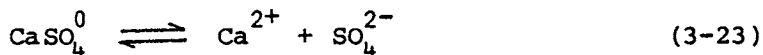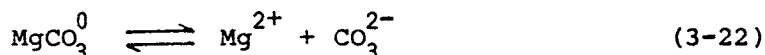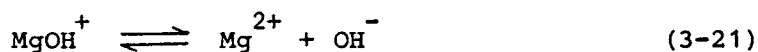
3.1.5 Ionic Strength Consideration

Ions in an infinitely dilute electrolyte solution are free from the influence of ionic forces, but this is not the case in a dilute soltuion. The long range inter-ionic forces are acting among all ionic species in the solution. The theory dealing with these forces was proposed by Debye-Hückel (Davies, 1967), because of these forces, the effective concentrations of ionic species in equilibrium according to the equilbirium equations are expressed as activities which are the products of molar concentration and activity coefficient of the respective ionic species.

Deby-Hückel proposed the following expression of mean activity coefficient:

$$-\log f_{\pm} = \frac{z_1 z_2 A_1 \sqrt{I}}{1 + B_1 a' \sqrt{I}} \tag{3-25}$$

where $f_{\pm}$ is the mean activity coefficient

z_1, z_2 are the charges on the ions considered

a' is the mean distance of closest approach

A_1 ,B_1 are constants characteristic of the systems studied

I is the ionic strength

The ionic strength is defined as:

$$I = 0.5\Sigma c_i z_i^2 \qquad (3-26)$$

where c_i is the molar concentration of ionic species with charge z_i

z_i is the charge on ith ionic species

The above equation breaks down for ionic strength greater than 0.005

A more practical but empirical equation was proposed by Davies (1967). This equation breaks down only when the ionic strength is greater than 0.1.

$$-\log f_{\pm} = 0.51z_1 z_2 [\frac{\sqrt{I}}{1+\sqrt{I}}-0.30I] \qquad (3-27)$$

Equation (3-27) is used to calculate activity coefficients throughout this project.

3.1.6 Temperature Consideration

Dissociation constants of ionic salts in equilibrium for a given aqueous matrix are temperature dependent. Therefore in order to calculate the chemical composition in water, dissociation constants require temperature correction in addition to correction for ionic strength. The following empirical equations are the temperature correction equations available in the literature on the respective dissociation constants used in this project.

$$pK_1 = (17052/T) + 215.21 \log T - 0.12675T - 545.56 \qquad (3-18)$$

where T is in degree Kelvin and the equation was determined for the range 0°C to 38°C (Harned and Davis, 1943).

$$pK_2 = (2902.39)/T + 0.02379/T - 6.498 \qquad (3-29)$$

determined in the range 0°C to 50°C (Harned and Scholes, 1943).

$$pK_w = 4787.3/T + 7.1321 \log T + 0.010365T - 22.801 \qquad (3-30)$$

determined in the range 0°C to 60°C (Harned and Hamer, 1933).

$$pK_{sp} = 0.01183t + 8.03 \qquad (3-31)$$

where t is the temperature in °C (Langmuir, 1968).

$$pK_{CaCO_3^0} = -27.3993 + 4114/T + 0.05617T \qquad (3-32)$$

(Reardon and Langmuir, 1974)

$$pK_{CaHCO_3^+} = -2.95 + 0.0133T \qquad (3-33)$$

(Jacobson and Langmuir, 1974)

3.1.7 Calcium Carbonate Solubility in a Given Aqueous Matrix

The solubility of calcium carbonate in a given aqueous matrix therefore requires definition of all the chemical equilibria. Assuming a closed system contains sodium and calcium as the cations, chloride and carbonic species as the anions. The system which contains calcium carbonate precipitate can be completely defined by the following equations:

(1) Carbonic species and water equilibra:

Equations (3-2), (3-3), (3-4) and (3-5)

(2) Ionic pair equilibria:

Equations (3-17), (3-18) and (3-19)

(3) Solid-liquid-phase equilibrium:

Equation (3-1)

A set of mass action equations can be developed to include ionic strength and temperature correction. They are written as follows:

$$\frac{[H^+][HCO_3^-]}{[H_2CO_3]}f_m^2 = K_1 \tag{3-34}$$

$$\frac{[H^+][CO_3^{2-}]}{[HCO_3^-]}f_d = K_2 \tag{3-35}$$

$$[H^+][OH^-]f_m^2 = K_w \tag{3-36}$$

$$\frac{[Ca^{2+}][HCO_3^-]}{[CaHCO_3^+]}f_d = K_{CaHCO_3^+} \tag{3-37}$$

$$\frac{[Ca^{2+}][CO_3^{2-}]}{[CaCO_3^0]}f_d^2 = K_{CaCO_3^0} \qquad (3-38)$$

$$\frac{[Ca^{2+}][OH^-]}{[CaOH^+]}f_d = K_{CaOH^+} \qquad (3-39)$$

$$[Ca^{2+}][CO_3^{2-}]f_d^2 = K_{sp} \qquad (3-40)$$

and

$$pH = -\log([H^+]f_m) \qquad (3-41)$$

where [ ] is molar concentration

f_m is activity coefficient for monovalent ions

f_d is activity coefficient for divalent ions

In addition, there are sets of species balance constraints.

$$T_{Ca} = [Ca^{2+}] + [CaHCO_3^+] + [CaCO_3^0] + [CaOH^+] \qquad (3-42)$$

$$C_T = [H_2CO_3^*] + [HCO_3^-] + [CO_3^{2-}] + [CaHCO_3^+] + [CaCO_3^0] \qquad (3-43)$$

$$[CaHCO_3^+] + [Na^+] + [H^+] + 2[Ca^{2+}] + [CaOH^+] =$$

$$[OH^-] + 2[CO_3^{2-}] + [HCO_3^-] + [Cl^-] \qquad (3-44)$$

where T_{Ca} and C_T are the total concentration of calcium and carbon in the solution respectively.

Equation for ionic strength is given as follows:

$$I = 0.5([H^+] + [Na^+] + 4[Ca^{2+}] + [OH^-] + 4[CO_3^{2-}] +$$

$$[HCO_3^-] + [Cl^-] + [CaHCO_3^+] + [CaOH^+]) \qquad (3\text{-}45)$$

Activity coefficients of mono and divalent ions are calculated from Equation (3-27).

The above equations allow calculation of the concentrations of species distribution in the aqueous system. Water samples can be analysed to determine the total concentration of cations and anions. The pH value can be measured. Total carbon content can be determined using an Inorganic carbon anaylyser (A.P.H.A-A.W.W.A.-W.P.C.F., 1980). If an Inorganic carbon analyzer is not available, total alkalinity of the solution determined by $H_2CO_3^*$ end point titration can be used to calculate carbonic species distribution.

$$[Alk] = 2[CO_3^{2-}] + [HCO_3^-] + [OH^-] - [H^+] \qquad (3\text{-}46)$$

$$[HCO_3^-] = \frac{[Alk] - [OH^-] + [H^+]}{(1 + 2K_2'/[H^+])} \qquad (3\text{-}47)$$

$$[CO_3^{2-}] = \frac{[Alk] - [OH^-] + [H^+]}{([H^+]/K_2' + 2)} \qquad (3\text{-}48)$$

$$[H_2CO_3^*] = \frac{[Alk] - [OH^-] + [H^+]}{(K_1'/[H^+] + 2K_2'K_1'/[H^+]^2)} \qquad (3\text{-}49)$$

where K_1' and K_2' are first and second dissociation constant of carbonic acid with ionic strength correction.

The product of the calculated $[Ca^{2+}]$ and $[CO_3^{2-}]$ of the system can be

used to describe the solubility of calcium carbonate.

3.2 COMPUTER PROGRAMMES

3.2.1 Programmes for Chemical Composition Calculation

3.2.1.1 Pure Calcium Carbonate System (PROG-CS)

The chemical compositions of solution after mixing sodium bicarbonate and calcium chloride can be calculated by the established equilibria. The following assumptions are made for the calculation:

1. Chemical equilibria among dissolved species are established instantaneously after mixing as compared to the equilibrium of calcium carbonate precipitate with $[Ca^{2+}]$ and $[CO_3^{2-}]$.

2. The contribution of $[CaOH^+]$ is insignificant below pH 10 as compared to $[CaHCO_3^+]$ and $[CaCO_3^0]$ (Wiechers and Sturrock, 1975).

3. It was observed that solutions of sodium bicarbonate under experimental stirring rates maintained a constant pH. Therefore carbon dioxide transfer between the liquid phase and the small gaseous space in the enclosed stirred reactor used for calcium carbonate precipitation experiments is insignificant (Chapter 4). As a result, a closed system is adopted to describe the carbonic species distribution.

A computer programme was established to calculate concentrations of all relevant species in the solution by an iterative method. Subsequently the degree of supersaturation, S, defined as:

$$S = \frac{[Ca^{2+}][CO_3^{2-}]f_d^2}{K_{sp}} \qquad (3-50)$$

can be calculated.

The listing of the programme is given in Appendix F.

3.2.1.2 Calcium Carbonate in the Presence of Magnesium (PROG-CMS)

The calculation is basically the same as PROG-CS except $MgCl_2$ is included in the programme. Therefore the concentration of total magnesium is included in the input of the programme. In addition two more ion pairs of magnesium, namely $[MgHCO_3^+]$ and $[MgCO_3^0]$ are considered. The dissociation constants at 25°C and unit activity are $K_{MgHCO_3^+} = 0.06918$ and $K_{MgCO_3^0} = 0.000398$ respectively (Garrels and Thompson, 1962). The basic programme is exactly the same except for the addition of the species due to magnesium. The listing of the programme is given in Appendix F.

3.2.1.3 Calcium Carbonate in the Presence of Magnesium and Sulphate - Lake Liddell Water (PROG-CMSS)

In the studies of scaling potential of Lake Liddell water (Chapter 7), water samples were taken from the pipe and the pH measured immediately. Although an open pool was used to cool down the water, the pH values of the water were similar to the HCO_3^- end point of carbonic acid distribution. Carbon dioxide transfer is therefore insignificant under one atmospheric pressure. Again, a closed system carbonic acid distribution equilibria was adopted to calculate

concentrations of species distribution in the water.

The major inorganic cations and anions in Lake Liddell water are $[Na^+]$, $[Ca^{2+}]$, $[Mg^{2+}]$, $[Cl^-]$ and $[SO_4^{2-}]$ and the carbonic species. Together with the ion pairs they form the matrix of the entire aqueous system. The listing of the programme is given in Appendix F. The dissociation constants of $MgSO_4^0$, $CaSO_4^0$ at 25°C at unit activity are 0.004365 and 0.00450 respectively (Garrels and Thompson, 1962).

3.2.2 Programmes for Precipitation Calculation

3.2.2.1 Pure Calcium Carbonate System (PROG-PCS)

Calcium carbonate precipitation experiments were conducted in an enclosed stirred reactor with in-situ pH measurements. The concentrations of species in water after mixing known amount of $NaHCO_3$ and $CaCl_2$ can be calculated by PROG-CS. When calcium carbonate precipitates the following reactions take place:

$$Ca^{2+} + 2HCO_3^- \rightarrow CaCO_3 \downarrow + H_2O + CO_2 \uparrow \qquad (3\text{-}51)$$

$$CO_2 + H_2O \rightarrow H_2CO_3 \qquad (3\text{-}52)$$

$$H_2CO_3 \rightarrow H^+ + HCO_3^- \qquad (3\text{-}53)$$

$$HCO_3^- \rightarrow H^+ + CO_3^{2-} \qquad (3\text{-}54)$$
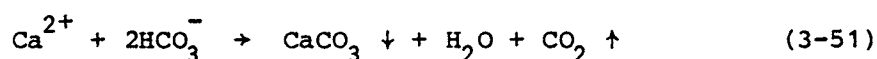
Therefore the nett result is a decrease in pH of the water. The concentration of the species will distribute among themselves according to the chemical equilibria. A method to calculate species concentration during precipitation was given by Wiechers et. al. (1975). The assumptions for PROG-CS are also applicable to the precipitation process. Therefore the decrease in total calcium due to calcium carbonate precipitation must be accompanied by a decrease in total carbon.

$$\Delta T_{Ca} = \Delta C_T \tag{3-55}$$

$$\Delta T_{Ca} = T_{Ca_i} - T_{Ca} = ([Ca^{2+}]_i + [CaHCO_3^+]_i + [CaCO_3^0]_i)$$

$$- ([Ca^{2+}] + [CaHCO_3^+] + [CaCO_3^0]) \tag{3-56}$$

$$\Delta C_T = C_{T_i} - C_T = ([H_2CO_3^*]_i + [HCO_3^-]_i + [CO_3^{2-}]_i + [CaHCO_3^+]_i$$

$$+ [CaCO_3^0]_i) - ([H_2CO_3^*] + [HCO_3^-]$$

$$+ [CO_3^{2-}] + [CaHCO_3^+] + [CaCO_3^0]) \tag{3-57}$$

where $[\ ]_i$ disignate initial molar concentrations at time, $\theta = 0$

$[\ ]$ designate molar concentrations at time θ.

The supersaturation of the water is depicted by $[Ca^{2+}]$ and $[CO_3^{2-}]$. Therefore the change of $[Ca^{2+}]$, ΔCa^{2+} can be solved from Equations (3-56) and (3-57).

$$\Delta Ca^{2+} = [Ca^{2+}]_i - [Ca^{2+}] = ([H_2CO_3^*]_i + [HCO_3^-]_i + [CO_3^{2-}]_i)$$

$$- ([H_2CO_3^*] + [HCO_3^-] + [CO_3^{2-}]) \qquad (3-58)$$

Applying the above equations, when $[Ca^{2+}]$ is reduced by a finite quatity from the initial $[Ca^{2+}]$ calculated from PROG-CS, the corresponding species concentration in the water can be recalculated again by an iterative method. Again the new $[Ca^{2+}]$ can be reduced by this finite quantity and the whole process repeated. Each calculation will also calculate $[H^+]$ which can be converted to pH. Therefore from the pH values measured in-situ during precipitation, the respective species concentration distribution can be known and allows subsequent kinetic derivation of the process. The listing is given in Appendix F. All the input data are obtained from the initial species concentration calculated by PROG-CS.

3.2.2.2 Calcium Carbonate in the presence of Magnesium (PROG-PCMS)

The initial concentrations can be calculated from PROG-CMS. Similar principles apply except the additional terms due to the contribution of magnesium ion pairs to total carbon calculation:

$$\Delta C_T = C_{T_i} - C_T = ([H_2CO_3^*]_i + [HCO_3^-]_i + [CO_3^{2-}]_i$$

$$+ [CaHCO_3^+]_i + [CaCO_3^0]_i + [MgHCO_3^+]_i$$

$$+ [MgCO_3^0]_i) - ([H_2CO_3^*] + [HCO_3^-] + [CO_3^{2-}]$$

$$+ [CaHCO_3^+] + [CaCO_3^0] + [MgHCO_3^+] + [MgCO_3^0]) \qquad (3-59)$$

The listing of the programme is given in Appendix F.

CHAPTER 4

EXPERIMENTAL STUDIES OF PRECIPITATION OF CALCIUM CARBONATE

4.1 NUCLEATION AND CRYSTALLIZATION OF CALCIUM CARBONATE - A LITERATURE REVIEW

4.1.1 Introduction

The precipitation of calcium carbonate is an important phenomenon in many process. Although the precipitation in water supplies and cooling water systems, followed by subsequent build up of calcium carbonate scale has been known in both domestic and industrial practice for many years, there are many beneficial applications of calcium carbonate. In water softening of potable water, precipitation of calcium carbonate plays a vital role to remove hardness. Calcium carbonate is also extensively used in industry as a filler for plastic materials, rubber, paper etc. The control of the calcium carbonate precipitation process, either to avoid scaling or for industrial application, therefore has important implications. Consistent control of the process can only be acheived with detailed understanding of the crystallization process of calcium carbonate, and this has become a substantial research interest during the past decades.

4.1.2 Nucleation of Calcium Carbonate

The rate of nucleation is influenced by various factors in the solution, such as the presence of heteronuclei and impurities, the degree of supersaturation and the mixing energy. Truely homogeneous nucleation of calcium carbonate is probably never observed, however under a very high degree of supersaturation, the influence of heteronuclei can be reduced to a minimum and the nucleation process is approximately homogeneous. In all the studies reported in the literature for calcium carbonate nucleation, rate of nucleation was measured in terms of an experimentally measured induction period and this was used to calculate the interfacial tension between calcium carbonate nuclei and the solution. Roques and Girou (1974) studied calcium carbonate crystallization by gasing the known concentration of calcium carbonate solution with a constant stream of air/carbon dioxide mixture in which the partial pressure of carbon dioxide was equal to the equilibrium pressure. Once the solution reached the desired temperature, the supersaturation was created with air/carbon dioxide mixtures of lower carbon dioxide partial pressure. The solution was stirred by the gas. Appropriate stirring was achieved by adjusting the gas flow rate. They also studied the process with mechanical stirring in addition to gasing to create supersaturation. Three temperatures, namely 10°C,, 30°C and 50°C were studied. An empirical correlation between the nucleation velocity and inital crystal growth velocity was given as:

$$V_G = 1.22 \times 10^{-2} V_0^{0.88} \quad \text{at } 30°C \tag{4-1}$$

where V_G is the germination (nucleation velocity), min^{-1}

V_0 is the initial crystal growth velocity, mg/L min

All three types of calcium carbonate, namely vaterite, calcite and aragonite were observed under the experimental conditions used. They calculated the interfacial energies based on Volmer, Becker and Dörring's classical formulae:

$$\log T_G = 1/\log^2 \text{(degree of supersaturation)} \qquad (4-2)$$

where T_G is the latency time (germination period) as defined. The results are shown in Table (4-1).

TABLE 4-1

Values of Interfacial Energies Obtained for each

Variety of Calcium Carbonate (after Roque and Girou)

Temp. (°C)	Vaterite	Aerated Systems Calcite	Aragonite	Mechanically agitated Systems Aragonite
10	15 MJ/m^2	3 MJ/m^2	-	-
30	14 MJ/m^2	7 MJ/m^2	7 MJ/m^2	7 MJ/m^2
50	-	23 MJ/m^2	11 MJ/m^2	-

Germination (nucleation) was found to be influenced by the method of gas bubbling employed to create supersaturation. It is believed that heterogeneous nucleation was created under such condition. Therefore this also explains the low values of interfacial energies obtained in their experiments which are more than 10 times less than the data obtained from other investigators (Söhnel and Mullin, 1978, 1982).

Söhnel and Mullin (1978,1982) used various methods to measure the experimental induction period, which is the time taken for the first measurable change of solute concentration in the form of turbidity, conductivity or by simple observation with the naked eyes for the first sign of crystals They developed a stopped-flow method (Söhnel and Mullin, 1978) to detect the induction period by conductivity. The principle of the stopped-flow method was already commonly used in studying the kinetics of very fast reactions. This method could detect induction periods as short as 5 ms which therefore enabled them to study nucleation of calcium carbonate under very high degrees of supersaturation. Under such high degree of supersaturation, hetero-geneous nucleation is negligible. Adopting the theory of Nielsen and Söhnel (1971) derived for homogeneous nucleation based on the diffu-sional growth of the created nuclei, the logarithm of induction period is a linear function of $(\log S)^{-2}$ in the form:

$$\log \theta_{ind} = K_{(4-3)} + \alpha_t/(\log S_a)^2 \qquad (4-3)$$

where $K_{(4-3)}$ is a constant

S_a is the degree of supersaturation based on activity

α_t is the gradient based on the induction period and

$$\alpha_t = 2\beta' \sigma^3 V_m^2 / 5(KT\ln 10)^3 \qquad (4\text{-}4)$$

where β' is a geometry shape factor

σ is the interfacial energy

V_m is the mean ionic volume

K is the Boltzman constant

T is the absolute temperature in $°K$

Therefore σ could be calculated from the gradient of the plot of $\log\theta_{ind}$ versus $(\log S_a)^{-2}$.

From a microscopic count of the number of crystals in the precipitation suspension it was found that the logarithm of number of crystal per unit volume is a linear relationship to $(\log S)^{-2}$ (Nielsen, 1967) in the form:

$$\log N = K_{(4\text{-}5)} - \alpha_N / (\log S_a)^2 \qquad (4\text{-}5)$$

where $K_{(4\text{-}5)}$ is a constant

α_N is the gradient based on crystal number

N is the number of crystals per unit volume

and

$$\alpha_N = 3\beta' \sigma^3 V_m^5 / 5(KT\ln 10)^3 \qquad (4\text{-}6)$$

The interfacial energies of calcium carbonate determined are 83 mJ/m^2 (Söhnel and Mullin, 1978) , 98 and 107 mJ/m^2 for the pure and Mn^{2+} contaminated systems respectively (Söhnel and Mullin, 1982).

The interfacial energy for calcite was calculated based on the assumption of surface hydration which gave reasonable estimates of at least 30 other substances (Nielsen and Sohnel, 1971). The value is 120 mJ/m^2 and obviously compared well with the above values. Other values have been reported in the literature, such as 7 mJ/m^2 (Roques and Girou, 1974), 19.5 mJ/m^2 (Kharim, 1974) 205 mJ/m^2 (Möller and Rajogopalan, 1976) and 280 mJ/m^2 (Goujonand Mutaftschiev, 1976) for calcite, 10 mJ/m^2 (Kharim, 1974) and 14 mJ/m^2 (Roques and Girou, 1974) for vaterite and 150 mJ/m^2 (Möller and Rajagopalan, 1976) for aragonite. Based upon the range of experimentally studies Söhnel and Mullin (1982) made the following comments:

Low values in the range of 7 - 20 mJ/m^2 were due to heterogeneous nucleation. The extremely high value 280 mJ/m^2 was derived from doubtful equations. The values of 205 mJ/m^2 and 150 mJ/m^2 were derived from experiments based on the assumption of polynuclear growth however under the experimental conditions there was a strong possibility of a spiral growth mechanism. Therefore it was concluded that the value 120 mJ/m^2 for calcite was valid. Kharim et. al. (1980) also reported 110 mJ/m^2 as the interfacial energy of calcium carbonate.

Impurities in the form of cations can affect the nucleation of calcium carbonate. In general, cations having atomic radii smaller than that of calcium and hydration energies higher than calcium are capable of altering the crystal form from calcite to aragonite, simultaneously the induction period is increased. This fact has been reported frequently in the literature. Roques and Girou (1974) observed an increase in induction period (latency time as they termed it) with an increase in the concentration of magnesium. Möller and

Rajagopalan (1975) also observed the increase in induction period with the increase in Mg/Ca ratio. They also reported there was a pronounced discontinuity at Mg/Ca = 4 which indicated that beyond Mg/Ca = 4, aragonite was formed. The nucleation rate of aragonite was lower than calcite under similar conditions. Both papers reported the observation under conditions of heterogeneous nucleation. Söhnel and Mullin (1982) reported a similar trend of increasing induction period for an increasing Mg/Ca ratio. The experiment was predominantly of homogeneous nucleation. For the precipitation suspension with a degree of supersaturation less than 100 the number of crystals was less in the presence of foreign cations (Mg, Mn) as compared to a pure system.

4.1.3 Crystallization of Calcium Carbonate

The early research work stemmed from a realisation of the importance of the role played by calcium carbonate in geochemistry and oceanography (Weyl, 1958; Pytkowicz 1965; Kitano et. al. 1962; 1965; 1966). Reddy and Nancollas (1971a, 1971b) avoided the possible complications caused by both the nucleation process during crystal growth and heterogeneous nucleation. They conducted the study by using seed crystals with known surface area in a supersaturated metastable solution. The measured growth rate in terms of the rate of decrease in total calcium concentration in the solution followed a second order equation with respect to the concentration, this suggested a surface-controlled process. The crystallization process was studied over temperature ranged from 10 to 40°C. The activation energy for crystal growth was measured as 46.0±4.2 KJ/mole. The growth rate was independent on the stirring applied to the system. In their study, they proposed that the rate of calcium carbonate precipitation was the nett

rate of the flux of lattice ions incorporated into the crystal at the growth. The flux of solute on the surface,

$$J_G = K_{(4-7)} A [Ca^{2+}] [CO_3^{2-}] \tag{4-7}$$

The diffusional flux of solute away from the surface of the crystal,

$$J_K = K_{(4-8)} A \tag{4-8}$$

where $K_{(4-7)}$ is the growth rate constant

   A is the surface area in unit volume

   $K_{(4-8)}$ is the diffusional flux constant where

$$K_{(4-8)} = K_{(4-7)} A (K_{sp}/f_d^2) \tag{4-9}$$

   K_{sp} is the solubility product of calcium carbonate

   f_d is the divalent activity coefficient

   $[Ca^{2+}]$ and $[CO_3^{2-}]$ are the molar calcium and carbonate ion concentration respectively.

Assuming that diffusion is not rate limiting, the growth rate of calcium carbonate is therefore expressed as

$$- \frac{dT_{Ca}}{d\theta} = J_G - J_K = K_{(4-7)} A [Ca^{2+}] [CO_3^{2-}] - K_{sp}/f_d^2 \tag{4-10}$$

where T_{Ca} is the total molar calcium concentration.

House (1981) explained the Nancollas and Reddy equation by assuming that the adsorbed ions combined in the surface layer to form the ion-pair $CaCO_3^0$. This is subsequently incorporated into the crystal lattice. The influx of $CaCO_3^0$ ion-pair can be expressed as:

$$\text{Influx of } CaCO_3^0 = K_{(4-11)}A[CaCO_3^0] \qquad (4-11)$$

where $K_{(4-11)}$ is the rate constant.

$[CaCO_3^0]$ is the molar concentration of ion-pair

At the same time, the efflux of $CaCO_3^0$ is expressed as:

$$\text{Efflux of } CaCO_3^0 = K_{(4-12)}A[CaCO_3^0]^e \qquad (4-12)$$

where $K_{(4-12)}$ is a rate constant

$[CaCO_3^0]^e$ is the equilibrium molar concentration of $CaCO_3^0$ ion-pair.

The activity of $CaCO_3^0$ can be expressed as follows:

$$CaCO_3^0 = f_d^2[Ca^{2+}][CO_3^{2-}]/K_4 \qquad (4-13)$$

where K_4 is the thermodynamic dissociation constant of $CaCO_3^0$.

Therefore combining Equations (4-11), (4-12) and (4-13), assuming $f_{CaCO_3^0}=1$,

$$-\frac{dT_{Ca}}{d\theta} = K_{(4-11)}A[CaCO_3^0] - [CaCO_3^0]^e$$

$$= \frac{K_{(4-11)}Af_d^2}{K_4}[Ca^{2+}][CO_3^{2-}] - K_{sp}/K_d^2$$

(4-14)

This equation was later verified by Wiecherst et. al. (1975), also using a seeding technique. The value of activation energy determined is 43 ± 3.8 KJ/mole.

A similar rate equation also proposed by Reddy and Nancollas (1973) is of the form

$$- \frac{dT_{Ca}}{d\theta} = - \frac{d[Ca^{2+}]}{d\theta} = K_{(4-15)} A\Delta^2 \qquad (4-15)$$

where $[Ca^{2+}]$ is the ionic calcium molality in solution

θ is the time in minutes

$- \frac{dT_{Ca}}{d\theta}$ or $- \frac{d[Ca^{2+}]}{d\theta}$ is the crystal growth rate

K is the rate constant for crystal growth

A is the effective surface area of the growing crystals

Δ is the amount of calcium carbonate remaining to be precipi-
  tated from the solution before the equilibrium concentration
  is reached

$$\Delta = ([Ca^{2+}]_0 - [Ca^{2+}]_\infty) - ([Ca^{2+}]_0 - [Ca^{2+}]) \qquad (4-16)$$

$$\Delta = [Ca^{2+}] - [Ca^{2+}]_\infty \qquad (4-17)$$

ie. $\quad - \frac{dT_{Ca}}{d\theta} = - \frac{d[Ca^{2+}]}{d\theta} = KA([Ca^{2+}] - [Ca^{2+}]_\infty)^2 \qquad (4-18)$

where $[Ca^{2+}]_0$ and $[Ca^{2+}]_\infty$ are the initial and equilibrium calcium con-
centration respectively.

The effect of some phosphonic acid derivatives was studied and found that the rate of growth of calcite seed crystals was greatly reduced. Equation (4-15) were also later adopted by Reddy to express calcium carbonate crystallization (Reddy, 1977; Reddy and Wang, 1980; Reddy and Gaillard, 1981).

Plummer et. al. (1978) studied the kinetics of semi-optical grade crystals of Iceland spar dissolution at fixed values of P_{CO_2} (0.0 to 1.0 atm.) and at temperatures which ranged from 5 to 60°C. When the concentration is far from equilibrium, they identified that the rate of dissolution consists of three forward rates:

1. First order dependence on the bulk fluid activity of H^+.

2. Linear dependence on the bulk fluid P_{CO_2}.

3. A constant forward rate in the near absence of H^+ and dissolved CO_2.

At near equilibrium, a backward reaction at constant P_{CO_2} and temperature, was identified as the linear relationship of the product of the activities of Ca^{2+} and HCO_3^- in solution. As a result, the nett rate of dissolution (R') is given by an equation of the form:

$$R' = k_1\{H^+\} + k_2\{H_s2CO_3^*\} + k_3\{H_2O\} - k_4\{Ca^{2+}\}\{HCO_3^-\} \qquad (4-19)$$

where k_1, k_2, k_3 are first order rate constants dependent of temperature

k_4 is a function of both temperature and P_{CO_2}

$\{H_2CO_3^*\}$ which is the the carbon dioxide is equal to

$\{H_2CO_3\} + \{CO_2\}$
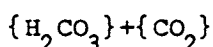
{} indicates activity

Plummer et. al. (1978) used the adsorption layer heterogeneous reaction model described by Mullin (1972) to derive their mechanistic model. The adsorption layer model assumes a thin adsorption layer between the surface of the crystal and the hydrodynamic boundary layer. Species in the adsorption layer were assumed to have relative low mobility as compared to species in the hydrodynamic layer. The surface of the crystal is believed to be sparsely covered by reaction sites at molecular-scale discontinuities in the surface. They also assumed that forward and backward reactions involve kinetic interaction of boundary layer species and product species with the adsorption layer species at the reaction sites. The following reactions were considered to take place simultaneously:

$$CaCO_3 + H^+_{(o)} \rightarrow Ca^{2+}_{(s)} + HCO^-_{3(s)} \qquad (4-20)$$

$$CaCO_3 + H_2CO_{3(o)} \rightarrow Ca^{2+}_{(s)} + 2HCO^-_{3(s)} \qquad (4-21)$$

$$CaCO_3 + H_2O_{(o)} \rightarrow Ca^{2+}_{(s)} + HCO^-_{3(s)} + OH^-_{(s)} \qquad (4-22)$$

with the backward reactions:

$$|Ca^{2+} + HCO^-_3|_{(o)} + CO^{2-}_{3(s)} \rightarrow CaCO_3 + HCO^-_{3(s)}$$

$$HCO^-_{3(s)} \rightarrow H^+ + CO^{2-}_{3(s)}$$

$$|Ca^{2+} + HCO^-_3|_{(o)} \rightarrow CaCO_3 + H^+_{(s)} \qquad (4-23)$$

$$|Ca^{2+} + HCO_3^-|_{(o)} + HCO_{3(s)}^- \rightarrow CaCO_3 + H_2CO_{3(s)} \qquad (4-24)$$

$$|Ca^{2+} + HCO_3^-|_{(o)} + OH_{(s)}^- \rightarrow CaCO_3 + H_2O_{(s)} \qquad (4-25)$$
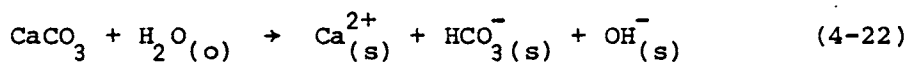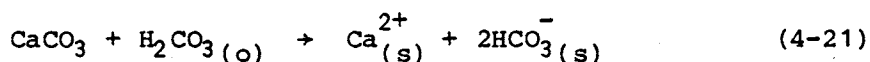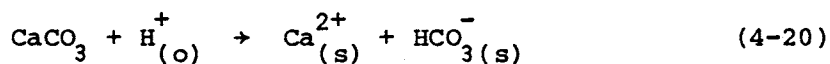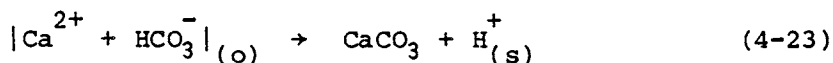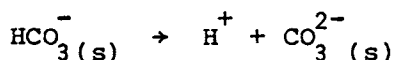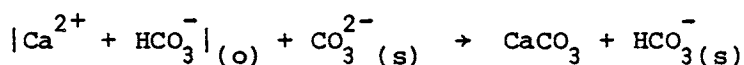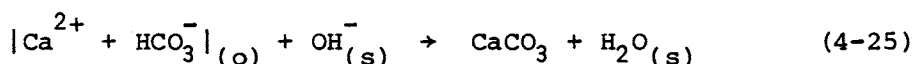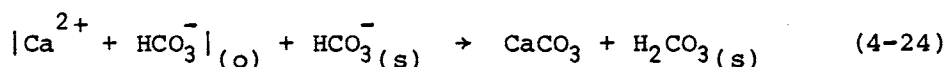
where the subscript (s) and (o) indicate the species in the adsorption (surface) layer and at the bottom of the boundary layer respectively.

The form of Ca^{2+}, and HCO_3^- involved in the backward reaction was not certain, therefore the notation $|Ca^{2+} + HCO_3^-|_{(o)}$ was used. The backward rates can be considered as the rate of crystallization as against the rate of dissolution of calcium carbonate. Therefore these nett rates of reactions from Equations (4-20) and (4-23), (4-21) and (4-24), (4-22) and (4-25) are:

$$R_1' = k'\{H^+\}_{(o)} - k_4'\{Ca^{2+}\}_{(o)}\{HCO_3^-\}_{(o)} \qquad (4-26)$$

$$R_2' = k_2'\{H_2CO_3\}_{(o)} - k_4''\{Ca^{2+}\}_{(o)}\{HCO_3^-\}_{(o)}\{HCO_3^-\}_{(s)} \qquad (4-27)$$

$$R_3' = k_3'\{H_2O\}_{(o)} - k_4'''\{Ca^{2+}\}_{(o)}\{HCO_3^-\}_{(o)}\{OH^-\}_{(s)} \qquad (4-28)$$

Total dissolution rate (R') is therefore

$$R' = R_1' + R_2' + R_3' \qquad (4-29)$$

At the high Reynolds numbers of their experiment, Plummer and Wigley (1976) showed that bulk concentration is nearly equal to the concentration at the bottom of boundary layer, except for $\{H^+\}$ where pH is less than or equal to 4. Also if reaction (4-20) is very rapid relative to reactions (4-21) and (4-22), $\{H_2CO_3^*\}_{(s)}$ and $\{H_2O\}_{(s)}$ are both

equal to their bulk concentrations. For the application of calcium carbonate precipitation, the approximation of $\{H^+\}_{(s)} = \{H^+\}$ in the bulk solution is not important because reaction (4-20) is negligible when compared to the total rate at pH 7. At equilibrium, $R_1' = R_2' = R_3' = 0$. Rearranging the Equations (4-26), (4-27) and (4-28) by the substitution of K_1, K_2, K_{sp} and K_w which are the dissociation constants of carbonic acid, the dissociation of bicarbonate, the solubility of calcium carbonate and the dissociation constant of water respectively, the final form of k_4 is

$$k_4 = \frac{K_2}{K_{sp}}\{k_1 + \frac{1}{\{H^+\}_{(s)}}[k_2\{H_2CO_3^*\}_{(s)} + k_2\{H_2O\}_{(s)}]\} \tag{4-30}$$

To apply to calcium carbonate precipitation, substitute Equation (4-30) into (4-19),

$$R' = k_1\{H^+\} + k_2\{H_2CO_3^*\} + k_3\{H_2O\} - \{Ca^{2+}\}\{HCO_3^-\} \times \frac{K_2}{K_{sp}} +$$

$$\frac{1}{\{H^+\}_{(s)}[k_2\{H_2CO_3^*\}_{(s)} - k_3\{H_2O\}_{(s)}]} \tag{4-31}$$

At low P_{CO_2} (<0.03 atm) and pH greater than 7.0, $k_1\{H^+\}$ and $k_2\{H_2CO_3^*\}$ can be neglected compared to $k_3\{H_2O\}$. As a result, the rate equation is approximated by

$$R' = -\frac{dT_{Ca}}{d\theta A} = k_3\{H_2O\}(\frac{\{H^+\}}{\{H^+\}_{(s)}} \Omega - 1) \tag{4-32}$$

$$\text{where} \quad \Omega = \frac{\{Ca^{2+}\}\{Ca_3^{2-}\}}{K_{sp}} \quad (4-33)$$

Therefore in order to use this rate equation, the surface pH value is required. The dissolution experiments carried out by Plummer et. al. (1978) were at relatively high P_{CO_2}. The P_{CO_2} and $H^+_{(s)}$ are close to the bulk concentration due to the rapid reaction with H^+, therefore the surface pH which is in equilibrium with calcite can be calculated using an aqueous solution thermodynamic model, however this is not true for precipitation at low P_{CO_2} (Plummer et. al., 1979). The validity of using this rate equation assuming that surface P_{CO_2} and bulk P_{CO_2} are the same was tested by Reddy and Plummer (1981) and was shown to be of restricted validity. Unfortunately, in order to calculate the rate of calcium carbonate precipitation at low P_{CO_2} (<0.03 atm) using a mechanistic model requires a value of surface P_{CO_2}.

House (1981) studied the kinetics of crystallization of calcite from calcium bicarbonate solution using a seeding technique and adjusting the pH of the solution by bubbling a CO_2/N_2 gas mixture into the metastable solution. He tested the available kinetic models with the experimental data and concluded that the mechanistic model suggested Plummer et. al. (1978) gave the best fit to experimental data. The growth model of Davies and Jones gave good agreement when the extent of precipitation as defined in his paper (House, 1981) was between 0.1 and 0.45. This Davies and Jones model was previously used by Sturrock et. al. (1976) and Kazmlierczak (1979) and subsequently used by House (1982). This equation is based upon a double-layer model that allows for a difference in concentration of the adsorbed

ions and ions in the bulk of solution (Davies and Jones, 1955). The potential set up between the crystal and bulk solution is such that the concentrations of the cations and anions of the inorganic salt taking part in the precipitation are equal in the monolayer. The influx of cations and anions into the monolayer is proportional to their concentrations at the surface of the monolayer. The efflux of cations and ions from the monolayer is proportional to the solubility of the inorganic salt in the aqueous solution. The nett influx of cations and anions (ie. influx in excess of the efflux) equals the flux available for precipitation. Applying Boltzman distribution law:

$$\text{Concentration of } Ca^{2+} \text{ in the monolayer} = \{Ca^{2+}\}e^{-2\psi/RT} \qquad (4\text{-}34)$$

$$\text{Concentration of } CO_3^{2-} \text{ in the monolayer} = \{CO_3^{2-}\}e^{+2\psi/RT} \qquad (4\text{-}35)$$

where $\{Ca^{2+}\}$ and $\{CO_3^{2-}\}$ are the activities of calcium and carbonate in bulk solution

R is the gas constant

T is the temperature in °K

ψ is the potential difference between crystal and bulk solution

When the solution is saturated with calcium carbonate crystals, in the monolayer,

$$(\{Ca^{2+}\}e^{-2\psi/RT})(\{CO_3^{2-}\}e^{2\psi/RT}) = K_{sp} \qquad (4\text{-}36)$$

therefore

$$\{Ca^{2+}\}e^{-2\psi/RT} = \{CO_3^{2-}\}e^{2\psi/RT} = K_{sp}^{1/2} \qquad (4\text{-}37)$$

Thus for a saturated solution the influx (or efflux) of calcium and carbonate are

$$\text{Influx (or efflux) of } Ca^{2+} = K_{(4-38)} K_{sp}^{1/2} \tag{4-38}$$

$$\text{Influx (or efflux) of } CO_3^{2-} = K_{(4-38)} K_{sp}^{1/2} \tag{4-39}$$

where $K_{(4-38)}$ is the rate constant.

If the supersaturated solution in which the concentration of Ca^{2+} is higher than CO_3^{2-}, the potential defference, ψ, will be established between the adsorbed layer and the bulk solution in such a way that the concentrations of Ca^{2+} and CO_3^{2-} are equal at the monolayer surface. The influx of calcium and carbonate are

$$\text{Influx of } Ca^{2+} = K_{(4-38)} \{Ca^{2+}\} e^{-2\psi/RT} \tag{4-40}$$

$$\text{Influx of } CO_3^{2-} = K_{(4-38)} \{CO_3^{2-}\} e^{2\psi/RT} \tag{4-41}$$

The efflux from the layer is given by Equations (4-38) and (4-39). Therefore the nett fluxes are:

$$\text{Nett flux of } Ca^{2+} = K_{(4-38)} (\{Ca^{2+}\} e^{-2\psi/RT} - K_{sp}^{1/2}) \tag{4-42}$$

$$\text{Nett flux of } CO_3^{2-} = K_{(4-38)} (\{CO_3^{2-}\} e^{2\psi/RT} - K_{sp}^{1/2}) \tag{4-43}$$

The rate of formation of ion pair $CaCO_3^0$ (to be incorporated into the crystal lattice) is proportional to the nett influx of Ca^{2+} and CO_3^{2-}.

Rate of formation of $CaCO_3^0$/unit crystal surface =

$$K_5(\{Ca^{2+}\}e^{-2\psi/RT} - K_{sp}^{1/2})(\{CO_3^{2-}\}e^{2\psi/RT} - K_{sp}^{1/2}) \qquad (4-44)$$

The rate of precipitation of calcium carbonate is proportional to the rate of formation of $CaCO_3^0$ and the total crystal surface area available for growth, ie.

$$-\frac{dT_{Ca}}{d\theta} = K_{DJ}A(\{Ca^{2+}\}e^{-2\psi/RT} - K_{sp}^{1/2})(\{CO_3^{2-}\}e^{2\psi/RT} - K_{sp}^{1/2}) \qquad (4-45)$$

where A is the total crystal surface area in unit volume

K_{DJ} is the rate constant

Since the concentration of calcium equals the concentration of carbonate in the monolayer:

$$e^{2\psi/RT} = (\{Ca^{2+}\}/\{CO_3^{2-}\})^{1/2} \qquad (4-46)$$

Substituting for $e^{2\psi/RT}$ from Equation (4-46) to (4-45),

$$-\frac{dT_{Ca}}{d\theta} = K_{DJ}A(\{Ca^{2+}\}^{1/2}\{CO_3^{2-}\}^{1/2} - K_{sp}^{1/2})^2 \qquad (4-47)$$

Incorporating activity coefficients,

$$-\frac{dT_{Ca}}{d\theta} = K_{DJ}Af_d^2\{[Ca^{2+}]^{1/2}[CO_3^{2-}]^{1/2} - (K_{sp}/f_d^2)^{1/2}\}^2 \qquad (4-48)$$

Sturrock, et. al. (1976) investigated the kinetics of calcium carbonate precipitation in seeded batch experiments at 20°C. The rates were expressed as a function of seed mass instead of surface

area and supersaturation by both the Nancollas and Reddy equation (Equation (4-14)) and the Davies and Jones equation (Equation (4-48)). The kinetic constants were found to be a function of the initial supersaturation when applying the Nancollas and Reddy equation. This suggested that the hypothesis of Nancollas and Reddy was not sustained. However, the kinetic constants were independent of initial supersaturation when the Davies and Jones equation was applied. Sturrock et. al. (1976) concluded that the hypothesis of Davies and Jones applied well for cacium carbonate precipitation.

Crystallization of calcium carbonate is influenced by many factors such as the presence of heterogeneous nuclei, initial degree of supersaturation, temperature and also the presence of foreign ions which affect the size and morphology of the final crystals. Crystal growth also is greatly reduced or completely inhibited in the presence of some foreign ions. Studies on the effect of magnesium on calcium carbonate crystallization have been published by many investigators (Taft, 1967; Kitano, 1967; Roques and Girou, 1974; Reddy and Nancollas, 1976; Reddy and Wang, 1980). Sufficient magnesium in the solution tends to reduce the crystal growth rate and favours the formation of aragonite rather than calcite. It was reported that at a concentration of 10^{-3} M magnesium ions the rate of crystallization was greatly reduced, at 10^{-5} M of magnesium ions there was no effect (Reddy and Wang, 1980). Besides magnesium, other metal ions such as Ni^{2+}, Co^{2+}, Fe^{3+}, Zn^{2+} and Cu^{2+} also encourage the formation of aragonite, while Mn^{2+}, Cd^{2+}, Sr^{2+}, Pb^{2+} and Ba^{2+} favour calcite. In general, metal ions with a small ionic radius and higher hydration energy than that of Ca^{2+} result in aragonite formation (Roques and Girou, 1974).

The crystallization process is usually studied in a batch stirred reactor, a continuous stirred reactor can be used to study the process especially to acquire information for industrial crystallizer operation. Calcium carbonate crystallization has been studied using continuous stirred tank reactors (Maruscak et. al., 1971; Attarian et. al., 1976; Schierholz and Stevens, 1975; Swinney and Stevens, 1982). The studies investigated product size control and crystallization kinetics. Schierholz et. al. (1975) used the population balance concept (Radolph and Larson, 1971) to investigate calcium carbonate crystalization kinetics in a mixed suspension mixed product removal (MSMPR) crystallizer which was applicable to water softening. Calcium carbonate was precipitated out by continuously adding fixed concentrations of calcium sulphate and sodium carbonate reagents to the stirred reactor, while a fixed quantity of mixed suspension was removed periodicaly to maintain the required residence time. Calcite was found to form at low residual supersaturation and aragonite at higher supersaturation. Crystallization was found to follow a power law model.

4.2 EXPERIMENTAL METHOD - A GENERAL SURVEY

4.2.1 Nucleation Studies

4.2.1.1 Homogeneous Nucleation Studies

It is not unusual to find contradictory results on nucleation studies reported in the literature. This is especially true when one attempts to study homogeneous nucleation and fails to realise the experimental problems involved becuase it is difficult if not impossible to create a dust-free solution for homogeneous nucleation.

Furthermore, there are experimental difficulties because of the extremely small size and fast rate of nuclei formation for homogeneous nucleation. Some results reported on homogeneous nucleation were believed to be distorted by the presence of impurities and hence were really studies of heterogeneous nucleation. Homogeneous nucleation has to be studied using dust-free solutions and then allowed to proceed with the solution isolated from all possible contaminants both from the atmosphere and from containers or equipment. These problems were believed to be solved by Vonnegut (1948) who subdivided a liquid system into a large number of tiny, non-communicating droplets whose number greatly exceeded the number of impurities (foreign nuclei). Therefore the impurities were only present in relative few droplets and the effect was reduced to a minimum, hence reproducible rate measurements became possible. This principle was subsequently used and further developed by other investigators (Pound and La Mer, 1952; Turnbull, 1952; White and Frost, 1959; Melia and Moffitt, 1964; Newkirk and Turnbull, 1955). An apparatus developed by White and Frost (1959) was modified by Melia and Moffitt (1964) to study homogeneous nucleation. This apparatus was designed to produce droplets of aqueous solution suspended in oil. The aqueous solution was contained in a reservoir as a temperature above the saturation temperature of the solute. The solution was allowed to flow from the reservoir through the capillary jet and droplets were stripped off by the flow of oil past the capillary tip. The size of the droplets could be closely adjusted by the rate of flow of oil past the capillary tip and coarsely adjusted by the dimentisons of the capillary. The temperature of the oil below the tip was regulated by a thermostatically-controlled flowing water jacket. The temperature could be set at below the saturation temperature of the solution to cause nucleation.

Furthermore the composition of the oil could be arranged to solidify at that temperaure. As a result, the droplets, about 100 - 200 in a typical run could be fixed and observed over long periods of time. The droplets could be observed with a microscope fitted with crossed Nicol prisms to detect the presence of crystallization. Therefore the percentage of droplet nucleate with respect to time could be followed. However this technique has it shortcomings:

1. The number of crystal formed in the droplets cannot be counted,

2. The beginning of nucleation of sparingly soluble salts and sats with a low temperature-coefficient of solubility cannot be detected visually because only a small amount of precipitate forms.

Melia suggested that these problems could be overcome by the method similar to that used by Newkirk and Turbull (1955). They developed a method to allow microscopic observation and to take photographs during the course of nucleation and crystal growth. They dispersed the aqueous solution into many small drops in warm liquid paraffin or silicone oil by rapid mixing with a stirrer and a draught tube. A drop of this dispersion was placed on a glass slide covered with a thin glass cover slip and then examined on a special microscope stage whose temperature was adjustable and controlled. Nucleation of solute could be triggered by cooling of the emulsion so that the solute saturation was exceeded. The under cooling required to form crystals in the droplet was detected to the accuracy of $\pm 2°C$ and the supersaturation created corresponds to or is nearly equal to the critical supersaturation for homogeneous nucleation. Therefore the solute interfacial energy can be calculated.

4.2.1.2 Metastable Zone Width

Nyvlt (1968) suggested a method to study kinetics of nucleation by measuring the width of the metastable zone of concentrations. When supersaturation corresponds to the labile zone of the solute, the nucleation rate increases rapidly. However, if solute supersaturation is gradually achieved by moderate cooling, it is practically impossible to exceed the limit of metastable supersaturation. Accoring to Nyvlt's reasoning, the nucleation rate at the beginning of nucleation should be identical for a limited period of time, therefore the nucleation rate can be expressed in the form:

$$J' = \frac{dm_z}{d\theta} = K_n P_1^n = K' b'$$

(4-49)

where J' is the mass nucleation rate

m_z is the mass of crystals of size z which do not redissolve into

    solution

$d\theta$ is the period of time during which the mass is formed

P_1 is the metastable zone width which is the difference in metastable limit concentration and equilibrium concentration of the solute

K_n and n are the nucleation rate constant and nucleation order respectively

K' represents the weight of the substance precipitated by a unit volume of saturated solution by 1°C

b' is the cooling rate

In addition, K' can be expressed as

$$K' = \varepsilon' \frac{dc_s}{dt} \qquad (4\text{-}50)$$

where c_s is the equilibrium concentration of the solute

t is the temperature ^0C

$\varepsilon' = (1-c/\mu'\rho)^{-1}$

μ' is the ratio of molecular weights of hydrate to anhydrous

salt

ρ is the solution density

The metastable zone width may be expressed as

$$P' = (\frac{dc_s}{dt})\Delta t_{max} \qquad (4\text{-}51)$$

where Δt_{max} is the maximum allowable undercooling defined as the difference of temperature at which the crystals appear and the temperature at which they dissolve again.

Substitute Equation (4-51) into Equations (4-49) and (4-50) gives

$$\varepsilon'(\frac{dc_s}{dt})b' = K_n [(\frac{dc_s}{dt})\Delta t_{max}]^n \qquad (4\text{-}52)$$

Assuming $\frac{dc_s}{dt}$ is over the range of temperature considered,

$$\log b' = \text{const.} + n \log \Delta t_{max} \qquad (4\text{-}53)$$

Therefore by plotting the cooling rate against maximum allowable undercooling, the kinetic order n can be determined as the gradient of the plot of $\log b$ and $\log \Delta t_{max}$. Substituting back to Equation (4-52), K_n can be calculated.

The experimental technique is relatively simple, a solution of known saturation temperature is agitated and cooled at a specified rate in a 50 mL Erlenmeyer flask and the temperature at which nuclei first appear is recorded. The difference between the saturation and nucleation temperature is the maximum allowable undercooling, Δt_{max}, for the particular cooling rate, b. This method was applied by some investigators to study the nucleation of salts from solution (Mullin and Osman, 1973; Mullin and Ang, 1977). In theory the metastable zone width method proposed by Nyvlt is applicable to both homogeneous and heterogeneous nucleation. However, the experimental setup proposed invariably involved difficulties in providing dust-free solution for true homogeneous nucleation. Therefore, the results obtained by using this method apply to heterogeneous nucleation, which is evident in the investigation by Mullin and Ang (1977). If the same principle is applied to the Newkirk and Turbull method as described previously, it is possible to investigate homogeneous nucleation.

4.2.1.3 Induction Period Method

Another completely different approach to nucleation study is by mesasurement of induction period. A number of authors (Turnbull, 1953; Khamskii, 1969; Mullin and Osman, 1973) made simplifying assumptions to suggest that the induction period was basically the time involved in nucleation. Therefore, it was inversely proportional to the rate of nucleation:

$$J = K_{(4-54)} \theta_{ind}^{-1} \qquad (4-54)$$

where J is the number rate of nucleation

$K_{(4-54)}$ is a constant of proportionality

Based on the classical nucleation relationship (see Equation (2-13)),

$$\log(\frac{1}{\theta_{ind}}) \propto \{\frac{\sigma^3}{T^3 (\log S)^2}\} \qquad (4-55)$$

Therefore the plot of $\log \theta_{ind}$ versus $(\log S)^{-2}$ should result a straight line and the gradient allows σ, the interfacial energy to be calculated. Under very high degrees of supersaturation, the induction period is very small, but this is the situation where homogeneous nucleation is more likely to take place because very high concentrations of nuclei are generated and the conditions minimize the influence of heteronuclei. Therefore, to measure a very short induction period becomes the major experimental difficulty. The simplest way to measure induction period is by direct visual observation under a beam of strong light. Two reagents required to produce the precipitate are mixed rapidly into a beaker with a magnetic stirrer mixing the beaker contents. The time taken for the first appearance of shiny crystals is taken as the induction period. The first change of physical property, such as conductivity can also be taken as the induction. This presents no problems if the induction period is longer than 5 seconds, but under conditions of very high degrees of supersaturation, the induction period is normally less than 5 seconds, in fact it is in the range of milliseconds. This direct simple method becomes unsuitable. Nielsen (1967) had devised a modified stopped- flow method by forcing the reacting solutions into a mixing chamber of the Roughton type and the mixture flows into an illuminated outlet channel. The induction period was measured by means of a record on a 35 mm film moved continuously at 50 cm per second in a Shackmann Oscilloscope Camera. At

low supersaturation, the induction period was measured as the time that passed from the moment the pistons stopped to the appearance of a visible precipitate. At high supersaturation, the length of the clear zone between the mixing chamber and the place in the outflow channel where the precipitate became visible was measured and converted to induction period.

Söhnel and Mullin (1978) used Nielsen's stopped-flow and mixing apparatus to measure the induction period by detecting changes of conductivity with a storage oscilloscope. The apparatus permitted time measurements from 10 s to 1 μs. The oscilloscope sweep was triggered when the flow of solution stopped, ie. mixing was completed. The mixed solution than flowed backward and the period of conductivity 'steadiness' was therefore the induction period. This method detects induction periods as short as 5 ms.

4.2.2 Crystallization Studies

4.2.2.1 Conventional Methods

Numerous experimental methods have been used to measure crystal growth rate. Since the growth rate of crystals can be described by face growth rates of a single crystal as well as overall growth rate on single and multi crystals, each method used is designed to provide information only on certain aspects of crystal growth. These methods include direct microscopic observation, photography and interferometry to study single crystal face growth rate. The face growth rate of single crystals is generally expressed in the empirical form:

$$G = K_{(4-56)} \Delta C^n \qquad (4-56)$$

where G is the linear growth rate, length per unit time

$\Delta = C - C_s$ where C is the solute concentration and C_s is the equilibrium saturation

$K_{(4-56)}$ is the constant dependent on the velocity of the fluid

n is the order with respect to supersaturation

Alternately a much more convenient way of measuring crystal growth is to determine the overall growth rate which is the mass deposited per unit time per unit surface area of the crystal. This is especially useful for a multiparticle system. It can be studied in a fluidised bed or in a batch stirred reactor from a known quantity of seed crystals. It is also common to study the crystallization process in a batch stirred reactor without separate seed addition. In such experiments the precipitation of the crystals stems from nucleation (O'Rourke and Johnson, 1955; Ang and Mullin, 1979; Konak, 1971; Söhnel and Mullin, 1982). The empirical form of the overall growth rate expression is:

$$R_G = K_G \Delta C^n \qquad (4-57)$$

where R_G is the overall growth rate and K_G is the overall growth rate constant.

When growth rate is also a function of crystal size, then

$$R_G = K_{(4-58)} L^m \Delta C^n \qquad (4-58)$$

where $K_{(4-58)}$ and m are constants and L is the mean crystal size.

4.2.2.2 Population Balance by MSMPR Crystallizer

A completely different approach to study the kinetics of crystal growth is by the population balance method. Kinetic data is best obtained from a continuous mixed suspension mixed product remover (MSMPR) crystallizer, where a stirred reactor is continuously fed with precipitating reagents and the suspension in the reactor is intermittently removed to maintain a specified residence time. Information obtained is applied to industrial crystallizer design to provide required product size and yield. The concept of population balance was first proposed by Randolph (1964) and Hulburt, et. al. (1964) to describe the crystal size distribution (CSD) in a system. The detailed mathematical treatment is given in the reference (Randolph and Larson, 1971). In a MSMPR crystallizer, some assumptions are made:

1. Steady state operation.

2. Perfect mixing.

3. No attrition of the particles.

4. Uniform shape factor.

The distribution of crystal sizes is represented in terms of population density N, defined as

$$\Delta N = \int_{L_1}^{L_2} n dL \qquad (4-59)$$

where ΔN is the number of crystals in size range L_1 to L_2 per unit volume of suspension

n is a function of L

When the system is operating at steady state, the number rate of crystals entering a size range must be equal to the number rate leaving. Therefore, in an incremental time $\Delta\theta$, the number of crystals entering size L_1 to L_2 because of growth is:

$$Vn_1 G_1 \Delta\theta \qquad\qquad (4-60)$$

where n is the population density of L_1

$\quad$ G_1 is the linear growth rate of crystals of size L_1

The number of crystals leaving size range L_1 to L_2 because of growth is

$$Vn_2 G_2 \Delta\theta \qquad\qquad (4-61)$$

If the feed stream contains seed crystals in this range, then the input to the distribution in the volume V is

$$Q_i \bar{n}_i \Delta L \Delta\theta \qquad\qquad (4-62)$$

where Q_i is the volumetric flow rate

$\quad$ $\bar{n}_i$ is the average population density in the size range,

$\quad$ $\Delta L = L_2 - L_1$.

Similarly, the withdrawal stream particles in the size range is

$$Q\bar{n} \Delta L \Delta\theta \qquad\qquad (4-63)$$

At steady state, input = output, therefore

$$Q_i \bar{n}_i \Delta L \Delta \theta + V G_1 n_1 \Delta \theta = Q \bar{n} \Delta L \Delta \theta + V G_2 n_2 \Delta \theta \qquad (4\text{-}64)$$

rearranging,

$$V(G_2 n_2 - G_1 n_1) = (Q_i \bar{n}_i - Q \bar{n}) \Delta L \qquad (4\text{-}65)$$

when $L \rightarrow 0 \Delta$

$$\frac{V d(Gn)}{dL} = Q n_i - Q n \qquad (4\text{-}66)$$

assuming there are no crystals in the feed stream $n_i = 0$, then

$$\left(\frac{V}{Q}\right) \frac{d(Gn)}{dL} + n = 0 \qquad (44\text{-}67)$$

Assuming McCabe's ΔL law holds, ie. the growth rate is independent of crystal size, also defining $\theta = \frac{V}{Q}$, which is the residence time of the drawdown time, the equation becomes

$$G\theta \left(\frac{dn}{dL}\right) + n = 0 \qquad (4\text{-}68)$$

Integrating Equation (4-68), and letting n^0 be the population density of zero-size crystals (the nuclei population density),

$$\int_{n_0}^{n} \frac{dn}{n} = \int_0^L \frac{L dL}{G\theta} \qquad (4\text{-}69)$$

$$n = n^0 \exp(-L/G\theta) \qquad (4\text{-}70)$$

Therefore the plot of log n versus L gives a straight line with an intercept at L=0 equal to n^0 and a gradient of $\frac{-1}{G\theta}$. Therefore G the

linear growth rate can be determined with known residence time of the crystallizer.

Kinetics of nucleation and crystal growth can also be calculated by the following equations:

$$\frac{dN^0}{d\theta} + K_{(4-71)}\Delta c^m \tag{4-71}$$

where $\dfrac{dN^0}{d\theta}$ is the rate of nucleation.

$$G = \frac{dL}{d\theta} = K_{(4-72)}\Delta c^l \tag{4-72}$$

Now

$$\frac{dN^0}{d\theta} = \frac{dN}{d\theta}\Big|_{L=0} = \frac{dN}{dL}\Big|_{L=0}\frac{dL}{d\theta} = n^0 G \tag{4-73}$$

Therefore

$$\frac{dN^0}{d\theta} = K_{(4-74)} G^{m/l} \tag{4-74}$$

or

$$n^0 = K_{(4-75)} G^{\frac{m}{l} - 1} \tag{4-75}$$

Therefore a plot of $\log n^0$ versus $\log G$ gives a straight line of gradient $\dfrac{m}{l} - 1$. If l is known from the empirical equation of power law of supersaturation, m may be evaluated for the kinetic order of nucleation.

4.3   INTERPRETATION OF DESUPERSATURATION CURVE

A single batch crystallization experiment can conveniently generate crystal growth data covering a wide range of degrees of supersaturation. The solute concentration with respect to time can be followed by measuring parameters such as conductivity, refractive index and pH of the solution. The resulting plot of concentration against time is known as the desupersaturation curve of crystallization. A typical desupersaturation curve is shown in Figure (4-1).

At point A, $\theta=0$, supersaturation is created and is followed by a period of nucleation. At point B, visible nuclei are formed and the time taken is called the induction period, θ_{ind}. The mass precipitated out from the solution at this point is still insignificant to cause a decrease in the measured solute concentration. However, the precipitation process proceeds until the measured concentration begins to decrease. This occurs at point C and the time taken is called the latent period. The solute concentration continues to experience a steep decline where point C' represents the commencement of this steep decline. This decline gradually slows down as indicated by region D and E in Figure (4-1). Such a plot based upon a carefully controlled batch experiment can give information about the kinetics of crystallization. Methods are available to retrieve kinetic data from such experiments and they are discussed below:
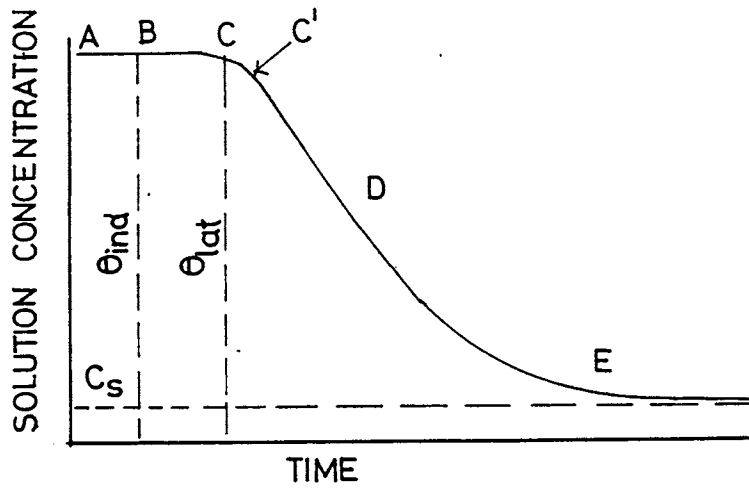
FIGURE 4-1 A Typical Desupersaturation Curve;
c_s = Equilibrium Saturation, θ_{ind} =
Induction Period, θ_{lat} = Latent Period
(after Mullin, 1972)

4.3.1 Chronomal Analysis

Chronomal (short term for chronometric integral) analysis was first used by O'Rourke and Johnson (1955), the Chronomal, I, corresponding to an assumed curve, can be plotted against time. A straight line plot therefore confirms the growth law assumed. Nielsen (1955,1964)) applied this technique to the precipitation process for a range of compounds. Crystal growth mechanisms such as diffusion control, surface nucleation control as defined by Nielsen can be identified with this method. There are some major assumptions when applying this method;

1. The crystals have identical size and shape.

2. The crystals retain their initial shape during growth.

3. Supersaturation is generated only at the beginning of an experiment.

4. No growth dispersion occurs.

5. No nucleation occurs during an experiment (ie. number of nuclei is fixed).

With the above assumptions, the kinetics of crystallization can be determined as follows:

Assuming empirical linear growth rate

$$\frac{dL}{d\theta} = K_{(4-76)}{}^{\sigma}$$

(4-76)

where L is the characteristic length of the crystal

σ is the supersaturation defined as $\dfrac{c - c_s}{c_s}$

c is the solute concentration at any given time

c_s is the equilibrium concentration

$K_{(4-76)}$ is a constant

The mass balance on the solute in a batch experiment is

$$\sigma = \sigma_i [1 - (\frac{L}{L_f})^3]$$ (4-77)

where σ_i is the initial supersaturation $= \dfrac{c_i - c_s}{c_s}$

c_i is the initial solute concentraton

L_f is the final crystal size

From Equations (4-76) and (4-77),

$$\frac{dX}{d\theta} = (\frac{1}{3\theta_1})(1 - x^3)$$ (4-78)

where

$$X \equiv \frac{L}{L_f} = (1 - \frac{\sigma}{\sigma_i})^{1/3}$$ (4-79)

θ_1 is a time constant for growth

$$\sigma_1 = L_f/(3K_{(4-80)}\sigma_i)$$ (4-80)

The factor 3 is introduced to maintain consistency with Nielson's (1955) work on diffusion controlled chronomal. From Equation (4-78)

$$3\int_{x_i}^{x} \frac{dx}{1-x^3} = \int_{\theta_1}^{\theta} \frac{\theta}{\theta} d\theta$$ (4-81)

hence

$$I_1(x) - I_1(x_i) = \frac{\theta}{\theta_i} \qquad (4\text{-}82)$$

where $I_1(x)$ is the first order chromonal.

$$I_1 \equiv 3\int_0^x \frac{dx}{1-x^3} =$$

$$\frac{1}{2}\ln\{\frac{1-x^3}{(1-x)^3}\} + \sqrt{3}\tan^{-1}(\frac{\sqrt{3}x}{2+x}) \qquad (4\text{-}83)$$

Therefore if the plot of $I_1(x)$ against time is a straight line, the first order growth rate holds. The gradient is equal to θ_1. If σ_i and L_f are known, the growth constant $K_{(4\text{-}79)}$ can be calculated.

Similarly, an empirical equation in the form of mth order kinetics

$$\frac{dL}{d\theta} = C_m \sigma^m \qquad (4\text{-}84)$$

$$I_m(x) - I_m(x_i) = \frac{\theta}{\theta_m} \qquad (4\text{-}85)$$

where $\theta_m = L_f/(3C_m\sigma_i^m)$

$$I_m \equiv 3\int_0^x \frac{dx}{(1-x^3)^m} \qquad (4\text{-}86)$$

Again, a straight line plot confirms the empirical growth law and the growth constant can be calculated from θ_m provided L_f and σ_i are known.

4.3.2 Turnbull's Characteristic Curve

Turnbull (1953) published his work on the kinetics of precipitation of barium sulphate. He defined the fraction of barium sulphate precipitated in time θ by $x = \dfrac{c_i - c}{c_i - c_s}$ where x is a function of time. He plotted the curve of x against time for different initial supersaturation experiments. When he applied a suitable scaling factor, he noticed that all data fell onto a single characteristic curve described by the general relations:

$$x = f(S_1, \theta) \tag{4-87}$$

where S_1 is the scaling factor which is also a function of initial supersaturation. Equation (4-87) also can be written in the form:

$$\frac{\sigma}{\sigma_i} = f(\frac{\theta}{\theta_B}) \tag{4-88}$$

where θ_B is the time constant similar to that described in Section (4-3-1). Turnbull reported that the rate of linear growth of barium sulphate was independent of crystal size at the earliest stage of precipitation. After the crystals reached a certain size their growth rate became limited by diffusion. Therefore the linear growth rate can be expressed in the form:

$$\frac{dL}{d\theta} = C_B \sigma^a L^b \tag{4-89}$$

where σ_B, a and b are constants. If the expression of chronomal analysis is used,

$$I_B(x;a,b) - I_B(x_i;a,b) = \frac{\theta}{\theta_B} \qquad (4\text{-}90)$$

where

$$I_B(x;a,b) = 3\int_0^x \frac{dx}{x^a(1-x^3)^a} \qquad (4\text{-}91)$$

and

$$\theta_B = 1/(3C_B\sigma_i^a L_f^{b-1}) \qquad (4\text{-}92)$$

Equation (4-92) provides a more general method to analyse the kinetics of crystal growth. Three batch experiments with different initial supersaturation can be carried out which leads to different final crystal sizes. All these desupersaturation data can be superimposed onto a single characteristic curve obtained by applying an appropriate scaling factor to individual desupersaturation curves represented by plotting σ_i against time. With the data of three sets of Equation (4-92) having C_B, a and b as unknown, these can therefore be solved from the simultaneous equations and obtain a more general form of the linear growth rate equation.

4.3.3 Size Distributon Consideration

The above mentioned methods of interpreting desupersaturation data of crystal growth are based on mono-sized crystals. In reality, crystals precipitated out from solution in different sizes which can be characterised by some form of size distribution function. Therefore, to describe the crystal growth kinetics closely, a size

distribution of the crystals during growth process has to be incorporated into the interpretation of desupersaturation curve. To simplify the problem, the crystal growth kinetics can be assumed to be independent of crystal size. This is true for the case of calcium carbonate in the size range of 5 to 100μm (Schierholz and Stevens, 1975). Again, from a mass balance on solute in a batch precipitation experiment generated by spontaneous nucleation,

$$\frac{\sigma}{\sigma_i} = \frac{\overline{L_f^3} - \overline{L^3}}{\overline{L_f^3}} \qquad (4\text{-}93)$$

where σ and σ_i is the supersaturation as defined previously

$\overline{L_f^3}$ and $\overline{L^3}$ are the normalised third moment of the size distribution of final size and size at any time respectively

The normalised sth moment size is defined as:

$$\overline{L^s} = \int_0^\infty dL L^s n(L,\theta) / \int_0^\infty dL n(L,\theta) \qquad (4\text{-}94)$$

where $n(L,\theta)$ is the number density of crystals of size L at θ.

For size independent kinetics, the shape of the size distribution is unaltered by growth. As a result, the normalized moments about the mean, μ_s, are constants.

$$\mu_s = \int_0^\infty dL (L-\overline{L})^s n(L,\theta) / \int_0^\infty dL n(L,\theta) \qquad (4\text{-}95)$$

where $\overline{L}$ is the arithmetic mean of the number size distribution. Now

$$\overline{L^3} = \mu_3 + 3\mu_2\overline{L} + \overline{L}^3 \qquad (4-96)$$

if $\mu_s' = \dfrac{\mu_s}{\overline{L}^s}$ and $x = \dfrac{\overline{L}}{\overline{L}_f}$, Equation (4-93) becomes;

$$\frac{\sigma}{\sigma_i} = \frac{3\mu_2'(1-x)+1+x^3}{\mu_3'+3\mu_2'+1} \qquad (4-97)$$

Therefore with the information of final arithmetic mean size, initial supersaturation and number size distribution, together with the desupersaturation curve data, arithmetic mean size with respect to time can be derived from Equation (4-97). Thus means that the empirical linear growth rate can be derived from the usual curve fitting procedure. When applied to calcium carbonate precipitation experiments, the arithmetic mean size of the precipitate at any given time of bulk crystallization can be calculated by the following procedure:

1. Calculate the value of σ/σ_i for x ranging from 0 to 1 from Equation (4-97).

2. Construct a best polynomial fit equation for x as function of σ/σ_i.

3. Since $x = \overline{L}/\overline{L}_f$, $\overline{L}$ can be calculated from the desupersaturation curve with respect to time.

4. Construct a best polynomial fit equation for $\overline{L}$ against time and then calculate $d\overline{L}/d\theta$, which is the mean linear growth rate of the bulk crystallization. Therefore from a single batch experiment, the mean linear growth rate kinetics can be determined.

The chronomal analysis can still be applied to incorporate size distribution. If the empirical growth law is

$$\frac{d\overline{L}}{d\theta} = C_m \sigma^m, \quad I_m(x;\mu_2') - I_m(x_i;\mu_2') = \frac{\theta}{\theta_m'} \qquad (4\text{-}98)$$

where

$$\theta_m' = \frac{\overline{L}_f}{3C_m \sigma_i^m} \{\overline{L_f^3}/\overline{L}_f \overline{L_f^2}\}^m$$

$$I_m(x;\mu_2') = 3(\overline{L}_f \overline{L_f^2}/\overline{L_f^3})^m \int_0^x dx (\frac{\sigma_i}{\sigma})^m$$

$$= 3\int_0^x dx [\frac{1+\mu_2'}{3\mu_2'(1-x)+(1-x^3)}]^m \qquad (4\text{-}99)$$

The analytical solution of chronomal integral $I_m(x;\mu_2')$ can be obtained, eg. for the 1st order chronomal:

$$I_1(x;\mu_2') = \frac{1}{2}\ln[\frac{1+3\mu_2' + x + x^2}{(1-x)^2(1+3\mu_2')}]$$

$$+ \sqrt{(\frac{3}{1+4\mu_2'})}\tan^{-1}[\frac{\sqrt{3}x/(1+4\mu_2')}{x+2+6\mu_2'}] \qquad (4\text{-}100)$$

Therefore consideration of the size distribution on chronomal analysis only introduces the coefficient of variation, $\sqrt{\mu_2'}$. The Turnbull characteristic curve method cannot be applied unless the product from different initial degrees of supersaturation are the same, which is normally not the case.

4.3.4 Overall Growth Rate (Simplified)

The overall growth rate, ie. the mass deposited per unit time per unit surface area of the crystal can be expressed by the general equation as follows (O'Rourke and Johnson, 1955):

$$\frac{dc}{d\theta} = -K_{(4-101)} \cdot f(S) \cdot f(C) \tag{4-101}$$

where f(S) is a function of the available surface area and f(C) is a function of precipitating solute. The precipitating solute, according to Davies and Jones (1955), is in the form of supersaturation, ie. $(c_b - c_s)^n$, which is the solute available for precipitation and n is a constant. Apparently, the overall growth rate requires information on the surface area available with respect to time in the course of crystallization (precipitation). When precipitation produces small crystals, or the shape of the crystals comprises more than one form, an approximate overall growth rate can be derived with the two major assumptions (O'Rourke and Johnson, 1955):

1. The growth of large crystals in the system causes the majority of the decreases of the solute concentration. The contribution of small particles is considered insignificant. As a result, the mass of the deposited crystals can be redistributed onto all crystals to assume a monosized pattern.

2. The total number of crystals throughout the crystallization process is considered to be constant.

Therefore the volume per mono-sized particle per unit system volume is proportional to $\frac{c_{in} - c_b}{N}$. Where N is the total number of the mono-sized crystals per system volume.

Surface area per particle is proportional to $(\frac{c_{in}-c_b}{N})^{2/3}$.
The function of total surface area per unit system volume available at any given supersaturation,

$$f(S) = (\frac{c_{in}-c_b}{N})^{2/3} \cdot N = (c_{in}-c_b)^{2/3}N^{1/3} \qquad (4-102)$$

combines with Equation (4-101),

$$\frac{dc}{d\theta} = -K_{(4-103)}(c_{in} - c_b)^{2/3}N^{1/3}(c_b - c_s)^n \qquad (4-103)$$

where $K_{(4-103)}$ is the rate constant containing shape factors. This method has been used by Söhnel and Mullin (1982) to interprete the growth rate constants of calcium carbonate from the desupersaturation curves obtained from their experiments.

Where applying to the calcium carbonate bulk crystallization experiments,

$$\frac{dc}{d\theta} = \frac{dT_{Ca}}{d\theta} \qquad (4-104)$$

where T_{Ca} is the total calcium content at any given time, θ. Assuming constant crystal number throughout the crystallization process, the increase of crystal surface area per liter, $f(S)$ can be expressed as follows:

$$W(\theta) = NV(\theta)\rho = N\rho\alpha_v L(\theta)^3 \qquad (4-105)$$

Where $W(\theta)$ is the weight of crystal in 1 litre at time θ

N is the number of crystals in 1 litre

$V(\theta)$ is the volume of crystal in 1 litre at time θ

ρ is the densty of crystal = 2710 g/L

$L(\theta)$ is some characteristic length of the crystal at time θ

α_v is the volume shape factor of the crystal

$$f(S) = N\alpha_a L(\theta)^2 \qquad (4-106)$$

where α_a is the surface shape factor of the crystal. From Equation (4-105)

$$f(S) = [\frac{\alpha_a}{(\rho\alpha_v)^{2/3}}] [W(\theta)^2 N]^{1/3} \qquad (4-107)$$

since

$$W(\theta) = [T_{Ca_{in}} - T_{Ca}] M \qquad (4-108)$$

where $T_{Ca_{in}}$ is the initial total calcium concentration

T_{Ca} is the total calcium concentration at time θ

M is the molecular weight of calcium carbonate.

Therefore

$$\frac{-dT_{Ca}}{d\theta} = - k \{\frac{\alpha_a}{(\rho\alpha_v)^{2/3}} M^{2/3} N^{1/3} (T_{Ca_{in}} - T_{Ca})^{2/3}\} f(C) \qquad (4-109)$$

The popular empirical rate equation for calcium carbonate crystallization is expressed according to Davies and Jones (1955) theoretical treatment in Equation (4-48).

$$- \frac{dT_{Ca}}{d\theta} = K_{DJ} \ A \ f_d^2 \{ [Ca^{2+}]^{1/2} [CO_3^{2-}]^{1/2} - (K_{sp}/f_d^2)^{1/2} \}^2$$

Putting

$$f(C) = \{ [Ca^{2+}]^{1/2} [CO_3^{2-}]^{1/2} - (K_{sp}/f_d^2)^{1/2} \}^2 \qquad (4-110)$$

The final equation is expressed as

$$- \frac{dT_{Ca}}{d\theta} = k' N^{1/3} f_d^2 (T_{Ca_{in}} - T_{Ca})^{2/3} \ f(C) \qquad (4-111)$$

where

$$k' = k \ f_d^2 \ \frac{\alpha_a}{\rho \alpha_v} \ M^{2/3} \qquad (4-112)$$

$[Ca^{2+}]$, $[CO_3^{2-}]$ are calcium and carbonate concentration at a given time respectively.

$\alpha_a = \pi$ (sphere) and 3.681 (rhomb)

$\alpha_v = \frac{\pi}{6}$ (sphere) and 0.484 (rhomb)

The shape factors used for rhombohedral calcite are calculated theoretically in Section (5.2.1).

4.3.5 Overall Growth Rate with Size Consideration

Ang and Mullin (1979) had proposed a method to calculate the surface area of precipitate during crystallization from the final crystal size distribution, ie. by the medium size, coefficient of variation and final mass of crystals. Normal size distribution was assumed in the calculation. Surface area of the crystal with respect to

supersaturation measured in the course of crystallization is calculated by decremental size procedure for the corresponding mass precipitated, together with the precised determination of surface and volume shape factor. However when the number distribution of the final precipitate is available, assumption for normal distribution is not necessary. The desupersaturation curve can be interpreted by modifying the method proposed by Ang and Mullin (1979) as belows:

The weight of the sample sized by Micro Videomat Image Analyzer (Section(4.4.3.3)) is expressed as:

$$W = \sum_{i=0}^{\infty} N_i \rho_c \alpha_v L_{in}^3 \qquad (4-113)$$

where W is the weight of the sample precipitate sized by image analyzer

N_i is the number of crystals in each size range

ρ_c is the crystal density

α_v is the volume shape factor

L_{in} is the chord length of the crystal measured by the image analyzer

n is the number of size class for the number distribution

$$A = \sum_{i=0}^{n} N_i \alpha_a L_{in}^2 \qquad (4-114)$$

where A is the surface area of the sample precipitate sized by image analyzer

α_a is the surface shape factor

The summation of weight calculated from Equation (4-113) can be compared with the total weight of the final precipitate, consequently a weight factor can be calculated by dividing the total weight with the sample weight. The total surface area of the precipitate is simply the sample surface area multiplied by this factor. The size of each class of the final precipitate can then be reduced by a small quantity and the summation of weight and surface area over the entire size range can be calculated again. The total decremental weight of the precipitate can be compared with the weight calculated from the desupersaturation curve. Hence the surface area of the crystal with respect to time and degree of supersaturation can be calculated. The process can be repeated to cover a wide range of the desupersaturation curve. By substituting the corresponding values of surface area and supersaturation into Equation (4-48), the overall growth rate constant can be calculated. A programme was developed to calcuate the total weight and surface area of the precipitate for each decremental size reduction. This can be found in Appendix F (PROG-SIZE).

4.4 EXPERIMENTAL

4.4.1 Introduction

Calcium carbonate crystallization was investigated under bulk crystallization condition in a batch stirred reactor at constant temperature. Spontaneous crystallization (bulk crystallization without crystal seeds) was the mode of crystallization for all studies. This allowed nucleation and crystallization of calcium carbonate to be studied in a single experiment. The unseeded crystallization experiments were also the better representation of the precipitation in the

cooling water system. Experiments were carried out at four different temperatures, viz. 25°C, 36°C, 44°C and 55.8°C. Two geometries for stirred reactor, viz. Geometry A and Geometry B in conjunction with different stirring speed were used to study the effect of different power input to crystal growth rate of calcium carbonate. A wide range of initial degrees of supersaturation for spontaneous crystallization was investigated to study its effect on the crystal growth rate constants. Apart from crystallization of calcium carbonate in a pure calcium system, the presence of magnesium equal to calcium molar concentration was also studied. In a batch crystalization experiment, the degrees of supersaturation was recorded continually by registering the pH values of the solution, which could be converted into degree of supersaturation using programme PROG-CS (see Appendix F). A desupersaturation curve was constructed for each batch experiment and interpreted for crystal growth rate. Numbers of crystal were counted under a microscope at the end of each experiment, which was run for at least four hours. The information about crystal number was required for crystal growth rate calculation as described in Section (4.3.4). Some crystal products were sized and photomicrographs were taken. The scanning electron microscope was also employed to provide detailed crystals morphology (Appendix B).

4.4.2 Equipment

The major equipment used in the crystallization experiment is a stirred reactor made of perspex. The detail of the experimental set up is shown in Figures (4-2) to (4-4). Two geometries, viz. Geometry A and Geometry B were used in the studies to provide a range of different stirring conditions. The individual equipment used is

described as follows (Figure (4-2)):

(1)   Stirred Reactor

This is a 190 mm I.D. diameter cylindrical vessel made of perspex glass. It comprises one six-bladed brass turbine stirrer with a stainless steel rod. The stirrer was painted with epoxy paint to prevent any form of brass corrosion. It was positioned at 1/6 of the vessel diameter from the base. Four baffles of the width 1/10 vessel diameter in Geometry A and 1/12 vessel diameter in Geometry B were installed. The baffles were used to prevent swirling of the solution and hence achieve even mixing. The vessel was enclosed with a lid made of perspex. This lid contains openings for pH and temperature probes. There are also two adaptors to receive the cylindrical tap funnels by which the reagents are introduced into the reactor. The joints were sealed with silicone grease. The silicone sealent was used to seal the joints of pH and temperature probes on the lid. Such arrangement allowed easy removal of the probes for calibration and cleaning. The bearing used for the stirrer rod was a sealed bearing further secured by a O-ring (Figure (4-3)). Another O-ring was placed in the circular groove on the flange of the reactor. When the reactor was closed by putting the lid in position and tightened by the nuts and bolts, the stirred reactor was completely air-tight. Subsequently the reactor was immersed in a constant temperature water bath.

(2)   Constant Temperature Water Bath

A constant temperature water bath was set up with a Julabo P water circulator of ±0.02°C accuracy. This provided the necessary temperature control of the solution in the reactor throughout the crystallization experiment.

(3)   Resistance Thermometer

Temperature of the solution in the stirred reactor was measured
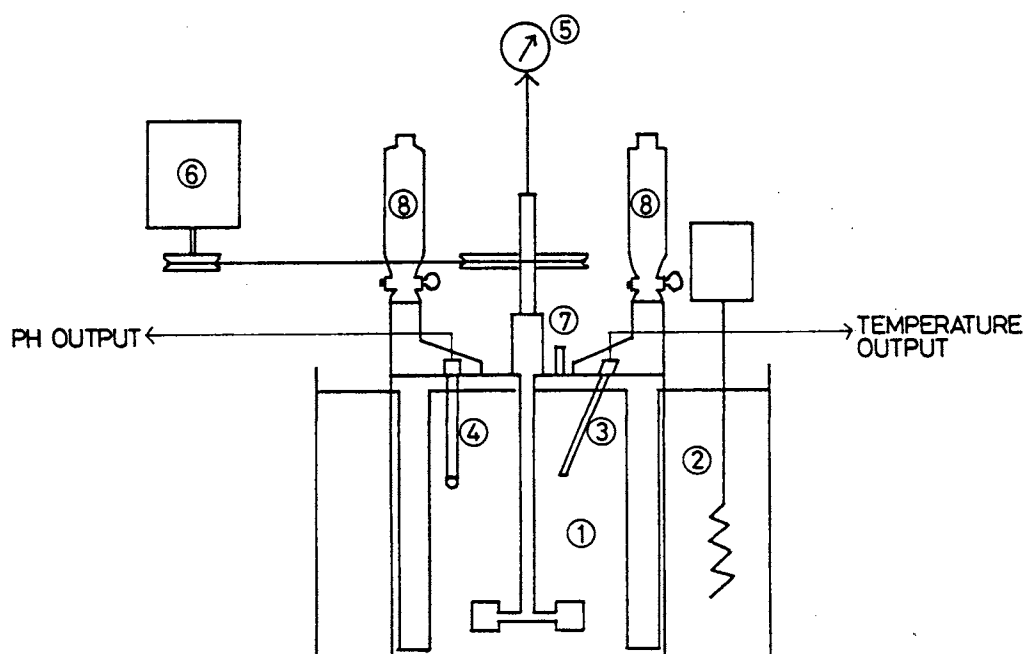
FIGURE 4-2 Schematic Representation of the Apparatus
for CaCO$_3$ Precipitation Study

FIGURE 4-3 Cross-sectional View of the Stirred Reactor

OIL-SEALED
BEARING

SAMPLING
PORT
PLUG

PH

RT

∅127

DIMMENSION : mm
NOT TO SCALE

T/12

3.2

D/4

D/5

D

T/6

3.2

∅T=187
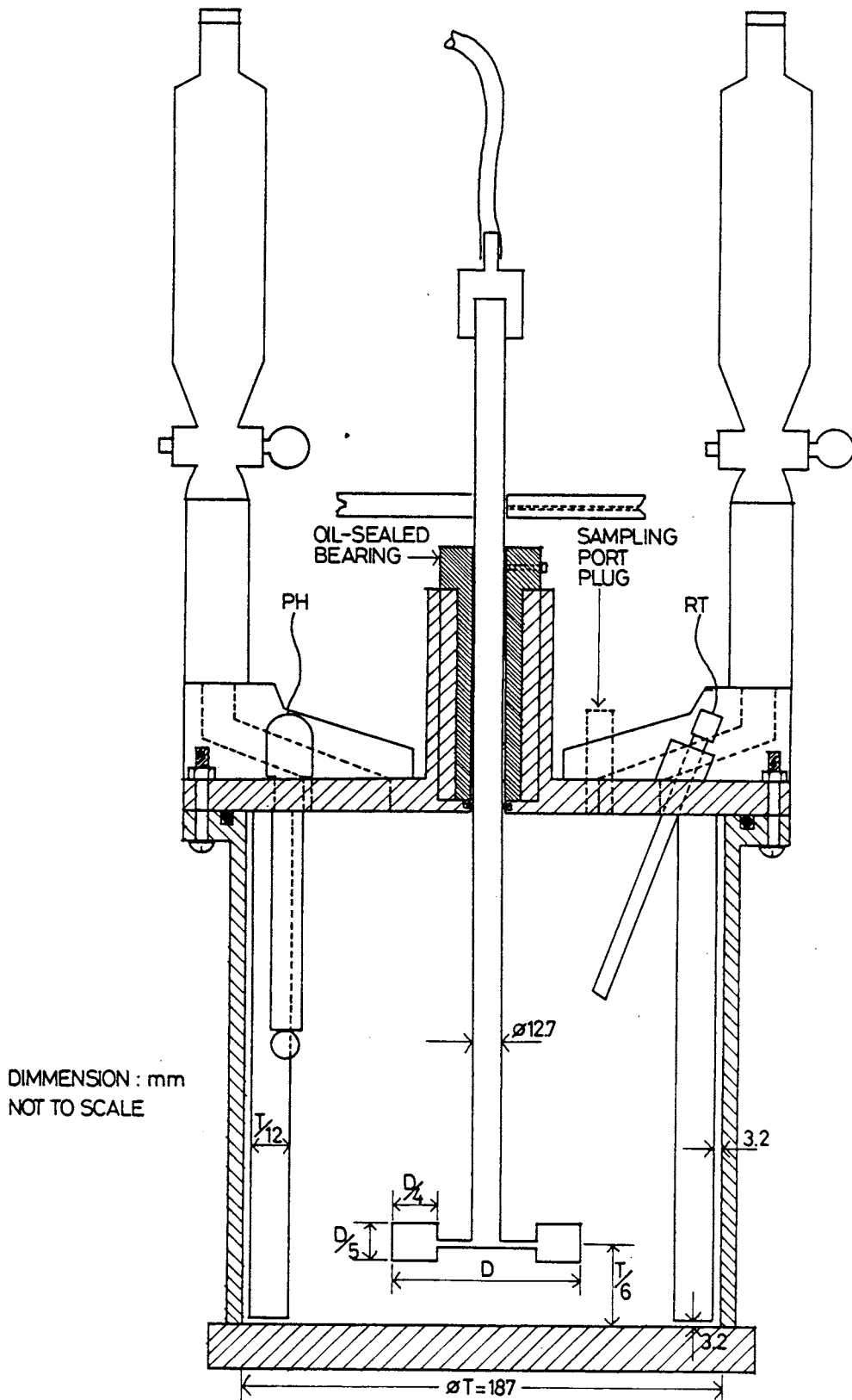
FIGURE 4-4 Schematic Representation of Geometry A
and Geometry B
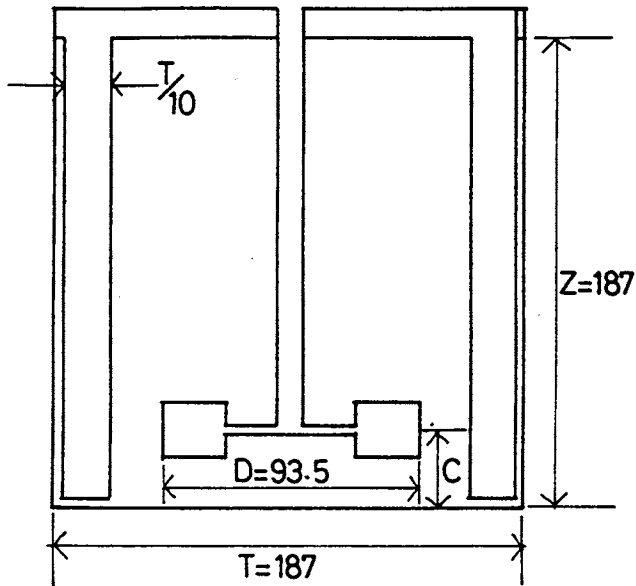
GEOMETRY   A

$$\frac{D}{T} = \frac{1}{2}$$

$$\frac{Z}{T} = 1$$

$$\frac{C}{T} = \frac{1}{6}$$

$$\frac{C}{D} = \frac{1}{3}$$
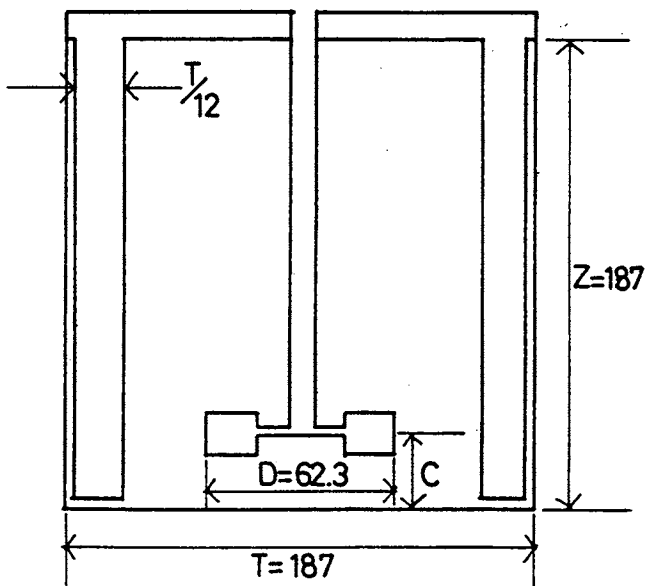
GEOMETRY B

$$\frac{D}{T} = \frac{1}{3}$$

$$\frac{Z}{T} = 1$$

$$\frac{C}{T} = \frac{1}{6}$$

$$\frac{C}{D} = \frac{1}{2}$$

DIMMENSION : mm
NOT TO SCALE

separately by a 3 wire Pt 100 resistance thermometer (Richard Foot Pty. Ltd., Australia) with ±0.1°C accuracy. The temperature was indicated by a digital display temperature indicator.

(4)   pH Probe and Meter

The pH measurement was conducted by a combination pH probe and registered by 1852 TPS digital pH meter with readout to the second decimal point.

(5)   Tachometer

The speed of revolution was registered by connecting a flexible tubing between the stirring rod and the tachometer (Type M.B., Everett Edgcumbe, England) which generated current in the form of analog read out in revolutions per minute.

(6)   Motor

A fixed rate motor (Parvalux Electric Motors Ltd., Australia) was used to drive the stirrer at the required speed achieved by different combination of pulley size on the motor shaft and on the stirrer rod. The pulleys were fabricated out of perspex glass. A 1/4 in. nominal section with 10 in. nominal diameter Merco O-ring (Bestobell Merco) was used as the belt. Once the tension was fixed, the speed of revolution remained constant throughout the experiment.

(7)   Sampling Port

An opening was available on the lid to allow crystals sampling. During the process of crystallization, this opening was closed tightly by a plug.

(8)   Funnels

Two 100 ml cylindrical tap funnels were placed in the adaptors of the lid. The calcium chloride and sodium bicarbonate reagents were introduced into the reactor simultaneously via these two funnels. Once the addition process was completed, these funnels remained closed

throughout the experiment.

4.4.3 Procedures

4.4.3.1 Batch Stirred Reactor Crystallization Experiments

Distilled water filtered through $0.22\mu m$ Millipore membrane filter was used for all the experiments. All glasswares and the stirred reactor were thoroughly washed by the following procedure:

The stirred reactor was soaked in 1N hydrochloric acid over night to remove all the calcium carbonate residue. Subsequently the reactor together with all the glassware were soaked in 40°C washing liquid made of 2 - 3 g/L of Pyroneg (a surgical detergent) for two hours. They were subsequently brushed and rinsed with plenty of tap water followed by distilled water. The washing procedure was to minimize dust in the solution although complete dust-free solution was impossible. All the chemical reagents used were A-R grade. The saturated solution of calcium carbonate was prepared by mixing sodium bicarbonate and calcium chloride in distilled water. The required quantity of sodium bicarbonate for the respective supersaturation was carefully weighed out and dissolved in 100 mL filtered distilled water. The solution was filtered again through 0.22 μm membrane filter. Calcium chloride solution was prepared volumetrically to 100 mL from standardised stock solution. Both solutions were then equilibrated to experimental temperature in a constant temperature water bath. 4900 mL of distilled water was carefully measured and transferred into the stirred reactor and stirred at the required speed in the enclosed environment. The temperature of the solution eventually reached

equilibrium with the water bath temperature. The experimental temperature of the solution in the stirred reactor was separately measured by the Pt100 resistance thermometer to 0.1°C . A torch light equipped with 4.8V globe was placed at the back of the stirred reactor to provide the sight of 'zero' turbidity of the solution. pH of the distilled water was sometimes adjusted by sodium hydroxide solution to the required reading for high initial degree of supersaturation intended. To prepare the crystallization experiment for 1:1 Mg/Ca molar concentration system, magnesium chloride was weighed out separately to the required quantity and dissolved into 4900 mL of distilled water in the stirred reactor. Once all these initial preparations were completed, solutions of calcium chloride and sodium bicarbonate were drained simultaneously through two separate cylindrical tap funnels. The sampling port was left open during the addition of the reagents. Once the transfer was completed, two stop watches were started simultaneously and the taps of the funnels and the sampling port were closed. pH of the solution was recorded with respect to time followed on one of the stop watch. The other stop watch was used to register the time taken for the first appearance of shiny nuclei, ie. the induction period measured by visual observation. The pH readings would continue to decrease once crystallization was evident. The process was given at least four hours to complete. The solution was then filtered through a 0.22 µm membrance filter. The calcium carbonate crystals were retained on the filter and washed with 200 mL of distilled water followed by 200 mL of 70% ethyl alcohol to remove the last traces of residual solution. These crystals were subsequently dried in the oven at 70°C overnight and stored in a dessicator for further microscopic observation.

4.4.3.2 Microscopic Observation and Crystal Number Count

The solution was stirred continuously with the speed which was able to suspend all crystals. The minimum speed was 300 r.p.m. of Geometry B. This is vital to ensure a uniform sample. A 20 µL sample of crystals suspension was taken from the sampling port by a Gilson micropipette. The sample was then transferred onto the surface of a counting chamber. The counting chamber has a depth of 0.22 mm and a total counting area of 9 mm^2. A cover slip was placed onto the counting chamber carefully to spread the crystal suspension evenly over the counting surface. The 20 µL size was chosen because it wetted the entire covered area. Care was taken to spread the crystals over the entire covered area as evenly as possible, nevertheless the crystals tend to spread evenly over the counting area which was about 90% of the entire covered area. Therefore the crystal number is considered to be slightly higher than the actual number. This error is compensated by the possible aging effect of the crystal product by the end of the experiment. (Section (5.1.5)).

The crystals were examined and counted under 10X objective. For detail examination the 40X objective was used. The number of crystals within the counting area was counted and converted to number of crystal per litre solution. For each batch experiment, sufficient number of samples were taken and counted under the microscope to achieve a statistical significance tested by the χ^2 test. The mean was used to calculate the overall growth rate constant of the bulk crystallization of calcium carbonate.

4.4.3.3 <u>Crystal</u> <u>Size</u> <u>Measurement</u>

Some dried crystal samples were sized to enable overall growth rate constant determination by size consideration. The crystal samples inevitably contained agglomerates. These agglomerates can be redispersed in 0.2% sodium pyrophosphate solution. A small quantity of dried crystal sample was transferred into an approximatley 0.5 mL of 0.2% sodium pyrophosphate. This crystal suspension was placed in a ultra-sonic bath generated by a Labsonic 1510 ultra-sound generating unit at the power input of 10 watts for one minute. This range of power and duration was found to be suitable to disperse most of the agglomerates. A drop of this well dispered crystal suspension was transferred by Pasteur pipette onto a microscope slide. Another drop of glycerine was added onto the previous drop and subsequently covered by a cover slip. Glycerine formed the periphery and prevented evaporation during crystal counting. Crystals were than sized by Micro-videomat 2 in the School of Mining Engineering (Zeiss, 1978, 1980). This is a instrument with precision television scanning system, often described as image analyzer. The instrument is comprised of a mono-chrome camera, display, control panel and central processor. Input comes from a Zeiss Universal microscope fitted with Interference Mono-chromometer for contrast enhancement and transmitted light optics with highly planar characteristics for flat field coverage. The TV lines scan the display image from the microscope aerial image. The operator sets the discriminating level manually. When brightness intensity deviates from the selected level, a square wave pulse is produced. The length of scan line within the discriminated image is proportional to the time parameter on the square wave. The discriminated signal pulse selected from the continuous background oscillator pulse is

further processed, if required, before proceeding to the digital out-
put stage. Horizontal TV scan lines and vertical pulses produce
between 10^5 and 10^6 picture points scanned in 40 milliseconds. The
control panel may be operated either manually or via HP 9825A computer
keyboard and software. Multiple fields are controlled from the calcu-
lator via stepping motors operating in 10 micrometer units. Crystal
numbers as high as 60,000 were scanned and the size was registered as
the TV lines scanned from left to right of the screen. The data input
was presented as first moment distribution (Appendix D).

4.5 RESULTS

4.5.1 Primary Nucleation of Calcium Carbonate Precipitation

4.5.1.1 Experiments at Constant Stirring Speed

A series of experiments were conducted on the stirred reactor
with Geometry A as described in Section (4.4.2) for the crystalliza-
tion studies. The induction periods were determined by visual obser-
vation at different temperatures over a wide range of initial degrees
of supersaturation. The degree of supersaturation throughout this
project is defined as $S = \dfrac{[Ca^{2+}] [CO_3^{2-}] f_d^2}{K_{sp}}$. The time taken for the
first appearance of shiny crystals was registered as induction period
(θ_{ind}). The latent period (θ_{lat}) was also registered as the time
taken for the first detection of pH decrease from the maximum pH value
created after mixing. The stirring speed was 220±5 r.p.m. The total
volume of the solution in the reactor was 5.1 litre. The results are
tabulated in Tables (4-2) and (4-3).

TABLE 4-2
Induction and Latent Period of Calcium Carbonate Nucleation Determined in Geometry A Stirred Reactor at 220 r.p.m.

Expt. No.	Temp. (°K)	Degree of Sup. S	Induction period $\theta_{ind}(s)$	Latent period $\theta_{lat}(s)$
PE21	298.0	51.6	53	484
PE20	298.0	22.6	150	-
E13	298.0	26.1	390	660
E14	298.0	20.7	570	960
E15	298.0	20.6	522	1740
E19	298.0	16.7	1098	3840
E20	298.0	35.0	270	1200
E21	298.0	50.2	151	720
E22	298.0	62.0	85	495
E23	298.0	72.4	68	462
E24	298.0	76.4	70	322
E26	298.0	78.9	60	289
E27	298.0	81.5	43	249
E29	309.0	54.8	68	248
E30	309.0	45.9	234	769
E32	317.0	49.4	62	298
E33	317.0	48.3	78	379
E34	317.0	37.2	72	323
E35	328.8	35.4	102	311
E36	328.8	34.3	117	702

TABLE 4-3
Calculation of Results for Calcium Carbonate
Induction and Latent Period Determined in
Geometry A Stirred Reactor

Expt. No.	$\log \theta_{ind}$	$\log \theta_{lat}$	$(\log S)^{-2}T^{-3}$ x10^8 (°K)$^{-3}$	$(\log S)^{-2}$	$\sigma = S-1$	$\log \sigma$ x10^3	$\theta_{ind}^{-1}(s^{-1})$
PE21	1.72	2.68	1.29	0.341	50.6	1.70	18.90
PE20	2.18	-	2.06	0.545	21.6	1.33	6.70
E13	2.59	2.82	1.88	0.498	25.1	1.40	2.60
E14	2.76	2.98	2.18	0.577	19.7	1.29	1.75
E15	2.72	3.24	2.19	0.579	19.6	1.29	1.92
E19	3.04	3.58	2.53	0.669	15.7	1.20	0.91
E20	2.43	3.08	1.58	0.426	34.0	1.53	3.70
E21	2.18	2.86	1.31	0.346	49.2	1.69	6.62
E22	1.93	2.69	1.18	0.311	61.0	1.78	11.76
E23	1.83	2.66	1.09	0.289	71.4	1.85	14.71
E24	1.85	2.51	1.07	0.282	75.4	1.88	14.29
E26	1.78	2.46	1.05	0.278	77.9	1.89	16.67
E27	1.63	2.40	1.04	0.274	81.5	1.91	23.26
E29	1.83	2.39	1.12	0.328	54.8	1.74	14.71
E30	2.37	2.89	1.23	0.362	44.9	1.65	4.27
E32	1.79	2.47	1.10	0.348	48.4	1.68	16.13
E33	1.89	2.58	1.11	0.353	47.3	1.67	12.82
E34	1.86	2.51	1.27	0.405	36.2	1.56	13.89
E35	2.01	2.49	1.17	0.417	34.4	1.54	9.80
E36	2.07	2.85	1.19	0.424	33.3	1.52	8.55

4.5.1.2 Experiments at Different Stirring Speed

A series of experiments were conducted at 300, 400, 500, 700 and 880 r.p.m. using Geometry B at 25°C. The results are tabulated in Tables (4-4) and (4-5).

4.5.1.3 Experiments at Different Stirring Speed of 1:1 Mg/Ca Molar Concentration

The presence of magnesium cations is known to retard the rate of nucleation and crystallization of calcium carbonate. In this experiment the effect of stirring was investigated at 1:1 Mg/Ca molar ratio at 25°C under similar supersaturation condition. Geometry B stirred reactor was used for this series of experiments. The results are tabulated in Table (4-6) for both induction period and latent period.

4.5.2 Secondary Nucleation of Calcium Carbonate Precipitation

Secondary nucleation is heterogeneous nucleation and occurs due to the collision of crystals against other crystals and the collision of crystals against other objects. Therefore, it is not unreasonable to expect secondary nucleation in a stirred reactor as used in these experiments. In fact this mode of nucleation is considered to be the major source of new crystals in a industrial crystallizer when stirrers and pumps are used to move the crystals suspension in the crystallizer (Bennett, et. al., 1973). In a batch reactor crystallization process, nucleation takes place after the precipitating solutions are mixed together. This continues for a period of time until crystallization predominates, which is indicated by a significant decline of

TABLE 4-4

Induction and Latent Period of Calcium Carbonate
Nucleation in Geometry B Reactor at 25°C under
Different Stirring Speed and Supersaturation

Expt. No.	Degree of Sup. S	Induction Period θ_{ind} (s)	Latent Period θ_{lat} (s)	Stirring Speed (r.p.m.)
PE5	57.0	126	920	500
PE7	58.0	120	751	500
PE11	25.6	174	3518	500
PE14	39.3	96	2757	500
PE16	76.5	39	303	500
PE8	57.0	84	724	400
PE9	57.0	192	1083	400
PE13	25.6	174	10560	400
PE6	62.8	162	1066	300
PE3	59.0	96	948	300
PE15	57.0	84	324	700
PE4	57.0	156	965	880
PE12	35.6	132	16020-16440	880

TABLE 4-5
Calculation of Results for Calcium Carbonate
Induction and Latent Period Determined in
Geometry B Stirred Reactor

Expt. No.	$\log\theta_{ind}$	$\log\theta_{lat}$	$(\log S)^{-2}T^{-3}$ $\times 10^8 (°K)^{-3}$	$(\log S)^{-1}$	$\sigma = S-1$	$\log \sigma$
PE5	2.10	2.96	1.23	0.324	56.0	1.75
PE7	2.08	2.88	1.22	0.322	57.0	1.76
PE11	2.24	3.55	1.91	0.504	24.6	1.39
PE14	1.98	3.44	1.49	0.393	38.3	1.58
PE16	1.59	2.48	1.07	0.282	75.5	1.88
PE8	1.92	2.86	1.23	0.324	56.0	1.75
PE9	2.28	3.03	1.23	0.324	56.0	1.75
PE13	2.24	4.02	1.91	0.504	24.6	1.39
PE6	2.21	3.03	1.17	0.309	61.8	1.79
PE3	1.98	2.98	1.21	0.319	58.0	1.76
PE15	1.92	2.51	1.23	0.324	56.0	1.75
PE4	2.19	2.98	1.23	0.324	56.0	1.75
PE12	2.12	4.20-4.22	1.91	0.504	24.6	1.39

TABLE 4-6

Induction and Latent Period of Calcium Carbonate
Nucleation of S=24 determined in Geometry B
Reactor with 1=1 Mg/Ca Molar Ratio at 25°C

Expt.	Induction Period $\theta_{ind}(S)$	Latent Period $\theta_{ind}(S)$	Stirring Speed (r.p.m.)
PE17	128	3552	500
PE18	120	2076	700
PE19	219	7218	400

measurable properties such as conductivity or pH. During the period

of nucleation, the number of nuclei (miniature crystals) continues to

increase until it reaches a constant number, ie. crystal growth takes

over the process. This constant crystal number corresponds to the

commencement of the steep decline of the desupersaturation curve (see

Figure (4-1)). Assuming secondary nucleation is the major source of

nuclei generated, also assuming constant rate of increase in number of

nuclei over the entire period (this fact was observed and illustrated

in Figure (5-10)), then secondary nucleation is expressed as $\frac{\Delta N}{\Delta \theta}$ where

ΔN is the number of crystals counted at the end of crystallization. $\Delta \theta$

is the time taken to reach a constant crystal number.

Ottens et. al. (1972) derived the equation for nucleation due to

crystal-stirrer collision as well as crystal-crystal collision (see

Equations (2-24) and (2-25)). The energy dissipitated per unit mass

of slurry in the stirred reactor designed for the present experiment

can be calculated directly. The detailed calculation is described in

the following section.

4.5.2.1 The Calculation of Power Input in a Stirred Reactor

The power input from the impeller into the agitated liquid of the

stirred reactor can be calculated from the empirical equation derived

by dimensional analysis. The development of the generalized form of

an equation for correlating power has been covered by Johnstone and

Thring (1957) and Rushton, et. al. (1950a, 1950b). The general equa-

tion is expressed as:

$$\frac{Pg_c}{\rho N^3 D^5} = K_T (\frac{\rho ND^2}{\mu})^a (\frac{N^2 D^2}{g_c})^b (\frac{T}{D})^c (\frac{Z}{D})^d (\frac{C}{D})^e (\frac{p'}{D})^f (\frac{w}{D})^g (\frac{l}{D})^h (\frac{n_2}{n_1})^i \quad (4\text{-}115)$$

where P is the power

g$_c$ is the gravitational constant or conversion factor

ρ is the density

N is the impeller speed, r.p.s.

D is the impeller diameter

K$_T$ is a constant

μ is the viscosity

T is the vessel diameter

Z is the liquid depth

C is the impeller distance off vessel bottom, measured from
   underside of impeller

p' is the blade pitch

w is the impeller blade width

l is the blade length

n_1, n_2 are the numbers of impeller blades for
   condition 1 and 2

a,b,c etc. are the exponents

The dependent variable of Equation (4-115) is called the Power
number, N_p. The last seven terms on the right hand side of the equa-
tion are parameters of geometry. Therefore if geometric similarity is
stipulated and a non-swirling system is employed, the equation can be
reduced to:

$$N_p = K_T (Re)^a \quad (4\text{-}116)$$

where Re is the first dimensional group of the equation known as Reynolds number.

Bates, et. al. (1963) had conducted power input measurement on specified geometry and reported the Power number against Reynolds number of Newtonian fluids for various turbine impeller designs. The Power number is constant when the Reynolds number exceeds 10^4 for the radial six-blade turbine impeller. In this research project, the stirred reactor of Geometry B (see Figure (4-4)) was built according to the geometry specified by Bates, et. al. (1963) except the postiton of the impeller was at C/T=1/6. The Geometry A (Figure (4-4)) stirred reactor adopted 4 baffles with the width w_b=T/10 and the turbine impeller of D/T=1/2 diameter. Such disimilarities in the geometry incur some modification on the Power number based on the standard geometry specified by Bates, et. al. The corrections were also given by Bates et. al. (1963). The resulting Power numbers for Geometry A and Geometry B are 4.8 and 4.5 respectively. An example of the power input calculation based on the Power number of the corresponding Reynolds number and stirred reactor and impeller geometry is given as follows: Geometry B stirred reactor

$$N = 300 \text{ r.p.m.} = 5 \text{ r.p.s.}$$

$$D = 62.3 \text{ mm} = 62.3 \times 10^{-3} \text{ m}$$

$$\mu = 0.890 \text{ multiply } 10^{-3} \text{ kg/m s} \quad \text{at } 25°C$$

$$\rho = 997.04 \text{ kg/m}^3 \text{ at } 25°C$$

$$Re = \frac{D^2 N\rho}{\mu} = \frac{(62.3 \times 10^{-3})^2 \times 5 \times 997.04}{0.890 \times 10^{-3}}$$

$$= 2.174 \times 10^4$$

Therefore N_p is a constant which is equal to K_T. $K_T = 4.5$

$$P = \frac{K_T n^3 D^5 \rho}{g_c}$$

$$= 4.5 \times 5^3 \times (62.3 \times 10^{-3})^5 \times 997.04$$

$$= 0.5264 \text{ J/s}$$

Therefore the power input per unit volume, ε

$$= \frac{0.5264}{5.1} = 0.1032 \text{ J/L s}$$

4.5.2.2 Experiments of Pure Calcium Carbonate System

The Geometry B reactor was used for the investigation except for one experiment which used Geometry A reactor. The experimental procedure is exactly the same as crystallization experiment described in Section (4.4.3.1) except the numbers of crystals at the end of the experiment was counted in the counting chamber under a microscope. In experiment PE21 samples were taken during the nucleation process and the crystals number counted. The experiments were conducted at different initial degrees of supersaturation and different stirring speeds. All the experiments were conducted at 25°C. The data of desupersaturation curve with respective to time of the bulk crystallization are given in Appendix A and C. The results are summarised and tabulated in Table (4-7).

4.5.2.3 Experiments on 1:1 Mg/Ca Molar Concentration

Samples were taken during the nucleation process for crystals count in experiment PE19 (see Figure (5-13)). The final crystals counts were carried out for all experiments. The results are

TABLE 4-7
Secondary Nucleation of Calcium Carbonate at 25°C

Expt. No.	ΔN (L^{-1})	$\Delta\theta$ (s)	$J=\dfrac{\Delta N}{\Delta\theta}$ $(s^{-1}L^{-1})$	Degree of Sup. S' †	$M_x \times 10^4$ (g/L)	Stirring speed (RPM)	ε (J/Ls)
PE5	1.59×10^8	1380	1.15×10^5	56.3	10	500	0.4778
PE7	1.25×10^8	1500	8.30×10^4	57.2	10	500	0.4778
PE11	1.67×10^6	12786	1.30×10^2	25.1	6	500	0.4778
PE14	2.17×10^7	3762	5.77×10^3	38.5	10	500	0.4778
PE16	850×10^8	738	1.15×10^6	74.9	21	500	0.4778
PE8	5.7×10^7	1542	3.73×10^4	56.3	10	400	0.2446
PE9	3.00×10^7	2598	1.15×10^4	56.3	10	400	0.2446
PE13	2.99×10^5	22020	1.36×10	25.1	6	400	0.2446
PE6	5.17×10^7	2290	2.26×10^4	62.0	10	300	0.1032
PE15	2.6×10^8	768	3.37×10^5	55.8	11	700	1.3108
PE4	2.9×10^8	1422	2.07×10^5	56.3	10	880	2.6044
PE21*	9.13×10^7	1284	7.10×10^4	50.8	11	220	0.3218

† Degree of Supersaturation at the commencement of steep decline

* Geometry A stirred reactor, the rest of the experiments were were conducted in Geometry B stirred reactor.

tabulated in Table (4-8).

4.5.3 Crystallization of Calcium Carbonate Precipitation

4.5.3.1 Bulk Crystallization of Pure Calcium Carbonate System

A series of experiments were completed on Geometry A reactor at 220 ± 5 r.p.m. stirring speed. This series of experiments also studied different degrees of initial supersaturation bulk crystallization at 25°C, 36°C , 44.0°C and 55.8°C. No microscopic count for the final crystal products to derive rate constant were made mainly because crystal products at 36.0°C and above contained aggregates of aragonite which made individual crystal counts impossible. The photographs of these aragonite aggregates are presented in Appendix B. The experiments carried out at 25°C crystallization was the first series of experiments for this project. The role of crystal number for rate constant interpretation was not realised during this series of experiments. As a result, no data are available for the crystal number at 25°C as well. The summary of the crystal habits and the crystallographic forms of calcium carbonate produced in this series of experiments are summarised in Table (4-9). Appendix B presents the various crystallographic forms of calcium carbonate observed under light microscope and scanning electron microscope.

Another series of experiments were conducted at 25°C for different stirring speeds over a range of different initial degrees of supersaturation. Both Geometry A and B were used for the experiments. Desupersaturation curve from each batch experiment are shown in Appendix C. The pH values were converted into degrees of supersaturation

TABLE 4-8

Secondary Nucleation of Calcium Carbonate in
1:1 Mg/Ca Molar Concentration System at 25°C

Expt No.	ΔN (L^{-1})	$\Delta\theta$ (s)	$J=\frac{\Delta N}{\Delta\theta}$ $(s^{-1}L^{-1})$	log J	Degree of Sup. S'	$M_x \times 10^4$ (g/L)	Stirring Speed (r.p.m.)	(J/L s) (J/L s)
PE17	5.50×10^7	-	-	-	-	-	500	0.48
PE18	1.89×10^7	3382	5588	3.75	23.74	-	700	1.31
PE19	2.40×10^7	-	-	-	-	-	400	0.24

TABLE 4-9
Bulk Crystallization of Calcium Carbonate at Various
Temperatures at 220 r.p.m. (0.3218 J/Ls) Stirring Speed in Geometry A

Expt. No.	Temperature (°C)	Initial Degree of Supersaturation, S	Crystal Habit
E21	25.0	50.2	acicular aragonite entity[*]
E22	25.0	62.0	acicular aragonite entity
E23	25.0	72.4	acicular aragonite entity
E24	25.0	76.4	100% calcite rhombs
E26	25.0	78.9	100% calcite rhombs
E27	25.0	81.5	100% calcite rhombs
E28	36.0	77.5	mixture of calcite rhombs and
E29	36.0	54.8	acicular aragonite aggregates
E30	36.0	45.9	
E32	44.0	49.4	mainly acicular aragonite
E33	44.0	48.3	aggregates with some calcite
E34	44.0	37.2	rhombs
E35	55.8	35.4	100% acicular aragonite
E36	55.8	34.3	aggregates

[*] Acicular aragonite entity observed, probably due
to the continuing growth of centre aragonite aggregate
toward the calcium carbonate rich surrounding.
(See Plate B9 of Appendix B).

as well as the content of calcium with respective to time by the pro-
gramme PROG-CS. The data and results are available in Appendix A and
C. The final crystal number was counted in the counting chamber under
the microscope. The final crystals of some experiments were sized by
Micro-videomat 2 and the results are given Appendix D. The overall
growth rate constant was calculated for each batch experiment accord-
ing to Sections (4.3.4) and (4.3.5). The results are summarised in
Tables (4-10) and (4-11). The values of $dT_{Ca}/d\theta$ can be obtained from
the desupersaturation curve of T_{Ca} against time. A best straight line
can be drawn through the plot of $dT_{Ca}/d\theta/(T_{Ca_{in}}-T_{Ca})^{2/3}$ against
$\{[Ca^{2+}]^{1/2}[CO_3^{2-}]^{1/2}-(K_{sp}/f_d^2)^{1/2}\}^2$ for the overall growth rate constant
determined by simplified method and $dT_{Ca}/d\theta/A$ against
$\{[Ca^{2+}]^{1/2}[CO_3^{2-}]^{1/2}-(K_{sp}/f_d^2)^{1/2}\}^2$ for the overall growth rate constant
determined by surface area calculated based on size distribution. The
plots for all the experiments are shown in Appendix C. The gradient
of the former is therefore equal to $k'N^{1/3}$. The overall growth rate
constant k for bulk crystallization can be calculated from Equation
(4-111). The gradient of the latter is therefore equal to k'' and the
overall growth rate constant k can be calculated from Equation (4-48).
Some of the photomicrographs of the crystal samples are available in
Appendix B. All the three crystallographic forms of calcium car-
bonate, namely calcite, aragonite and vaterite were observed. The
calcite is in rhomohedral crystal habit. The aragonite is an aggre-
gate of acicular crystals. The vaterite appears in the form of spher-
ical crystals. The aragonite crystals were also observed in the
unique crystal habit which probably was the result of the continuing
growth of the bundle of acicular aragonite crystals. A typical ara-
gonite entity is shown in Plate 9 of Appendix B.

TABLE 4-10   Bulk Crystallization of Calcium Carbonate at 25°C at Various Stirring Speeds (Simplified)

Expt No.	Stirring Speed r.p.m.	Initial Degree of Super-satur'n S	Final Number of Crystals (L^{-1})	f_d	Gradient $k'N^{1/3}$ $\times 10^4$	Overall Growth Rate Const $k \times 10^{-3}$ $(\frac{L^2}{mole\,min\,m^2})$	Crystal Habit
			GEOMETRY A				
PE21	220	51.6	9.13×10^7	0.58	2.0180	24.96	mainly spherical vaterite with some calcite rhombs & polyhedral calcite
PE20	220	22.6	7.23×10^5	-	-	-	100% calcite rhombs
			GEOMETRY B				
PE13	400	25.6	2.78×10^5	-	-	-	100% calcite rhombs
PE11	500	25.6	1.67×10^6	0.65	0.3478	10.47	100% calcite rhombs
PE12	880	25.6	2.09×10^4	-	-	-	100% calcite rhombs
PE14	500	39.3	2.17×10^7	0.62	0.6667	10.40	mixture of calcite rhombs & spherical vaterites
PE6	300	62.8	5.17×10^7	0.60	1.038	11.69	mixture of calcite & hybrid
PE8	400	57.0	5.77×10^7	0.60	1.587	21.38	spherical vaterite with calcite rhombs
PE9	400	57.0	3.00×10^7	0.59	0.8909	12.44	mainly calcite rhombs with few vaterite
PE5	500	57.0	1.58×10^8	0.60	2.0150	19.40	mainly spherical vaterite with some calcite (much less than 400 r.p.m. expt
PE7	500	58.0	1.25×10^8	0.60	1.9565	20.39	
PE15	700	56.7	2.60×10^8	0.60	2.2721	18.53	
PE4	880	57.0	2.94×10^8	0.60	2.9270	22.84	almost 100% spherical vaterite
PE16	500	76.5	8.50×10^8	0.60	2.3090	12.70	mainly vaterite with some calcite - agglomorates evident, linked by spherical vaterite

TABLE 4-11
Bulk Crystallization of Calcium Carbonate at 25°C
at Various Stirring Speed (Size Consideration)

Expt. No.	Stirring Speed (r.p.m.)	Initial Degree of Sup.	f_d	gradient k'' $\left(\dfrac{L^2}{mole\text{-}min.cm^2}\right)$	Overall growth rate $k_w \times 10^{-3}$ $\left(\dfrac{L^2}{mole\ min\ m^2}\right)$ *	constant Habit
		S				
geometry A						
E22	220	62.0	0.58	1.168	34.7	calcite rhombs and
E23	220	72.4	0.61	1.275	34.3	acicular aragonite entity
E24	220	76.4	0.61	0.938	25.2	100% calcite rhombs
geometry B						
PE4	880	57.0	0.60	1.45	40.2	Almost 100% spherical vaterite
PE7	500	57.0	0.60	1.32	36.7	Almost 100% spherical vaterite
PE8	400	57.0	0.6	1.017	28.3	Spherical vaterite with some calcite
PE9	400	57.0	0.60	0.6033	17.3	Mainly calcite rhombs with few vaterite
PE11	500	25.6	0.65	0.725	17.2	100% calcite rhombs
PE15	700	56.7	0.60	2.02	56.1	mainly vaterite with some calcite

* $k_w = \dfrac{k'' \times 10^4}{f_d^2}$

4.5.3.2 <u>Bulk</u> <u>Crystallization</u> <u>of</u> <u>Calcium</u> <u>Carbonate</u> <u>in</u> <u>1:1</u> <u>Mg/Ca</u> <u>Molar</u>

<u>Concentration</u>

Some experiments were also conducted in Geometry B stirred reactor to study the effect of stirring speed (power input) to bulk crystallization of calcium carbonate with the presence of magnesium. The results are shown in Table (4-12).

TABLE 4-12

Bulk Crystallization of Calcium Carbonate at 25°C
in the presence of 1:1 Mg/Ca molar Concentration
Solution at Different Stirring Speed

Expt. No.	Stirring Speed (RPM)	Initial Degree of Supersatn. S	Final Number of Crystal (L^{-1})	f_d	Gradient $k N^{\frac{1}{3}}$ $\times 10^{-4}$	Crystal Habit
PE17	500	23.38	5.50×10^7	0.57	-	Mainly Aragonite aggregates with some polyhedral calcite
PE18	700	24.10	1.89×10^7	0.57	1.0667	100% polyhedral calcite
PE19	400	22.40	2.4×10^7	0.57	-	Almost 100% aragonite aggregates with few polyhedral and rhombohedral calcite. Growth of ancicular Aragonite on polyhedral calcite is evident

CHAPTER 5

DISCUSSION OF CALCIUM CARBONATE PRECIPITATION STUDIES

5.1 NUCLEATION OF CALCIUM CARBONATE

5.1.1 General

The study of nucleation of calcium carbonate has adopted the approach of induction period. Induction period can be related to the classical nucleation period to calculate other importat information such as interfacial energy, critical nucleus size and 'order' of nucleation.

5.1.2 Visual Induction Period Data

In Figure (5-1), the induction periods measured from experiments conducted under constant and different speed of mixing are readily grouped into two regions. The boundary of these two regions is indicated by $(\log S)^{-2} T^{-3}$ at 1.23×10^{-8} °K. For $(\log S)^{-2} T^{-3} > 1.23 \times 10^{-8}$, line B can be constructed. Line B passes through points obtained from experiments at 200 r.p.m. stirring speed that produced mixture of calcite and aragonite (Section (4.5.3.1)). This region clearly shows the effect of heterogeneous nucleation which reduces the induction period and is expected at lower initial degrees of supersaturation. Particles of diameter less than 1 μm cannot be observed easily in an intense beam of light. Hence for low particle concentrations it is very difficult to observe the nucleus sized particles. The problems

FIGURE 5-1   The Plot of LOG Induction Period Against $(LOG\ S)^{-2}T^{-3}$
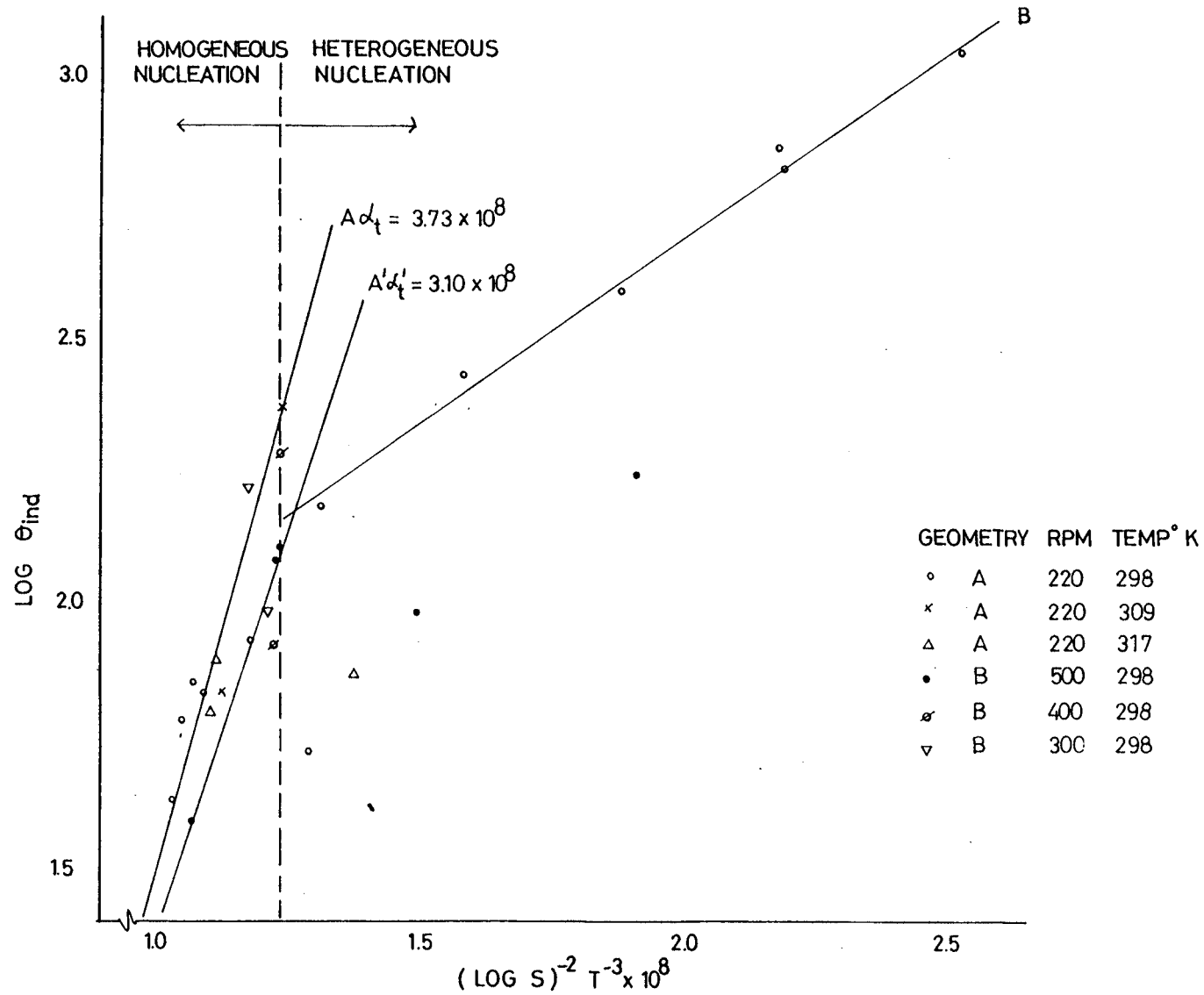
are compunded by the presence of heteronuclei in solutions of lower degrees of supersaturation. Hence data on heterogeneous nucleation are considered to be less reliable and subject to greater error than for other experimental conditions. The effect of stirring speed (power input) is not certain especially because heteronuclei have a strong influence in this region. However, lines A and A' have a steeper gradient than lines B and B'. These points were obtained from stirred reactor experiments with higher degrees of supersaturation. The gradient of the straight line is the result of homogeneous nucleation of calcium carbonate.

Söhnel and Mullin (1982) used Nielsen's (1967, 1969) approach to assume homogeneous nucleation, followed by diffusional growth of the created nuclei. The induction period of precipitation may be considered to obey the Equations (4-3) and (4-4) (Section (4.1.2)). The derivation of these equations was given in the papers published by Nielsen (1964, 1967, 1969, 1971). The diffusional growth of the created nuclei to the size that is either visible or causes changes of a measurable property is considered a valid assumption. Crystals less than 10 μm have relatively slow velocity through the solution in a normal gravity field or at normal stirring rates, ie. for submicroscopic crystal growth, convection can be neglected (Nielsen, 1964; Konak, 1971). In some experiments, samples of solution at the initial stage of crystallization were observed under the microscope and the nuclei (closely resembling a spherical shape) were as small as 1 μm. It is well known that bacteria (which are approximately 1 μm in size) in large populations can be detected visually as turbidity in solution. Therefore, the induction period measured by visual observation is an indication of the presence of nuclei (miniature crystals) of at

least 1 μm size but the nuclei are still small enough to be considered due to diffusion controlled growth. The characteristic time or time scale (θ_1) is expressed in the following equation (Nielsen and Söhnel, 1971):

$$\alpha_1 = \frac{c_{in} - c'}{c_{in} - c_s} = \frac{16\pi\sqrt{2}}{15} JD^{2/3} [V_m(c_{in} - c_s)]^{1/2} \theta_1^{5/2} \tag{5-1}$$

where α_1 is some arbitrary constant characteristic of the degree of precipitation when diffusion-controlled growth is still valid

c' is an arbitrary concentration to establish a characteristic constant

c_{in} is the initial concentration

When c_{in} is increased, θ_{ind} decreases so θ_1 decreases to reach α_1 when homogeneous nucleation predominates. θ_{ind} is a significant measure of the time required for nuclei to grow to 1 μm size. Therefore, θ_1 is proportional to the induction period within the range of the diffusion controlled growth mechanism. From Equation (5-1),

$$\theta_1 = [\frac{15\theta_1}{16\pi\sqrt{2}JD^{3/2}[V_m(c_{in} - c_s)]^{1/2}}]^{2/5} \tag{5-2}$$

Inserting $\qquad J = \frac{2D}{d_m^5} \exp(-\Delta G^*/KT) \qquad$ (Nielsen, 1964)

and $\qquad \Delta G^* = \beta' \sigma^3 V_m^2/(KT \ln S)^2$

where D is the diffusion coefficient

d_m is the molecular diameter

Taking logarithm and rearrange Equation (5-2)

$$\ln\theta_1 = \ln\left[\frac{15\alpha_1 d_m^5}{16\pi\sqrt{2}D^{5/2}V_m^{1/2}(c_{in} - c_s)^{1/2}}\right]^{2/5} + \frac{2\beta'\sigma^3 V_m^2}{5(KT)^3(\ln S)^2} \quad (5-3)$$

Since θ_1 is proportional to θ_{ind} which is measured experimentally, tanking $\theta_1 = \theta_{ind}$,

$$\log \theta_{ind} = \text{const.} + \alpha_t/(\log S)^2 \quad (5-4)$$

where

$$\alpha_t = \frac{2\beta'\sigma^3 V_m^2}{5(KT\ln 10)^3} \quad (5-5)$$

Therefore, the plot of $\log\theta_{ind}$ against $(\log S)^{-2}$ and $(\log S)^{-2}T^{-3}$ (in the case of data available from more than one temperature) enables the calculation of interfacial energy from the gradient of the plot. Figure (5-1) gives the value $\alpha_t = 3.73\times10^8$ for homogeous nucleation of calcium carbonate. The straight line passes through data obtained from calcite nucleation at 25°C and the mixtures of calcite and aragonite from 36°C and 44°C. The value $\alpha_t' = 3.10\times10^8$ is obtained from line A' which passes through data obtained from vaterite nucleation at 25^0 C. Substituting the following values for calcite:
$\beta = 32$ (cube), $V_m = 3.067\times10^{-23}$ cm^3 and $K = 1.3805\times10^{-23}$ J°K^{-1},

$$\sigma^3 = \frac{5K^3(\ln 10)^3\alpha_t}{2\beta V_m^2} = 9.95\times10^{-16} \ (J/cm^2)^3$$

$$\sigma = 101 \ mJ/m^2$$

The value of $\beta' = \dfrac{16\pi}{3}$ (sphere) for vaterite,

$$\sigma^3 = \frac{5K^3 (\ln 10)^3 \alpha'_t}{2\beta' v_m^2} = 1.58 \times 10^{-15} \ (J/cm^2)^3$$

$$\sigma = 118 \ mJ/m^2$$

The value of calcite interfacial energy is similar to values reported by other workers (Nielsen and Söhnel, 1971; Söhnel and Mullin, 1978; Kharin et. al., 1980; Söhnel and Mullin, 1982). Although vaterite was found to possess a slightly higher interfacial energy than calcite, the lower α'_t (therefore a smaller free energy required for nucleation) indicates an overall faster nucleation rate than calcite.

The empirical relationship (see Equation (4-49)):

$$J = K_n (c - c_m)^n = K_n \Delta c^n \qquad\qquad (5-6)$$

based on the concept of metastable region (Miers and Isaac, 1906) has frequently been used.

where K_n is the nucleation rate constant

c is the solute concentration

c_m is a concentration greater than the saturated concentration

below which nucleation does not occur.

In inorganic salt system, c_m also can be replaced by the saturated concentration c_s without affecting significantly the empirical relationship (Randolph and Larson, 1971). Therefore by defining σ' as the

supersaturation:

$$\sigma' = S - 1 = \Delta c / c_s \qquad (5\text{-}7)$$

From Equations (4-54) and (4-55)

$$\theta_{ind} = K' K_n^{-1} (\sigma' c_s)^{-n} \qquad (5\text{-}8)$$

Taking logarithm:

$$\log \theta_{ind} = \log (K' / K_n c_s^n) - n\log \sigma' \qquad (5\text{-}9)$$

Therefore the plot of $\log \theta_{ind}$ against $\log \sigma'$ will result in a straight line with the gradient n, which is the 'order' of nucleaton. In Figure (5-2), the data from the experiments at 220 r.p.m. using Geometry A were plotted. The order of homogeneous nucleation was found to be equal to 8. In Figure (5-3), the plot of nucleation rate in terms of $1/\theta_{ind}$ against initial degree of supersaturation indicates that the metastable limit degree of supersaturation, below which $\frac{1}{\theta_{ind}} \to \infty$, ie. nucleation does not take place, is approximately 10.

5.1.3 Latent Period Data

Latent period is measured by the time required for the first measurable decline in the pH value from the maximum pH value after mixing. The pH value achieved a steady number instantaneously at degrees of supersaturation which cause homogeneous nucleation. For the degree of supersaturation apparently in the region of heterogene-ous nucleation, it takes a finite time (few minutes) to achieve

FIGURE 5-2   The Plot of LOG θ_{ind} Against LOG σ Using Data
from Geometry A, 220 r.p.m. Experiments at 25°C

HETEROGENEOUS
NUCLEATION

HOMOGENEOUS
NUCLEATION

n = 8

LOG θ_{ind}

LOG σ
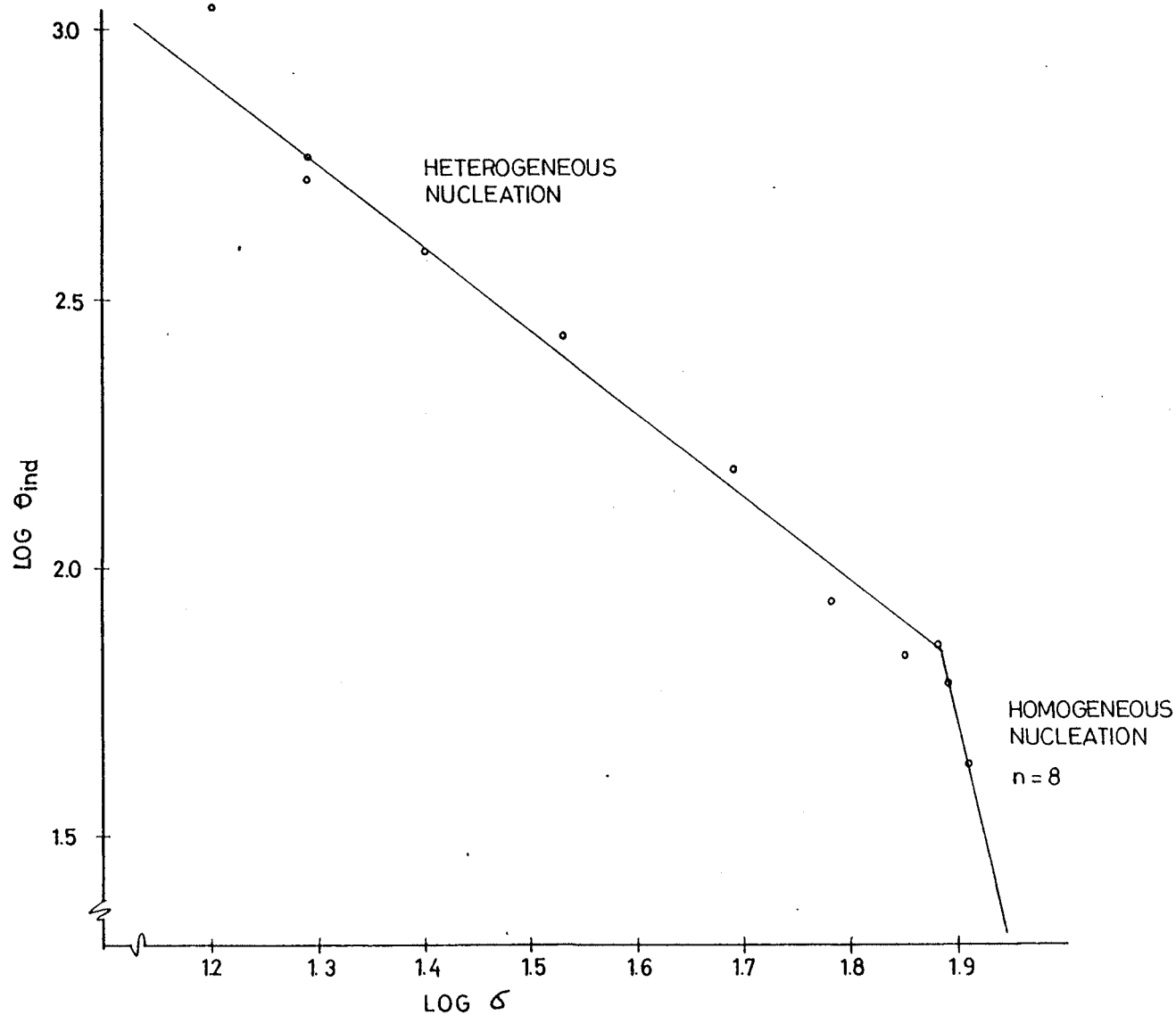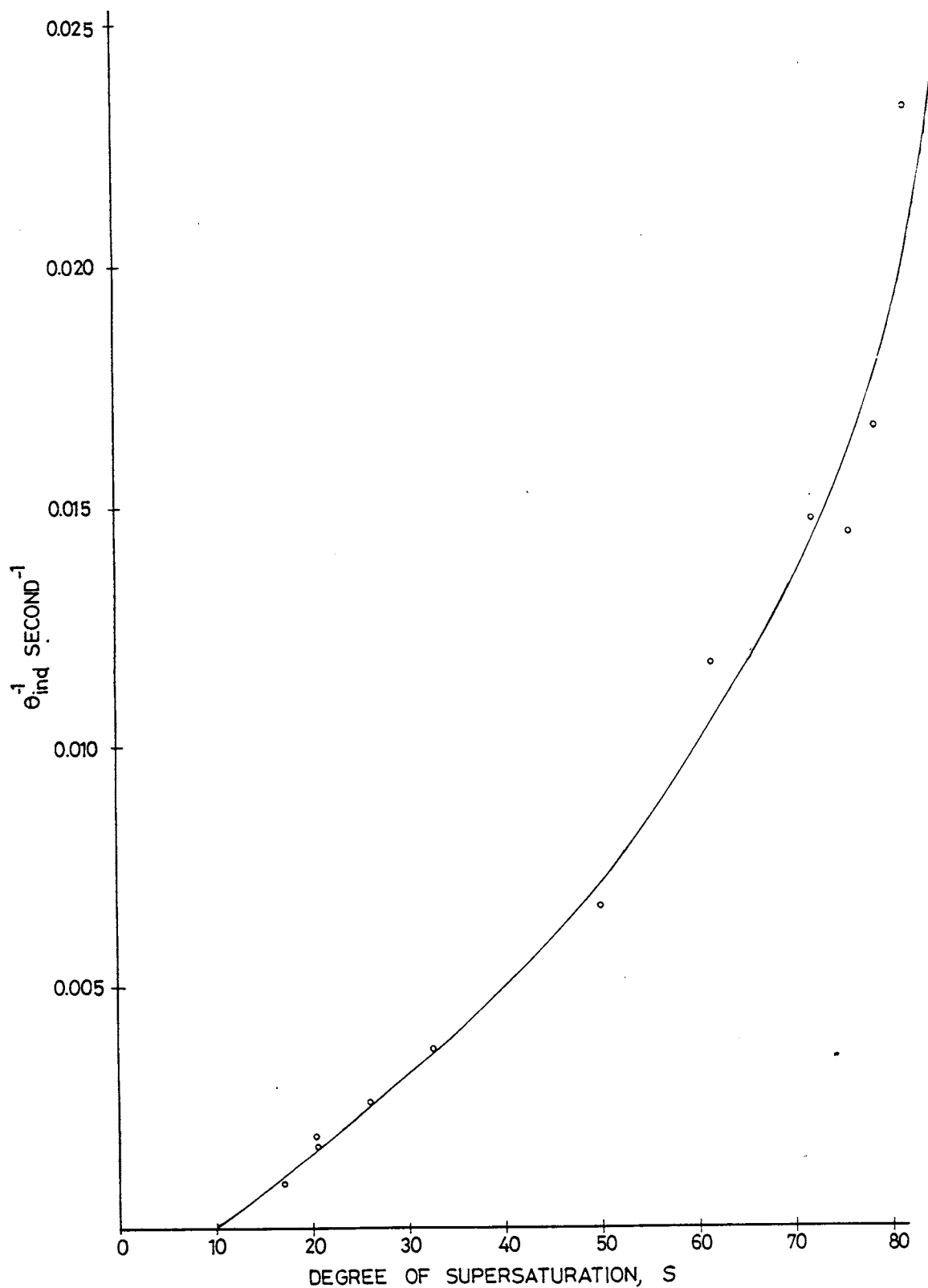
FIGURE 5-3   The Plot of Reciprocal of Induction Period Against
            Degree of Supersaturation using Data from Geometry
            A, 220 r.p.m. Experiments at 25°C

constant pH because of the relatively slow rate equilibration of car-
bon dioxide between the gaseous phase and the solution. Therefore,
significant errors are to be expected in θ_{ind} and θ_{lat} for heterogene-
ous processes, as such no attempt was made to interprete heterogeneous
nucleation data.

Using the approach of classical homogeneous nucleation theory
combined with diffusion control growth of the nuclei created, nuclei
growth continue to deplete the solute available until the decline of
solute concentration reaches the pH which can be detected by the pH
meter and registers a finite decline of 0.01 pH unit. Again usng
Equation (5-1)

$$\alpha_1 = \frac{c_{in} - c'}{c_{in} - c_s} = \frac{16\pi\sqrt{2}}{15} J D^{3/2} [V_m(c_{in} - c_s)]^{1/2} \theta_1^{5/2} \qquad (5-10)$$

In the present cases, c' is the solute concentration that causes a
drop of 0.01 pH unit from the initial pH. θ_1 is the time taken, which
is the latent period, θ_{lat}. From Equation (5-10),

$$\frac{c_{in} - c'}{c_{in} - c_s} = 1 - \frac{c'}{c_{in}} \qquad \text{for } c_{in} \gg c_s$$

when c_{in} increases, c' also increases, therefore $1 - \frac{c'}{c_{in}}$ is approxi-
mately a constant, ie α_1 is constant.
Again from Equation (5-10),

$$\theta_1 = \theta_{lat} = [\frac{15\alpha_1}{16\pi\sqrt{2}JD^{3/2}[V_m(c_{in} - c_s)]^{1/2}}]^{2/5} \tag{5-11}$$

Inserting the classical homogeneous nucleation equation for J, taking logarithm and rearranging, Equation (5-11) becomes

$$\log \theta_{lat} = const. + \phi_t/(\log S)^2 \tag{5-12}$$

where

$$\phi_t = \frac{2\beta'\sigma^3 v_m^2}{5(KT\ln 10)^3} \tag{5-13}$$

From Figure (5-4), α_t value is obtained from the straight line plot of $\log \theta_{lat}$ against $(\log S)^{-2}$, indicated by line A for calcite.

$$\phi_t = 18.33$$

$$\sigma^3 = \frac{5(KT\ln 10)^3 \alpha_t'}{2\beta' v_m^2} = 1.29 \times 10^{-s15} \ (J/cm^2)^3$$

$$\text{therefore } \sigma = 110 \ mJ/m^2$$

Again this value compares well with the value obtained by the induction period method as well as values reported in the literature. In fact, since the latent period measurement is more reliable than visual measurement for the induction period, the latter is subjective and less reproducible. The value of interfacial energy $\sigma = 110 \ mJ/m^2$ determined from the latent period data is the more reliable figure. In the light of all these values and because the latent period

FIGURE 5-4   The Plot of LOG θ_{lat} Against $(LOG\ S)^{-2}$ using Data from the Homogeneous Nucleation Region at 25°C
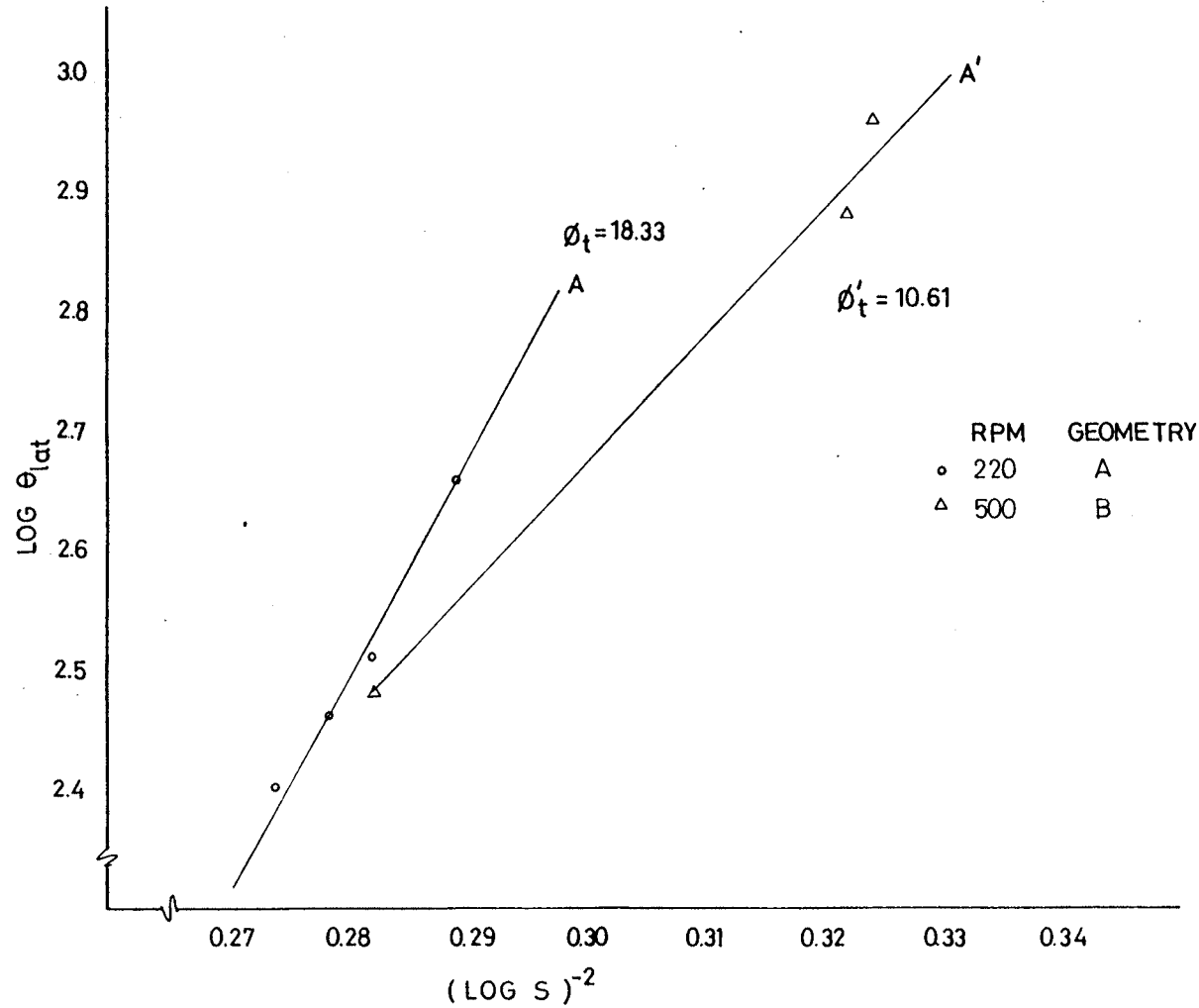
measurement is an additional piece of information obtained from crystallization experiments, it seems that there is no need to conduct induction period measurement by separate sophisticated methods (Section (4.2.1.3)).

Similarly, line A' gives a gradient

$$\phi'_t = 10.61 \text{ for the vaterite}$$

$$\sigma^3 = \frac{5(KT\ln 10)^3 \phi'_t}{2\beta' V_m'^2} = 1.43 \times 10^{-15} \ (J/cm^2)^3$$

therefore $\sigma = 114 \ mJ/m^2$

Again the value obtained is similar to the value obtained by the induction period method.

The results of experiments to determine the effects of stirring on both the induction period and the latent period of calcium carbonate crystallizaton under constant initial degree of spersaturation are plotted in Figures (5-5) and (5-6). It is difficult to be certain whether there is a definite decline of induction and latent period from 300 r.p.m. to 500 r.p.m., but 700 r.p.m. represents the minimum θ_{ind} and θ_{lat} before the values increase at 880 r.p.m. The effect of stirring has been reported by Mullin and Raven (1961), subsequently Roques and Girou (1974) reported that the critical supersaturation for nucleation decreases as the stirring speed increases, but beyond certain mixing speed, critical supersaturation actually increases.

The results of magnesium experiments are shown in Figure (5-7). The sharp decline of the induction period from 400 r.p.m. to 500 r.p.m. seems to suggest a significant effect of magnesium which

FIGURE 5-5   The Plot of Induction Period Against Power
             Input for S = 57 - 63 at 25°C
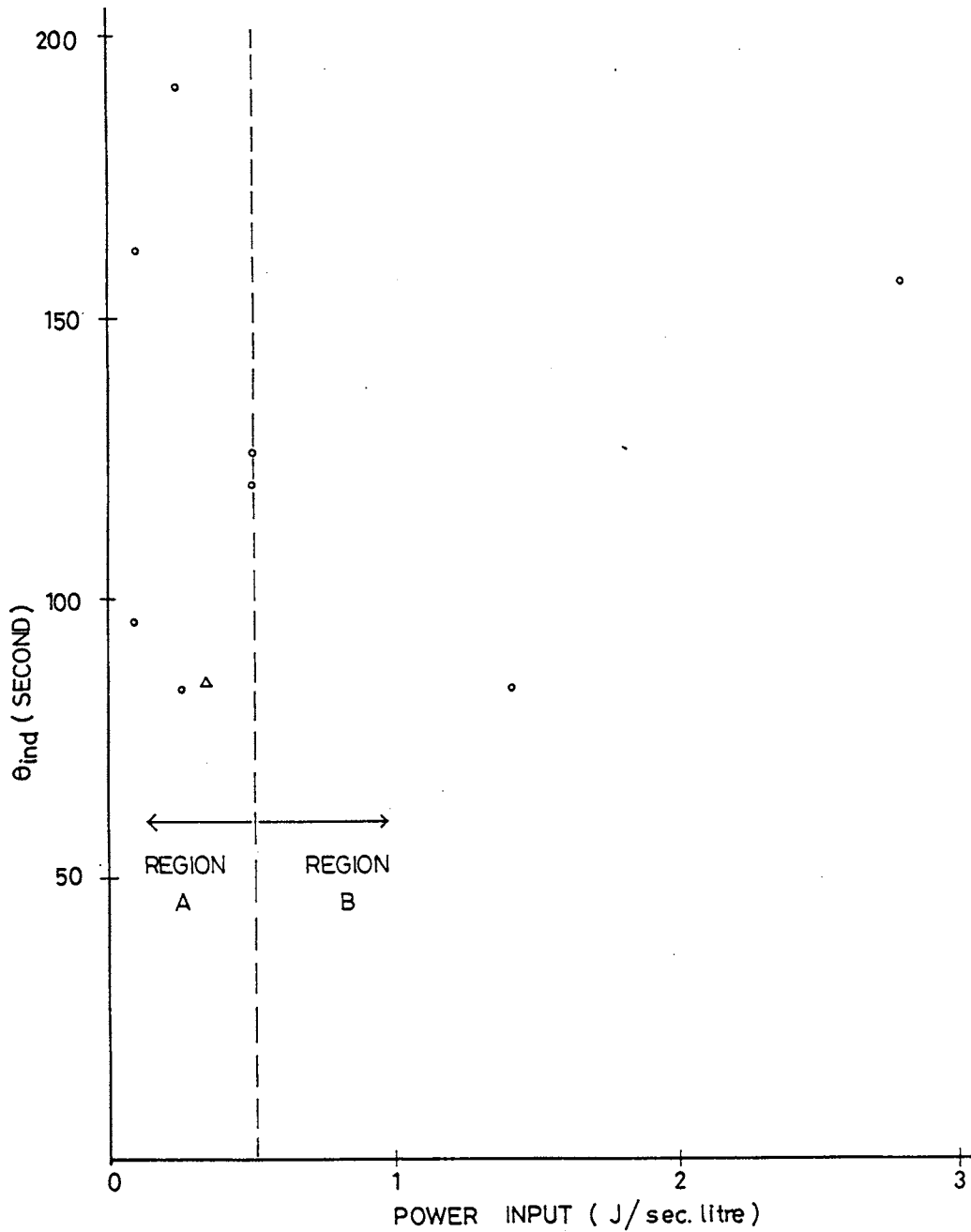
REGION A : MIXTURE OF CALCITE/ARAGONITE ENTITY AND
           CALCITE/VATERITE IN VARIOUS PROPORTION

REGION B : VATERITE PREDOMINANT WITH SOME CALCITE

    △   220 RPM OF GEOMETRY A

    ○   GEOMETRY B

FIGURE 5-6   The Plot of Latent Period Against Power
             Input for S = 57 - 63 at 25°C

REGION A : MIXTURE OF CALCITE/ARAGONITE ENTITY AND
           CALCITE/VATERITE IN VARIOUS PROPORTION

REGION B : VATERITE PREDOMINANT WITH SOME CALCITE

  △   220 RPM OF GEOMETRY A

  o   GEOMETRY B

decreases the rate of formation calcium carbonate nuclei. The physical significance will be discussed in detail in the section on secondary nucleation (Section (5.1.6)). A very similar pattern was observed for the determination of the latent period (Figure (5-8)).

5.1.4 An Explanaton for the Formation of Different Crystallographic Forms of Calcium Carbonate

A mechanism is proposed in order to explain the observation on nucleation and crystallization in the stirred reactor crystallization experiments. The following are the bases of this proposed mechanism:

1. Calcite is thermodynamically more stable than aragonite and vaterite (Wray and Daniels, 1957).

2. Vaterite nucleates fastest among these three crystallographic forms since vaterite nucleates faster than calcite as indicated by the induction experiment (Section (5.1.1)). Aragonite has the slowest nucleation rate. The induction period of aragonite is longer than calcite as reported by Möller and Rajagopalan (1975).

3. According to a statistical thermodynamic basis the macroscopic view of energy of the fluid system at constant temperature and pressure is constant. However, the microscopic view presents the fluctuations of energy level about the constant mean value. Thus means there is a statistical distribution of energy, or molecular velocity, in the molecules constituting to the system. Supersaturation represents this energy level. Therefore, there is a fluctuation of supersaturation about the constant mean supersaturation.

4. All of the three crystallographic forms of calcium carbonate can
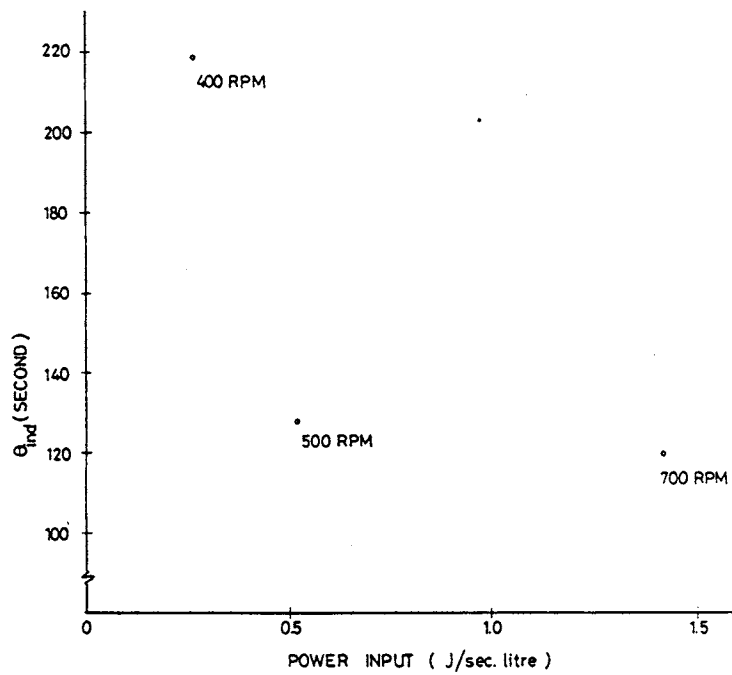
FIGURE 5-7   The Plot of Induction Period Against Power Input
            for 1:1 Mg/Ca System (S = 24) at 25°C
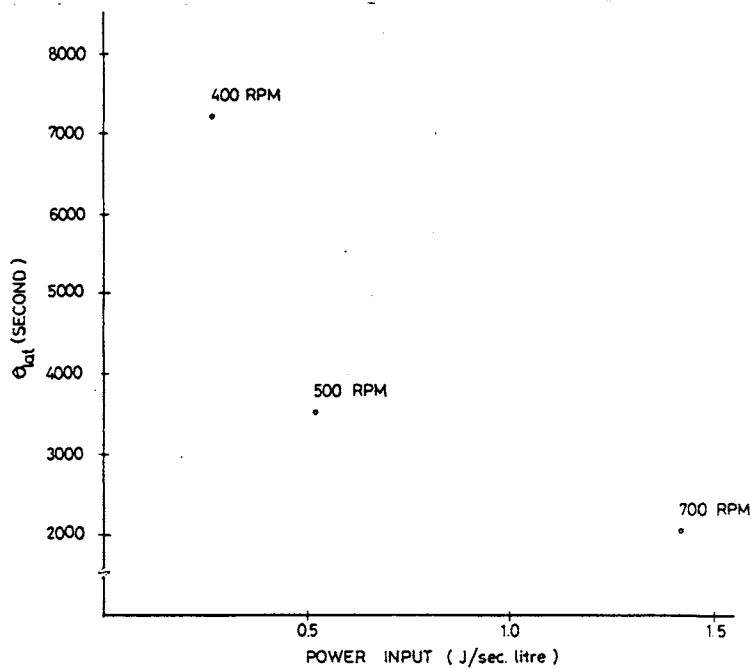
FIGURE 5-8   The Plot of Latent Period Against Power Input
            for 1:1 Mg/Ca System (S = 24) at 25°C

exist at the subcritical nucleus state, ie. molecular cluster or embryo as proposed by Roques and Girou (1974).

It is clear that from the stirred reactor experiments, irrespective of the degree of the degree of stirring, calcite will be formed at low initial degrees of supersaturation (see Tables (4-9) and (4-10)). This fact was reported by Brooks et. al. (1950) that slow precipitation rate favours the formation of calcite , whereas the more rapid the precipitation rate, the greater the tendency to form metastable states. The higher the inital degree of supersaturation, the faster the precipitation rate. From the experiments, this degree of supersaturation within the range of power input from 0.10 to 2.60 J/L s might be 25 beyond which metastable forms will form. From the proposed basis, the transient fluctuation of energy level represented by degrees of supersauration at 25 and below does not provide sufficient energy required for the formation of metastable crystallographic forms of calcium carbonate.

When the effect of stirring was singled out from the experiments conducted, there is a change of crystallographic form from mixtures of calcite and acicular aragonite entity at 300 r.p.m. to vaterite predominating at 700 r.p.m. and beyond at the degree of supersaturation of 57 (Figures (5-5) and (5-6)). 400 r.p.m. - 500 r.p.m. is the range of the transitional stirring speed (power input) where mixtures of calcite and aragonite entity and mixtures of calcite and vaterite in different proportions were observed. In accordance with the proposed basis, at S = 57.0 - 63.0, supersaturation is considered high. Therefore, the fluctuations of energy are more pronounced. Additionally vaterite has the fastest nucleation rate. Therefore if any

embryo can survive in competition with calcite, vaterite has the greatest probability. In deed this is the case. As the stirring speed increases, the mechanical stirring is also introducing the additional transient increase of energy in the form of heat to the already present transient increase of energy due to supersaturation. At 300 r.p.m. the advantage of the faster nucleation rate possessed by the vaterite is still insignificant. However, within the range of 400 r.p.m. to 500 r.p.m. of Geometry B which also includes 220 r.p.m. of Geometry A, the competition of all three crystallographic forms of calcium carbonate is evident. The resulting crystal products varied from batch to batch with different proportion of calcite/aragonite or calcite/vaterite under similar stirring condition and initial degree of supersauration. However when the stirring speed was increased beyond 500 r.p.m. the excess transient increase in energy due to stir-ring apparently supply the higher energy required by the formation of metastable vaterite. Although calcite is thermodynamically more stable then vaterite, this is off set by the faster nucleation rate of vaterite. The overall result is therefore a majority of vaterite rather than calcite beyond 500 r.p.m. From these experiments, it also shows that aragonite is thermodynamically more stable than vaterite at room temperature and moderate stirring speeds. This is the reason of the relativey scarce deposit of vaterite in nature compared to calcite and aragonite.

5.1.5 Secondary Nucleation of Pure Calcium Carbonate System

The final crystal numbers were plotted against stirring speed at approximately constant initial degrees of supersauration ($S = 57 - 63$) (see Figure (5-9a)). It is clear that the number of crystals

FIGURE 5-9a The Final Number of Crystals per Litre at
Different Stirring Speed at 25°C (S = 57 -63)
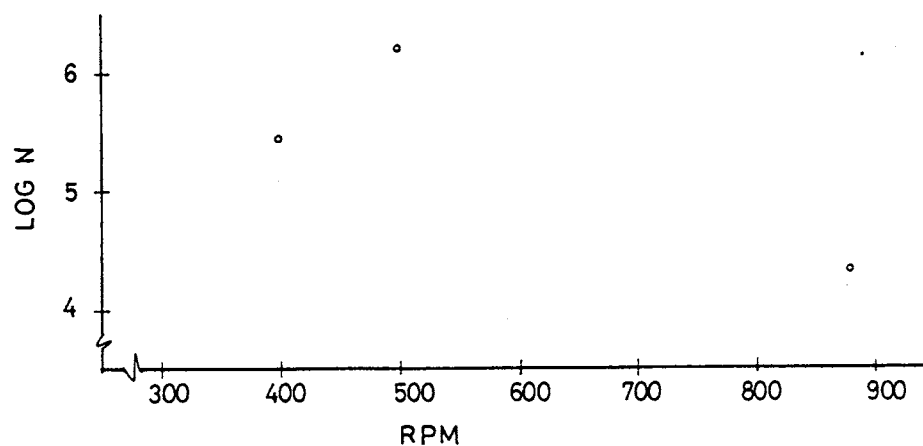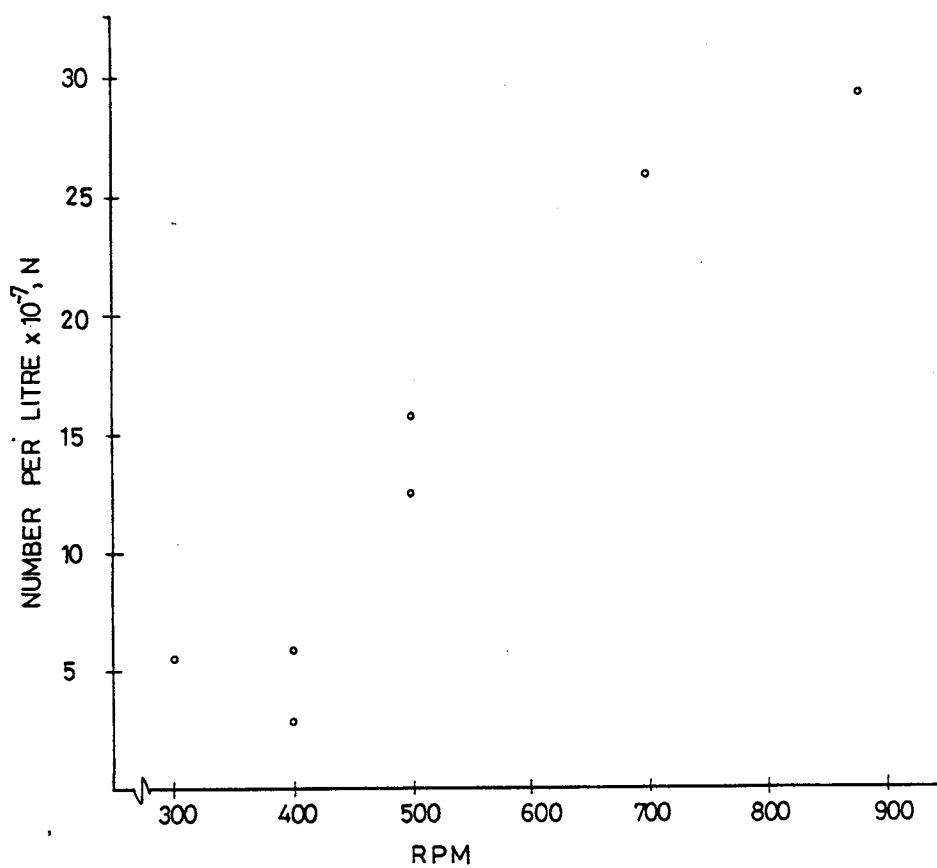
FIGURE 5-9b The Final Number of Crystals per Litre at
Different Stirring Speed at 25°C (S = 25.6)

increases rapidly with stirring speed from 400 r.p.m. to 700 r.p.m. and then gradually levels off beyond 700 r.p.m.. Apparently, stirring speed has an effect on the number of crystals generated in a batch stirred reactor experiments. This also implies that the number of nuclei generated is affected by the stirring speed, an indication of the presence of secondary nucleation. At 880 r.p.m., the number of crystals increases only sightly. If nuclei are formed from stable clusters of molecules, the stability of molecular clusters (embryos) can be jeopardised by vigorous stirring which breaks down the molecular clusters. Therefore, the number of crystals at 880 r.p.m. is only sightly greater than that observed at 700 r.p.m. The effect will be more significant at low degrees of supersaturation where nuclei are already less stable compared to medium and high degrees of supersaturation. To examine this effect, experiments were also conducted at low degrees of supersaturation (S = 25.6) over a range of stirring speeds. The effect is much more pronounced than expected. The number of crystals increases by an order of magnitude from 400 to 500 r.p.m. and decreases by order of magnitude at 880 r.p.m. (Figure (5-9b)).

In experiment PE21, crystallization of calcium carbonate was conducted in Geometry A stirred reactor at 220 r.p.m.. Samples were taken to count the number of crystals (nuclei) during the course of crystallization. The results are shown in Figure (5-10). Crystal number increases linearly and is approximately constant beyond 25 minutes. Emergence of new spherical nuclei approximately 1 - 2 μm in size were observed under the microscope. The birth of new nuclei appears to stop beyond 25 minutes and the process continues with crystal growth predominating. This indicates insignificant secondary nucleation as compared to crystal growth. The final crystal number is

FIGURE 5-10   The Number of Crystals Counted with respect
to Time for Experiment PE21 (220 r.p.m.,
Geometry A)
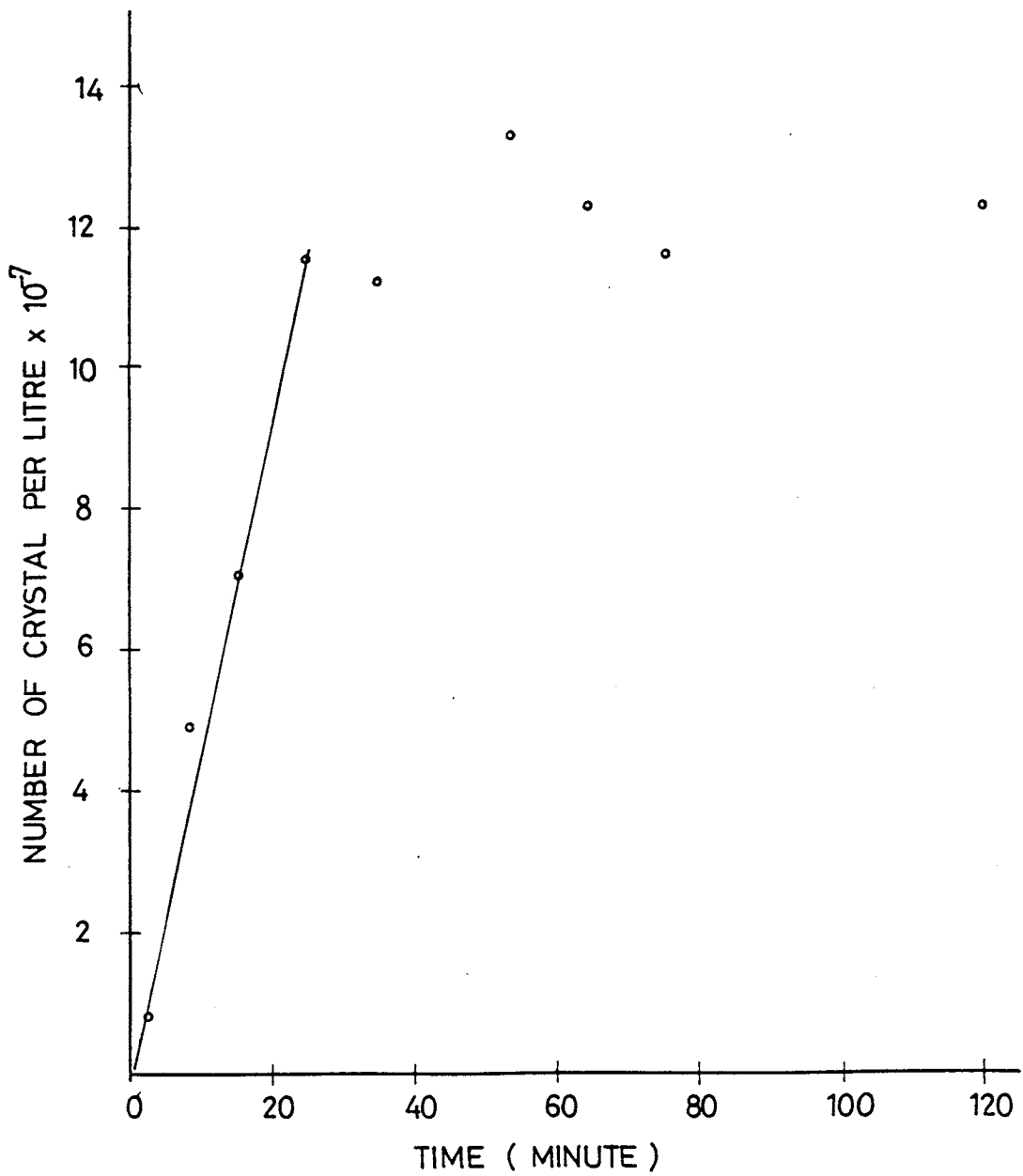
approximately 76% of the crystal number at the end of the nucleation
process. This implies that ageing (ripening) takes place during the
final stage of the batch crystallization process. The final crystal
number is 9.13×10^7 per liter as compared to 1.23×10^8 per litre counted
during crystallization. The nucleation rate is therefore approxi-
mately 30% higher compared to that calculated from the final crystal
number as defined in Section (4.3.4). This may be the case for all
the rest of the experiments on crystallization. However, not all
nuclei generated by secondary nucleation are able to survive to grow
into big crystals (Section (2.2.3)). Small nuclei seem to grow very
slowly or not at all. As a result their presence during the course of
crystallization should only incur a minimum error on growh rate con-
stant based on final crystal numbers. These nuclei are most likely to
be incorporated into big crystals via ageing process and render a
smaller crystal population at the end of the process. Therefore, the
effect of ageing can be considered tolerable when the final crystal
number is used in nucleation rate calculations and crystallization
rate calculations. From this experiment, the nucleation rate appears
to be a constant. By plotting nucleation rate $(\frac{\Delta N}{\Delta \theta})$ as defined in Sec-
tion (4.5.2.1)) for the same degree of initial supersaturation against
stirring speed expressed in power input per unit volume, a linear
relationship can be established (Figure (5-11)). Since the final cry-
stal number also increases with the power input per unit volume, the
presence of secondary nucleation in the mode of nucleation is evident.
The effect of high stirring speed is more apparent when the number of
crystals is expressed in the nucleation rate. At 880 r.p.m., the
sharp decline of nucleation rate indicates the unstable environment
for viable embryos (molecular clusters) during vigorous mixing. The
experimental data presented in Table (4-7) covering different initial

FIGURE 5-11 The Linear Relationship of Secondary Nucleation Rate
with respect to Power Input for S = 57 - 63 at 25°C
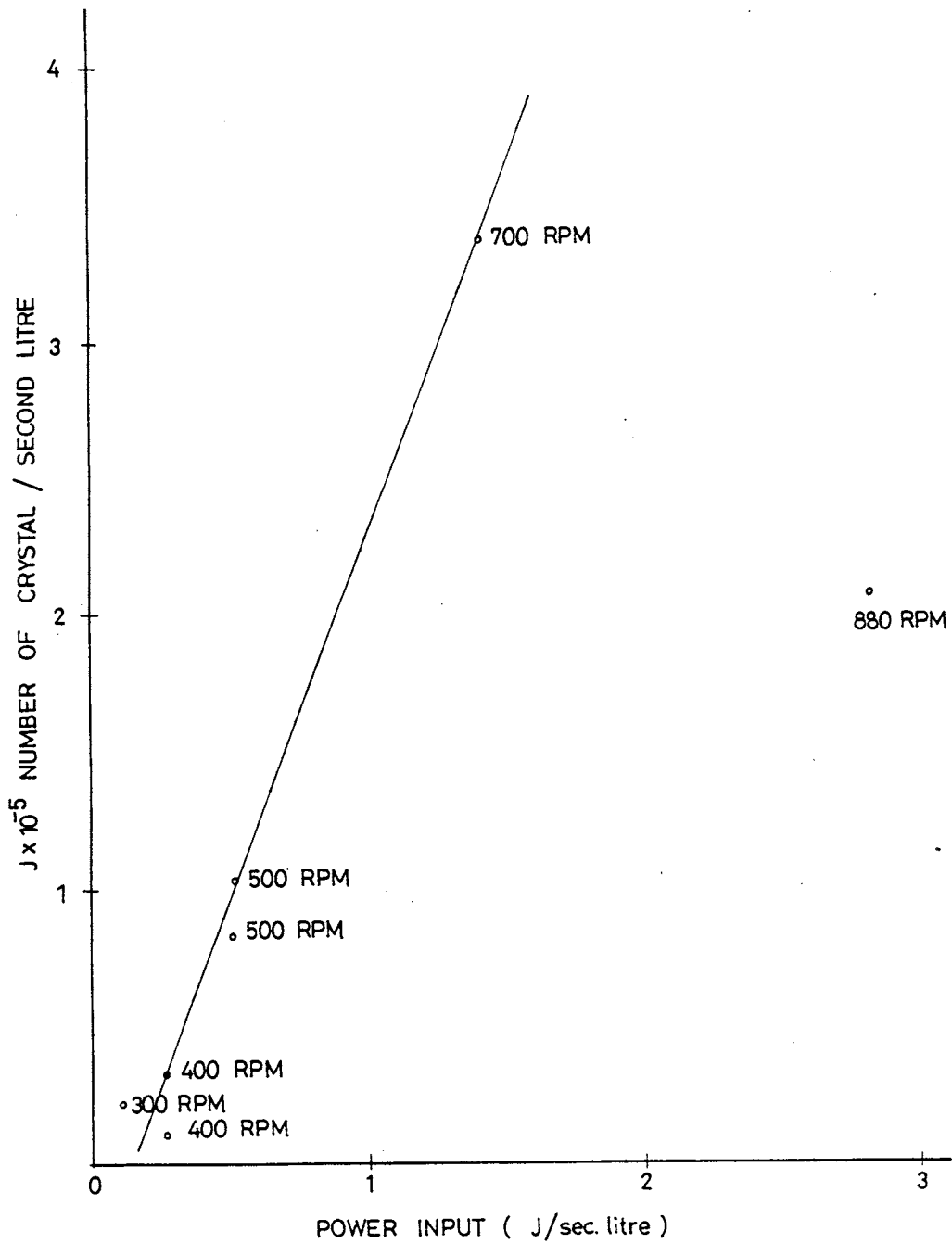
degrees of supersaturation and stirring speeds were plotted based on the empirical expression

$$J_{c-ms} = K_{(2-25)} (\Delta c)^p \varepsilon M_x \qquad (2-25)$$

where Δc is substituted by S $(S = \dfrac{f_d^2 [Ca^{2+}] [CO_3^{2-}]}{K_{sp}})$

M_x is the weight concentration of calcium carbonate precipitated at the respective degree of supersaturation

ε is the energy dissipitated by the stirring per unit mass of slurry by the stirring and is calculated from the power number (Section (4.5.2.2))

The best fit for all this data is obtained for p=7.9 (Figure (5-12)) which has a correlation coefficient = 0.9713. Apparently, the effect of degree of supersaturation is still the single major parameter governing the rate of nucleation. The exponent of the degree of supersaturation, p=7.9 is in agreement with the order of nucleation of the homogeneous nucleation with respect to supersaturation defined as S-1. The order of nucleation n is equal to 8 (Section (5.1.2)) The absence of significant secondary nucleation during crystallization is because of the rapid decline of the available degree of supersaturation.

The linear relationship also suggests that stirrer-crystal collision is responsible for secondary nucleation in stirred reactors as suggested by Ottens et. al. (1972). Secondary nucleation studies reported in the literature were usually studied in a MSMPR system under steady state condition. The number of nuclei was calculated by

FIGURE 5-12   Empirical Correlation of Secondary Nucleation
Rate of Calcium Carbonate at 25°C in a Batch
Stirred Reactor
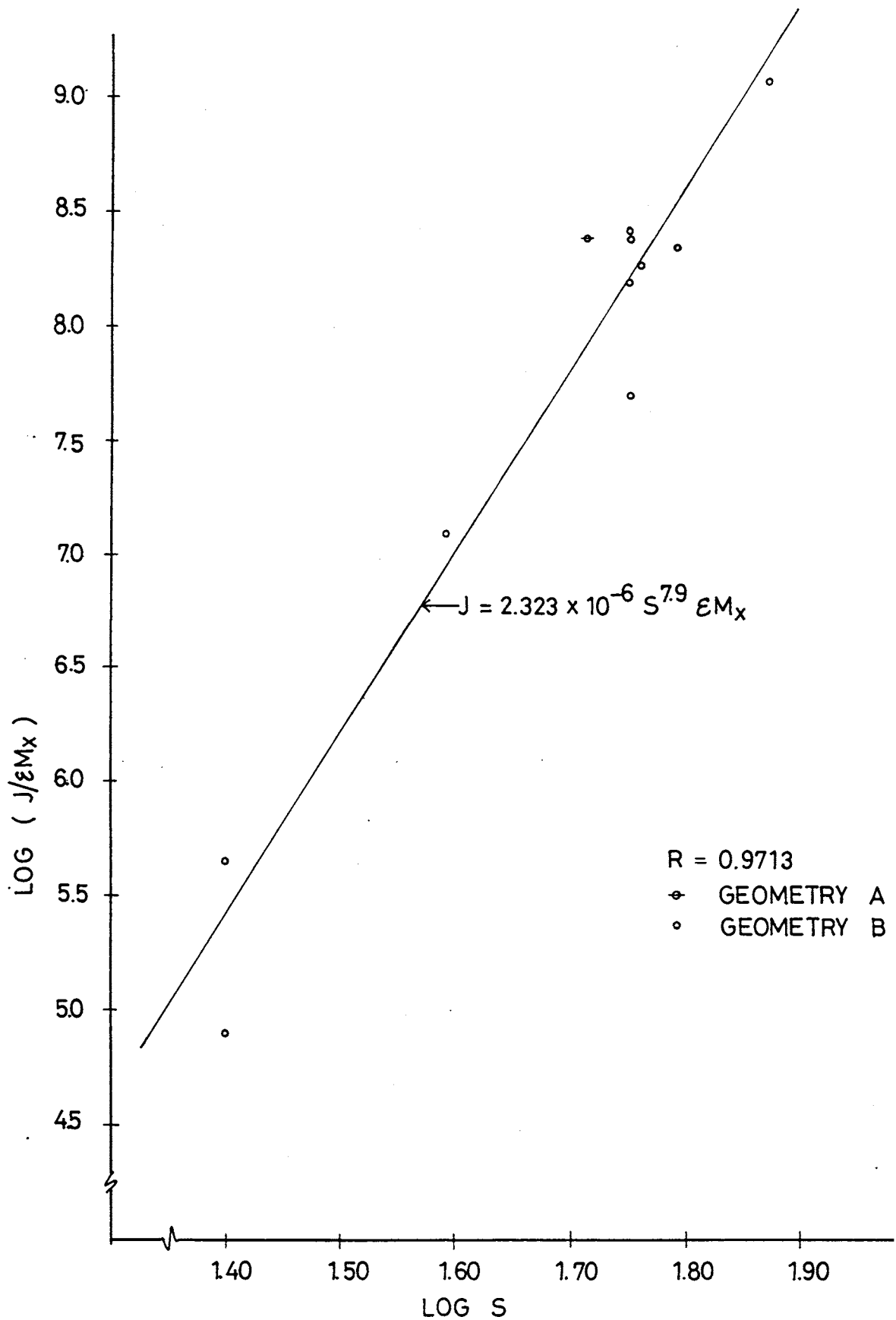
constructing a curve of particle population density against its size determined by the Coulter counter. The nucleation rates were related to system retention time. A rigorous treatment of the crystal size distribution pattern related to nuclei birth and stirring speed was possible with Coulter counter data. However a MSMPR system always mantains a concentrated crystal magma under steady state conditions, even $8 - 60$ kg/m^3 weight concentration was considered low (Ottens et. al., 1972). Therefore, it does not give an insight into secondary nucleation for extremely low crystal concentration systems. In fact, all the nucleation rate data obtained by MSMPR methods are probably better described as secondary nucleation rather than primary nuclea- tion studies. Cooling water does not contain such a high crystal con- centration (for calcium carbonate crystals). Therefore, a batch reac- tor was used for unseeded experiments. Nuclei were generated after mixing due mainly to primary nucleation and then subsequently com- pounded by secondary nucleation. A constant increase of nuclei number took place within the nucleation process during which the crystal con- centration rose from 0.001 to 0.005 Kg/m^3. It is impossible to sample the solution to count the crystals without disturbing the solution supersaturation. Therefore, only experiment PE21 as described previ- ously was used to check the pattern of nucleation after mixing and the accuracy of the crystalization data was sacrificed Although the present method appears to be less rigorous for crystal number determi- nation, the result is a closer representation of cooling water precip- itation involving a secondary nucleation mechanism such as nuclei generation due to pumping of water in the cooling water system.

5.1.6 Secondary Nucleation of 1:1 Mg to Ca Molar Concentration System

The presence of magnesium in 1:1 molar ratio to calcium seemed to complicate the interpretation of nucleation data. Experiments were conducted at three different stirring speeds. Both 400 and 500 r.p.m. experiments produced final crystals dominated by needle-like aragonite and hexagonal shaped calcite (Plate B15 Appendix B). Sampling for crystal count and identification was carried out during nucleation and crystalization of EP19 (400 r.p.m.). No crystals were observed under microscope for 193 minutes after mixing. Beyond 193 minutes a shower of crystals appeared and the number continued to increase rapidly as both calcite and aragonite. At 224 minutes, another shower of crystals occured, this time in shower of needle-like crystal splinters pressumbly from attrition of aragonite (Figure (5-13)). Final crystal number is only approximately 30% of the number at 251 minutes due to the ripening process. Therefore, the presence of aragonite, which is always an aggregate of needle-like aragonite crystals, together with the batchwise increase in nuclei number make secondary nucleation rate calculation impossible.

Aragonite is thermodynamically less stable than calcite at $10^{-3.5}$ atmospheric P_{CO_2} and 25°C. It was suggested by Roques and Girou (1974) that three forms of calcium carbonate can exist at the subcritical nuclei (embryo) state. The survival probability of these embryos to nucleate and grow to macroscopic scale is determined by their thermodynamic stability under crystallization conditions. Magnesium cations can be adsorbed onto some preferrable forms of embryo. This actually slows down the rate of embryo growth to reach critical nuclei size and therefore reduces the survival probability of such embryos in

FIGURE 5-13   The Number of Crystal Counted with respect
to Time for Experiment PE19 (400 r.p.m.,
Geometry B)
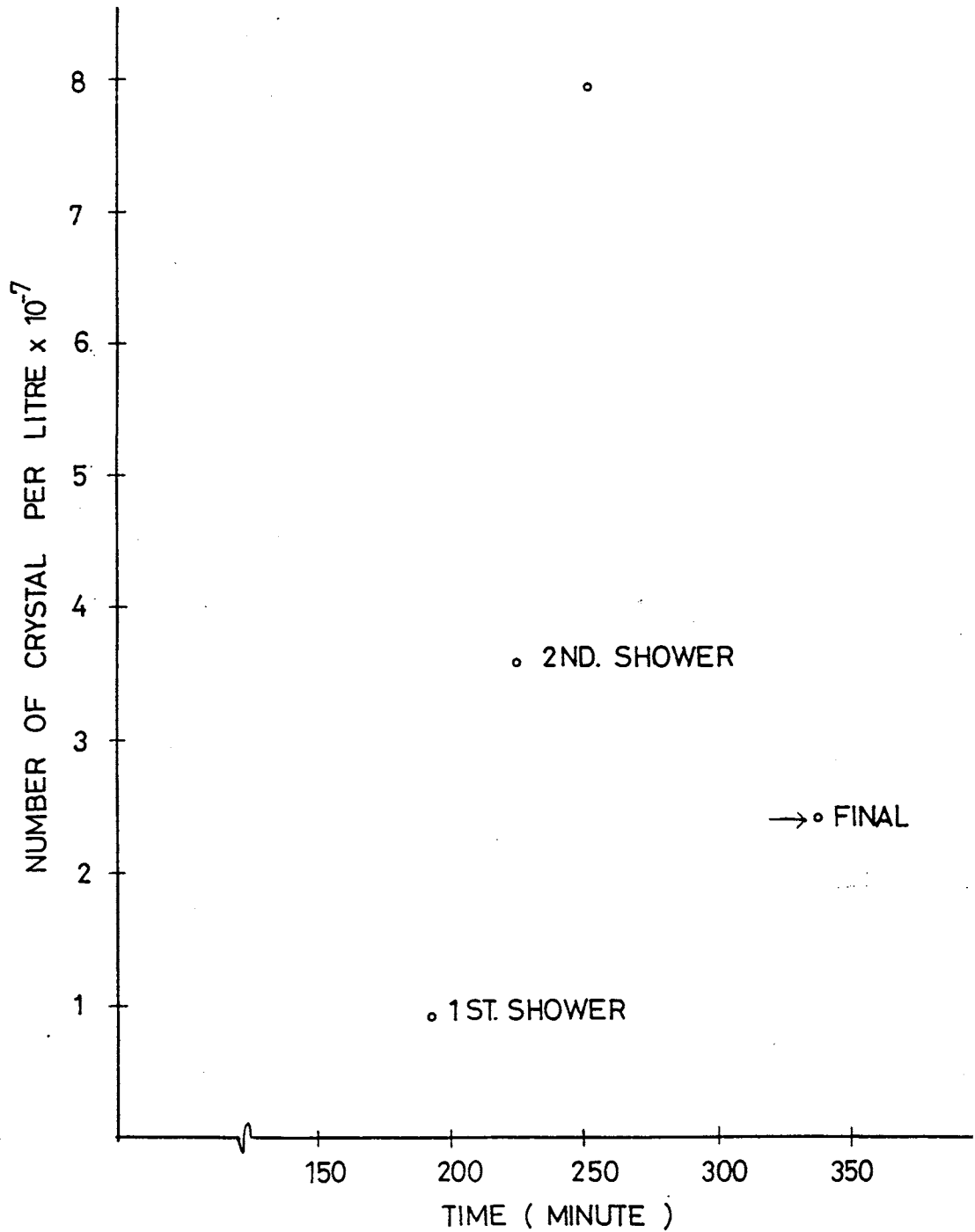
competition with other forms of embryo. Therefore, with this postulate, magnesium cation have been adsorbed onto calcite and vaterite embryos, hence reducing the number of calcite crystals and completely inhibits the formation of vaterite. If aragonite embryos are not affected by magnesium cation adsorption, they will have a higher survival probability and grow despite being a less thermodynamically stable entity. This postulate can also explain the general increase in induction period in the presence of magnesium because of the overall reduction of embryo survival probability and the rate of embryo growth to reach critical nuclei size.

Möller and Rajagopalan (1975) proposed a different explanation of the effect of magnesium. They suggested that small dehydrated magnesium ions present in subcritical nucleus (embryo) of calcite distort the lattice to such an extent that formation of stable calcite nucleus becomes impossible at Mg/Ca > 4. The presence of smaller magnesium cations may lead to a denser lattice structure and therefore favours the formation of aragonite.

Precipitation of calcium carbonate was carried out in a quiescent solution at 1 atmospheric pressure and 25°C at a initial degree of supersaturation of 24. Only hexagonal shaped calcite crystals similar to the 700 r.p.m. experiment were produced (Plates B12 and B13 of Appendix B). This conforms to Möller and Rajagopalan's finding that the formation of aragonite requires Mg/Ca > 4. However, in stirred experiments at 400 r.p.m. and 500 r.p.m., both aragonite and calcite were formed for a similar initial degree of supersaturation (S = 24). In fact the final crystal mixture was nearly 100% aragonite in the 400 r.p.m. experiment. The 500 r.p.m. experiment still produced more

aragonite than calcite.

The proposed mechanism in Section (5.1.4) can also be used to explain this observation. During the initial stage of nucleation at 400 r.p.m. (PE19), an almost equal percentage of aragonite and calcite were present. Although Mg/Ca is only 1 and not sufficiently high to suppress the growth of calcite, the transient increase in energy in the form of heat due to stirring has increased the probability of aragonite survival. The aragonite aggregates generated eventually dispersed or produced secondary nuclei in the form of crystal splinters under the effect of stirrer-crystal collison. The sudden increase of aragonite crystals population allows aragonite to continue to form new aggregates out of crystal splinters or onto the hexagonal calcite already present. Such transitional crystal habit (aragonite crystals on hexagonal calcite crystals) were observed in the final crystal products (Plate B15 of Appendix B). The nett result is the aragonite predominating crystal products.

There was no sign of aragonite in the 700 r.p.m. experiment. Crystallization growth rate interpretations from Section (5.2.3) also indicates no apparent retardation of the crystalliztion growth rate constant due to the presence of magnesium. However, the secondary nucleation rate does not obey the empirical equation derived for pure calcium carbonate systems. Aragonite embryos did not have the chance to grow to stable nuclei. This is probably due to the vigorous stirring which tends to redissolve the thermodynamically less stable aragonite nuclei. Because aragonite are acicular crystals, they have a very high surface area to volume ratio which implies high dissolution rates. The 500 r.p.m. experiment produced an aragonite dominated

precipitate rather than almost 100% aragonite precipitate in the case of the 400 r.p.m. experiment, this also illustrates the effect of increasing stirring on aragonite dissolution.

5.2 CRYSTALLIZATION OF CALCIUM CARBONATE

5.2.1 Crystal Surface and Volume Shape Factors

The weight and surface area of a crystal can be calculated from the characteristic length measured provided the shape factors of the crystal are known. In this project, calcium carbonate was formed in three main crystal habits, namely rhombohedral, spherical and acicular form (Section (4.5.3.1)). Since all the acicular aragonite crystals formed aggregates, it is impossible to calculate either the weight or surface area based on the characteristic lengths of the aggregates measured, consequently no attempt was to derive the shape factors of aragonite aggregates. Fortunately at 25°C. the calcium carbonate precipitates from the bulk crystallization experiments are mainly discrete calcite or vaterite which are rhombodhedral and spherical respectively. The instrument used for crystal size measurement is a computerized image analyzer (Section (4.4.3.3)) which measures the sizes of the particle images shown on the screen from left to right. Therefore the characteristic lengths of the particles are the chord lengths which also depend on the orientation of the particle. When the shape of the particle is spherical , it presents no problem because the chord length is the diameter of the sphere, as is the case for vaterite. The surface and volume shape factors are simply π and $\pi/6$ respectively. However, it is not so in the case of calcite rhombs. These calcite rhombs are monoclinic and with a inclined angle

of 80° (Appendix B). Therefore the chord lengths measured from the left to the right of the crystals are very much subject to the orientation of the crystals. Assuming a random orientation, the minimum chord length measured will be the actual length of the crystals irrespective of which side the crystals rest on the slide. This is because the calcite crystal is trigonal with the length, breadth and thickness in equal length. The schematic representation of calcite crystal is shown in Figure (5-14).

The maximum chord length that can be measured is apparently the diagonal length of the two dimensional crystal surface. From Figure (5-14), the minimum chord length measured due to the orientation is x, the maximum chord length measured due to the orientation is $2x\cos 40°$ which is equal to $1.532x$. Therefore the range is from 1 to 1.532 units. Assuming a normal distribution of chord length measured within the range, ie. $\pm 3\sigma_s = 0.532x$.

$$\text{Therefore } \sigma_s = \frac{0.532x}{6} = 0.089x$$
$$\text{mean (d)} = x + 3\sigma_s = 1.267x$$

The mean of normal distribution is considered to be the most probable chord length measured by the image analyzer for calcite rhombs subject to random orientation.

Based on Figure (5-14), the theoretical shape factors based on most probable chord length can be calculated as follows:

$$\text{Volume} = (x-y) \times x\sin80° + x\sin80° \times y$$
$$\tan80° = \frac{x\sin80°}{y} = \frac{0.9848x}{y} = 5.671$$
$$\text{Therefore } y = \frac{0.9848}{5.671} = 0.1736x$$
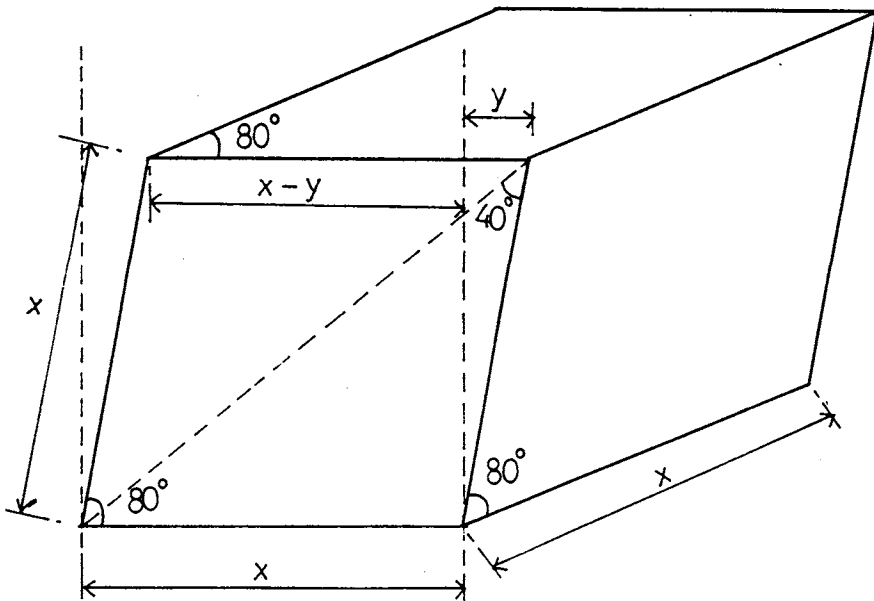
FIGURE 5-14 Schematic Representation of Rhombohedral Calcite

Volume = (x-0.1736x) x 0.9848x + 0.9848x (0.1736x x)

$$= 0.8138x^3 + 0.1710x^3 = 0.9848x^3$$

Volume based on most probable chord length

$$= \alpha_v d^3 = \alpha_v (1.267x)^3$$

$$= \alpha_v 2.034x^3$$

$$\alpha_v = \frac{0.9848x^3}{2.034x^3} = 0.484$$

Surface area = {(x-y) xsin80° + y xsin80° } . 6

$$= 0.8138x^3 + 0.1710x^3 . 6$$

$$= 5.9088x^2$$

Surface area based on most probable chord length

$$= \alpha_a d^2 = \alpha_a (1.267x)^2$$

$$= \alpha_a 1.605x^2$$

$$\alpha_a = \frac{5.9088x^2}{1.605x^2} = 3.681$$

Similarly, if the characteristic length of the rhombohedral calcite crystal, ie. x is used to calculate the shape factors, α_v=0.484 and α_a=3.681. These are used in the calculation of overall growth rate constant based on crystal number counted at the end of the crystallization process. (Section (4.3.4)).

5.2.2 Overall Growth Rate of Crystallization of Pure Calcium Carbonate System

The rate of reduction of total calcium content in the batch crystallization experiments can be expressed by the following general empirical equation:

$$\frac{dc}{d\theta} = K_{(5-14)} f(S)(c_b - c_s)^2 \tag{5-14}$$

where c_b and c_s are the bulk and saturation concentrations respectively

     $K_{(5-14)}$ is the rate constant

     f(S) is the crystal surface area which is also a function of time

The 'order' of reaction is 2 which suggests a surface-reaction controlled mechanism also confirmed by previous investators on calcium carbonate crystallization (Reddy and Nancollas, 1971a; 1971b; Wiechers et. al., 1975). Referring to Figure (4-6), a best straight line was drawn through the points. At the early stage of the precipitation, the linear relationship does not hold. This is because at this stage of precipitation, nucleation is still the predominating process and is continously generating new nuclei. The crystallization process only predominates when the linear relationship begins to apply. The rate of bulk crystallization can be calculated from the gradient and crystal shape factors (Equation (4-111)). Vaterite and calcite are considered to assume a spherical shape and rhomb respectively as evident from the scanning electron photomicrographs (Appendix B). The overall growth rate (simplified) method based on the number of crystals counted at the end of each crystallization experiment and assuming a mono-sized precipitate was used to calculate the overall growth rate constants (Section (4.3.4)). From Table (4-10), there are two major groups of crystal products, namely vaterite and calcite, also indicating different overall growth rate constants. Although there are different percentages of calcite present in vaterite dominating crystal products, the rate is still consistent to within ±11%. The rate of calcite is consistent to within ±9%. The arithmetic mean of overall growth rate constants for vaterite and calcite are 20.5±2.3 and

11.5 ± 1.0 L^2/min mole m^2 respectively. Crystallization of vaterite is apparently faster than calcite.

In comparison to the simplified method, the overall growth rate method with size consideration was used to calculate the rate constants (Section (4.3.5)). There are two major difficulties in determining the surface area accurately by this method. Firstly, it is due to the agglomerates. Although the dispersion method mentioned in Section (4.4.3.3) has significantly reduced the number of agglomerates in the samples used for crystal sizing, it is practically impossible to remove all agglomerates without also breaking the crystals. The presence of these agglomerates consistently causes an underestimation of the total crystal surface area during the crystallization process. This can be demonstrated in principle as follows::

The total weight of the sample calculated by summing over the entire size range was used to obtain the arbitary weight factor (n') required to achieve the final weight of precipitate. The total crystal surface area of the precipitate is therefore the sample surface area obtained by summing the surface area over the entire size range multiplied by n'. However, when agglomerates are present, the total surface area of the precipitate will be underestimated. To illustrate this point, consider a crystal agglomerate and the final precipitate is n' times the weight obtained from the size of this agglomerate of size L_{agg}. Assuming this agglomerate comprises n crystals with size L_{act} where $L_{act} < L_{agg}$. Therefore, the weight of the agglomorate is actually

$$W_{act} = n\alpha_v L_{act}^3 \qquad (5\text{-}15)$$

The arbitary factor based on weight should be

$$n_w' = \frac{n' \alpha_v L_{agg}^3}{n\alpha_v L_{act}^3} = \frac{n' L_{agg}^3}{nL_{act}^3} \qquad (5\text{-}16)$$

Therefore, this arbitary factor should be used to obtained the actual surface area of the precipitate.

$$A_{act} = n_w' n\alpha_a L_{act}^2 = \frac{n' L_{agg}^3 \, n\alpha_a L_{act}^2}{nL_{act}^3} = \frac{n' \alpha_a L_{agg}^3}{L_{act}} \qquad (5\text{-}17)$$

The surface area based on agglomerate size L_{agg} is

$$A_{agg} = n' \alpha_a L_{agg}^2 \qquad (5\text{-}18)$$

Therefore the ratio of A_{act} and A_{agg} is

$$\frac{A_{act}}{A_{agg}} = \frac{n' \alpha_a L_{agg}^3}{L_{act}} \times \frac{1}{n' \alpha_a L_{agg}^2} = \frac{L_{agg}}{L_{act}} \qquad (5\text{-}19)$$

Since $L_{agg} > L_{act}$, therefore the actual surface area of the precipitate is always greater than the surface area determined from the sample which contains some agglomerates. This leads to a higher value of the overall growth rate constant of the bulk crystallization of calcium carbonate.

To minimise this error, a maximum size was predetermined as the ceiling of the size range. This is to avoid the inclusion of unrealistically large agglomerates of the sample into the size measurement.

Secondly, only grab samples were taken for the size measurement because of the physical limitions of the instrument to count and size the total precipitate for each experiment. This apparently will introduce an uncertainty about whether the sample is representative of the total precipitate. From Table (4-11), the results of the calcium carbonate growth rate constants demonstrate a wide scatter compared to the simplifed overall growth rate method. Experiments E22 and E23 apparently suffered the shape factor complication due to the presence of aragonite crystals and produce a high value of the rate constant calculated. Nevertheless, these two values are reproducible for this kind of precipitate. The rate constants of calcite are extracted from experiments E24, PE9 and PE11. Except E24, the growth rate constants calculated from PE9 and PE11 are virtually identical. Therefore $17.3 \times 10^3 \, L^2/mole \, mim \, m^2$ is taken as the value of calcite overall growth rate constant determined by the size consideration method. The arithmetic mean of calcite growth rate constants calculated from the simplified overall growth rate method is $11.5 \pm 1.0 \, L^2/mole \, min \, m^2$. Therefore, these values from two different methods compare reasonably well. The growth rate constant reported by Karmlerczak, et. al. (1982) was $17.8 \pm 1.2 \times 10^3 \, L^2/mole \, min \, m^2$. They also recalculated the rate constant reported by Nancollas and Reddy (1971) as $15 \times 10^3 \, L^2/mole \, min \, m^2$. The reported values suggest that the rate constants calculated from PE9 and PE11 based on size consideration are identical to the seeded crystal growth method if the complications due to agglomeration of the grab samples and non-uniform shape factors are

not significant. The simplified overall growth rate method registered the lower values for the growth rate constants. Nevertheless, they are more reproducible to with ±9% of the arithmetic mean. This reproducibility is attributed to the significant number of samples counted under the microscope to acquire a statistical significance tested by the χ^2 test (Section (4.4.3.3)). If compared with the values of rate constant obtained from the seeded crystal growth method (Nancollas and Reddy, 1971) and the overall growth rate with size consideration, the simplified method is overestimating the precipitate surface area by making an assumption of monosized crystal. Taking PE9 for example, the surface area of the precipitate calculated by the result of size distribution is:

$$A_f = n'_w \sum_{i=1}^{n} N_i \alpha_a \bar{L}_i^2 = 135 \text{ cm}^2 \text{ per liter} \tag{5-20}$$

where A_f is the surface area of the final precipitate per liter solution

n'_w is the factor based on the final total weight of the precipitate per liter solution

N_i is the number of crystals in class i

$\bar{L}_i$ is the mean size of crystals in class i

n is the total number of size classes

α_a is the surface shape factor = 3.681

The surface area of precipitate per litre of solution calculated by the simplified method is:

$$A_f = \frac{\alpha_a}{(\rho_c \alpha_v)^{2/3}} M^{2/3} N^{1/3} (T_{Ca_{in}} - T_{Ca_f})^{2/3} \tag{5-31}$$

where α_a is the surface shape factor = 3.681

α_v is the volume shape factor = 0.484

M is the molecular weight of calcium carbonate = 100

ρ_c is the calcite density = 2.71 g/cm^3

$T_{Ca_{in}}$ is the initial total calcium content = 0.001999 M

T_{Ca_f} is the final total calcium content = 0.0008594 M

N is the number of crystal per liter = $3x10^7$

Therefore

$$A_f = 223 cm^2$$

This indicates an increase of 65% surface area compared to that calculated from grab samples of the final precipitate.

The overall growth rate constants of vaterite can be extracted from experiments PE4, PE7, PE8 and PE15. Only PE7 and PE8 are reproducible. PE15 is not within the normal range of data. The surface area of the final precipitate calculated is 145 cm^2 which is only 66% of the final precipitate from PE4, yet these two experiments generated almost the same crystal population ($2.60x10^8$/L of PE15 compared to $2.94x10^8$/L of PE4). As a result, the rate constant calculated is 40% higher then the mode, namely $40.0x10^3$ L^2/mole min m^2. From the simplified method (Table (4-10)), the rate constant calculated is the smallest value and still within ±11% of the normal. The rate constant of PE4 calculated by size consideration has a value of $28.3x10^3$ L^2/mole min m^2. This is the closest to the arithmetic mean growth rate constant calculated by the simplifiedmethod. No growth rate constant of vaterite has been reported in the literature,

therefore the reliability of these values cannot be checked. However, using rate constant of calcite as a guideline, the overall growth rate constant of vaterite should lie between 20×10^3 and 30×10^3 L^2/mole min m^2.

In conclusion, the spontaneous precipitation method present greater difficulties to produce highly reproducible rate constants based on true surface area calculated from size distribution measurement by the image analyzer for the final precipitate. However, the simplified overall growth rate method is highly reproducible but the crystal surface area may be overestimated. If the rate constant of calcite crystallization is taken as 15×10^3 L^2/mole min m^2 obtained by Nancollas and Reddy (1971), then the value 11.5×10^3 L^2/mole min m^2 calculated from the simplified method represents a 23% difference. This is considered tolerable for kinetic growth rate determination of such a complicated process like precipitation. The reproducibility of seeded crystal growth rate were apparent. However, the seeded crystal growth method requires the crystal seeds to be carefully prepared and the surface area measured. During the process of crystallizaion, the crystal seeds continue to grow. Therefore, the transient surface area has to be calculated by some normalization procedure (Karmlerczak, et. al., 1982). Again the determination of true transient crystal surface area is difficult. Consequently, although the seeded crystal growth method was claimed to be a well controlled method to determine the growth rate of calcium carbonate, the accuracy of the value still suffers from the uncertainty incurred in calculating the transient crystal surface area during the process of crystallization. The method also requires careful preparation of the crystal seed and special instrumentation such as BET apparatus applying nitrogen

adsorption to determine the crystal surface area. In view of these factors, there are certainly merits in recommending the simplified overall growth rate method due to its simplicity and reproducibility. The crystals suspension only required to be sampled at the end of the crystalization process by laboratory micropipette. The counting is perfomed under ordinary light transmitting microscope with the sample placed in the counting chamber. The tools used are all common laboratory items and no special technique is required. The method is simple and results reproducible. The lower (23%) growth rate constant may be due to a consistent systematic error introduced by the micropipette during sampling. Because of the suction effect of the micropipette during sampling, a more concentrated crystal suspension than the true concentration can be sampled consistently. As a result, the surface area of the crystals in the reactor can be overestimated and produces a lower calculated growth rate constant. Obviously the accuracy of the growth rate constant determined by this method can be improved by modifying the sampling device to avoid the suction effect during sampling. However, a systematic error in crystal counting on a 20 μL sample as high as 90% will only produce a 23% difference in the final value of crystal growth rate constant calculated, because the crystal number is to the one third power in Equation (4-111).

Finally, the kinetic data of the spontaneous precipitation method interpreted by overall growth rate method with size consideration can still be valid. The accuaracy of the growth rate constants can be improved if a large quantity of the uniform precipitate suspension at the end of the crystallization experiment can be sized by a Coulter counter. A more representative sample can prepared on a microscopic slide for size measurement by image analyzer if the crystal population

in the suspension is sufficiently high for crystal counting and sizing. Although spontaneous precipitation experiments have been criticised by some workers (Nancollas and Reddy, 1971; Kazmlerczak, et. al., 1982) because of the complications due to nucleation, the present study demonstrates that the complications due to nucleation can be ignored in the mode of crystallization and at the same time provides new insight about the effect of power input on nucleation as well as crystallization.

Both calcite and vaterite follow surface-reaction controlled mechanism. The growth rate constants of vaterite determined by both methods are higher than calcite. Until now, theoretical calculation of the rate constant of crystallization is still not possible although some interesting progress has been made (Nielsen, 1982). From the theories of crystal growth, rate constant comprises many fundamental parameters that are characteristic of individual crystals and its crystallographic form. Surface reaction controlled mechanism implies that processes such as adsorption and desolvation of growth unit, surface diffusion of growth unit, the creation of energetically favourable kinks either by surface nucleation or screw dislocation all govern the crystal growth rate. No information is available about rates of these surface processes of calcite and vaterite. However, the nucleation rate of vaterite seems to be faster than calcite as indicated by the lower free energy required for nucleation (Section (5.1.2)). If the surface nucleation process is singled out to be important especially at high degree of supersaturation, vaterite should grow faster than calcite. At this stage, it is still very difficult to be certain exactly what is the controlling surface meachanism because the growth theories are still inadequate to allow

prediction of crystal growth rate from first principles. Therefore, it is only appropriate at this stage to say that irrespective of calcite or vaterite crystallization, they are different crystallographic forms of sparingly soluble calcium carbonate and following an overall surface reaction controlled crystallization mechanism. Vaterite crystallizes faster than calcite. The surface reaction controlled mechanism is further justified because the results of overall growth rate constant are not affected by different stirring speeds. The 300 r.p.m. in Geometry B is the minimum speed required to suspend all crystals formed during crystallization. Total suspension of crystals is important so that there is no inhibition of reaction due to crystal surface limitation. Experiment PE16 indicates an exceptionally low growth rate constant of vaterite. It is believed that this is due to agglomeration of high crystal population and subsequently reduces the available surface area for crystal growth.

5.2.3 Formation of Different Crystal Habits in Pure Calcium Carbonate System

The presence of different habits of calcium carbonate crystal especially at high degrees of supersaturation and stirring speeds of 300 r.p.m. and beyond is evident. In the discussion on the results of nucleation studies, qualitative explanation was attempted from the concept of statistical thermodynamics. Crystal habits are known to be affected by many factors such as the presence of impurities , the degree of supersaturation, the temperature of crystallization, and the degree of agitation.

The unique shaped aragonite was observed at 25°C from Geometry A experiments and experiment PE6 using Geometry B (Tables (4-9) and (4-10)). Under the high magnification of the scanning electron microscope, these aragonite crystals appeared to be the result of the continuous outward growth of crystals from a bundle of acicular aragonite into the calcium carbonate rich environment (Plates B5 and B9 of Appendix B).

At low initial degrees of supersaturation, discrete calcite crystals were formed, for example PE13 (Plate B6 of Appendix B). The crystals were imperfect and showed a trail of layer growth. This provides evidence to support the conventional crystal growth theories (Chapter 2).

When the initial degrees of supersaturation are 76.4 and beyond, 100% calcite was formed in the Geometry A experiment (Table (4-9)). Similar observations on some inorganic systems were mentioned by Walton (1967). He mentioned the presence of three distinct induction regions. At low supersaturation, heterogeneous nucleation and discrete growth occurred. It is consistent that both Geometry A and Geometry B experiments irrespective of degrees of stirring produced a discrete calcite precipitate. As the supersaturation was increased, dentritic growth might develop. This was demonstrated by the fact that aragonite was present when the degree of supersaturation was below 76.4. At high supersaturation homogeneous nucleation predominated and the particle size of the precipitate was greatly reduced. This is in the region of 76.4 and beyond where the degree of stirring is not sufficiently vigorous to generate vaterite, a shower of relatively small calcite crystals were formed as observed in Geometry A

experiments.

When the crystallization experiments were conducted at 36°C, aragonite began to appear in long needle-like crystals aggregates in the midst of calcite. Compared to the experiments at 25°C, this indicated that the aragonite nuclei are more abundant and grew into discrete acicular crystals which agglomerated during the latter stage of crystallization. These aggregates of aragonite were in irregular pattern due to the result of random agglomeration compared to the consistent pattern of aragonite aggregates observed in 25°C experiments. These aggregates broke off easily under ultrasonication whereas the aggregates from 25°C experiments remained intact. At 44°C, crystals were mainly aragonite. At 55.8°C, crystals were 100% aragonite (Plate B14 of Appendix B). This indicates that aragonite becomes thermodynaically more stable as the temperature increases. Since aragonite formed from these bulk crystallization experiments are acicular crystals, they are grouped together in agglomerates. This makes a crystal count virtually impossible. Therefore no attempt was made to calculate the overall growth rate constant from the experiments conducted at 35°C and above.

5.2.4 The Effect of Magnesium in Calcium Carbonate Bulk Crystallization

Out of the three crystalliztion experiments on 1:1 Mg/Ca molar ratio system, only the 700 r.p.m. experiments was able to provide the bulk crystallization growth rate. This is because of the aragonite agglomerates precipitated in the other two experiments which makes crystal counts impossible. Magnesium is known to encourage the growth of aragonite. But at the Mg/Ca ratio equals to 1, Mg is believed to

be still insufficient to generate aragonite predominant nuclei for bulk crystallization. Since all experiments were conducted on more or less similar initial degree of supersaturation for precipitation, the only difference was the degree of mixing. It seems that it is this difference that triggers the otherewise thermodynaically less stable aragonite in bulk crystallization at 25°C at 1:1 Mg/Ca. In Section (5.1.5), the formation of aragonite at 25°C was discussed.

Under scanning electron microscope, calcite appeared differently from the simple rhombohedral habit (Plates B12 and B13 of Appendix B). The crystals are polyhedral. They are the combination of prism with rhombohedron. Under light transmitting microscope, the crystals look like hexagonal crystals in two dimension. Similar type of crystal hibit was observed when crystals were formed without stirring. The final appearance of crystals are due to the result of slow growth faces that bind together. In other words, the fast growth faces of the crystals grow themselves out of the formation of the final crystals (Mullin, 1972). In pure supersaturated calcium carbonate solution, all the fast growing faces disappear in the formation of rhombohedral calcite. However, when magnesium is present, certain degree of hindrance is experienced by the fast growing faces. As a result, they survive and the crystals appear in the polyhedral form. Because of the complex geometry of these crystals, the shape factors are difficult to determined. However, from the overall gradient, $k'N^{1/3}$, of experiment PE18 (Table (4-12)), the value 1.0667×10^4 seems to indicate the growth rate at least is comparable to the pure calcium carbonate system. Therefore, the overall growth rate of the bulk precipitation of calcium carbonate with 1:1 Mg/Ca molar ratio at 700 r.p.m. at 25°C is considered not to be retarded by the magnesium cation.

CHAPTER 6

CALCIUM CARBONATE SCALING IN HEAT EXCHANGERS

6.1 INTRODUCTION

One important application of calcium carbonate precipitation studies is to understand and predict precipitation fouling (scaling) in heat exchangers when water is used for cooling. Cooling water used in industries and utilities will contain a range of calcium and magnesium which are two of the most common cations in natural water. Calcium carbonate has an inverse solidity with temperature. The cooling water flowing over the heat transfer surface is able to precipitate out calcium carbonate if the solubility product of calcium carbonate is exceeded.

Calcium carbonate crystals deposit onto the heat exchanger surface and are able to grow into thick scale under supersaturated conditions. The result of such chemical scale is a decrease of heat transfer efficiency of the heat exchanger.

The overall heat transfer coefficient of the heat exchanger is expressed as follows:

$$\frac{1}{U_o} = \frac{1}{U_o} + \frac{D_o}{h_i D_i} + \frac{x_w D_o}{k_m \overline{D}_L} + \frac{D_o}{h_d D_i} + \frac{1}{h_d}$$

(6-1)

where

U_o is the overall heat transfer coefficient based on outside

diameter

h_o is the film coefficient of the outside tube

h_i is the film coefficient of the inside tube

k_m is the thermal conductivity of the tube wall

x_w is the thickness of the tube wall

D_i is the inside diameter of the tube

D_o is the outside diameter of the tube

$\overline{D}_L$ is the logarithmic mean diameter of the tube

h_{d_i} is the fouling factor of the inside tube

h_{d_o} is the fouling factor of the outside tube.

$$R_f = \frac{D_o}{h_i D_i} + \frac{1}{h_{d_o}} \qquad . \qquad (6\text{-}2)$$

which is the thermal resistance due to the fouling deposit.

Therefore when the tubes are clean, R_f is not included in the expression. The current information on heat exchanger fouling is still scarce. Fouling factors are selected for a heat exchanger design based on broad design guidelines as outlined in Tubular Exchangers Manufacturers Association. T.E.M.A. Standards (1968).

Heat exchanger fouling is a complex process depending on a range of physical and chemical factors. In the case of calcium carbonate, the fouling factor is a function of calcium carbonate scale thickness which is also a function of time and thermal conductivity. Recently, some efforts have been made to determine the asymptotic fouling

resistance of calcium carbonate under specified conditions based on the assumption that scale is deposited and is removed by the hydraulic flow through the tube such that eventually a steady state will be reached. Such asymptotic fouling resistance will be a more rational number for design purpose.

6.2 MATHEMATICAL MODELS OF FOULING

According the Kern and Seaton (1959)

Net rate of fouling = Rate of formation of the fouling deposit
- Rate of removal of the fouling deposit

The Kern and Seaton model was considered as the accepted starting point for all models of fouling (Somerscales, 1979). The general form of the model is

$$k_f \cdot \frac{dR_f}{d\theta} = \frac{dX_f}{d\theta} = \frac{dW_T/d\theta}{A\rho_f} - \frac{x_f \tau}{B} \tag{6-3}$$

where

k_f is the thermal conductivity of the deposit

R_f is the fouling resistance

$dW_T/d\theta$ is the total wall deposition rate

(ionic and particulate matter)

x_f is the thickness of the deposit

A is the deposition surface area

ρ_f is the bulk density of deposit

τ is the fluid wall shear stress

B   is an adherence parameter

which lead to the expression of asymptotic fouling resistance,

$$R_f = R_f^* [1 - \exp - (\theta - \theta_D)/\theta_C] \qquad (6-4)$$

where

θ_D is the induction period

θ_C is a time constant characterizing the tenacity of deposit

R_f^* is the asymptotic fouling resistance

$$R_f^* = \frac{\frac{dW_T}{d\theta}/A}{\rho_f k_f} \cdot \quad \theta_C = \frac{\frac{dW_T}{d\theta}/A}{\rho_f k_f} \cdot \frac{B}{\tau} \qquad (6-5)$$

Therefore if θ_C is very large, which signifies a very adherent scale, from Equation (6-3).

$$\frac{x_f \tau}{B} = 0 \qquad (6-6)$$

ie. $\quad \dfrac{dx_f}{d\theta} = \dfrac{dW_T}{d\theta}/A\rho_f$ which predicts a linear fouling curve.

6.2.1 Rate of Deposition

The rate of deposition in the Kern-Seaton model is governed by diffusion (mass transfer) and surface reaction on the heat transfer surface. In general, there are two approaches to describe the rate of deposition;

* driving force

*   kinetic

6.2.1.1 Driving Force

The rate of deposition will depend on the concentration gradient of the substance deposited between the bulk and the heat transfer surface. The general equation is:

$$\frac{dW}{d\theta} = K_G A (c_b - c_s)^z \qquad (6\text{-}7)$$

where

W   is the weight of the deposit

K_G is the combined diffusion - reaction mass transfer constant

c_b is the bulk concentration

c_s is the surface concentration

z   is the constant exponent

A   is the surface area

when z=1, then the process is mass transfer controlled and K_G becomes K_d, which is the mass transfer coefficient.

6.2.1.2 Kinetic

This approach is to ignore the detailed description of the process such as crystallization or particulate deposition, instead the approach describes the overall growth rate of the deposit by a rate equation:

$$\frac{dW}{d\theta} = K_{(6-8)} K_r (c_r)^n \qquad\qquad (6-8)$$

where

$K_{(6-8)}$ is a constant

c_r is the concentration of material which undergoes the reaction

n is the order of the reaction and

K_r is given by the Standard Arrhenius equation:

$$K_r = K_{(6-9)} e^{-E/RT_s} \qquad\qquad (6-9)$$

where

$K_{(6-9)}$ is a constant

E is the activation energy of the reaction

R is the Standard gas constant

T_s is the fluid/solid interface temperature (°K) at which

       the reaction takes place

6.2.2 Rate of Removal

The rate of deposition in the heat exchanger decreases with time mainly due to two reasons:

1. the decrease in temperature at the scale/liquid interface in the case of constant temperature medium heating,

2. the fluid shearing effect on the deposit.

The rate of removal of calcium carbonate is generally expressed by the equation:

$$\left(-\frac{dW}{d\theta}\right)_r = \frac{\tau \cdot W_T}{A \cdot B} \tag{6-10}$$

where

$\left(-\dfrac{dW}{d\theta}\right)_r$ is the rate of removal

τ is the fluid wall shear stress

A is the surface area

B is the adherence parameter

W_T is the total mass deposit

B/τ is extracted by Morse and Knudsen (1977) in their study as the time constant θ_c. This seems to be a good indicator of the strength of the deposit. The larger θ_c, the more tenacious is the deposit.

Shear stress at the fluid - deposit interface can be calculated by the following equation:

$$\tau = -\frac{D_h}{4} \frac{dP}{dL} \tag{6-11}$$

where

D_h is the hydraulic diameter of the pipe. $\left(D_h = \dfrac{4A}{p}\right.$, where

       A is the cross sectional area of the flow stream, and p

       is the wetted perimeter of the stream.)

$\dfrac{dP}{dL}$ is the pressure gradient in the direction of the flow.

Integrating over the length L,

$$\frac{\Delta P}{L} = \frac{f}{D_h} \frac{\rho_w \overline{v}^2}{2}$$

(6-12)

where

    f   is the Blasius friction factor

    $\overline{v}$ is the fluid velocity averaged over the cross section of the pipe

    ρ_w is the density of the fluid

6.3 FACTORS AFFECTING SCALING (Suitor, et. al., 1977)

6.3.1 Velocity

Velocity of the fluid can affect the fouling process by modifying deposition and removal processes. The rate of deposition is controlled either by mass diffusion or surface reactions. In the case of scaling, the crystal growth mechanism is generally shifted from a diffusion controlled mechanism to surface reaction controlled mechanism when the velocity is increased. This is because the overall growth rate is attributed to mass transfer for the substrate to the scale/liquid interface, followed by incorporation into the crystal lattice by reaction at the interface. When the velocity of the fluid is increased, force convective mass transfer becomes rate-unlimiting relative to the surface reaction, therefore, the rate - controlled mechanism is that of the surface reaction.

6.3.2 Temperature

The temperature of the liquid that contains inversely soluble salts such as $CaCO_3$, $CaSO_4$ etc is critical to precipitation processes. When the temperature is sufficiently high that the solubility product of the salt is exceeded, supersaturation is created and eventually will lead to precipitation.

Temperature of the heat transfer surface therefore also strongly affects the scaling process. With sufficiently high temperature, local supersaturation can be created. In addition, the rate of crystallization is governed by temperature in the form of an Arrhenius equation, therefore the higher the temperature, the faster is the rate of scaling. In the case of a constant temperature heating medium system, the temperature at the scale/liquid interface will gradually decrease when scale builds up. This will lead to a natural decrease in the rate of scaling.

6.3.3 Tube Surface

The structure of the tube surface may be important for the initial nucleation of the scaling process. If cavities of appropriate size are present on the tube surface, scaling crystals nuclei can be retained in the cavity and subsequently grow into crystals. In other words, crystallization sites are available on the tube surface.

Additionally if scaling chemicals precipitate onto the surface via a deposition fouling process, they have to overcome the energy barrier at the tube surface before the particles can get to the wall

(Ruckenstein and Prieve, 1973; Spielman and Friedlander, 1974; Dahneke, 1973; Bowen et. al., 1976). This energy barrier is the result of London-van der Waals and electrical double layer interaction forces. The latter can be attractive or repulsive depending on the charges of the particles and wall. Whereas London-van der Waals forces are always attractive.

6.3.4 Water Chemistry

Water chemistry is the primary factor which controls scaling. If the water is supersaturated with scaling-potential chemicals, then the water is likely to foul the heat exchanger. The primary driving force is therefore the degree of supersaturation of scaling chemicals. The degree of supersaturation of a specific scaling chemical is governed by temperature, pH, dissolved solids and other chemical species present. For example, $CaCO_3$ supersaturation is strongly controlled by pH which determines the concentration distribution of $H_2CO_3^*$, HCO_3^- and CO_3^{2-} species as described in chapter 3. If the solubility product of $CaCO_3$ is exceeded, the water is supersaturated with $CaCO_3$. The presence of other hardness species such as Mg also alter the degree of supersaturation of $CaCO_3$. The effect of mixtures of salts can be significant due to formation of complex species, hence changing the concentration driving force.

6.4 CALCIUM CARBONATE SATURATION INDEXES

The solubility of calcium carbonate is the primary cause of calcium carbonate scaling in heat exchangers, conversely low concentrations can cause corrosivity of water. Attempts to define corrosivity

and scaling have focused on predicting the ability of the water to deposit $CaCO_3$ films. Several indexes of calcium carbonate saturation have been proposed. The existence of many indexes shows that no single index has proved to be entirely satisfactory. Recently Rossum and Merrill had made an evaluation on six calcium carbonate saturation indexes and discussed the reliability of the indexes for predicting the water's capacity for $CaCO_3$ deposition or dissolution. (Rossum and Merrill, 1983).

6.4.1 Langelier Index (LI)

This is the most commonly used index. Langelier (1936) developed the concept of a Saturation index, often referred to as the Langelier Index (LI) to characterise a water as to whether it is scale forming or scale dissolving.

$$LI = pH_{actual} - pH_s \qquad (6-13)$$

The pH_{actual} value is the pH value of the water. pH_s is defined by Langelier as 'pH value at saturation' to mean that theoretical pH value at which in water of a given alkalinity and calcium content would be just saturated with $CaCO_3$.

$[CO_3^{2-}]$ can be expressed in terms of measured alkalinity (Equation (3-48)) and substituted into the calcium carbonate solubility product equation. The corresponding $[H^+]$ to satisfy calcium carbonate saturation is calculated as pH_s. The trial pH_s can be calculated from the equation.

$$pH_s = pK_2 - pK_{sp} + p[Ca^{2+}] +$$
$$p([Alk] - [OH^-]_s + [H^+]_s) + \log(1+2K_2/[H^+]_s) - \log f_m \quad (6-14)$$

where

[Alk]   is the total alkalinity in equivalents per litre

$[\ ]_s$ designates a saturated molar concentration

For most waters, a number of simplifying assumptions can be made in specific pH ranges:

(1) For $9.5 < pH < 10.3$, hydrogen and hydroxide ion concentrations are negligible in the term $([Alk]-[OH^-]_s + [H^+]_s)$.

$$pH_s = pK_2 - pK_{sp} + p[Ca^{2+}] + p[Alk]$$

$$+ \log(1+2K_2/[H^+]_s) - \log f_m \quad (6-15)$$

This equation has to be solved by an iterative technique

(2) For $6.5 < pH < 9.5$, the term $2K_2/[H^+]_s$ is negligible.

$$pH_s = pK_2 - pk_{sp} + p[Ca^{2+}] + p[Alk] - \log f_m \quad (6-16)$$

(3) For $pH < 6.5$ the terms $2K_2/[H^+]_s$ and $[OH^-]_s$ are negligible.

$$pH_s = pK_2 - pK_s + p[Ca^{2+}] + p([Alk] + [H^+]_s) - \log f_m \quad (6-17)$$

Again pH_s has to be solved by an iterative technique.

A positive LI indicates that the water is scale forming, a negative LI indicates that the water is scale dissolving.

Snoeyink and Jenkins (1980) have redefined pH_s as the pH of the system if saturated with $CaCO_3$ at the measured calcium and bicarbonate concentrations instead of basing the index on alkalinity. This simplifies the calculation of pH_s. According to Rossum and Merill (1983), such an index (LI_n) better relates to a water's capacity to precipitate $CaCO_3$ than the LI index.

6.4.2 Ryznar Stability Index (RI)

Ryznar Stability Index was proposed by J.W. Ryznar (1944) as an empirical index to indicate the state of water. The index is equal to $2pH_s - pH$ where pH_s is the Langelier Saturation pH and pH is the measured pH value of the water. Ryznar correlates this index with experimental results as well as field data and concluded that below 6.0 the water is scale-forming while beyond 7.0 the water is corrosive. Therefore, the water is considered stable between index number of 6.0 and 7.0.

6.4.3 Driving Force Index (DFI)

This is defined as

$$DFI = \frac{[Ca^{2+}][CO_3^-]}{K_{sp}}$$

(6-18)

A DFI of 1.0 indicates the water is saturated with $CaCO_3$. A number

greater than 1.0 indicates supersaturation, whereas a number less than 1.0 denotes an undersaturated water.

6.4.4 Aggressiveness Index (AI)

This index was developed for asbestos - cement pipe and water temperatures in the range of 4°C-27°C. It is defined as:

$$AI = pH + \log_{10}\{Ca^{2+}\}\{Alk\} \qquad (6-19)$$

where {} is designated for concentration of the component in mg $CaCO_3$ /L.

Waters with an AI less than 10 are aggressive, between 10 and 12 waters are moderately aggressive, and waters which exceed an AI of 12 are considered to be non aggressive.

6.4.5 Momentary Excess (ME)

This index was developed by J.F. Dye (1952) and stated that ME was equal to the moles of $CaCO_3$ that must precipitate to satisfy the following equation:

$$([Ca^{2+}] - ME)([CO_3^{2-}] - ME) = K_{sp} \qquad (6-20)$$

A positive ME denotes a supersaturated water, a negative ME denotes a corrosive water, and a zero ME denotes a water saturated with $CaCO_3$.

6.4.6 Calcium Carbonate Precipitation Potential (CCPP)

This index has been used by Merrill and Sanks (Merrill, 1976; Merrill and Sanks, 1977a; 1977b; 1978) to indicate theoretical quantity of $CaCO_3$ that can precipitate from supersaturated waters or are dissolved by undersaturated waters. During the process of precipitation the concentrations of calcium and carbonic species change. Therefore the equilibrium concentrations at the end of the process will not be the same as described by pH_s of the Langelier Index which assumes the initial calcium concentration and the initial total alkalinity.

During $CaCO_3$ precipitation, the equivalents of calcium carbonate precipitated is equal to alkalinity precipitated (Lowenthall and Marais, 1976). An equal number of equivalents of calcium and alkaline are precipitated as calcium carbonate. Therefore, at equilibrium

$$2(.[Ca^{2+}]_i - [Ca^{2+}]_{eq}) = Alk_i - Alk_{eq} \qquad (6-21)$$

where $[Ca^{2+}]_i$ and $[Ca^{2+}]_{eq}$ are initial and equilibrium calcium molar concentrations.

Alk_i and Alk_{eq} are initial and equilibrium total alkalinity in equivalents per litre.

The index is expressed as follows:

$$CCPP = 50000 (Alk_i - Alk_{eq}) \qquad (6-22)$$

where CCPP is in $mg/CaCO_3$

Alk_{eq} has to be calculated by trial and error from the following

equations:

$$2[Ca^{2+}]_i - Alk_i = \frac{2K_{sp}r_{eq}P_{eq}}{t_{eq}(Acy_i - S_{eq})} - \frac{t_{eq}(Acy_i - S_{eq})}{P_{eq}} + S_{eq} \qquad (6-23)$$

$$r_{eq} = \frac{[H^+]_{eq} + 2k_2}{k_2} \qquad (6-24)$$

$$S_{eq} = [H^+]_{eq} - \frac{k_w}{[H^+]_{eq}} \qquad (6-25)$$

$$P_{eq} = \frac{2[H^+]_{eq} + K_1}{K_1} \qquad (6-26)$$

$$t_{eq} = \frac{2K_2 + [H^+]_{eq}}{[H^+]_{eq}} \qquad (6-27)$$

$$Acy_i = Acy_{eq} = (\frac{Alk_{eq} + S_{eq}}{t_{eq}})P_{eq} + S_{eq} \qquad (6-28)$$

$$Alk_{eq} = \frac{t_{eq}}{P_{eq}}(Acy_i - S_{eq}) - S_{eq} \qquad (6-29)$$

where Acy_i and Acy_{eq} are initial and equilibrium acidity in equivalents per litre. A positive CCPP denotes a supersaturated water, a negative value denotes an undersaturated water and a zero value denotes a saturated water. According to Rossum and Merrill, CCPP is the best index to describe $CaCO_3$ precipitation and dissolution. It is also directly related to the rate equation of calcium carbonate precipitation in the form such as proposed by Reddy (Equation (4-15)).

6.4.7 Comparison of Indexes

The prediction of water corrosivity and scale-forming potential by the indexes can be best realised by calculating their values on the actual waters. Two water samples from Lake Liddell experiment (see chapter 7) and two water samples from Ryznar's report (Ryznar, 1944) are used. The values of water quality and indexed calculated are tabulated in Table (6-1).

The values of free calcium cation, $[Ca^{2+}]$, free carbonate anion $[CO^{2-}]$ and the divalent activity coefficient for the indexes calculation can be obtained from the programme PROG-CMSS developed in chapter 3. The values of calcium carbonate precipitation potential (CCPP) were calculated based on the iterative procedure mentioned by Rossum, et. al. (1983).

From Table (6-1), all the indexes except R.I. and A.I. are consistent in predicting the quality of the water samples. The indexes such as L.I., R.I. and D.F.I. only indicate the state of water that is whether the water has a corrosive tendency or a scale-forming tendency. They do not calculate the quantity of calcium carbonate that will be dissolved or precipitated theoretically. However, indexes such as A.I., M.E. and CCPP not only indicate the state of water, but give the theoretical quantity of calcium carbonate that will be dissolved or precipitated out.

A.I. is less reliable because of its empirical nature of the equation (see Equation (6-19)). This is also indicated by the values shown in Table (6-1). Although the values of M.E. follow the similar

TABLE 6-1   The Comparison of Calcium Carbonate Indexes

Water Quality \ Water Sample	Lake Liddell Expt. 5	Lake Liddell Expt. 7	La Grange, 111 Well Water	La Grange, 111 Well Water
Total Calcium (ppm $CaCO_3$)	264	331	526	526
Total Magnesium (ppm $CaCO_3$)	261	344	326	326
Total Alkalinity (ppm $CaCO_3$)	126	362	397	397
Sulphate (ppm SO_4^{2-})	480	663	450	450
Chloride (ppm Cl^-)	346	328	51	51
Temperature ($^\circ$C)	24.7	25.5	15	60
pH	7.90	8.52	6.8	6.8
L.I.	0.28	1.37	-0.23	0.56
R.I.	7.34	5.78	7.26	5.68
D.F.I.	1.86	22.2	0.59	3.64
A.I. (ppm $CaCO_3$)	12.3	13.4	12.0	12.0
M.E. (mole/L $CaCO_3$)	6.62×10^{-6}	1.72×10^{-4}	-2.00×10^{-6}	4.12×10^{-6}
CCPP (ppm $CaCO_3$)	4.3	56.6	-44.4	96.8

direction compared to CCPP and other indexess, it is based on a less rigorous theoretical basis compared to CCPP. Hitherto, CCPP is the best index to describe calcium carbonate precipitation and dissolutions (Rossum and Merrill, 1983) for the value not only indicates the state of water, but also suggests a theoretical quantity of calcium carbonate precipitation and dissolution. The values of these indexes are a good starting point to predict the impact of water onto heat exchangers. However a more rigorous treatment is required in order to predict the behaviour of the water more precisely because of other physical factors involved such as temperature, tube surface and velocity of the fluid. In fact one major approach of modeling of calcium carbonate scaling in the heat exchangers follows the line of empirical growth rate equation of the scale in the form of Arrhenius rate equation with little or no emphasis on the chemistry of the water (Knudsen and Story, 1975; Morse and Knudsen, 1977). The review of calcium carbonate scaling models are given in the following section.

6.5 LITERATURE REVIEW ON CALCIUM CARBONATE SCALING (PRECIPITATION FOULING)

The first fouling study published is on chemical deposition in evaporators by McCabe and Robinson (1924). They proposed the mathematical model under constant heat flux:

$$d(\frac{1}{U}) \ / \ d\theta \ = \ K_{(6-30)} U \tag{6-30}$$

$$\frac{1}{U^2} \ = \ \frac{1}{U_i^2} + K_{(6-31)} \theta \tag{6-31}$$

where U is the overall heat transfer coefficient

U_i is the initial (clean tube) overall heat transfer coefficient

$K_{(6-30)}$, $K_{(6-31)}$ are constants

θ is time

Rewritting Equation (6-31) in terms of the fouling resistance R_f

$$R_f = [(1 + K_{(6-31)} U_i^2 \theta)]^{1/2} - 1] / U_i \qquad (6-32)$$

With this equation the fouling resistance is increased with time.

After the Kern-Seaton model which also considered the removal process was published, Hasson (1962) published a general expression for the tube side fouling assuming that:

$$d(\frac{1}{U})/d\theta = K_{(6-33)} U^a \qquad (6-33)$$

$$dR_f/d\theta = K_{(6-34)} q(t_b - t_{in})^{a-1} \qquad (6-34)$$

therefore

$$\frac{1}{U^{a+1}} = \frac{1}{U_i^{a+1}} + K_{(6-35)} (a+1)\theta \qquad (6-35)$$

where $K_{(6-33)}$, $K_{(6-34)}$, $K_{(6-35)}$ are constants

q is the heat flux

t_b is the bulk temperature

t_{in} is inlet water temperature.

The experimental data fitted to this model resulted in a value of 2.5 for a at low velocity. With higher velocity such as 1m/s, the removal process became important. However Hasson suggested that the use of a higher value a would correlate the higher velocity data with the low velocity data confirming the unlimited growth model.

Hasson also proposed the deposition process of $CaCO_3$ based on the diffusion theory of crystallization,

$$\frac{dW}{d\theta} = K_G A (c_b - c_s)$$
(6-36)

where A is the surface

  K_G is the overall growth rate

  c_b is the bulk concentration

  c_s is the saturated concentration

Assuming a first-order surface reaction.

$$\frac{1}{K_G} = \frac{1}{K_d} + \frac{1}{K_r}$$
(6-37)

where K_d is the mass transfer coefficient

  K_r is the surface reaction rate coefficient for the $CaCO_3$

    molecules to be arranged into crystal lattice

K_d is evaluated empirically by

$$Sh = K_d d/D = 0.023 Re^{0.83} Sc^{0.53}$$
(6-38)

and

$$K_r = K_{(6-39)} \exp[-E/(RT_s)] \qquad (6-39)$$

where Sh is the Sherwood number

d is the particle diameter

D is the molecular diffusivity

Re is the Reynolds number

Sc is the Schmidt number

$K_{(6-39)}$ is a constant

E is the activation energy

R is the universal gas constant

T_s is the surface temperature, $^{\circ}K$

At low velocity, the experimental data fitted well. At higher velocity the model breaks down because of the absence of a removal term and also the crystallization process tends to be surface reaction controlled. The reaction was suggested to be second order by Nancollas and Reddy (Reddy and Nancollas, 1971; Nancollas and Reddy, 1971).

Reitzer (1964) developed the fouling rate equation based on the inverse solubility of the salt, crystallization velocity, scale properties and heat transfer conditions. He introduced the linear relationship of concentration of inversely soluble salt with temperature.

$$c = K_{(6-40)} - bt \qquad (6-40)$$

where c is concentration

$K_{(6-40)}$ is a constant

b is the slope of the solubility curve

t is the temperature

which leads to

$$s = b(t_s - t_b) \tag{6-41}$$

where s is the supersaturation

t_s is the temperature at inner surface of scale

t_b is the temperature of the liquid in the tube

with the general crystal growth expression

$$\frac{dW}{d\theta} = K_G A s^n \tag{6-42}$$

and

$$\frac{1}{U} = \frac{1}{U_i} + \frac{x_f}{k_f} \tag{6-43}$$

the rate of increase of scale thickness is

$$\frac{dx_f}{d\theta} = \frac{K_G b^n}{\rho_f} (t_s - t_b)^n \tag{6-44}$$

with constant Δt, he derived the final equation

$$\frac{1}{U^{n+1}} = \frac{1}{U_i^{n+1}} + (n+1) \left(\frac{K_G}{k_f \rho_f}\right) \left(\frac{b\Delta t}{h_i}\right)\theta \tag{6-45}$$

where K_G is the combined of diffusion-reaction mass transfer coeffi-
cient

k_f is the thermal conductivity

Δt is the total temperature drop from heating to cooling medium

ρ_f is the scale density

when n=1, Equation (6-44) becomes

$$\frac{1}{U^2} = \frac{1}{U_i^2} + \frac{2bK_G\Delta t}{\rho_f k_f h_i}\theta \qquad (6-46)$$

which is similar to $\frac{1}{U^2} = \frac{1}{U_i^2} + \beta\theta$ derived by McCabe and Robinson where

β is a constant.

Under constant heat flux condition the final equation becomes

$$\frac{1}{U} = \frac{1}{U_i} + \frac{K}{\rho_f} k_f \left(\frac{b}{h_i}\right)^n \left(\frac{q}{A}\right)^n \theta \qquad (6-47)$$

where q is the heat load.

For unsaturated solutions, the final equation derived is

$$\frac{1}{U} = \frac{1}{U_i} + \frac{K_G}{\rho_f} k_f \left[(c_1 - c'_1) + \frac{b}{h_i}\frac{q}{A} \right]^n \theta \qquad (6-48)$$

where c_1 is the concentration of liquid and c'_1 is the hypothetical concentration of liquid saturated with scaling component at t_1.

Hasson (1968) measured the rate of $CaCO_3$ scale deposition on the surface of annular constant heat flux exchanger, with the scale surface temperature maintained constant irrespective of scale layer thickness. Effects of flow velocity, scale surface temperature and

water composition were examined according to the rate model presented. The rate model considered the mass transfer of HCO_3^- and Ca^{2+} toward the reaction surface and followed by surface reaction between Ca^{2+} and CO_3^{2-} to form $CaCO_3$. The backward diffusion rate of dissolved CO_2 formed during the reaction is also taken into account.

Overall reactions occurring in the crystallization of $CaCO_3$ scale are represented by

$$2HCO_3^- \longrightarrow CO_3^{2-} + CO_2 + H_2O \qquad (6-49)$$

$$Ca^{2+} + CO_3^{2-} \longrightarrow CaCO_3(s) \qquad (6-50)$$
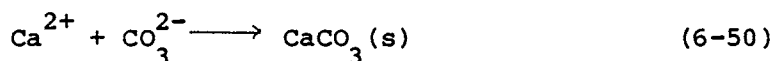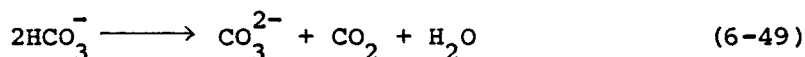
mass transfer coefficient was obtained from heat transfer correlation derived experimentally,

$$\frac{h_i D_e}{k_w} = 0.0608 \, (Re)_f^{0.716} \, (Pr)_f^{1/3} \qquad (6-51)$$

where D_e is the equivalent diameter of annular flow passage

$(Re)_f$ is the Reynolds number of water based on average film temperature

$(Pr)_f$ is the Prandtl number of water based on average film temperature

k_w is the thermal conductivity of water

combined with j-factor analogy between heat and mass transfer

$$\frac{K_d}{h_i} = (\frac{1}{C_p \rho}) \cdot (Pr/Sc)_f^{2/3} \qquad (6\text{-}52)$$

where C_p is the specific heat of water

ρ is the density of water

$(Sc)_f$ is the Schmidt number based on average film thickness

K_d is the mass transfer of the species considered

The experiment was carried out at surface temperatures $67^{\circ}C$ to $85^{\circ}C$ and Reynolds numbers from 13,000 to 42,000. $CaCO_3$ deposition is mainly controlled by the forward diffusion rate of Ca^{2+} and HCO_3^- ions. In certain cases it is also controlled by the backward diffusion rate of dissolved CO_2 formed during the reaction.

Taborek et. al. (1972a, 1972b) reviewed the mechanisms of fouling and established a mathematical model verified by a massive data bank accumulated by Heat Transfer Research Incorporated (HTRI). The model also includes a removal term, probability function of the scale as well as the water characterization factor to account for the effect of water chemistry.

For

$$\frac{d(x_f/k_f)}{d\theta} = \phi_d - \phi_r$$

$$\phi_d = K_{(6\text{-}53)} P_d (\Omega)^n \exp(-E/RT_s) \qquad (6\text{-}53)$$

$$\phi_r = K_{(6\text{-}54)} \frac{\tau}{\psi} x_f^m \qquad (6\text{-}54)$$

where $K_{(6-53)}$ and $K_{(6-54)}$ are constants

P_d is the probability function

Ω is the water characterization factor which is a function of Langelier Index

ψ is a function of the deposit structure

τ is the shear stress of the flow

m is a constant to be determined experimentally

x_f is the thickeness of deposit

k_f is the thermal conductivity of deposit

ϕ_d is the rate of deposition

ϕ_r is the rate of removal

Equation (6-53) is derived from the general reaction controlled expression

$$K_{(6-53)} \; K_r \; (c_r)^n$$

where c_r is the reaction concentration described by P_d and Ω. If $m=1$, equations (6-22) and (6-23) can be combined

$$\frac{x_f}{k_f} = R_f = R^*_f (1-e^{-B'\theta}) \tag{6-55}$$

$$\text{where} \quad R^*_f = \frac{K_{(6-53)} \; P_d \; (\Omega)^n \; \exp(-E/RT_s)}{k_f \; K_{(6-54)} \; \tau/\psi} \tag{6-56}$$

$$\text{and} \quad B' = K_{(6-54)} k_f \frac{\tau}{\psi} \tag{6-57}$$

Watkinson and Martinez (1975) studied scaling of calcium carbonate inside copper tubes. The scaling process was studied under accelerated scaling conditions. They also derived the mathematical model based on Kern-Seaton model. The deposition term was a generalization of the Reitzer model,

$$\frac{dx_f}{d\theta} = \frac{K_r}{\rho_f} (c - c_i)^n \tag{6-58}$$

where K_r is crystallization rate constant in terms of wall temperature t_w and including a removal term:

$$\frac{dx_f}{d\theta} = \frac{K_r}{\rho_f} \left[\frac{b (t_w - t_b)}{1 + h_i x_f / k_f} \right]^n - K_{(6-40)} \tau \, x_f \tag{6-59}$$

where a is a constant and $\tau = f v^2 \rho / 2$.

The asymptotic fouling resistance can be obtained by setting $\frac{dx_f}{d\theta}$ = 0 in Equation (6-58) and putting $R_f^* = x_f / k_f$.

$$R_f^* (1 + R_f^* h_i)^n = \frac{2 \, b^n K_r \, (t_w - t_b)}{K_{(6-40)} k_f \, f v^2 \rho_f \rho} \tag{6-60}$$

Knudsen and story (1975) studied the effect of heat transfer surface temperature on the scaling behaviour of simulated cooling tower water using equations (6-55), (6-56) and (6-57). Under constant heat flux condition, they derived the final results on asymptotic fouling resistance with respect to surface temperature:

$$R_f^* = (3 \times 10^{11}) \ \exp(- 11000/RT_s) \qquad (6-61)$$

The coefficient (3×10^{11}) is specific for the experiments carried out and embodies the velocity, water quality, and scale properties which were constants for all runs.

Morse and Knudsen (1977) investigated the effect of alkalinity on the scaling of simulated cooling tower water also based on the Taborek et. al. (1972a, 1972b) model. They noticed that there was frequently a delay time between the start of the run and the formation of deposit. Therefore, in order to fit the data to Equation (6-55), the equation was modified to the form

$$R_f = R_f^* \ [1 - \exp(-(\theta-\theta_D)/\theta_c)] \qquad (6-62)$$

where θ_D is the delay time

$\theta_c = 1/B'$ is the time constant where $B' = K_{(6-54)} k \frac{\tau}{f\phi}$

The alkalinities studied were from 115 to 187 mg/L $CaCO_3$. Flow rate, bulk and surface temperatures were maintained constant for all runs. The velocity was 1.04 m/s through the annular section. Surface temperature was around 70° C. Exact correlation of alkalinities and fouling resistance could not be established. They concluded that the actual effect of alkalinity is complex since changing alkalinity will change water quality and also will change the composition of the deposited scale.

Hasson et. al. (1975) considered the kinetic of $CaCO_3$ crystallization and mass transfer of ionic species. The approach is similar to the diffusion theory of crystallization which leads to the general crystal growth rate equation:

$$\frac{1}{A}\frac{dW}{d\theta} = K_d (c_b - c_i) \qquad (6-63)$$

$$= K_r (c_i - c_s)^z \qquad (6-64)$$

$$= K_G (c_D - c_s)^n \qquad (6-65)$$

where A is the surface area

c_b is the bulk concentration of the species

c_i is the interfacial concentration

c_s is the saturated concentration

K_d is mass transfer coefficient

K_r is surface reaction coefficient

K_G is the overall growth rate

z,n is the order of reaction for surface controlled and overall reaction respectively

In Hasson's paper, Equation (6-64) became

$$\frac{1}{A}\frac{dW}{d\theta} = K_r \{ [Ca^{2+}]_i [CO_3^{2-}]_i - K_{sp}' \} \qquad (6-66)$$

as the crystallization rate equation well established (Reddy and Nancollas, 1971; Nancollas and Reddy, 1971; Grazit and Hasson, 1975; Wiechers, et. al., 1975).

Equation (6-63) became

$$\frac{1}{A}\frac{dW}{d\theta} = K_d\{ [CO_3^{2-}] - [CO_3^{2-}]_i \} = K_d\{ [Ca^{2+}] - [Ca^{2+}]_i \} \qquad (6-67)$$

Combine equations (6-65) and (6-67) and calculate K_d which is the convective diffusion coefficient of $CaCO_3$ from correlation (Linton and Sherwood, 1950).

$$\frac{K_d}{v} Sc^{2/3} = 0.023 Re^{-0.17} \qquad (6-68)$$

where v is the flow velocity in tube

Re is the Reynolds number

Sc is the Schmidt number

The final simplified equation, with the unknown interfacial concentrations eliminated from equations (6-65) and (6-67),

$$\frac{1}{A}\frac{dW}{d\theta} = K_d [CO_3^{2-}] \left[\frac{1 - \dfrac{K'_{sp}}{[Ca^{2+}][CO_3^{2-}]}}{1 + \dfrac{K_d}{K_r [Ca^{2+}]} + \dfrac{[CO_3^{2-}]}{[Ca^{2+}]}} \right] \qquad (6-69)$$

for pH. The chemical species were calculated from the chemistry of CO_2 - H_2O system. K'_{sp} is the solubility product of $CaCO_3$ after temperature and total dissolved solids correction.

For low pH values, the diffusion equations are

$$\frac{1}{A}\frac{dW}{d\theta} = \frac{K_d}{2} \{ [HCO_3^-] - [HCO_3^-]_i \}$$
$$= K_d \{ [CO_2]_i - [CO_2] \}$$
$$= K_d \{ [Ca^{2+}] - [Ca^{2+}]_i \} \qquad (6-70)$$

The final simplified equation is

$$\frac{1}{A}\frac{dW}{d\theta} = K_d[CO_3^{2-}]\left[\frac{1 - K_{sp}'/[Ca^{2+}][CO_3^{2-}]}{\dfrac{K_d}{K_r[Ca^{2+}]} + \dfrac{4\,[CO_3^{2-}]}{[HCO_3^-]} + \dfrac{K_{sp}'}{[Ca^{2+}][CO_2]}}\right] \qquad (6-71)$$

This rate of deposition equation was tested on data published by Morse and Knudsen. θ_c from Equation (6-62) is a good indicator of the strength of scale. Generally a large value corresponds to deposits mainly consisting of $CaCO_3$. The deposit is highly tenacious. The deposition equation was tested on large θ_c runs with good agreement. This deposition model therefore is able to predict the fouling rate due to $CaCO_3$ deposition on a heat exchanger tube under various flow and supersaturated conditions, without significant removal of $CaCO_3$ scale.

Steinberg and Hasson (1979) studied the scaling process by considering bulk precipitation tendency of brine circulating in the desalination plant. The population balance model (Randolph and Larson, 1971) was used to analyse the effects of brine circulation characteristics, retention time and supersaturation level on the degree of scale precipitation under mixed flow and plug flow conditions. They found that the mixed flow condition enhanced scaling potential. The induction period in mixed flow system was found to be shorter than plug flow system under similar supersaturation level and retention time. The following equations were used to derive the final equations for mixed flow and plug flow:

$$n = n^o \exp(-L/G\,\dot{\theta}_m) \qquad (6-72)$$

where n is particles population density (=dN/dL) where dN is the

number of particles between size L and L+dL

n^O is the nuclei population density

θ_m is the retention time defined by ratio of brine volume over

brine flow rate.

$$\theta_m = V/q \qquad\qquad (6-73)$$

$$B^O = n^O G \qquad\qquad (6-74)$$

$$B^O = K_N (c - c_s)^i \qquad\qquad (6-75)$$

$$G = K_G (c - c_s)^a \qquad\qquad (6-76)$$

where B^O is the nucleation rate

G is the linear growth rate

K_N and K_G are kinetic coefficients

i and a are empirically determined orders of the respective

processes.

The above equations lead to the final equations:

$$\frac{X}{(1 - X)^{i+3a}} = \left(\frac{\theta_m}{\theta_o}\right)^4 \qquad\qquad (6-77)$$

where $X = \dfrac{c_o - c}{c_o - c_s}$

θ_o is the characteristic time constant given by

$$\theta_o^4 = (c_o - c_s)^{3a+i-1} (6\alpha_v\rho\ K_N\ K_G^3) \qquad (6\text{-}78)$$

where c_o is incoming concentration

α_v is the particle volume shape factor

ρ is the particle density

For plug flow system, the differential population balance equations cannot be solved analytically, except for the limiting condition of a very low degree of precipitation (X<<1). The final result is

$$\frac{24X}{(1-X)^{i+3a}} = \left(\frac{\theta_p}{\theta_o}\right)^4 \qquad (6\text{-}79)$$

where θ_p is the retentin time of plug flow system.

6.6   CONCLUSIONS OF CHAPTER 6

Because calcium carbonate scaling in the heat exchangers is basically a chemical precipitation of calcium carbonate from the supersaturated water onto the heat transfer surface, the mathematical models based on the principles of calcium carbonate precipitation will be less empirical in nature. This can be realised from Hasson's model (Hasson, et. al., 1978). It is also realised that the water supersaturated with calcium carbonate will not generate scale· in the heat exchanger provided the degree of supersaturation exceeds a certain critical level. This is apparent in the power station cooling water practice which allows a positive Langelier Index (LI) of 1 as the maximum (Pincus,

1962). To test the validity of this practice and also the roles of other factors when using Langelier Index to monitor the quality of the cooling water for the scale-free operation of the power station cooling water system, the following chapter is devoted in setting up the pilot scale experiment on Lake Liddell power station cooling water.

CHAPTER 7

INVESTIGATION OF SCALING POTENTIAL OF LAKE LIDDELL WATER

TO POWER STATION CONDENSER TUBES

7.1 INTRODUCTION

Lake Liddell Power Station is one of the largest power stations installed by the NSW Electricity Commission. This base load station consists of four sets of 500 MW generators and is able to generate 2000 MW of electricity at full capacity. Each set of water cooling condensers used with a 500 MW generating set is one of the world's largest mass and heat transfer devices. It condenses steam from the turbine exhaust at low pressure and hence at low temperature, which ensures that the maximum amount of heat is extracted from the steam. The source of cooling water is an artificial cooling pond next to the station with an area of 1100 hectares. The water is circulating continously through the condenser tubes and back to one pond to dissipate heat. Water lost through evaporative cooling is replaced by natural inflow and by pumping from the nearby Hunter River. An investigation had been carried out to determine the scaling potential of Lake Liddell water to power station condenser tubes. The power station at the time of investigation was operated at positive Langelier Index (LI) of +1 as the maximum, which complied with the usual cooling water practice (Pincus, 1962). This was achieved by controlling the methyl orange alkalinity (total alkalinity) of the lake by dosing sulphuric acid. Owing to the size of the pond, the

sulphuric acid dosage required to control M.O. alkalinity is enormous. For example, it requires 4,670 tonnes of sulphuric acid to reduce the lake M.O. alkalnity from 130 p.p.m. to 100 p.p.m. The water quality during the time of investigation is given in Table (7-1).

TABLE 7-1   Data of Lake Liddell Water for 1979-1980

	Range	Typical
M.O. ALkalinity (mg/L $CaCO_3$)	97-134	118
Ca hardness (mg/L $CaCO_3$)	174-260	206
Total hardness (mg/L $CaCO_3$)	396-494	436
Sulphate (mg/L SO_4^-)	250-460	349
Chloride (mg/L Cl^-)	120-216	184
pH	7.7-9.1	8.2
Conductivity (μs/m) x 100	1270-1690	1370

Since Langelier Index (LI) was used to monitor the scaling potential of the lake water, the investigation was to determine experimentally the margins of reliability of the Langelier Index for scaling control of the condensing system. The requirement of sulphuric acid dosage could be calculated accordingly. This investigation was carried out by a test rig constructed to simulate the Lake Liddell power station condensing system as described in the next section. It was intended that these results would provide minimum sulphuric acid addition to Lake Liddell and hence minimum sulphate addition to the Hunter River without adverse effects on power generation due to loss of thermal conductivity.

7.2 EXPERIMENTAL

7.2.1 Experimental Design

Hawthorn and Perry (1980) of Central Electricity Generating Board of Midland Region, United Kingdom, had reported their investigation of tri-calcium phosphate fouling in power station condenser tubes where the cooling water was drawn from the River Trent. It was confirmed that the only reliable approach was to build a test rig and carry out investigations with actual water used in the stations. Based on their experience, a test rig was to be constructed to consist of heating and cooling systems.

TABLE 7-2 Rig Modelling Factors

Parameter	Full Scale	Model	Factor
Temperature Rise			
Winter	$16 - 25^{\circ}$ C	$16 - 25^{\circ}$ C	1
Summer	$26 - 36^{\circ}$ C	$26 - 36^{\circ}$ C	1
Tube	Al-Brass 25.4 mm OD	ex. Stock	1
Tube Length	14.5 m	3.5 m	1/4
Water Flow Rate	1.5-2.0 m/s	0.5 m/s	1/4
Water Supply	Lake Liddell	Lake Liddell	1
Heat Flux	20-26 kW/m^2	26 kW/m^2	1
Residence Time	7 s	7 s	1

Obviously it is not possible to simulate every aspect of the actual system in the power station. Nevertheless caution was taken to scale down the system to a manageable size without having to trade off

features that are important to scaling. The test rig was scaled down according to Table (7-2).

The velocity of the cooling water flow was reduced to 25% of the original flow rate in order to maintain the residence time, heat flux and temperature rise as in the actual plant. Fortunately, this velocity still falls into the region of turbulent flow as required for convective heat transfer in a heat exchanger. The slower velocity is thought to be more conducive for scale growth because of lower velocity shear stress on the tube wall. The rig is shown schematically in Figure (7-1).

7.2.2 Experimental Apparatus

7.2.2.1 Heating System

Instead of the low pressure condensing system in the power station, hot water was used as the heating medium to achieve a similar heat flux. A 4m length 1" 18 gauge Aluminium Brass condenser tube supplied by the Electricity Commission of New South Wales was surrounded by a hot water jacket with hot water recycled continuously from a 200 litre galvanized drum equipped with 2 x 4 kW heaters. The heaters were single phase stainless steel grade 316 Birko immersion heat (Birko-Electric (Sales) Pty Ltd, Australia). The hot water jacket was a 3.55 m length 200 mm nominal diameter asbestos cement pipe with both ends enclosed. The asbestos cement pipe was supplied by James Hardie and Coy Pty Ltd. The condenser tube was placed in the hot water jacket and secured by pressure fittings on both ends. The pressure fittings were brass hexagonal caps with 1" BSP female thread
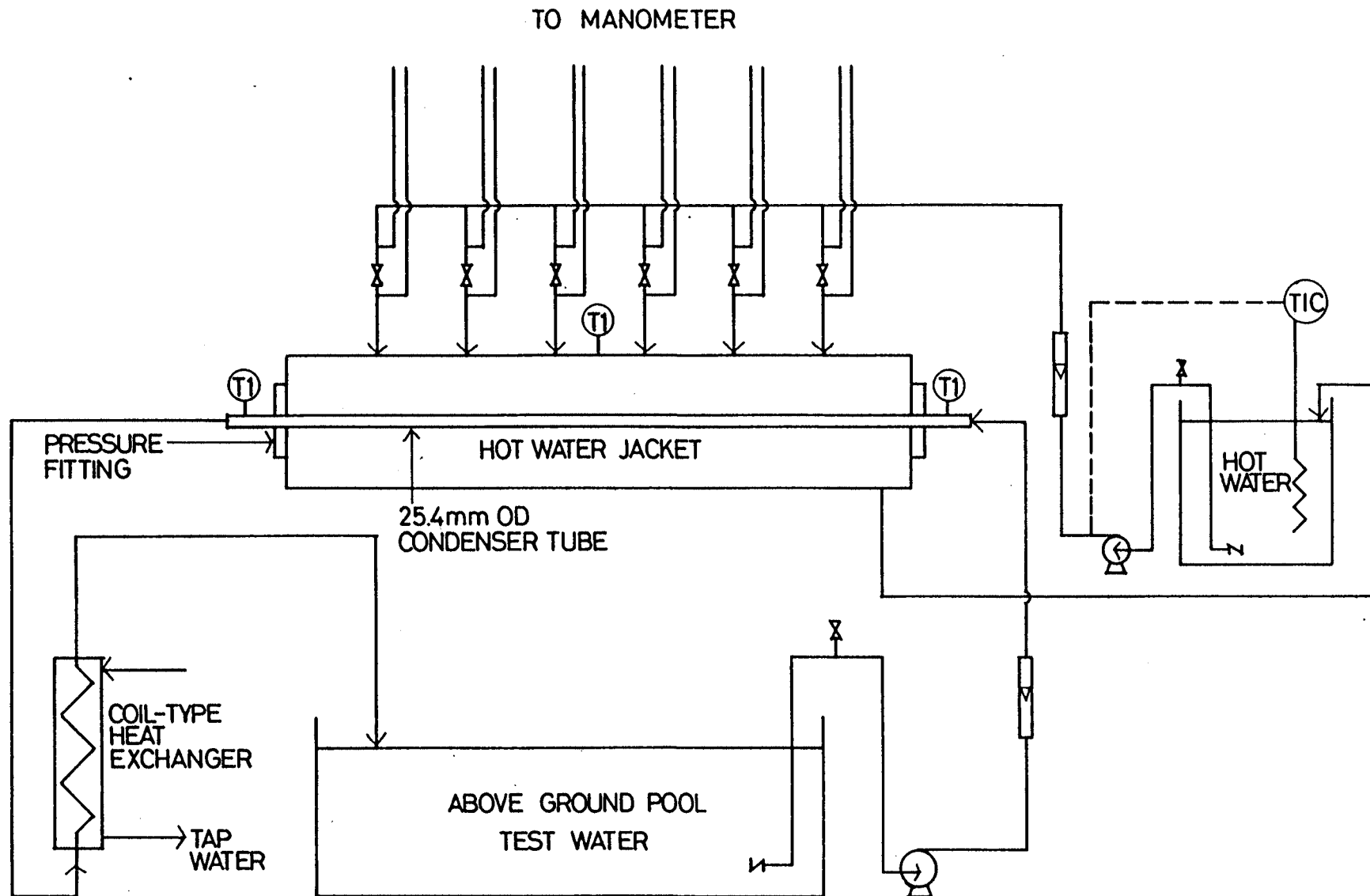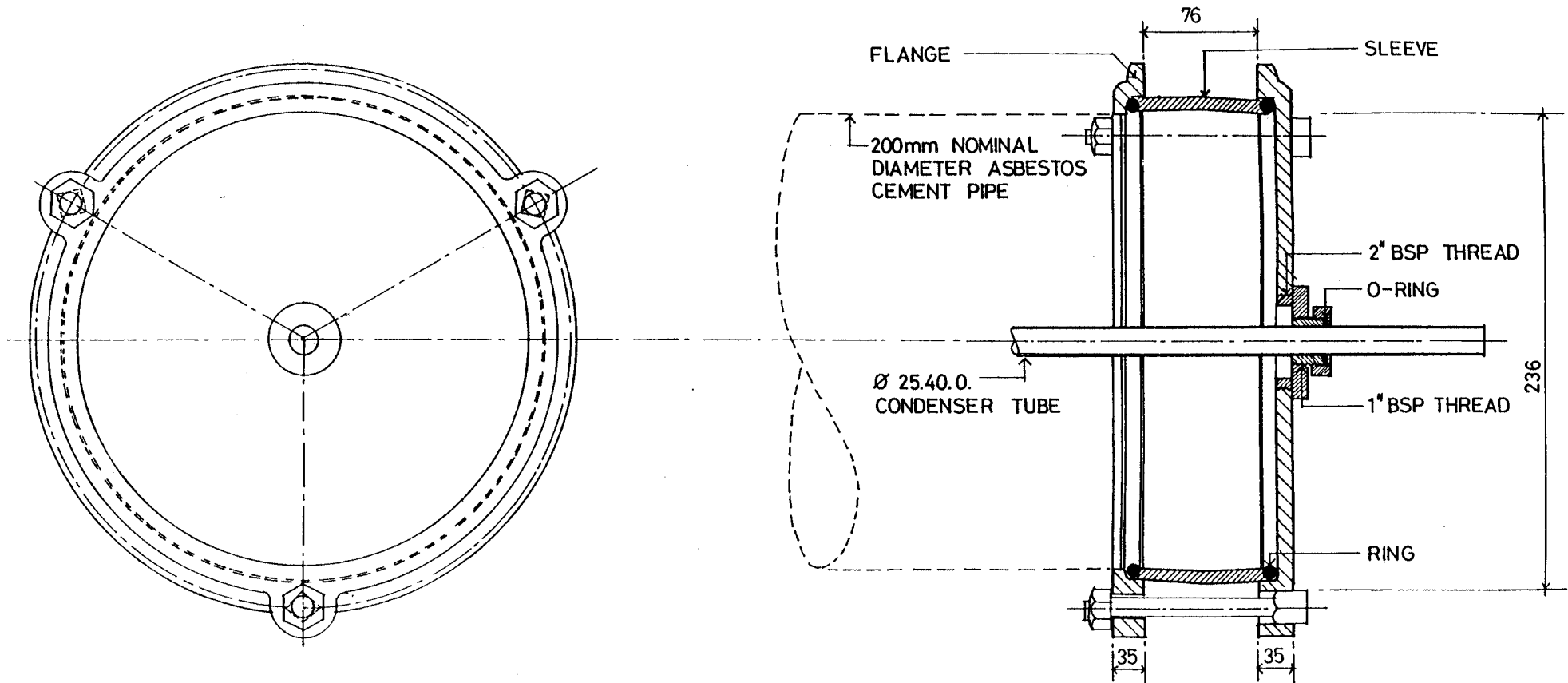
FIGURE 7-1 Schematic Representation of Test Rig

that screwed into a 1" BSP male brass plain nipple with the other end screwed into a 2" brass bush. An O-ring was placed between the hexagonal cap and plan nipple to secure a tight seal. A 1" opening on the hexagonal cap was available for the tube to move through the hot water jacket. Two Gibault fittings designed by the supplier, James Hardie and Coy Pty Ltd were used for both ends of the asbestos cement pipe. The fitting had a 2" BSP tapping to receive the pressure fitting. The whole arrangement made up the hot water jacket and was completely sealed at both ends of the pipe by the O-ring in the hexagonal cap tightened onto the tube. A new condenser tube was used for each experiment. Therefore with this arrangement, the hexagonal cap could be simply unscrewed and the tube removed from the hot water jacket. A drawing is shown in Figure (7-2).

The hot water was pumped into the jacket by a 3/4 hp single phase Volu-flo closed coupled centrifugal pump (Scruttons Pty Ltd, Australia) via 6 hot water regulating valves equally spaced apart. These hot water regulating valves were 1/2" Whitey regulating and shut-off valves (Sydney Valve and Fitting Pty Ltd, Australia) that allowed a precise flow rate to be regulated. The pressure drop across each valve measured by the water manometers was adjusted to achieve similar flow rates into the jacket. Therefore, a fairly uniform bulk temperature of the hot water in the jacket was possible. The bulk temperature of the hot water in the jacket was measured by a Pt100 element 3 wire lead resistance thermometer with 0.01% accuracy supplied by Richard Foot Pty Ltd, Australia. The hot water was pumped at the flow rate of 32 litres per minute at 58° C. The flow rate was measured by a Brass IGU Gapmeter with the measurement range 8-80 L/min (supplied by Duff and MacIntosh Pty Ltd, Australia). The temperature

FIGURE 7-2 Gibault Fittings and Removable Condenser Tube

FLANGE

SLEEVE

76

200mm NOMINAL
DIAMETER ASBESTOS
CEMENT PIPE

2" BSP THREAD

O-RING

Ø 25.40.0.
CONDENSER TUBE

1" BSP THREAD

236

RING

35   35

DIMENSION : mm
NOT TO SCALE

of the hot water was controlled by the temperature controlling unit comprising a West Guardian Q3X temperature controller with scale and calibration 0 to 100° C equipped with proportional, integral and derivative controlled function, a single phase 240 volts thyristor with maximum power of 16,000 watts and a special tolerance copper/constantant thermocuple for the temperature feedback. All these items were supplied by Richard Foot Pty Ltd, Australia. The resulting bulk temperature in the jacket was approximately 55° C. The designed heat flux was achieved when the inlet water was set for summer conditions. A 70 mm immersion mercury thermometer with 0.1° C resolution was installed at both ends of the tube with the thermometer bulb inserted in the flowing water to measure the inlet and the outlet temperatures. The whole heat system was insulated with 1" thick Rockwool insulator supplied by Bestobell Engineering Products. Alfloc 2000 from Catoleum was added to the hot water to serve as a corrosion and scaling control reagent.

7.2.2.2 Cooling System

The cooling system is to cool down the water after passing through the condenser tube and hence maintain the inlet water temperature constant. At the same time the cooling system has to simulate Lake Liddell used as the cooling pond which serves the Liddell power station. In view of these, an above-ground pool with 4.5 m^3 total volume and 7.3 m^2 total surface area supplied by Clark Rubber Ltd, Australia was installed to dissipate the majority of the heat. The rest of the heat was dissipated by a simple coil-type heat exchanger consisting of a 26 m length 1/2" 19 gauge helical copper coil packed in a 1.5 m tall 200 mm I.D. perspex column. The warm

lake water was fed into the bottom of the perspex column, rose up to the top and overflowed into the above-ground pool. A single-passed of tap water was used as the coolant. As a result there was no control over fluctuations of ambient temperature and tap water temperature. Nevertheless, the combination of above ground pool and coil-type heat exchanger was able to maintain the inlet water temperature for summer conditions to within 3°C. The Lake Liddell water was pumped continuously at the flow rate of 12 L/min by a 1/4 hp single phase all bronze Volu-flow closed coupled centrifugal pump supplied by Scruttons Pty Ltd, Australia. The flow rate was measured by a rotameter (Precision Bore Florimeter Tube No. FP-3/4-27-G-10/83 supplied by F & P Pty Ltd, Australia).

7.2.3 Experimental Procedure

The cooling water (Lake Liddell water) tested in the rig was pumped continuously at the flow rate of 12 L/min, which gave rise to the flow velocity of 0.5 m/s in the condenser tube. A rise of 8° C of the water when leaving the condenser tube was observed for a 25° C inlet water temperature throughout the experiment. The inlet and outlet temperatures of the water were constantly measured by the mercury thermometer of 0.1° C resolution at each end of the tube. The bulk temperature in the hot water jacket measured by resistance thermometer, the overall heat transfer coefficient of the unit was calculated. The reduction in overall heat transfer coefficient based on outside diameter of the tube serves as an indication of fouling. The chemistry of the water was constantly monitored by measuring pH, M.O. alkalinity, Ca hardness, Mg hardness, sulphate and chloride concentrations. Ca and Mg hardness were determined according to the

method given by Diehl et. al. (1950). The rest of the species were analysed according to Standard Methods (Standard Methods for the Examination of Water and Wastewater, 1980). Conclusion of each experiment was only made after the cooling water (lake water) had been pumped continuously for more than 100 hours.

The experiment was carried out in three stages.

Stage 1: Summer condition synthetic water experiment, with total alkalinity as the variable.

Stage 2: Summer condition Lake Liddell water experiment, with total alkalinity as the variable.

Stage 3: Summer condition Lake Liddell water experiment, with Ca hardness as the variable.

The chemical composition of each experiment was adjusted by dosing an appropriate quantity of technical grade $CaCl_2$, $MgCl_2$, $NaHCO_3$ and Na_2SO_4. pH adjustment was done by dosing sodium hydroxide. A new condenser tube was used for each experiment.

The chemicals and the quantity used for synthetic water to simulate typical lake water chemical composition are shown in Table (7-3).

TABLE 7-3   Chemicals Used for 4.5 m^3 Synthetic Water

Chemical	Weight (kg)	Typical Lake Water Composition
$CaCl_2$ (fused)	1.50	Ca hardness - 206 mg/L $CaCO_3$
$MgCl_2$	1.00	Mg hardness - 230 mg/L $CaCO_3$
Na_2SO_4	2.30	Sodium - 127 mg/L Na^+
		Sulphate - 349 mg/L SO_4^{2-}
		Chloride - 184 mg/L Cl^-
$NaHCO_3$	0.91	M.O. alkalinity 118 mg/L $CaCO_3$

7.3   RESULTS AND DISCUSSION

7.3.1   Methyl Orange Alkalinity Experiments

These are the experiments carried out at stage 1 and stage 2 on the rig using both synthetic and actual lake water with methyl orange alkalinity varied by dosing sodium bicarbonate to investigate the scale-forming tendency in the condenser tube.

A total of nine experiments were carried out, of which the first four experiments were with synthetic water which was prepared to simulate lake water by adding chemicals to tap water. Experiments 5, 6, 7, 8 and 11 were with lake water transported from Lake Liddell and deliberately dosed with sodium bicarbonate to specific methyl orange alkalinities. Results are tabulated in Tables (7-4) and (7-5).

TABLE 7-4   PHYSICAL DATA OF M.O. RUNS

Water	Run Nos.	Number of Hours	Average Inlet Temperature °C	Average Outlet Temperature °C	Average hot water Temperature °C	Overall heat transfer Coefficient (W/m²°C)		Percentage Reduction
						Initial	Final	
Synthetic	1	100	25.5	34.0	54.6 ± 0.2	1060	1030	2.80
Synthetic	2	197	27.5	35.7	54.6 ± 0.2	1060	1070	-0.94
Synthetic	3	335	30.0	37.3	55.1 ± 0.1	1014	1024	-0.99
Synthetic	4	278	23.0*	31.7@	55.0 ± 0.1	990	900	9.09
Lake	5	244	28.8	36.3	54.8 ± 0.2	1040	1060	-1.92
Lake	6	214	27.0	35.0	54.6 ± 0.1	1038	1027	1.06
Lake	7	261	26.4	34.4	54.6 ± 0.1	998	985	1.30
Lake	8	268	26.0	34.2	55.0 ± 0.1	1007	978	2.90
Lake	11	123	22.3*	31.0@	54.8 ± 0.1	954	856	10.27

*   Maximum Inlet Temperature

@   Minimum Outlet Temperature

TABLE 7-5   CHEMICAL DATA OF M.O. RUNS

Run Nos.	pH		M.O. Alkalinity (mg/L CaCO$_3$)		Ca Hardness (mg/L CaCO$_3$)		Mg Hardness (mg/L CaCO$_3$)		Sulphate (mg/L SO$_4^=$)		Chloride (mg/L Cl$^-$)	
	Initial	Final	Initial	Final	Initial	Final	Inital	Final	Initial	Final	Initial	Final
1	8.20	–	194	208	254	255	153	160	349	–	184	–
2	8.19	8.20	204	214	236	257	158	163	–	500	–	125
3	8.31	8.40	300	228	242	184	141	150	347	–	155	–
4	8.18	8.21	528	314	436	343	109	120	375	450	104	120
5	7.90	8.11	120	130	266	323	250	309	481	588	246	268
6	8.13	8.35	190	202	280	302	276	309	531	625	266	293
7	8.42	8.52	324	362	313	331	298	344	625	663	293	328
8	8.15	8.57	480	507	338	350	329	392	650	725	320	357
11	8.34	8.46	1016	869	241	49	279	288	450	475	290	306

Among these experiments, only experiments 10, 4 and 11 show significant scaling. Experiment 8 shows moderate scaling. This is indicated by a decrease in M.O. alkalinity and calcium hardness, and more importantly, the reduction in overall heat transfer coefficient. The scale samples were examined by scanning electron microscopy. The detailed results of scanning electron microscopy examination are presented in Appendix E. The profile of overall heat transfer coefficient against time for experiments 4, 8 and 11 are presented in Figures (7-3), (7-4) and (7-5) respectively. Scaling did not occur only in the condenser tube but in the entire pipe line of the test rig; the scale even covered the float surface of the rotameter prior to the condenser tube. Experiment 8 shows 2.9% reduction in overall heat transfer coefficient. Since experiment 7 has M.O. alkalinity similar to experiment 8, it is considered as the threshold of scaling. The rest of the experiments show no scaling and the concentrations of the chemical species increase at the end of each experiment because of the effect of evaporation.

7.3.2 Calcium Hardness Experiments

Another series of experiments were carried out to investigate the effect of calcium hardness on the tendency to scale. Ten times the concentration of calcium hardness encountered in the Lake Liddell water were investigated. Again the data obtained are presented in Table (7-6) for physical data and Table (7-7) for chemical data. Experiments 12, 13 and 14 show significant scaling. The profiles of overall heat transfer coefficient are presented in Figures (7-6), (7-7) and (7-8) respectively.
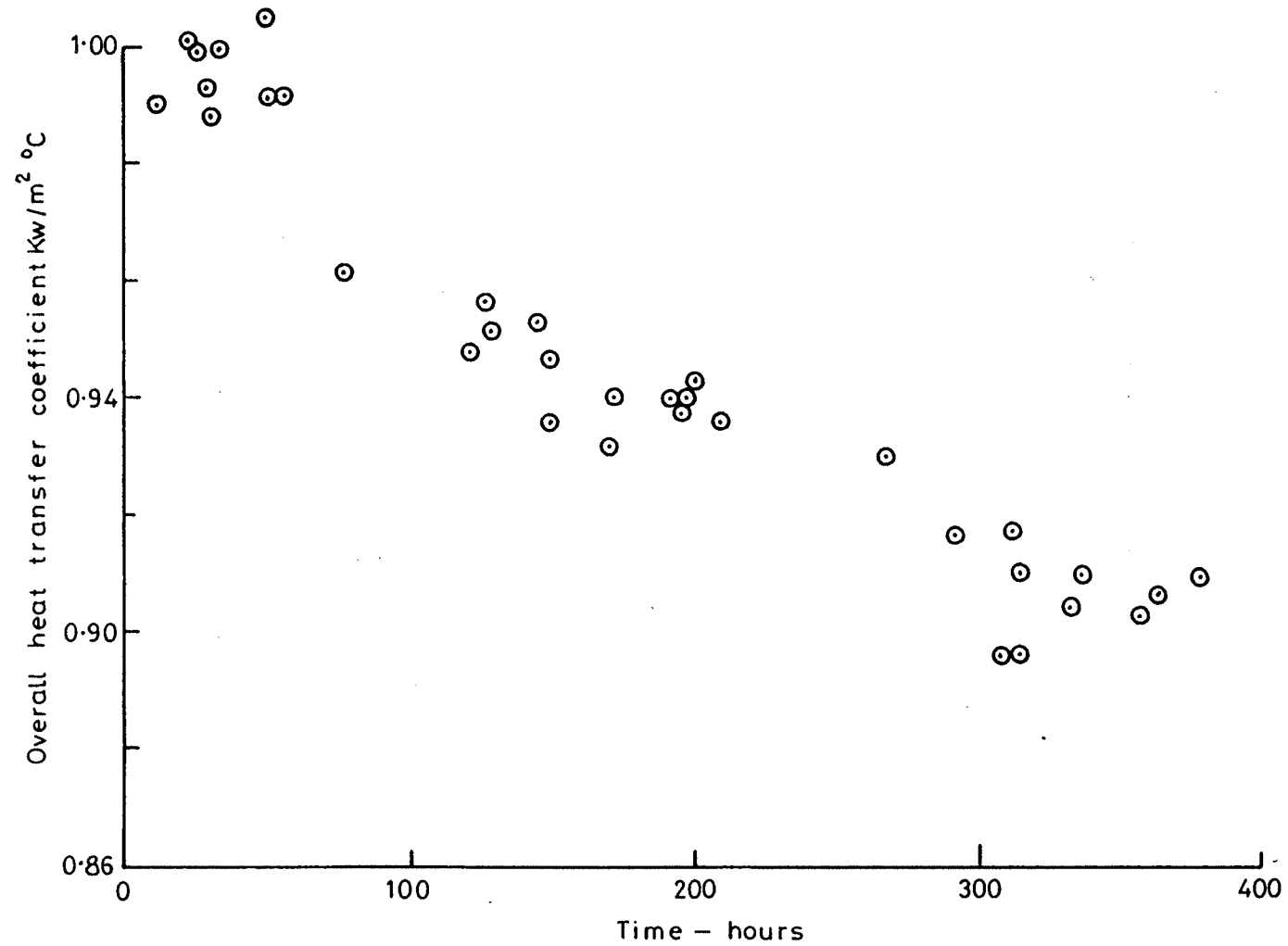
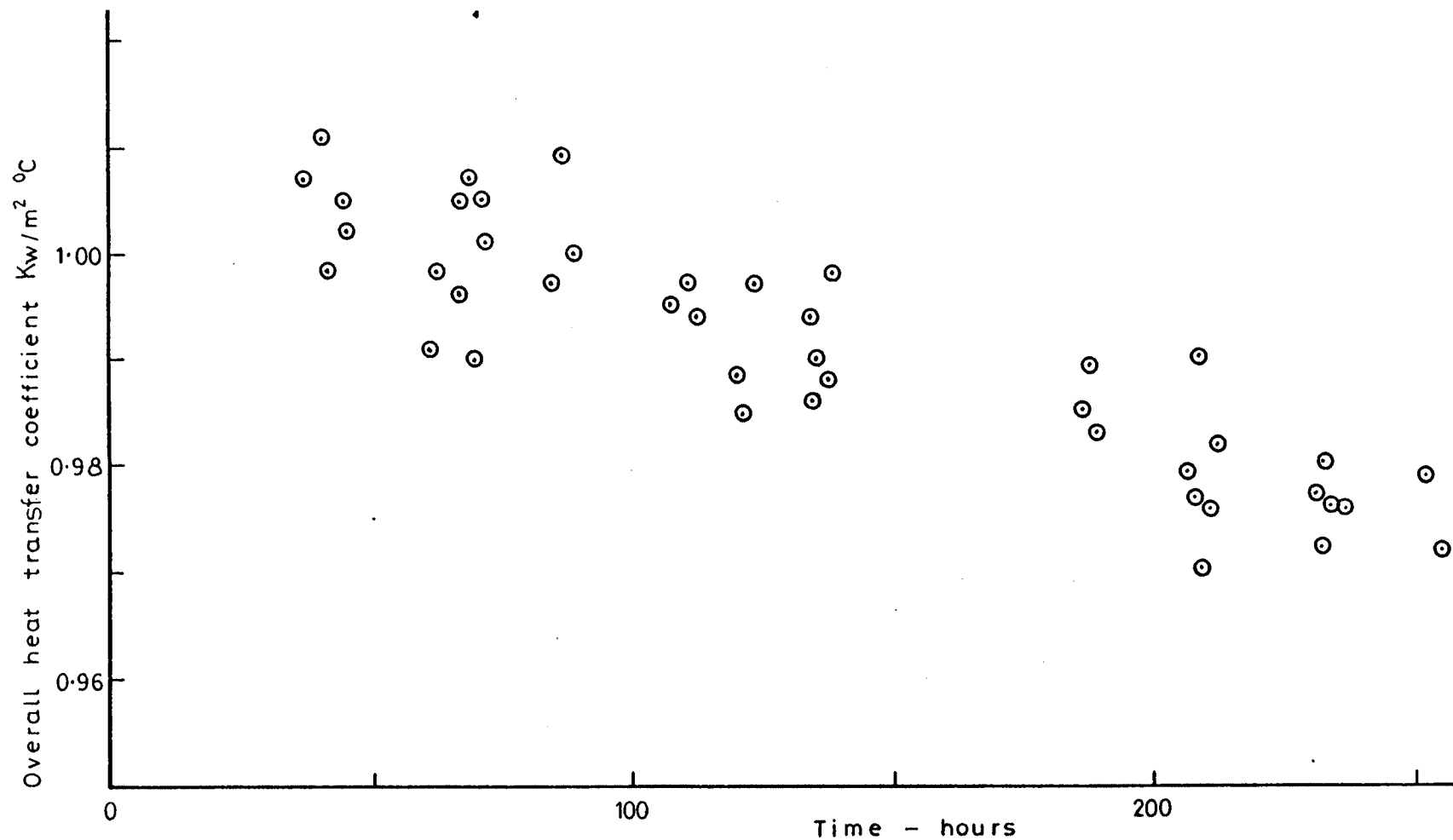FIGURE 7-3   Change of Overall Heat Transfer Coefficient with Time, Expt. 4

FIGURE 7-4   Change of Overall Heat Transfer Coefficient with Time, Expt. 8
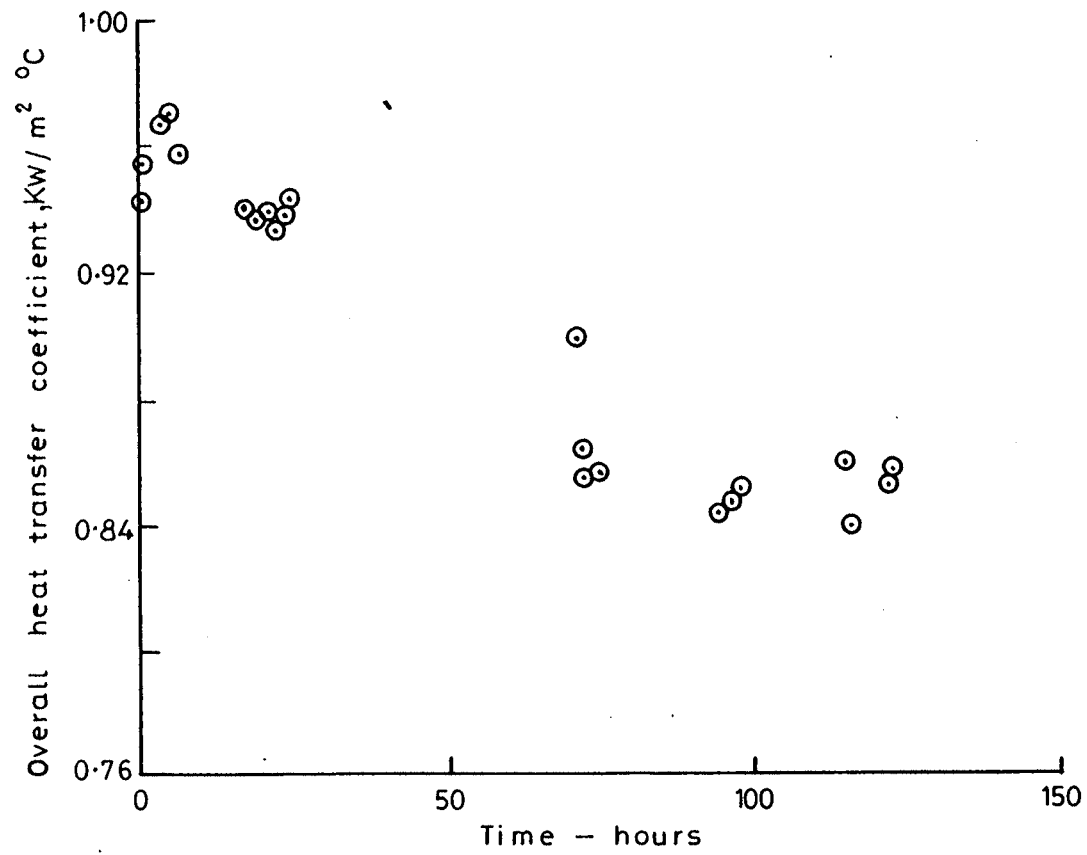
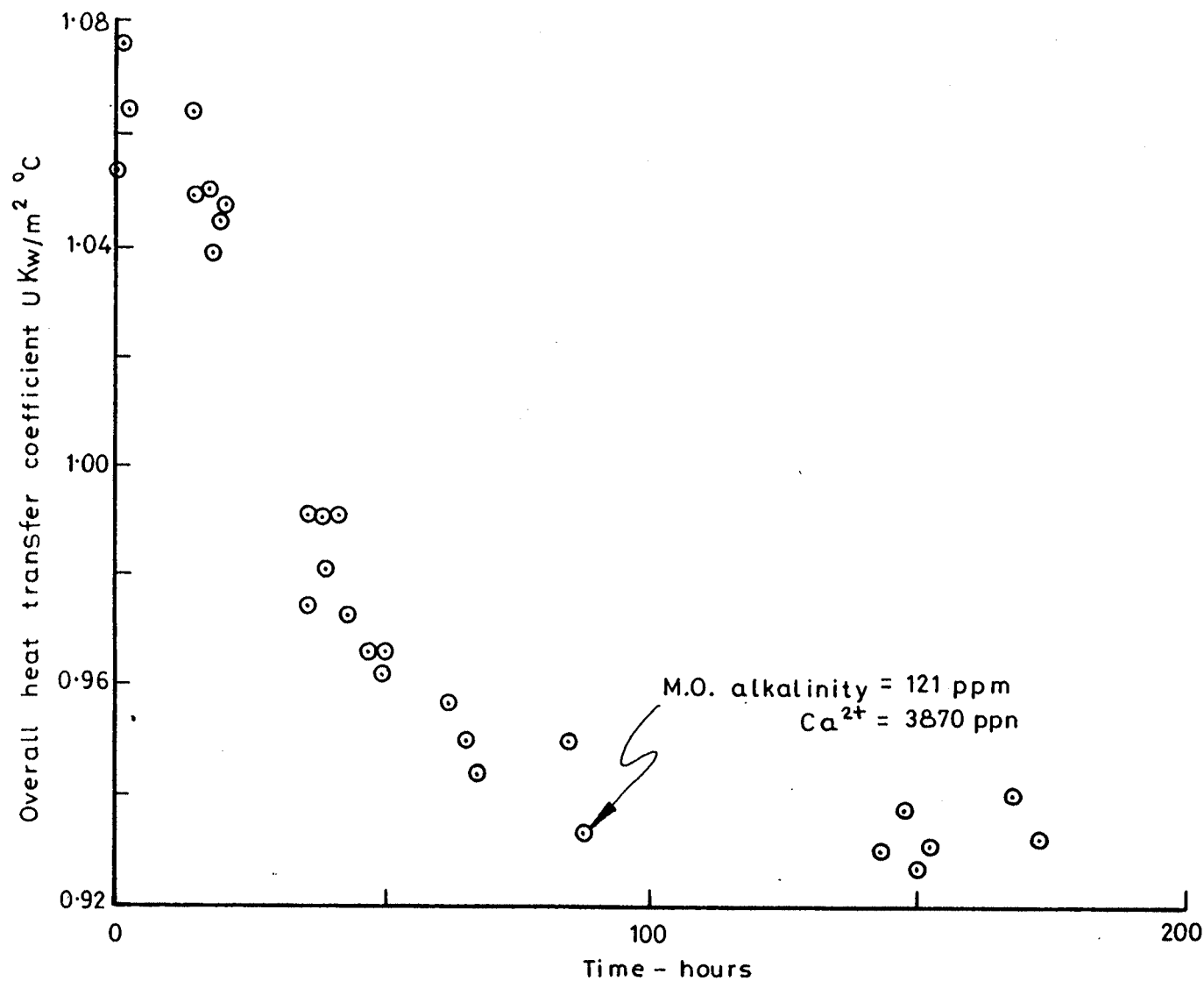FIGURE 7-5   Change of Overall Heat Transfer Coefficient with Time, Expt. 11

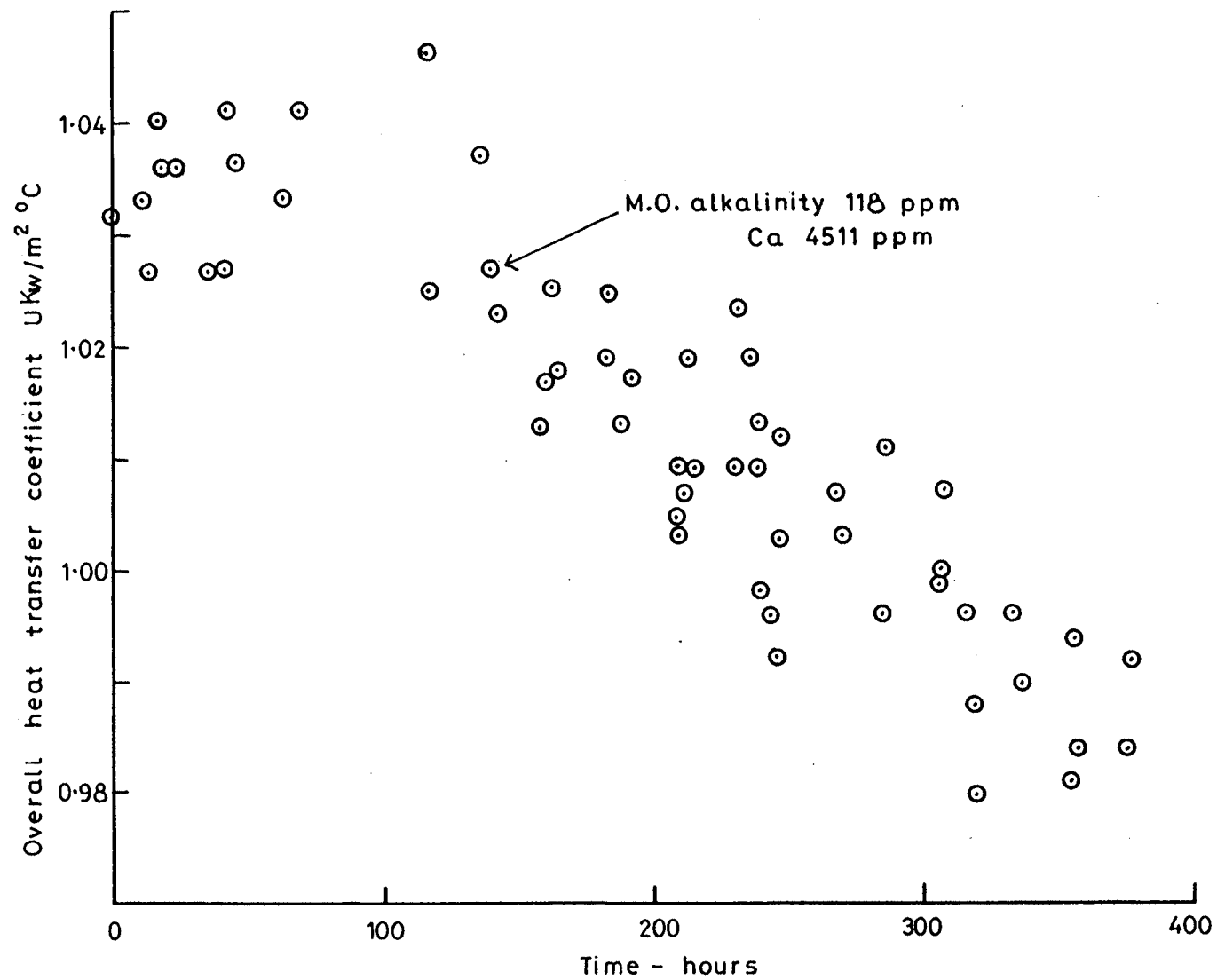FIGURE 7-6 Change of Overall Heat Transfer Coefficient with Time, Expt. 12

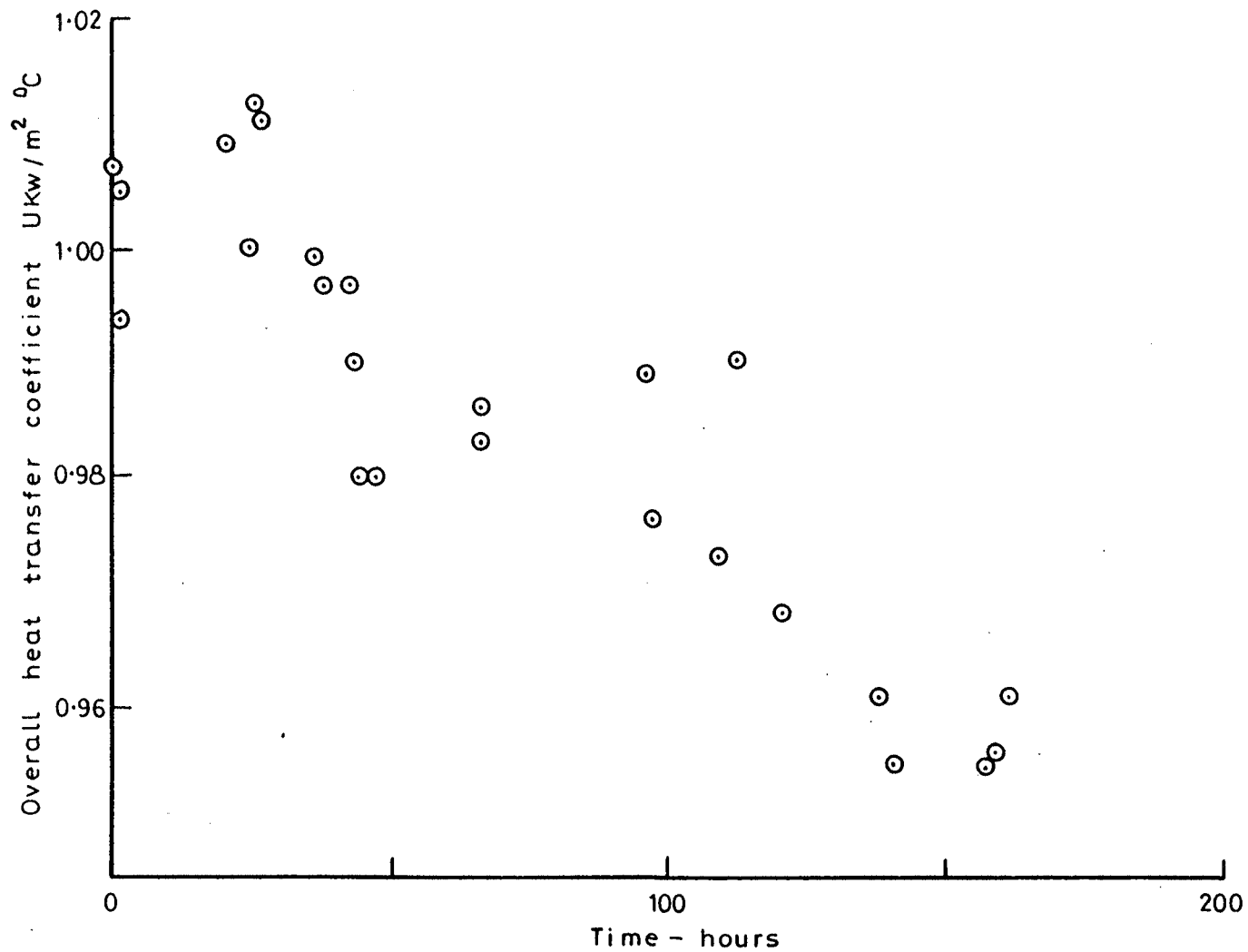FIGURE 7-7 Change of Overall Heat Transfer Coefficient with Time, Expt. 13

FIGURE 7-8   Change of Overall Heat Transfer Coefficient with Time, Expt. 14

TABLE 7-6 PHYSICAL DATA OF CALCIUM HARDNESS RUNS

Water	Run Nos.	Number of Hours	Average Inlet Temperature °C	Average Outlet Temperature °C	Average hot water Temperature	Overall heat transfer Coefficient (W/m²°C)		Percentage Reduction
						Initial	Final	
Lake	12	172	25.4 ± 2.0	38.8*	54.6 ± 0.1	1054	931	11.7
Lake	13	376	25.3 ± 0.4	34.6*	54.5 ± 0.1	1031	984	4.6
Lake	14	161	25.2 ± 0.5	35.9*	54.6 ± 0.1	1007	955	5.2
Lake	15	142	25.7 ± 0.4	33.8 ± 0.3	54.6 ± 0.1	990	992	-0.2

* The highest outlelt temperature of the run

TABLE 7-7   CHEMICAL DATA OF CALCIUM HARDNESS RUNS

Run Nos.	pH		M.O. Alkalinity (mg/L CaCO$_3$)		Ca Harness (mg/L CaCO$_3$)		Mg Hardness (mg/L CaCO$_3$)		Sulphate (mg/L SO$_4^=$)		Chloride (mg/L Cl$^-$)	
	Initial	Final	Initial	Final	Initial	Final	Initial	Final	Initial	Final	Initial	Final
12	8.00†	7.98	133	110	3721	4163	250	250	710	760	2903	3100
13	8.00	8.10	110	131	4163	5654	250	371	760	1057	3100	4312
14	7.91	8.01	128	140	3727	4021	321	383	750	800	2875	3061
15	7.94	-	121	-	2218	-	247	-	440	-	1781	-

† This pH value is estimated according to the quantity of NaOH added to the pool.

7.3.3 Threshold Langelier Index Calculated Based on Bulk Inlet Temperature

The results of experiment 7 are considered the threshold of scaling of Lake Liddell water for power station condenser tubes. Since the Langelier Index is used as the control parameter for scaling, it will be useful to calculate the corresponding Langelier Index for all the experiments. The Langelier Index of experiment 7 is therefore the threshold of which the water should not be operated at or exceeded. There are empirical expressions to calculate Langelier Index from the information of calcium hardness and total alkalinity. Temperature and ionic strength correction also are available. One of the commonly used expressions is by Larson and Buswell (1942). The Langelier Index also can be calculated based upon ion pair species. The pH calculated at saturation is believed to be more accurate. Water species concentrations are calculated from PROG-CMSS. The Langelier Index is calculated by the following equations:

(1) Larson and Buswell:

$$pH_s = pK'_2 - pK'_{sp} + p[T_{Ca}] + p[Alk] - \log f_m \qquad (7-1)$$

$$LI = pH - pH_s$$

(2) Ion Pair Consideration:

$$pH_s = pK'_2 - pK'_{sp} + p[Ca^{2+}] + p[Alk] - \log f_m \qquad (7-2)$$

$$LI = pH - pH_s$$

Together with the degree of supersaturation defined as

$$S = \frac{f_d^2 \, [Ca^{2+}] \, [CO_3^{2-}]}{K_{sp}}$$

the results are tabulated in Table (7-8). Figures (7-9) and (7-10) are the calculated values of both types of Langelier Index for all the experiments. The threshold level of scaling represented by the index applied to the inlet bulk lake water temperature is 1.40 for Larson and Buswell and 1.25 for Ion Pair Consideration. This is higher than the conventional practice of power stations which keep Langelier Index at 1 as the maximum. The degree of supersaturation of experiment 7 is 17. According to the results of calcium carbonate precipitation study in chapter 5, calcium carbonate can remain in the solution at supersaturation up to 10. Hence degree of supersaturation 17 represents a supersaturated water that will eventually precipitate out calcium carbonate from the bulk of water. Therefore if scaling took place, it was the result of bulk precipitation from the water combined with the wall crystallization of calcium carbonate on the condenser tube. Bulk precipitation was evident because the scale covered the entire pipe line especially for degrees of supersaturation higher than 19. The velocity shear stress on the tube may also account for the higher degree of supersaturation than the batch precipitation required in order to lay down adherent scale on the pipe line.

FIGURE 7-9 Langelier Index According to Larson and Buswell
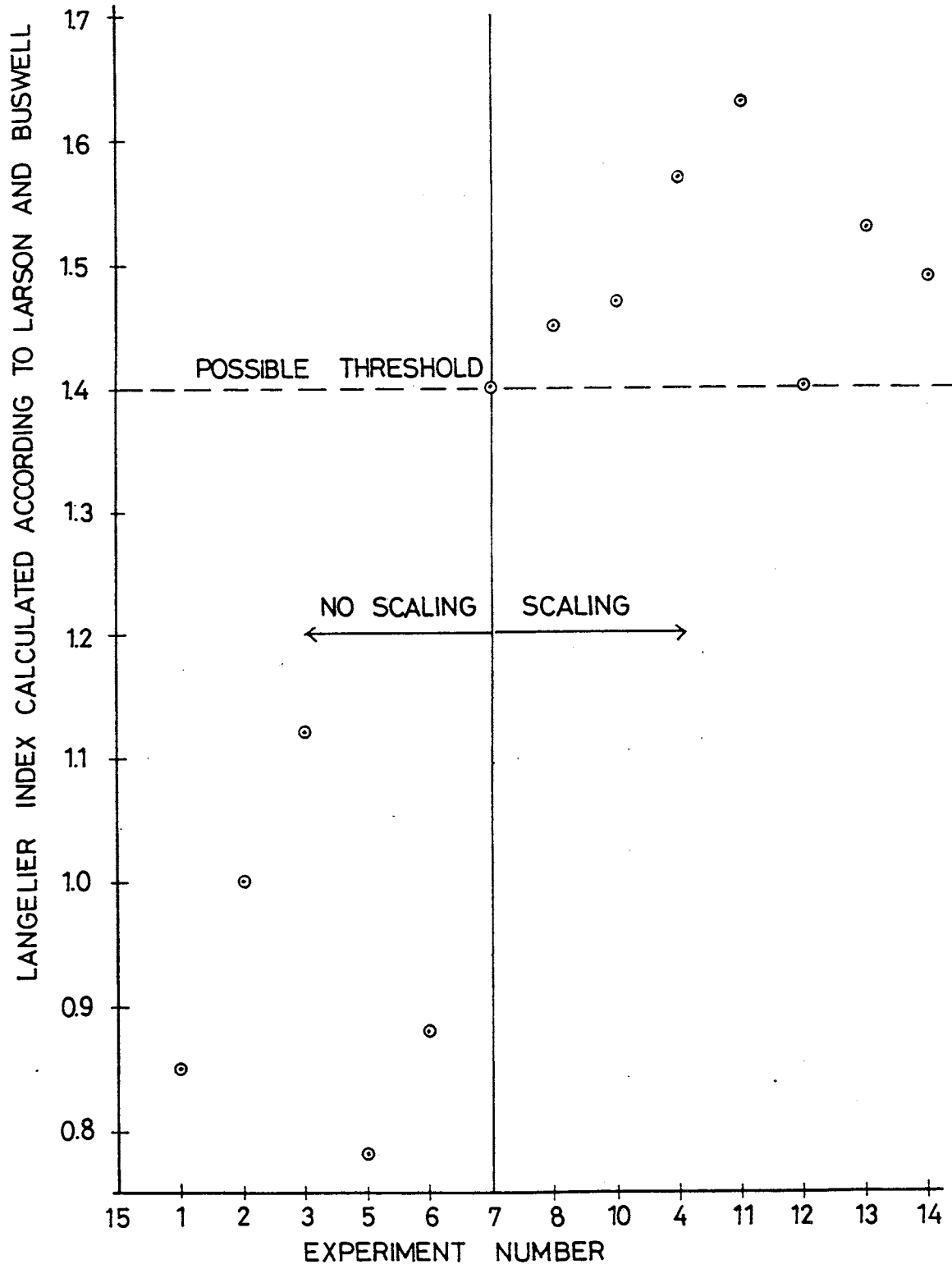at Bulk Inlet Temperature

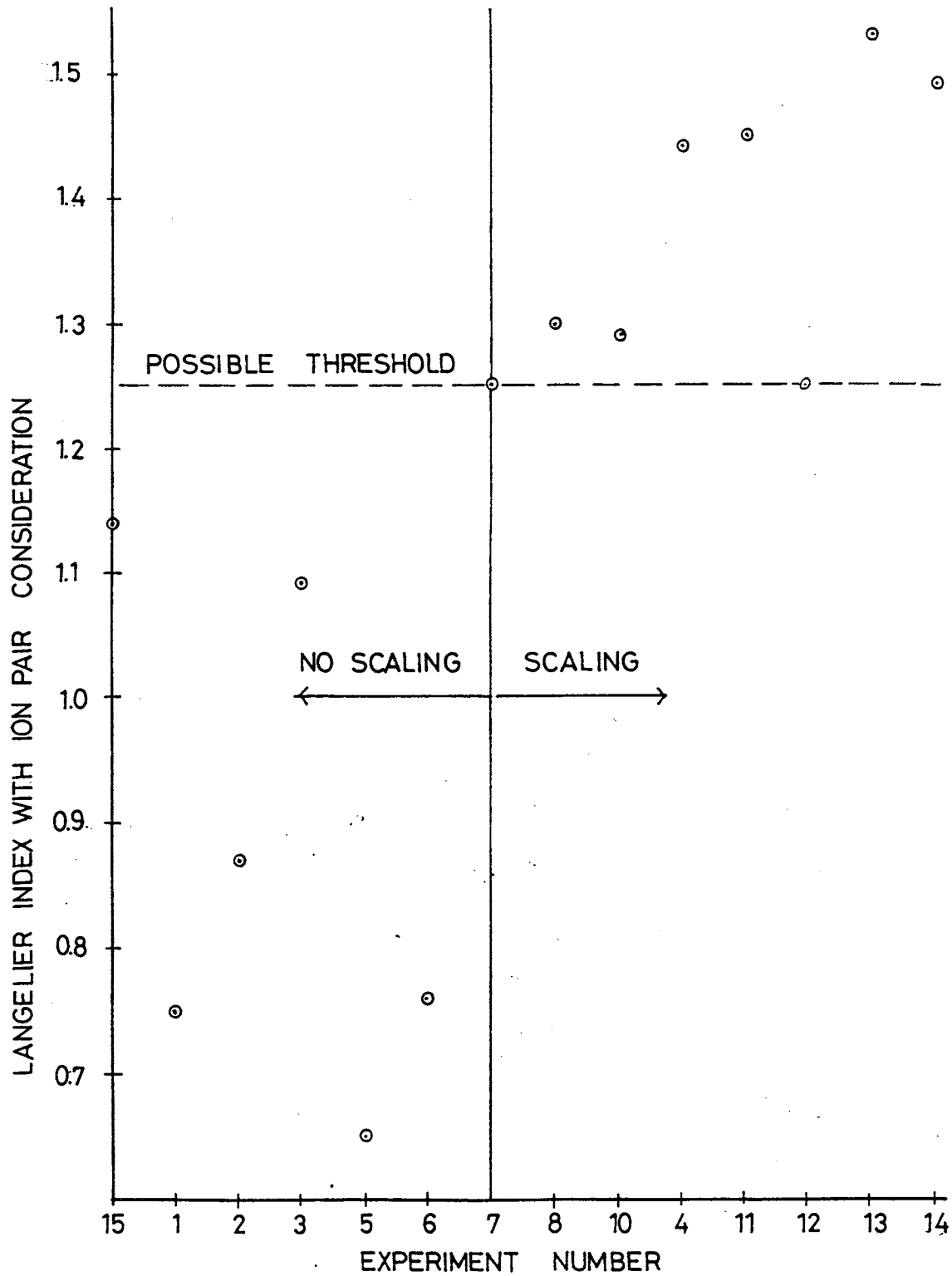FIGURE 7-10 Langelier Index with Ion Pair Consideration at Bulk Inlet Temperature

TABLE 7-8   Typical Langelier Index and Degree of Supersaturation

Calculated at Inlet Temperature

Expt. Nos.	Larson & Buswell	Ion Pair Consideration	Degree of Supersaturation	Remarks
1	0.85	0.75	5.4	no scaling
2	1.00	0.87	7.1	no scaling
3	1.21	1.09	11.8	no scaling
5	0.78	0.65	4.4	no scaling
6	0.88	0.76	5.6	no scaling
15	1.18	1.14	13.4	no scaling
7	1.40	1.25	17.0	no scaling
8	1.45	1.30	19.1	moderate scaling
10	1.47	1.29	18.7	scaling
4	1.57	1.44	26.7	scaling
11	1.63	1.45	27.0	scaling
12	1.40	1.35	22.2	scaling
13	1.58	1.53	32.6	scaling
14	1.49	1.43	26.5	scaling

Experiment 10 shows scaling at the degree of supersaturation equal to 18.7. Larson and Buswell's Langelier Index of this is 1.47. From the results of energy dispersive X-ray micro-analysis (Appendix E), the scale is not calcium carbonate based, rather it is a mixture of copper based inorganic salts. This is because of the copper sulphate salt added into the system which was intended to control algae growth in the pool. The dosage apparently triggered the delicate solubility balance of the water and precipitated out copper based inorganic salt.

The salt subsequently deposited in the tube. It is probably a more adherent scale than calcium carbonate scale because under similar flow conditions, a thickness of 2-15 μm was measured, whereas the scale from experiment 8 was difficult to be measured.

7.3.4 Threshold Langelier Index Calculated Based on Heat Transfer Surface Temperature

Calcium carbonate crystallization is surface reaction controlled as suggested by previous investigators and confirmed in Chapter 5. As a result, the heat transfer surface temperature can be a critical factor for scaling. The wall temperature can be estimated from the water film heat transfer coefficient established in the tube under fully turbulent flow (McCabe and Smith, 1967). An example to calculate wall temperature at experiment 8 is shown as follows:

Inlet temperature = 29.3° C

Outlet temperature = 36.7° C

Average temperature = (36.7 + 29.3)/2 = 33.0° C

Hot water jacket bulk temperature = 55.2° C

Linear velocity of water, v = 0.5 m/s

The physical properties of water at 33.0° C are:

Density ρ = 994 kg/m^3

Viscosity μ = 0.764 x 10^{-3} kg/m-s

Thermal conductivity k_w = 0.6197 J/m s °C

Specific heat C_p = 4.186 x 10^3 J/kg°C

Inside diameter of the tube D_i = 0.02286 m

Outside diameter of the tube D_o = 0.02530 m

Reynolds number Re = $\dfrac{D_i vP}{\mu}$ = $\dfrac{0.02286 \times 0.5 \times 994}{0.764}$ x 10^3 = 1.49 x 10^4

Prandtl number Pr = $\dfrac{C_p \mu}{k}$ = $\dfrac{4.186 \times 10^3 \times 0.764 \times 10^{-3}}{0.6197}$ = 5.16

Preliminary estimate of water film heat transfer coefficient can be obtained by the following empirical equation:

$$\frac{h_i}{c_p G} \left(\frac{C_p \mu}{k}\right)^{2/3} \left(\frac{\mu_w}{\mu}\right)^{0.14} = \frac{0.023 \left[1 + (D/L)^{0.7}\right]}{(DG/\mu)^{0.2}}$$

where G is the mass velocity (kg/s m^2), L is the length of the tube (m).

Omitting the corrections for tube length and for viscosity ratio:

$$h_i = \frac{0.023 \times 0.5 \times 994 \times 4.186 \times 10^3}{(1.49 \times 10^4)^{0.2} \times (5.16)^{2/3}} = 2345.7 \text{ W/m}^2 \text{ °C}$$

To determine wall temperature, the following equation can be used

$$\Delta T_i = \frac{D_o/D_i h_i}{1/u_o} \Delta T$$

where ΔT_i is the temperature drop through inside fluid, ^oC

ΔT is the overall temperature drop, ^oC

U_o is the overall heat transfer coefficient based on outside diameter, W/m^2 ^oC

The overall temperature drop $\Delta T = 55.2 - 33.0 = 22.2^oC$

The surface area of the condenser tube based on outside diameter = 2 x π x (0.02530/2) x 3.55 m = 0.282 m^2

The heat input = 0.5 x 4.186 x $(\frac{0.02286}{2})^2 \pi$ x 994 x (36.7 - 29.3)

$\quad\quad\quad\quad = 6.28$ KW

The log mean temperature difference = $\frac{(55.2-29.3)-(55.2-36.7)}{\ln[(55.2-29.3)/(55.2-36.7)]}$

The overall heat transfer coefficient = q/A Δ T = 1020 W/m^2 ^oC

The temperature drop over the water resistance:

$$\Delta T_i = \frac{0.02530 \text{ x } 1020}{0.02286 \text{ x } 2345.7} \text{ x } (55.2-33) = 10.7^oC$$

$$T_w = T + \Delta T_i = 43.7^oC$$

The viscosity of the water at T_w is now found:

$$\mu_w = 0.615 \text{ x } 10^{-3} \text{ kg/m s}$$

The viscosity-correction factors = 0.9701

The corrected coefficient h_i = 2275.5 W/m^2 ^oC

The temperature drop over the water resistance and the wall

temperature become

$$\Delta T_i \quad = \quad \frac{0.02530 \times 1020}{0.02286 \times 2275.5} \quad x \quad (55.2-33) \quad = \quad 11^{\circ}C$$

$$T_w \quad = \quad 33 + 11 \quad = \quad 44^{\circ}C$$

This is so close to the wall temperature calculated previously that a second approximation is unnecessary.

TABLE 7-9   Typical Langelier Index and Degree of Supersaturation Calculated
at Heat Transfer Surface Temperature

Expt. Nos.	Clean Wall Temp $^{\circ}C$	Larson & Buswell L.I.	Ion Pair Consideration L.I.	Degree of Super- saturation	Remarks
1	42.8	1.22	1.11	12.5	no scaling
2	44.2	1.28	1.14	13.3	no scaling
3	43.9	1.48	1.35	21.5	no scaling
5	41.8	1.01	0.88	7.4	no scaling
6	43.2	1.19	1.06	11.2	no scaling
15	42.3	1.50	1.45	27.4	no scaling
7	43.0	1.69	1.52	31.6	no scaling
8	44.0	1.72	1.55	34.1	moderate scaling
10	41.0	1.78	1.59	37.1	scaling
4	42.5	1.84	1.69	47.4	scaling
11	41.7	1.94	1.73	51.1	scaling
12	42.7	1.76	1.70	49.1	scaling
13	42.9	1.91	1.85	68.6	scaling
14	41.6	1.80	1.74	53.5	scaling

The Langelier Index and degree of supersaturation of all the
experiments at the heat transfer surface temperature are calculated
and tabulated in Table (7-9). Figures (7-11) and (7-12) show both
types of Langelier Index for all the experiments. The threshold level
of scaling is 1.69 pH above the saturation pH for Larson and Buswell
and 1.52 pH above the saturation pH for the Ion Pair Consideration.

FIGURE 7-11   Langelier Index According to Larson and
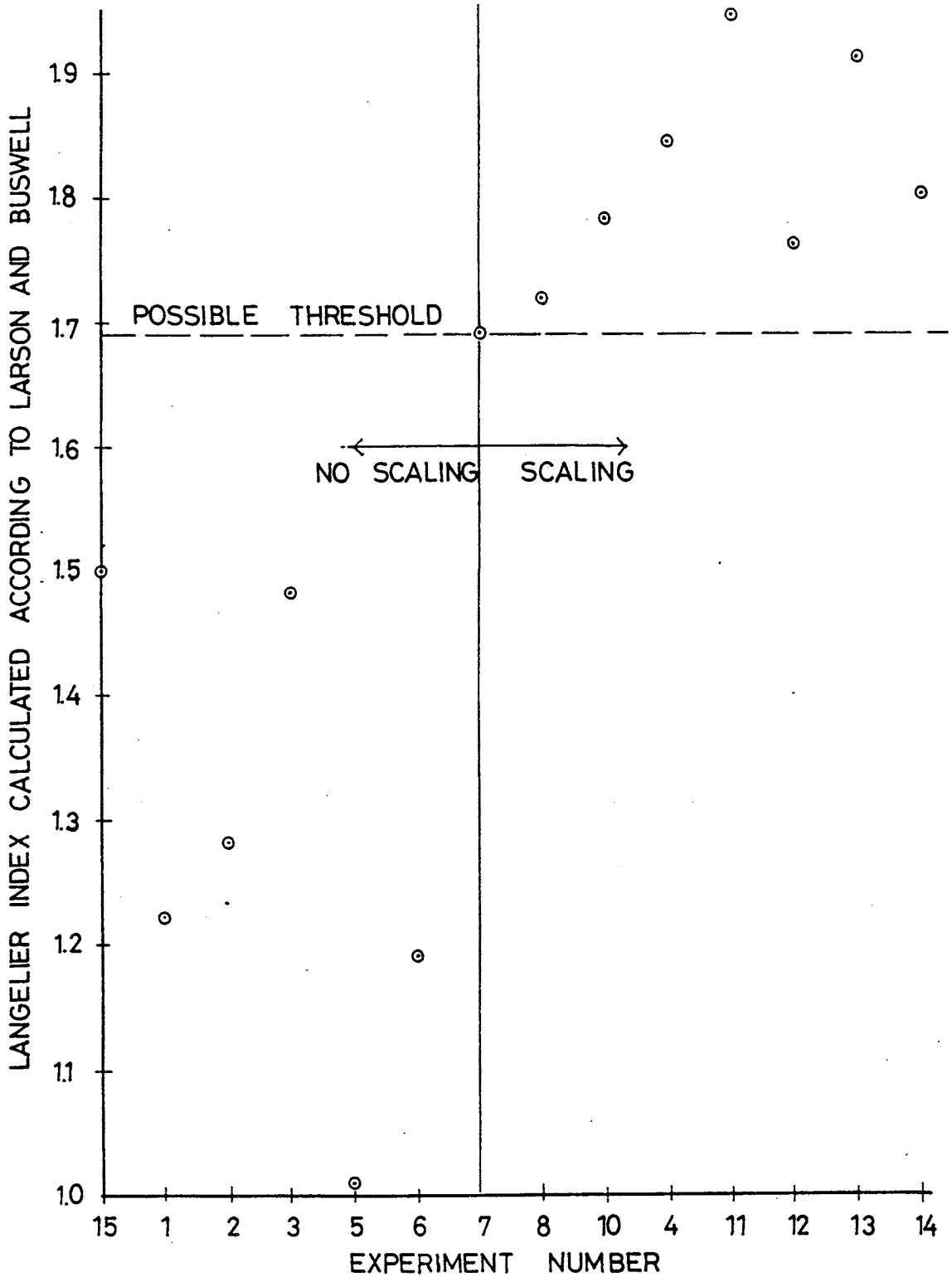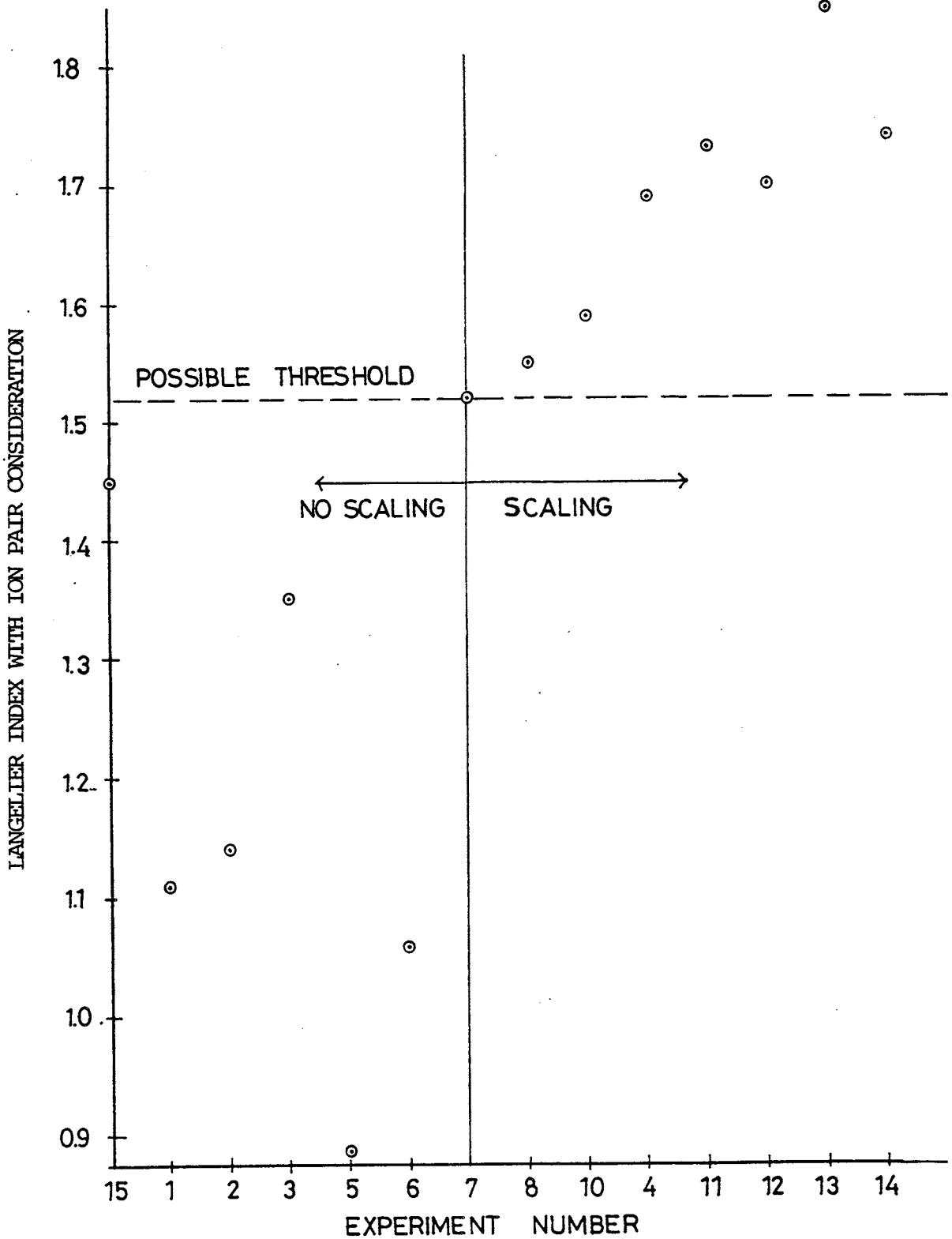Buswell at Surface Temperature

FIGURE 7-12 Langelier Index with Ion Pair Consideration at Surface Temperature

Feitler (1972, 1974, 1975) introduced the concept of critical pH which says that the precipitation from supersaturated solution will only happen at the pH which is exceeding the metastable limit represented by critical pH. The saturation pH described the condition of equilibrium between calcium carbonate solid and the ionic species. This is the boundary line that divides the metastable and the unstable region. It is known that calcium carbonate will not precipitate below a certain degree of supersaturation without the presence of calcium carbonate crystals. In fact this degree of supersaturaion is 10 as found in unseeded batch precipitation experiment of calcium carbonate described in Chapter 5. This means that there is a metastable region for calcium carbonate solubility. Feitler felt that critical pH is a more realistic index to predict the scaling tendency of the water. This critical pH is determined by adding incremental quantities of NaOH to the $CaCO_3$ water until the first sign of precipitation is detected by the pH scaling meter designed by himself. The corresponding pH is the initial pH which he believes is the boundary of the metastable region and the labile region. Experiments had been carried out by Feitler at 49° C for a range of calcium hardness and total alkalinity. Feitler reported that the critical pH is 1.7 to 2.0 pH units above pH_s. It is interesting to realise that 49° C is close to heat transfer surface temperature of the test rig condenser tube, which is also close to the actual Liddell Power station condenser. This piece of information therefore supports the reliability of the present findings. Obviously this is only applicable to heat transfer surface temperature consideration and should not be confused with the inlet cooling water Langelier Index.

Experiment 12 is an interesting run. This is the only experiment that shows scaling only in the condenser tube. Referring to Table (7-9), Langelier Index calculated for experiment 12 at bulk water temperature is 1.40 of Larson and Buswell and 1.35 of ion pair consideration. According to this number, scaling should not take place in the condenser tube. However, 1.76 and 1.70 for both types of Langelier Index are obtained at the heat transfer surface. This has exceeded the threshold Langelier Index, 1.69 and 1.52 represented by experiment 7. The result is significant scaling, due to wall crystallization rather than bulk precipitation as observed in experiment 12.

7.4 CONCLUSIONS

The test rig investigation of scaling potential of the Lake Liddell water to power station condenser tubes provides information to be related to the actual performance of the Liddell power station cooling water system. The normal operating Langelier Index at +1 recommended for cooling water practice (Pincus, 1962) without causing scaling in the condenser tubes is considered valid, in fact it is still conservative compared to the threshold Langelier Index found by this investigation. The threshold Langelier Index also has to be calculated based on the heat transfer surface temperature in addition to the bulk inlet temperature because the heat transfer and surface temperature was found to be a critical factor for scaling. It would be valuable to check the validity of the threshold Langelier Index found from this investigation to other cooling water systems to serve as a mean to predict calcium carbonate scaling potential. This is discussed in Chapter 8.

CHAPTER 8

PREDICTION OF CALCIUM CARBONATE SCALING IN THE HEAT

EXCHANGER OF A COOLING WATER SYSTEM

8.1 INTRODUCTION

It is important from both design and operating points of view to be able to predict calcium carbonate scaling potential of the operating cooling system as well as the rate of increase in scale resistance due to calcium carbonate growth in the heat exchanger. From the investigation described in chapter 7, several important conclusions were made regarding scaling threshold of the Lake Liddell power station cooling water system. These are separately tested on available operating data collected from other cooling water systems as described later in this chapter. Theoretical calculation of growth rate of calcium carbonate scale was proposed by Hasson, et. al. (1978) based on convective mass transfer consideration. The alternative is to calculate the growth rate based on overall growth rate constant of calcium carbonate crystallization. This method is used in precipitation studies of calcium carbonate in Chapter 5. Since forced convective heat transfer is the heat transfer mechanism in a shell-and-tube heat exchanger of the cooling water system, the flow rate is in the turbulent region. The growth of scale can be safely regarded as surface reaction controlled.

-

8.2 CALCULATION OF CALCIUM CARBONATE SCALING RATE IN THE HEAT EXCHANGER

If the growth of calcium carbonate scale in the heat exchanger tubes is not reduced or compensated by the velocity shear force, the theoretical growth rate can be calculated from the kinetics of calcium carbonate crystallization. In chapter 5, batch precipitation of calcium carbonate was studied and overall crystal growth rate was calculated. In order to apply the rate constant, the crystallization rate has to be converted to weight of calcium carbonate deposited per unit surface area of the heat exchanger tubes per unit time. The rate of precipitation is expressed in Equation (4-111)

$$\frac{-dT_{Ca}}{d\theta} = kf_d^2 \left\{ \frac{\alpha_a}{(\rho\alpha_v)^{2/3}} M^{2/3} N^{1/3} (T_{Ca_{in}} - T_{Ca})^{2/3} \right\}$$

$$\left\{ [Ca^{2+}]^{1/2} [CO_3^{2-}]^{1/2} - (K_{sp}/f_d^2)^{1/2} \right\}^2 \qquad (4-111)$$

$$f(S) = \frac{\alpha_a}{(\rho\alpha_v)^{2/3}} M^{2/3} N^{1/3} (T_{Ca_{in}} - T_{Ca})^{2/3} \qquad (8-1)$$

$$f(C) = \left\{ [Ca^{2+}]^{1/2} [CO_3^{2-}]^{1/2} - (K_{sp}/f_d^2)^{1/2} \right\}^2 \qquad (8-2)$$

where f(S) is the surface area of the precipitated crystal, $L_c^{2/3}$ / L

  L_c and L are volume of crystal and solution respectively

  f(C) is the function of concentration, $mole^2/L^2$

The weight of $CaCO_3$ deposition per m^2 of crystal surface area per minute can be expressed as:

$$\frac{dW}{dt} \cdot \frac{1}{f(S)} = k \times f_d^2 \times M \times f(C)$$

$$=k \times f_d^2 \times f(c) \times 100 \qquad (8\text{-}3)$$

where k is the overall rate constant, $\dfrac{L^2}{\text{mole min m}^2}$

$\dfrac{dW}{d\theta} = \dfrac{d^T Ca}{dt} \times M$, g/min

M is the molecular weight of calcium carbonate

A typical k value obtained from Chapter 5, for calcite based precipitate is 15×10^3 L^2/mole min m^2. The calcium carbonate scaling is considered to be due to an initial layer of calcium carbonate nuclei that covers the tube surfaces and subsequently grow into scale. Therefore the surface area of the tubes can be approximated as the surface area of the crystal in scaling calculation.

Scaling in the heat exchanger tube is represented schematically in Figure (8-1).
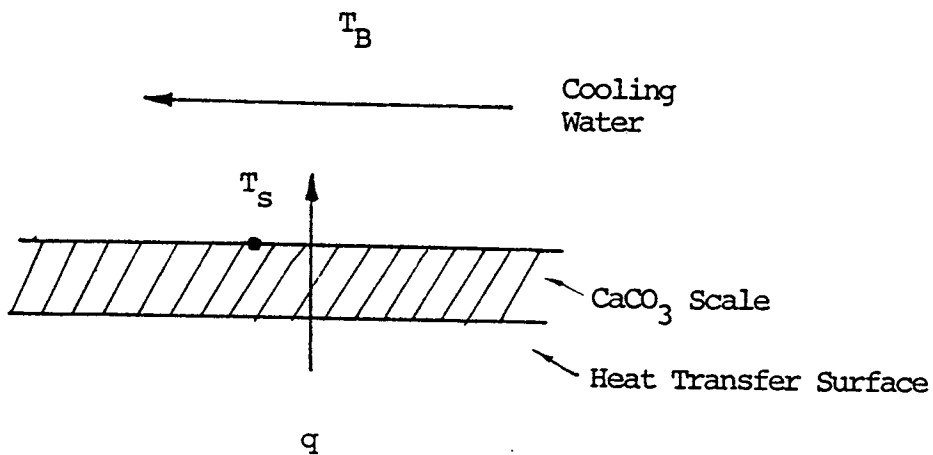

FIGURE 8-1 Schematic Representation of the $CaCO_3$ Scaling on a Heat Transfer Surface

The bulk temperature of the flowing cooling water in the tube is T_B. T_s is the surface temperature of the calcium carbonate scale at the solid/liquid interface. q is the heat flux. If the heating is a constant heat flux, T_s remains constant during the course of scaling. However, if the heating is achieved by constant temperature medium, wall temperature of the tube remains constant and T_s decreases gradually as the scale builds up. When calculating the concentration function of Equation (8-3), $(K_{sp}/f_d^2)^{1/2}$ is the saturation concentration at the solid/liquid interface. This saturation concentration, which is the solubility product of calcium carbonate, is temperature dependent. This has to be calculated at T_s. Computer programmes were developed to calculate species concentrations in water as described in Chapter 3.

Similarly, the overall growth rate constant is also a function of temperature following Van't Hoff-Arrhenius type equation. Therefore k has to be modified according to T_s. Wiechers, et. al. (1975) published the temperature dependent equation for calcite crystallization in the range of 10 - 40° C as:

$$k_t = 1.53 \times 1.053^{(t-20)} \qquad (8-4)$$

where k_t is the overall rate constant dependent on temperature

t is the temperature, ° C.

Therefore the first approximation of k modified by scale surface temperature can be calculated according to Equation (8-4). From Equation (8-4), k_{25} = 1.98, therefore the corrected

$$k_t = \frac{1.53 \times 1.053^{(t-20)}}{1.98} \times k \qquad (8-5)$$

If the scale adheres strongly onto the tube wall, the removal term in general fouling equation such as Equation (6-3) can be ignored. Therefore, the scaling rate of heat exchanger is:

$$k_f \cdot \frac{dR_f}{d\theta} = \frac{dX_f}{d\theta} = \frac{dW}{d\theta} \cdot \frac{1}{f(S)} \cdot \frac{1}{\rho_f} \qquad (8-6)$$

$$\frac{dR_f}{d\theta} = \frac{dW}{d\theta} \cdot \frac{1}{f(S)} \cdot \frac{1}{\rho_f} \cdot \frac{1}{k_f} \qquad (8-7)$$

where R_f = fouling resistance, $\dfrac{m^2 \,^{\circ}C \, s^2}{W}$

θ = time, s

ρ_f = scale density, g/m^3

k_f = thermal conductivity of scale, W/°C

8.3 SOME INVESTIGATIONS ON CALCIUM CARBONATE SCALING REPORTED IN THE LITERATURE

8.3.1 Morse and Knudsen (1977)

Morse and Knudsen conducted scaling studies on a portable fouling unit developed by HTRI (Coates et. al., 1980). The first section consisted of an annular duct with a 1.91 cm I.D. outer glass and a

1.08 cm O.D. core. The flow length was 44.5 cm. A 10.2 cm long portion of the core was electrically heated by an internal resistance heater. Four chromel-alumel thermocouples were embedded in the wall of the heated section. A constant heat flux was maintained throughout each test. The velocity of the water was 1.04 m/s. Heat flux was maintained at 276.3 kW/m^2. Both synthetic and actual cooling tower waters were tested. The water quality is given in Tables (8-1) and (8-2).

TABLE 8-1   Water Quality in Morse and Knudsen Investigation, Part I

Expt. No.	pH	(ppm as $CaCO_3$)			TDS (ppm)
		Alk	Ca	Mg	
24	8.62	134	147	54	495
26	8.58	130	143	59	498
27	8.60	128	139	62	490
28	8.64	146	142	59	527
29	8.54	145	140	64	563
22 (start)	8.73	187	146	54	528
22 (end)	8.68	137	94	55	498

TABLE 8-2   Water Quality in Morse and Knudsen Investigation, Part II

Expt. No.	P (ppm)	SO_4 (ppm)	Cl (ppm)	SiO_2 (ppm)	Zn (ppm)	Cu (ppm)	Fe (ppm)	Ni (ppm)
24	0.2	117	34	14.9	0.09	0.45	<0.05	1.5
26	0.07	110	33	14.5	0.12	0.32	<0.05	1.9
27	<0.01	109	33	13.9	0.18	0.38	0.13	0.3
28	0.07	115	35	13.2	0.11	0.28	<0.05	0.8
29	<0.01	123	39	13.2	0.07	0.30	<0.05	1.0
22	0.1	110	31	12.3	0.12	0.26	0.07	-

8.3.2   Coates and Knudsen (1980)

In this study, a 6m tall cooling tower was used together with a holding tank, three test sections, a circulation pump, a heat exchanger and a hot water system to control the bulk temperature of the test water (Lee et. al., 1978; Lahn, Jr. et. al., 1983; Coates et. al., 1980). The test section is a 40 cm length annular duct with 20 mm I.D. glass jacket and 12 mm O.D. heat core. The city water was used for the make-up. Four groups of synthetic waters were tested. The velocity of the water varied from 0.76 - 3.66 m/s. The average water qualities are summarised in Table (8-3).

TABLE 8-3   Average Water Qualities of Coates and Knudsen Investigation

	Group I Runs 28-31	Group II Runs 32-46	Group III Runs 47-65	Group IV Runs 66-83	City Water Make-up
Total Hardness (ppm $CaCO_3$)	210	220	470	370*(800)**	40
Calcium Hardness (ppm $CaCO_3$)	150	150	400	270(640)	30
M-Alkalinity (ppm $CaCO_3$)	210	300	115	160(600)	42
Chloride (ppm)	300	400	600	500	40
Silica (ppm SiO_2)	105	110	115	150	20
pH	9	9	9	9	7

(after Coates and Knudsen, 1980)

* - as analysed

** - numbers in parentheses represent values based on mass balance, ie effective concentration

8.3.3 Watkinson (1983)

Watkinson carried out scaling studies on heat transfer surface by circulating artificial hard waters through a steam-heated annular test section. The test section consisted of a 133 cm long, 1.91 cm O.D. copper tube which was mounted in a glass annulus of 3.72 cm I.O. Water passed through the annular section was heated by steam condensing in the tube. Water was made up in 140 litre batches by addition of $CaCl_2$ and $NaHCO_3$. The total alkalinity of the waters were between 90 to 700 ppm $CaCO_3$, pH was in the range 6.9 - 8.1. Velocity of the flow was maintained at 0.68 m/s. Steam temperature was at 107° C and raised to 130° C during scaling to maintain the heat flow of 10.6 kW. The water qualities of the investigation are given in Table (8.4).

TABLE 8-4   Water Quality of Watkinson Investigation

Run No.	Inlet Temp. ($^{\circ}$ K)	pH	T.A.	Ca^{2+}	S.S.	D.S.
			(mg/L as CaCO$_3$)		(ppm)	
50	330	7.22	400	-	250	2200
51	330	7.23	430	-	250	2200
54	330	6.80	450	950	275	2100
56	310	7.57	720	1130	85	1900
57	298	7.77	726	1055	10	2000
58	298	7.38	660	1230	8	2000
59	298	8.05	386	610	6	1000
60	298	7.55	680	867	20	2050
62	298	8.20	128	200	40	500
67	298	8.14	192	320	0*	483
68	298	7.57	483	1123	0	2475
69	298	7.62	497	1175	0	1700
70	310	7.80	578	1130	0	2612
71	298	8.05	337	635	0	575
72	298	8.10	96	207	0	100
74	332	7.30	350	835	0	1766

(after Watkinson (1983))

Note: Run 60 v = 0.343 m/s, otherwise v = 0.686 m/s.

Runs after 62 used in-line filter

S.S. = suspended solids

D.S. = dissolved solids

T_{steam} = 379° K at time zero

* not detected

8.4 COMPARISON OF CALCULATED AND EXPERIMENTALLY MEASURED SCALING RATE

The Lake Liddell water investigation (chapter 7) together with the investigation reported in the literature (Section 8.3) provide some data for calculating the rate of increase in fouling resistance due to scaling. Data are selected from nearly pure $CaCO_3$ scaling where no asymptotic fouling resistances are recorded. The overall growth rate model mentioned in Section (8.2) is used for the calculation. This is to compare the measured rates with the predicted rates calculated by Hasson's ionic diffusion model. The results are given in Table (8-5). Figures (8-2) and (8-3) plot the measured and predicted scaling rate calculated by overall growth rate model and Hasson's ionic diffusion model respectively.

From Figures (8-2) and (8-3), overall growth rate model seems to overestimate the scaling rate. In many instances, especially data obtained from the experiments of Coates and Knudsen; and Watkinson indicate an overestimation by as factor of 5 or more (see dotted line). On the other hand, the ionic diffusion model of Hasson predicts the scaling rate fairly well below 4 x 10^{-6} m^2 °C/KJ although more than 50% of the predicted rates are less than the measured rates (a factor of 2-6 as indicated by the dotted line).

The overall growth rate model has been employed using a value of rate constant calculated from the batch precipitation experiment. The rate constant calculated is based on total crystal surface area. For

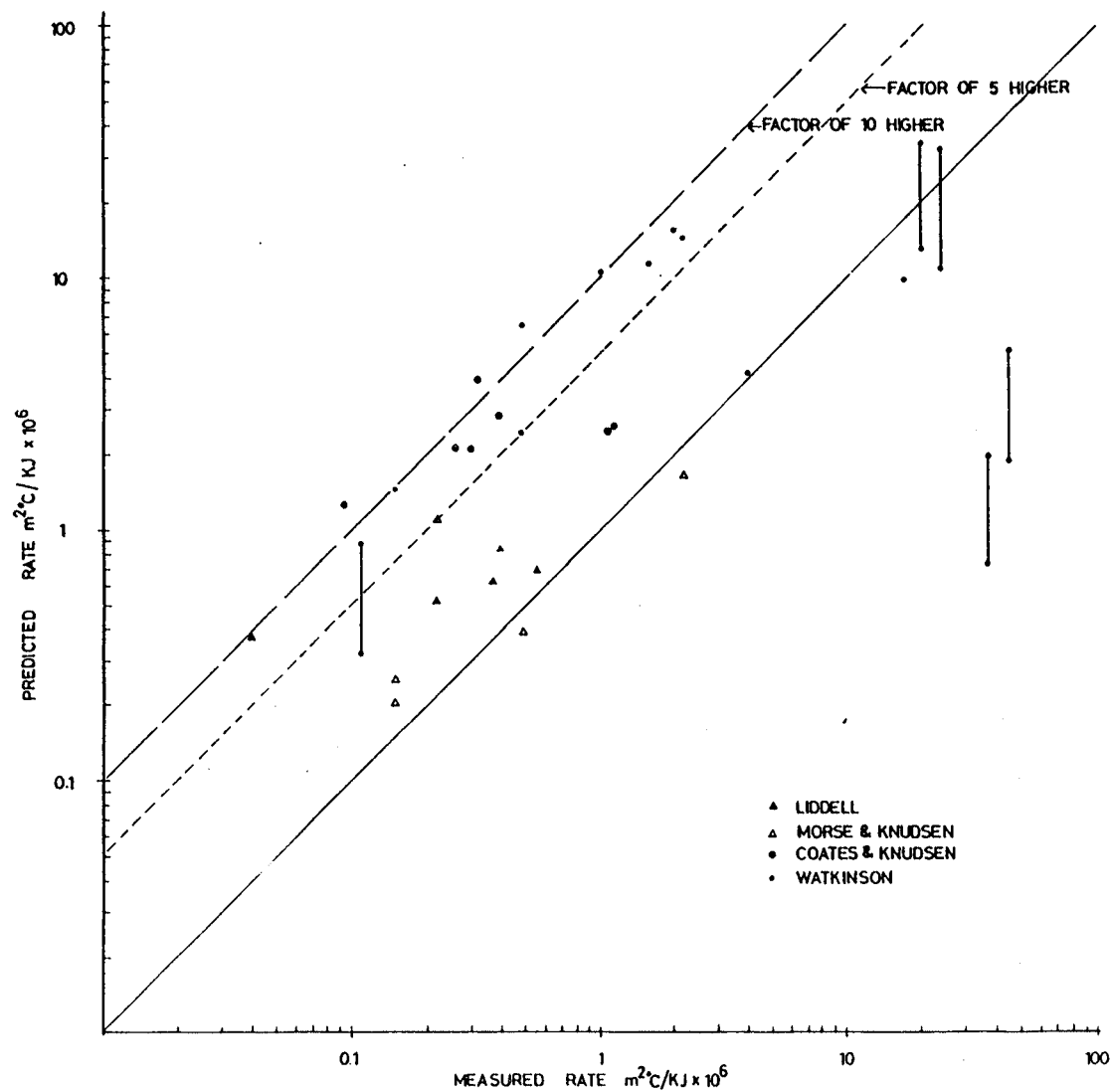FIGURE 8-2 Comparison of Measured and Predicted Scaling Rate by Overall Growth Rate Model

FIGURE 8-3   Comparison of Measured and Predicted Scaling Rate
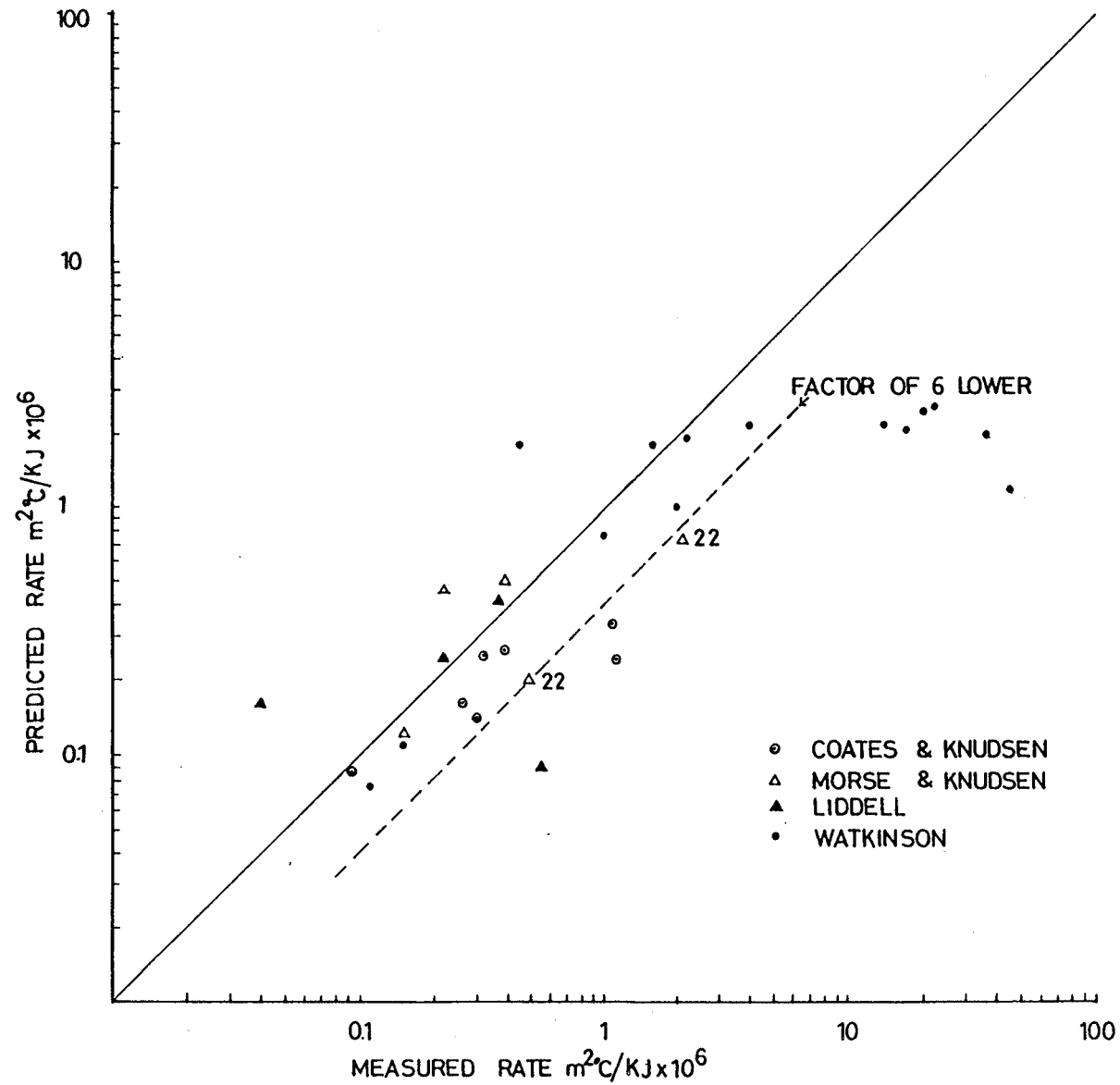by Hasson's Ionic Diffusion Model

TABLE 8-5   Rate of Scaling Measured and Calculated

Expt No.	Inlet Temp (°C)	Surface Temp (°C)	$f(c)$ x 10^8	k_f w/m°C	$\frac{dR_f}{d\theta}$ x 10^6 measured	Scaling Rate Overall Growth Model	(m²°C/KJ) Hasson Model
			Lake Liddell Investigation				
11	25.4	41.7	40.2	3.46[1]	0.37	0.62	0.41[2]
12	24.1	42.7	86.9	3.46	0.55	0.69	0.09
4	28.2	42.5	27.8	3.46	0.22	0.52	0.24
8	29.3	44.0	21.9	3.46	0.04	0.37	0.16
			Morse and Knudsen Investigation				
29	23.0	71.0	4.37	1.97-8.2	0.15-0.22	0.25-1.02	0.12-0.46[2]
28	22.0	65.0	5.08	1.97-8.2	0.15-0.39	0.02-0.83	0.12-0.49
22	22.0	65.0	9.62	1.97-8.2	0.49 2.2	0.39-1.64	0.20-0.73
			Coates and Knudsen Investigation				
38	35	62	37.7	3.46	1.09	2.47	0.33[3]
49	35	63	20.5	3.46	0.094	1.27	0.086
28	35	66	27.9	3.46	1.12	2.56	0.24
51	35	77	24.2	3.46	0.26	2.14	0.16
63	35	67	54.2	3.46	0.32	3.47	0.25
24	35	67	34.4	3.46	0.39	2.88	0.26
77	35	58	43.9	3.46	0.30	2.10	0.14
			Watkinson Investigation				
54	57	106	2.24[6]	1.7-4.6[5]	37	0.74-1.99	2.0[4]
56	37	106	37.5	1.7-4.6	24	10.9-32.8	2.6
57	25	106	45.2	1.7-4.6	20	13.0-35.3	2.5
58	25	106	16.0	4.6	4	4.4	2.2
59	25	106	22.2	2.6	2	15.6	1.0
60	25	106	17.0	2.5	17	9.8	2.1
62	25	106	1.39	2.6	0.15	1.46	0.11
67	25	106	4.64	1.7-4.6	0.48	2.42-6.55	1.8
68	25	106	16.8	2.1	1.6	11.2	1.8
69	25	106	21.6	2.1	2.2	14.3	1.9
71	25	106	19.8	3.4	1	10.6	0.76
72	25	106	5.28	1.7-4.6	0.11	0.32-0.88	0.075
74	59	106	7.01	1.7-4.6	45	2.4-6.8	1.2

(1) k_f value is selected for pure $CaCO_3$ as quoted by Coates & Knudsen

(2) The scaling rate is calculated based on the average of high and low pH model

(3) The high pH model is used for the calculation

(4) The low pH model is used for the calculation

(5) k_f value is not given; therefore the whole range of k_f value is used for overall growth rate calculation

(6) The concentration function is calculated based on bulk inlet temperature because K_{sp} value at 106°C is not reliable

calculation of this scaling rate of the tube under fully turbulent flow conditions, the tube surface area is used instead of the crystal surface area. It is evident that from the photomicrogram of the scale taken by scanning electron microscopy, scale is an aggregate of single calcium carbonate crystals (see Appendix E). Watkinson (1983) reported that the deposits consist of crystals of 50-100 microns in size. The actual crystal surface areas of the crystals can be a factor of 5 or more higher than the covered tube surface. The equation

$$\frac{dW}{d\theta} \cdot \frac{1}{f(S)} = K_G f(C) \qquad (8-8)$$

is used to calculate the rate of calcium carbonate deposition. $f(S)$ is a constant which is taken as the surface area of the tube. When crystals cover the tube surface, $f(S)$ due to crystals are higher than $f(S)$ of the tube and continue to increase with crystal growth and as new crystals are forming. As a result, $\frac{dW}{d\theta} \cdot \frac{1}{f(S)}$ is always higher than the rate calculated if the actual crystal surface is known. This is considered to be the probable reason that the overall growth rate model tends to overestimate the scaling rate as indicated in Figure (8-1).

Another approach to calculate the scaling rate was proposed by Hasson et al (1978). They considered mass transfer of ionic species in the fluid flowing through the pipe. Crystal growth can be described by mass transfer of the ionic species in the supersaturated solution by Equation (6-62).

$$\frac{1}{f(S)} \frac{dW}{d\theta} = K_d (c_b - c_i) \qquad (6\text{-}62)$$

where K_d is the mass transfer coefficient

$\quad$ $f(S)$ is the surface area

$\quad$ c_b is the bulk concentration

$\quad$ c_i is the interfacial concentration

Hasson determined the mass transfer coefficient for the ionic species in the water flowing through the tube by applying the j-factor analogy (see equation (6-67)). The unknown interfacial concentration is avoided by combining the equation for a surface reaction (equation (6-63)). The convective mass transfer coefficient of $CaCO_3$ determined is based on tube surface area. However, as the crystals deposit and grow on the tube surface, the available mass transfer area increases. As a result, more ions are able to be transferred onto a unit tube surface area. Therefore the Hasson model is expected to underestimate the actual scaling rate as indicated in Figure (8-3). This effect is more apparent when the scaling rate is beyond 4×10^{-6} m^2 $^\circ C/KJ$ because of the significant build up of deposited crystals - hence a significant increase in actual mass transfer surface. As a result, the model predicted the scaling rate an order of magnitude lower than the actual scaling rate indicated in Figure (8-3).

In comparing the overall growth rate model and Hasson's ionic diffusion model, the main transfer coefficient obtained from the j-factor analogy is based on well established physical data and consequently more reliable. The equations used (Equations (6-69) and (6-71)) indicate that K_d and $[CO_3^{2-}]$ are the two major terms that determine the results, the reaction constant, K_r plays an

insignificant role in the equations. Therefore, the predicted scaling rate by Hasson's ionic diffusion model is less susceptible to the values of the reaction constant used as well as to the accuracy of the chemical compositions of the water. On the other hand, the overall growth rate model uses kinetic values obtained from a different system, ie a batch reactor. The overall growth rate constant is also subject to uncertainty beyond 40° C. The predicted scaling rate is also strongly determined by the function of concentration, f(C) (Equation (8-2)). The accuracy of the chemical composition of the water becomes critical for the scaling rate prediction by the overall growth rate model. In most cases, the pH values strongly influence the final values of the concentration function calculated, this is particularly true for the data from the experiments of Coates and Knudsen and of Watkinson. The former reported approximate pH values for their experiments and the latter conducted the experiments on a 106° C heat transfer surface which requires a considerable extrapolation of the value of overall growth rate constant of calcite determined from the batch precipitation experiments. In view of all these, until more reliable kinetic data is obtained for the flow-through-pipe system, Hasson's ionic diffusion model is considered to be the more reliable.

Despite these difficulties associated with the use of the overall growth rate model the basic concepts embodied in this approach are still valid for flow through pipe systems. The overall growth rate model can still be used in parallel with the Hasson's diffusion model to counter check the possible underestimation by Hasson's diffusion model.

8.5 EFFECT OF SURFACE TEMPERATURE AND VELOCITY

From the investigation of the scaling potential of Lake Liddell water described in Chapter 7, heat transfer surface temperature is an important factor in causing scaling in heat exchangers. The possible threshold expressed as Larson and Buswell's Langelier Index is 1.69 under test conditions. This number can be checked with data from Morse and Knudsen as well as Coates and Knudsen Investigation (Table 8-6). In Morse and Knudsen investigation, Langelier Indexes calculated at bulk inlet temperature indicate no scaling if compared with 1.40 (Larson and Buswell's Langelier Index) and 1.25 (Ion Pair consideration Langelier Index) determined from Chapter 7, but when surface temperature is considered, the index number is 1.69. Runs 22, 28 and 29 precipitated calcium carbonate scale in the test secton, whereas Runs 24, 26 and 27 did not scale. This tends to suggest 1.68 is a possible threshold of scaling under the test conditions. Therefore, only calculating the Langelier Index of cooling water at bulk inlet temperature can be deceptive in determining the water scaling potential.

Langelier Indexes calculated from Coates and Knudsen data show that water is highly supersaturated for bulk precpitation to take place. However some of the runs actually did not scale at all. Scaling in general is considered a combined result of bulk precipitation in the system and wall crystallization on the heat transfer surface. If wall crystallization which is the main mechanism of adherent scale not prevailing, the precipitate due to bulk precipitation may not be able to adhere onto the tube surface under the effect of fluid shear stress. The Reynolds numbers and shear

TABLE 8-6 Calculated Results of Langelier Indexes and Shear Stress Based on Morse and Knudsen and Coates and Knudsen Data

Expt No.	Bulk Temp (°C)	Surface Temp (°C)	LBLI at Bulk Temp	LBLI at Surface Temp	IPLI at Bulk Temp	IPLI at Surface Temp	S at Bulk Temp	S at Surface Temp	Velocity (m/s)	Reynolds Number	Shear Stress (N/m²)	Remarks
					Morse and Knudsen Investigation							
29	23	71	0.89	1.69	0.83	1.51	6.4	29.2	1.04	9096	4.71	scaling
28	22	65	0.95	1.69	0.87	1.51	7.8	29.1	1.04	9096	4.71	scaling
22	22	65	1.19	1.93	1.11	1.71	12.1	45.1	1.04	9096	4.71	scaling
24	22	65	0.94	1.68	0.88	1.52	7.2	30.1	1.04	9096	4.71	no scaling
26	22	65	0.89	1.62	0.82	1.47	6.3	26.8	1.04	9096	4.71	no scaling
27	22	65	0.88	1.62	0.82	1.47	6.3	26.8	1.04	9096	4.71	no scaling
					Coates and Knudsen Investigation							
38	35	62	1.85	2.29	1.73	1.98	45.8	77.1	1.65	18257	9.20	scaling
49	35	63	1.45	2.30	1.42	2.15	24.4	108.0	1.65	18257	9.20	scaling
28	35	66	1.76	2.25	1.66	1.96	39.3	72.3	1.68	18590	10.20	scaling
51	35	77	1.85	2.48	1.80	2.26	53.3	130.0	1.52	16819	8.00	scaling
63	35	67	1.87	2.38	1.82	2.22	55.8	124.1	2.93	32420	27.10	scaling
24	35	67	1.81	2.32	1.71	1.99	43.4	77.1	1.62	17925	9.62	scaling
77	35	58	1.83	2.21	1.76	2.05	49.0	89.1	0.91	10069	3.51	scaling
53	35	40	1.77	1.86	1.73	1.81	44.8	53.3	2.26	25000	17.20	moderate scaling
70	35	40	1.77	1.86	1.70	1.78	43.0	50.7	0.94	10400	3.71	no scaling
37	35	57	1.87	2.24	1.74	1.96	46.9	74.2	1.65	18257	9.20	scaling
56	35	57	1.81	2.18	1.77	2.08	49.2	93.6	2.26	25000	17.20	no scaling
59	35	41	1.87	1.98	1.82	1.92	56.3	69.1	2.93	32420	27.10	no scaling
60	35	54	1.87	2.19	1.82	2.10	56.3	99.2	2.93	32420	27.10	no scaling

LBLI = Larson and Buswell's Langelier Index

IPLI = Langelie Index with Ion Pair Consideration

S = Degree of Supersaturation

stress are calcualated according to the fluid dynamics equations developed for fully turbulent flow in the circular tube. The friction factor calculated is increased by 8 percent in order to apply the concentric annular ducts (Olson, 1973). The equations used are presented as follows:

$$Re = \frac{vD}{\nu} \tag{8-9}$$

where V is velocity, m/s

D is tube diameter, in the case of concentric annular duct, the hydraulic diameter, m

ν is the kinematic viscosity of the water, m^2/s

$$f = \frac{0.316}{Re^{1/4}} \tag{8-10}$$

where f is the friction factor

$$\tau = \frac{f\rho v^2}{8} \tag{8-11}$$

where τ is shear stress, N/m^2

ρ is the water density, kg/m^3

The smallest shear stress encountered in Coates and Knudsen investigation is 3.51 N/m^2 of run 77 and 3.71 N/m^2 of run 70. According to Suitor et. al. (1977) who explained the anomaly regarding asymptotic fouling corresponding to Reynolds numbers reported by Hasson et. al. (1978) and Watkinson, et. al. (1975), the shear stress is the most likely reason for asymptotic fouling. Suitor et. al.

(1977) reported the presence of threshold shear stress between 0.685 -
0.847 N/m^2 below which no asymptotic fouling was observed. Therefore
it is possible that in run 70, precipitates due to bulk precipitation
were swept away by the high shear stress of the flow. On the other
hand, run 77 encountered wall crystallization of calcium carbonate on
the heat transfer surface and produced an adherent scale. This is
evident from the Langelier Index calculated at the surface
temperature. For run 77 the Langelier Index was 2.21 compared to 1.86
for run 70. However 1.86 is higher than the 1.69 or 1.68 in the case
of Morse and Knudsen's investigation. For Runs 56, 59 and 60, even
higher Langelier Indexes are tolerable without scaling. This might be
due to the very high shear stress of these runs which swept away even
the wall crystallization nuclei before they could grow into an
adherent scale. A bulk temperature of 35° C was used in Coates and
Knudsen investigation (Coates and Knudsen, 1980) compared to 22° C in
the Morse and Knudsen investigation (Morse and Knudsen, 1977). In the
batch precipitation of calcium carbonate experiments the crystals of
calcium carbonate produced at 35° consisted of at least 50% aragonite
for solution supersaturation which is conducive to bulk precipitation.
Although the crystalline form was not investigation it is possible
that the scales formed in this investigation contain some aragonite
and subsequently are less adherent compared to calcite which was the
likely product of the Coates and Knudsen investigation. Therefore in
addition to the effects of water chemistry the combined effect of heat
transfer surface supersaturation and the fluid shear stress has to be
considered in order to assess the scaling potential of a particular
cooling water.

The surface nucleation on heat exchangers was studied by Chandler (1964) using concurrent flow of warm saturated test solution and cooling water. The test solution flowed through the annular section of the heat exchanger over the cold tube surface. Supersaturation was created on the tube surface and where a scale formed. Chandler showed that the nucleus formation rate is a power function of surface supersaturation

$$\frac{dN^O}{d\theta} = K_{(8-12)} f(Re) \Delta c^n \qquad (8-12)$$

where N^O is the number of nuclei

θ is the time

$K_{(8-12)}$ is a constant

$f(Re)$ is a function of Reynolds number

Δc is the supersaturation of solution at the surface defined by Chandler

n is the empirical index for the solution studied.

Because the surface supersaturation was created by a temperature gradient across the film, the heat transfer coefficient will increase for an increase in Reynolds number. Chandler defined the critical heat transfer rate (q_{crit}) as the heat transfer rate able to produce 100 nuclei/ft^2 hr on the surface. The critical supersaturation is the supersaturation required to cause a nucleation rate at 100 nuclei/ft^2 hr. From the modified Dittus-Boelter equation, film heat transfer coefficient is proportional to $Re^{0.8}$. Chandler suggested that if

$$\frac{1}{\text{critical surface supersaturation}} = Re^{<0.8}$$

then there was the theoretical possibility that by increasing the

turbulence, the critical heat transfer rate that caused scaling could be increased. From his experimental study Chandler presented the following two empirical equations:

$$q_{crit} = K_{(8-13)}Re^{0.43} \qquad (8-13)$$

$$\text{Critical supersaturation} \propto Re^{-0.37} \qquad (8-14)$$

Therefore, the increase in the turbulence can increase the non-scaling heat transfer capacity of the surface. However the effect is also partly offset by a lowering of the critical supersaturation. This is obviously not applicable to the constant heat flux test section designed for the scaling studies. In those experiments the surface temperature of the scale can be maintained (Fischer, et. al., 1975). However, the actual heat exchanger used in industry relies on temperature gradient as well as the effect of turbulence to achieve heat transfer. Therefore there are advantages to increase the velocity of the cooling water. Apart from the higher shear stress introduced onto the tube surface to remove the scaling nuclei, in general there is an increase in non-scaling heat transfer capacity on the surface.

8.6   WALLERAWANG POWER STATION - ELECTRICITY COMMISSION OF NSW

The cooling towers are used in this power station to dissipate the waste heat. By March 1983, Wallerawang No. 7 condensers experienced back pressure and problems of higher temperatures condensate. Inspection of the condensers revealed considerable scaling (Little, 1984). Condenser tubes were cleared by specially

designed metal scrapers (pushed through by water pressure) and removed
700-800 g of scale and mud per tube. Analysis showed that this
material is approximately 70% calcium carbonate. A high manganese
content in the expelled scale/mud indicated the possible involvement
of chemical or biological manganese precipitation. The quality of the
cooling water between March 1982 and March 1983 are given in Table
(8-7). If a temperature of 43° C of the standard low pressure steam
is considered, the average condenser tubes wall temperature is
approximately 39° C. This is calculated as follows:

Inlet temperature = 25° C

Outlet temperature = 35° C

Saturated steam temperature = 43° C

Average temperature of the water = 30° C

The overall heat transfer coefficient based on outside diameter was
calculated by the Electricity Commission of NSW for 25.4 mm O.D. Al-
brass tubes for a water velocity of 1.28m/s at temperature of 21° C
using the equation

$$U = C \sqrt{(Velocity)} \qquad (8-15)$$

where C = 2623.8 (Heat Exchanger Institute, 1978). The calculated U_o
is 2968.5 W/m^2 $^\circ$C.

For the inlet temperature of 25° C, U_o = 2968.5 x 1.03 = 3057.6
where 1.03 is the correction factor (Heat Exchanger Institute, 1978).
The physical properties of water at 30° are:

TABLE 8-7   Water Quality of Wallerawang Power Station No. 7 Cooling Tower

Date	pH	Cond. (μs/m)	M.O. Alkalinity (ppm $CaCO_3$)	Total Hardness (ppm $CaCO_3$)	Ca Hardness (ppm $CaCO_3$)	SO_4^{2-} ppm	Cl^- ppm	SiO_2 ppm
4.3.82	8.6	150,000	138	490	250	487	72.8	13
10.3.82	9.0	115,000	142	400	210	622	66.8	10.5
16.3.82	8.9	180,000	153	600	280	784	104.7	15
6.5.82	7.85	28,000	-	-	65	48	-	-
14.5.82	8.4	85,000	158	470	220	500	12.5	21.8
18.5.82	8.3	72,000	118	460	120	260	14	-
26.5.82	8.55	110,000	164	372	180	297	57	22
2.6.82	8.3	110,000	116	365	215	363	58	19.6
9.6.82	8.3	110,000	104	480	280	487	54.6	10.6
18.6.82	8.4	55,000	96	220	130	118	30.3	6.8
24.6.82	8.7	110,000	122	370	190	490	55	11.6
30.6.82	8.5	110,000	116	400	190	433	67	21.5
7.7.82	8.2	170,000	138	640	300	487	72.8	11.7
15.7.82	8.3	240,000	-	-	410	720	-	-
23.7.82	8.7	340,000	224	1210	510	1190	174.5	32.8
27.7.82	8.65	420,000	196	1160	450	1298	211	44.2
4.8.82	8.5	360,000	190	1180	400	1149	149	60
11.8.82	8.55	320,000	195	1200	450	1203	143	53
20.8.82	8.65	285,000	210	1030	525	1041	152	55.5
26.8.82	8.6	245,000	195	910	410	1028	128	48.5
2.9.82	8.6	180,000	190	630	275	622	102	30.5
10.9.82	8.55	190,000	240	540	250	580	103	22
23.9.82	7.8	120,000	80	520	265	527	81	22
27.9.82	8.1	170,000	112	600	300	580	129	6
29.10.82	8.15	68,000	108	224	122	135	39.5	6.4
4.11.82	7.7	110,000	115	330	150	284	90	14.5
9.11.82	8.55	163,000	195	630	240	514	41	17
10.11.82	8.55	310,000	240	1150	500	1136	17.1	36.5
25.11.82	8.6	290,000	235	950	430	919	148	22
2.12.82	8.4	260,000	250	890	420	811	181	23.5
8.12.82	8.45	340,000	125	830	380	865	155	6.0
17.12.82	8.3	340,000	305	1350	630	1380	196	31
23.12.82	8.3	320,000	230	1160	540	1190	190	20.5
29.12.82	8.5	290,000	-	1100	440	1030	-	-
9.2.83	8.2	115,000	110	370	180	365	65	33.5
16.2.83	8.45	135,000	160	470	260	581	80	30.5
24.2.83	8.4	175,000	145	540	270	554	80	31.5
2.3.83	8.65	200,000	220	685	380	744	106	46
9.3.83	8.5	230,000	260	840	470	840	156	50.5
17.3.83	8.5	220,000	180	810	415	879	115	39.5
25.3.83	7.0	180,000	30	690	340	906	111	25.1
30.3.83	8.0	180,000	45	670	390	745	118	42

Density = 995.65 kg/m^3

Viscosity = 0.798 x 10^3 kg/m s

Thermal conductivity = 0.6145 J/m s °C

Specific heat = 4.186 x 10^3

Reynolds number Re = $\dfrac{D_i v \rho}{\mu}$ = $\dfrac{0.02286 \times 1.28 \times 995.65}{0.798 \times 10^{-3}}$

$\qquad\qquad\qquad$ = 3.65 x 10^4

$\circ$

Prandtl number Pr = $\dfrac{C_p \mu}{k}$ = $\dfrac{4.186 \times 10^3 \times 0.798 \times 10^{-3}}{0.6145}$

$\qquad\qquad\qquad$ = 5.436

Preliminary estimates of water film heat transfer coefficient can be calculated by the empirical correlation:

$$\frac{h_i}{C_p \mu}\left(\frac{C_p \mu}{k}\right)^{2/3}\left(\frac{\mu_w}{\mu}\right)^{0.14} = \frac{0.023[1+(D/L)^{0.7}]}{(DG/\mu)^{0.2}}$$

Omitting the corrections for tube length and for viscosity ratio:

$$h_i = \frac{0.023 \times 1.28 \times 995.65 \times 4.186 \times 10^3}{(3.65 \times 10^4)^{0.2} \times (5.436)^{2/3}}$$

The overall temperature decrease = 43 - 30 = 13° C

The temperature decrease over the water resistance:

$$\Delta T_i = \frac{0.02530 \times 3057.7}{0.02286 \times 4854.9} \times (43-30) = 9.1°C$$

$$T_w = T + \Delta T_i = 30 + 9.1 = 39.1°C$$

The viscosity of the water at T_w is then:

$$\mu_w = 0.653 \times 10^{-3} \text{kg/m s}$$

The viscosity-correction factor = 0.9723

The corrected coefficient = 4720.5 W/m^2 $^{\circ}C$

The temperature drop over the water resistance and the wall temperature become

$$\Delta T_i = \frac{0.02530 \times 3057.6}{0.02286 \times 4720.5} \times (43-30) = 9.3^{\circ}C$$

$$T_w = T + \Delta T_i = 30 + 9.3 = 39.3^{\circ}C$$

This is so close to the wall temperature calculated previously that a second approximation is unnecessary.

Some Langelier Indexes of the water calculated at bulk temperature, as well as tube wall temperature, are given in Table (8-8). Data show that there were prolonged periods of high supersaturation of the cooling water with respect to calcium carbonate. From 23/7/83 to 26/8/1982, the arithmetic mean of Larson and Buswell's langelier Index calculated at bulk temperature is 1.68 and 1.76 at heat transfer surface. From 16/11/82 to 23/12/1982, it is 1.57 and 1.64 respectively. From 2/3/83 to 17/3/83, it is 1.65 and 1.72 respectively. The condenser cooling water was maintained at a positive Langelier Index for the rest of the period to prevent corrosion. It is very likely that scaling began in the period from 23/7/82 to 26/8/82 because the water had the potential of both bulk precipitation and wall crystallization of calcium carbonate. In practice the power station condenser is operating at the higher flow velocity compared to the test rig (1.5 to 2.0 m/s compared to 0.5 m/s in the case of the Liddell power station study). Therefore there will

TABLE 8-8   Langelier Indexes Calculated for the Wallerawang Power Station

Date	LBLI* at Bulk Temp	LBLI at Surface Temp	IPLI** at Bulk Temp	IPLI at Surface Temp	S at Bulk Temp#	S at Surface Temp##
23.7.82	1.81	1.85	1.60	1.66	36.5	41.2
27.7.82	1.73	1.92	1.54	1.72	31.4	47.8
4.4.82	1.48	1.56	1.30	1.37	18.8	22.0
11.8.82	1.59	1.66	1.40	1.47	23.6	27.6
20.8.82	1.80	1.88	1.62	1.69	38.1	44.3
26.8.82	1.62	1.69	1.43	1.50	25.1	29.2
16.11.82	1.74	1.82	1.55	1.62	33.1	38.6
25.11.82	1.72	1.80	1.55	1.62	32.7	38.0
2.12.82	1.55	1.62	1.39	1.46	23.3	27.1
8.12.82	1.26	1.33	1.10	1.17	12.0	14.0
17.12.82	1.65	1.73	1.46	1.53	27.8	32.4
23.12.82	1.49	1.56	1.31	1.37	19.4	22.7
2.3.83	1.72	1.79	1.55	1.61	32.4	37.6
9.3.83	1.71	1.79	1.54	1.61	32.8	38.1
17.3.83	1.51	1.58	1.34	1.40	20.4	23.8

*   LBLI stands for Larson and Buswell's Langelier Index

**   IPLI stands for Ion Pair Consideration Langelier Index

Calculated at 35° C

Calculated at 39° C

be a higher shear stress. However, the heat flux is of a similar order, hence there is no additional tolerance due to increase in Reynolds number (Section (8.5)). It is likely that the shear stress of 4.66 N/m^2 calculated at 1.5 m/s for a 18 gauge Alumimum Brass tube, which is already 5 times higher than at 0.5 m/s (0.93 N/m^2) is still insufficient to remove the calcium carbonate scale. Further evidence was observed from the calculation of the threshold Langelier Index on data reported by Morse and Knudsen (1977) (Section (8.5)). The shear stress calculated was 4.71 N/m^2. After the formation of the first layer of calcium carbonate nuclei on the heat transfer surface, the scale continued to grow into a thick and adherent scale under the positive Langelier Index. The involvement of chemical or biofouling by manganese or the presence of clays worsens the situation because this also provides the sites for wall crystallization and may even reduce the threshold surface Langelier Index (supersaturation).

In view of all these factors, a cooling water therefore requires constant monitoring of water chemistry to ensure that langelier Index thresholds for both bulk precipitation and wall crystallization are not exceeded, although the surface threshold is considered more critical under designed heat flux and flow rate. The water, especially when a cooling tower is used, requires appropriate control on biofouling because of the nature of the cooling tower.

8.7 EFFECT OF MAGNESIUM

Watkinson (1983) had reported his findings on the effect of magnesium on scaling. He studied the effect on magnesium on both scaling rates where bulk precipiation is encouraged (at 57° C) and low

scaling rate (25° C). A range of Mg^{2+}/Ca^{2+} ratios between 0 and 1 were studied and a significant minimum scaling rate was observed for a Mg/Ca ratio of 0.2 at 57° C bulk temperature, a weak minimum was observed at 25° C. It is evident that at 57° C the presence of magnesium reduced the scaling rate, however this is not so apparent at 25° C. It is known that Magnesium can change the crystal habit of calcium carbonate from calcite to aragonite (Möller and Rajagopalan, 1975; Reddy and Nancollas, 1976), however a ratio of Mg/Ca exceeding 4 was required to change calcite to aragonite at 25° C (Möller and Rajagoplan, 1975). From the calcium carboante precipitation study (Chapter 5), there was no reduction in the rate of precipitation of calcium carbonate due to equal molar concentrations of magnesium present in experiments run at 700 r.p.m. The crystal habit is calcite and was similar to the crystals formed under non-stirring conditions. Again from the Lake Liddell water investigation (Chapter 7), the scale samples observed under scanning electron microscopy are very similar to the crystal habit (polyhedral) observed from the precipitation experiment. No magnesium was detected in the scale sample (see Appendix E). In the Lake Liddell study, bulk precipitation did take place. However, it is similar to precipitation of non stirred samples due to the 4.6 m^3 above-ground pool used to achieve evaporative cooling. The water temperature is approxmately 25° C. Together with the finding of Watkinson, it seems that the presence of magnesium has an insignificant effect to calcium carbonate scaling at 25° C within the range of 0 to 1 Mg/Ca ratio. However there is significant reduction in the scaling rate at 57° C. This is probably due to the already predominant aragonite form at higher temperatures further suffers blockage of magnesium cation during the process of crystallization to slow down the rate of formation. In addition, the

aragonite form is of low mechanical strength compared to calcite and therefore is less tenancious. The nett result is a significant reduction of scaling as observed by Watkinson. The reason for the minimum observed is not clear, but probably reflects the incorporation of magnesium into the calcium based scale.

CHAPTER 9

CONCLUSIONS AND RECOMMENDATIONS

9.1 CONCLUSIONS

The following list briefly describes the general conclusions drawn from the discussion of results given in Chapter 5, 7 and 8.

Calcium Carbonate Precipitation Studies

1. The interfacial energy of calcium carbonate (calcite predominating precipitate) is 101 mJ/m^2 as determined by visual induction period data and 110 mJ/m^2 as determined by latent period data. The recent published data on the interfacial energy by Söhnel and Mullin (1978) and Söhnel and Mullin (1982) is within the range 83 - 120 mJ/m^2.

2. The interfacial energy of calcium carbonate vaterite predominating precipitate) is 118 mJ/m^2 as determined by visual induction period data and 114 mJ/m^2 as determined by the latent period.

3. It is possible to obtain a reasonably accurate estimate of interfacial energy of calcium carbonate by bulk precipitation using the latent period data obtained from pH measurement.

4. The order of nucleation was found to be equal to 8 by plotting logarithm of induction period against logarithm of supersaturation defined as S-1. Mullin and Ang (1976) used the same approach to calculate the order of nucleation of nickel ammonium

sulphate and obtained a value of 3.2

5. The metastable limit of calcium carbonate is at the degree of supersaturation (S) equal to 10, below which nucleation does not occur.

6. At low initial degrees of supersaturation (S < 25) at 25°C, the bulk crystallization experiments invariably produced calcite crystals irrespective of stirring speed. Calcite is thermodynamically most stable at 25°C and 1 atmoshpheric pressure.

7. At higher initial degrees of supersaturation (S > 25) at 25°C, the final product invariably consists of more than one type of calcium carbonate. Both aragonite and vaterite were observed. The product was either the mixture of aragonite and calcite or vaterite and calcite. The calcite form was always present but in scattered proportion for the power input per litre within the range of 0.10 to 0.48 J/L s. The power input variation was achieved by changing the speed of stirring of the 62.3 mm diameter 6 blade turbine impeller in a 5.1 litre of liquid (Geometry B). However, when the power input was beyond 0.48 J/L s, the precipitate was predominantly vaterite with some calcite. At the moderate power input of 0.32 J/L s generated by the 93.5 mm diameter 6 blade turbine impeller stirring the 5.1 litre liquid at 220 r.p.m. (Geometry A), when the initial degree of supersaturation was 76.4 and beyond, only calcite crystals were formed. The details of the reactor and impeller geometry were defined in Chapter 4. Both the degree of stirring and the initial degree of supersaturation affect the crystal product, however, the degree of stirring as well as the pattern of stirring generated by different impeller and reactor geometry seems to exert a greater influence. The aragonite found in these batch experiments at

25°C appeared as aggregate of crystals in unique shape as the result of continuing outward growth of a bundle of aragonite crystals into the calcium carbonate rich environment.

8. The kinetics of bulk crystallization of calcium carbonate can be described by the Davies and Jones equation. The overall growth rate constants are independent of the initial degree of supersaturation and stirring speed (under fully suspended conditions). Therefore the crystallization of calcium carbonate is confirmed to be surface-reaction controlled.

9. The overall growth rates of calcium carbonate precipitation can be determined by the spontaneous precipitation method with results comparable with the values obtained from the seeded crystal growth method published in the literature (Reddy and Nancollas, 1971; Nancollas and Reddy, 1971). The overall growth rate of the vaterite predominating precipitate was found to be faster than calcite/aragonite precipitate as well as the pure calcite precipitate.

10. The overall growth rate constants calculated by simplified overall growth rate method (Section (4.3.4)) were found to be $11.5 \pm 1.0 \times 10^3$ L^2/mole min m^2 and $20.5 \pm 2.3 \times 10^3$ L^2/mole min m^2 for calcite and vaterite respectively.

11. The overall growth rate constants calculated by overall growth rate with the size consideration method (Section (4.3.5)) using Microvideomat 2 image analyzer to measure the size distribution of the final precipitate were found to be less reproducible. The rate constants of calcite were found to be in the range $17.2 - 25.2 \times 10^3$ L^2/mole min m^2. The rate constants of vaterite were found to be in the range $28.3 - 40.2 \times 10^3$ L^2/mole min m^2.

12. Kazmlierczak et. al. (1982) using a seeded precipitation

technique and reported the rate constant of calcite to be $17.8 \pm 1.2 \times 10^3$ L^2/mole min m^2. They also recalculated Nancollas and Reddy (1971) results and reported the value of 15×10^3 L^2/mole min m^2. Comparing the results obtained from this research, the value 15×10^3 L^2/mole min m^2 can be considered as the typical value of the calcite crystallization rate constant. There is no value published on vaterite crystallization hence comparison is not possible. However, using the values of calcite as the general guideline, the most probable value of vaterite crystallization rate constants lie within the range 20 - 30×10^3 L^2/mole min m^2.

13. The simplified overall growth rate method for interpreting the kinetic data generated by spontaneous precipitation experiments can be recommended for general crystallization studies for its reproducibility and simplicity. The accuracy can be improved if the sampling of crystal suspension can avoid the effect of suction and hence give rise a more representative sample.

14. The reproducibility of the overall growth rate method with size consideration may be improved if the final crystal suspension can be sized and counted for a large quantity by using an instrument such as Coulter counter to get a more representative crystal surface area.

15. At 220 r.p.m. using Geometry A, aragonite gradually became predominant, in the form of long needle-like aragonite aggregates of irregular pattern as temperature increased from 36°C to 55.8°C. At 55.8°C, crystal products were 100% aragonite aggregates. These aragonite aggregates were different from the one produced from 25°C experiments. They broke up easily into discrete aragonite crystals indicating the formation of

aggregates was due to agglomeration rather then the continuing growth of crystals as in the case of 25°C experiments.

16. The degree of mixing had an apparent effect on the number of nuclei generated. The number increased as stirring speed increased from 300 to 700 r.p.m. in Geometry B stirred reactor. However, very vigorous stirring had the opposite effect. At S = 25.6, 880 r.p.m. reduced the number of nuclei by an order of magnitude when compared to 500 r.p.m.

17. The stirrer-crystal collision was the major mechanism of secondary nucleation in the bulk precipitation. The empirical equation describing the kinetics of secondary nucleation of calcium carbonate was derived as $J = 2.323 \times 10^6 S^{7.9} \varepsilon M_x$ where J is rate of nucleation in number of nuclei per second, S is the degree of supersaturation, ε is the power in J/L s and M_x is the crystal concentration in g/L. The correlation coefficient was 0.9713. This empirical equation is applicable for the range of power input per unit volume of 0.10 to 1.31 J/L s and very low crystal concentrations (≤ 0.0021 g/L). The exponent of the degree of supersaturation p=7.9 is in agreement with the order of homogeneous nucleation expressed as the exponent of supersaturation (S-1) determined by induction period measurement. The order of nucleation determined is equal to 8.

18. The presence of magnesium in the molar concentration equal to calcium was found to prolong the induction period. However, the increase in stirring speed minimized such effects. The induction period was reduced sharply when the stirring speed was increased from 400 r.p.m. to 500 r.p.m.

19. There was a range of degrees of mixing represented by 400 to 500 r.p.m. using Geometry B of 1:1 Mg/Ca system in which aragonite

aggregates were the predominating crystallographic form at 25°C and S=24. However, both the extremes of zero and vigorous stirring (700 r.p.m.) produced polyhedral calcite (combination of prism with rhombodedron) which was the result of the survival of fast growing crystal faces which otherwise disappeared in pure calcium carbonate system.

20. In a 1:1 Mg/Ca system, the kinetics of secondary nucleation appeared to be different from pure calcium carbonate system.

21. In 1:1 Mg/Ca system at 25°C, there seemed to be no retardation of calcite due to magnesium.

Investigation of Scaling Potential of Lake Liddell Water to Power Station Condenser Tubes

22. A test rig consisted of a 3.55 m heating section and a 4.5 m^3 above ground pool water reservoir was used to simulate the Liddell power station cooling water system. The water from Lake Liddell was tested for its scale forming potential over a broad range of total alkalinity and total calcium content. The possible threshold level of scaling expressed as Langelier Index at bulk inlet temperature was found to be 1.40 calculated by Larson and Buswell empirical temperature and ionic strength correction and 1.25 calculated with ion pair consideration.

23. The heat transfer surface temperature was found to be a critical factor. Therefore threshold Langelier Index at heat transfer surface was calculated. The threshold Langelier Index at heat

transfer surface was 1.69 by Larson and Buswell and 1.52 by ion pair consideration.

24. The cooling water of Lake Liddell power station cooling system must not be operated at or beyond the experimental threshold Langelier Index for the bulk of water.

25. There was a critical degree of supersaturation for the bulk of water as well as heat transfer surface. The former was estimated as 17.0 and the latter as 31.6

26. The scaling of calcium carbonate in the condenser tubes was the result of bulk precipitation as well as wall crystallization under testing conditions. However, wall crystallization can be solely responsible for scaling when the effect of heat transfer surface temperature is apparent.

27. The profile of calcium carbonate scale thickness in the tube increased along the tube from the inlet to the outlet of the tube. This was in accordance with the bulk temperature profile on the cooling water along the tube.

28. The crystal habit of the scale observed by scanning electron microscopy was found to be identical with the crystal habit of the precipitate formed in the 1:1 Mg/Ca batch precipitation experiment at 700 r.p.m. at 25°C (Section (5.2.3)). The polyhedral calcite was the combination of prism with rhombohedon forms.

<u>Prediction</u> <u>of</u> <u>Calcium</u> <u>Carbonate</u> <u>Scaling</u> <u>in</u> <u>the</u> <u>Heat</u> <u>Exchanger</u> <u>of</u> <u>a</u> <u>Cooling</u> <u>Water</u> <u>System</u>

29. The overall growth rate model based on the growth rate calcium carbonate described by surface reaction controlled mechanism was developed for scaling rate prediction in the heat exchanger. The growth rate constant of calcium carbonate was obtained from batch precipitation kinetic study of calcium carbonate and modified by the Van't Hoff-Arrhenius equation for the heat transfer surface temperature. This model was tested on the scaling rate data obtained from Lake Liddel water investigation (Chapter 7) and published data from the literature. Data were selected from calcium carbonate predominant scale to avoid the complication of the removal of scale due to high fluid shear and less tenacious scale. The model predicted well on some data but showed consistent overestimation of scaling rate when significant discrepancy was evident. This was due to the underestimation of the actual reaction surface area, which was the crystal surface area deposited on the heat transfer surface compared to only the heat transfer surface area.

30. The Hasson's diffusion model was also tested in parallel with the overall growth rate model. The model predicted fairly well below 4×10^{-6} m^2 °C/KJ. However more than 50% of the data were less than the actual scaling rate by a factor of 2 - 6. Beyond 4×10^{-6} m^2 °C/KJ, the predicted values were an order of magnitude less than the actual scaling rate. The discrepency is believed to be again due to the failure to incorporate the actual deposited crystal surface area which is the actual mass transfer surface area instead of the surface of the tube. Nevertheless, because of the more reliable mass transfer coefficient value obtained from the j-factor analogy, this model is considered more reliable for moderate scaling rate ($dR_f/d\theta < 4 \times 10^{-6}$ m^2 °C/KJ).

31. Before the actual reaction or mass transfer surface area built up by the deposited crystal can be incorporated into either model, the overall growth rate model can be used in parallel with the Hasson's diffusion model to safeguard the possible underestimation due to Hasson's diffusion model.

32. The threshold Larson and Buswell Langelier Index based on heat transfer surface temperature determined from Lake Liddell water investigation as 1.69 was checked against published data from the literature. It seems that this number is valid (1.68-1.69) as the threshold Langelier Index calculated according to the surface temperature for other cooling water systems for the inlet water at 30°C or less. When the shear stress on the surface due to the velocity of the cooling water is higher than 4.71 N/m^2, it is possible that the effect of shear stress that sweeps away the deposited crystals and nuclei can increase the threshold Langelier Index. The effect will be more evident if the bulk inlet temperature is at 35°C or more which normally causes the formation of discrete aragonite crystals in the midst of calcite. The resulting scale will be less tenacious and easily swept away by the velocity shear stress. The threshold Langelier Index under this condition (the data reported by Coates and Knudsen, 1980) was found to be 1.86 or more.

33. The threshold Larson and Buswell Langelier Index was also checked against the actual operating data of the Wallerawang power station of Electricity Commission of New South Wales which experienced condenser tubes scaling. The shear stress calculated was 4.66 N/m^2. The operating data showed substantial periods of time when both Langelier Indexes based on bulk inlet and heat transfer surface temperatures were above the threshold calculated from

Lake Liddell water investigation (1.68 and 1.76 respectively).
Therefore the threshold Langelier Index based on heat transfer
surface temperature (1.69) successfully explains and predicts the
scaling encountered.

34. In general, the constant heating medium heat exchangers will be
less susceptible to scaling if operating under high cooling water
velocity because of higher shear stress to remove the scale from
the surface as well as an increase in non-scaling heat transfer
capacity on the surface.

35. The presence of magnesium has an insignificant effect to calcium
carbonate scaling at 25°C within the range of 0 to 1 Mg/Ca ratio.

9.2 RECOMMENDATIONS

The following are recommendations for further research into this
topic:

1. The growth rate constants of calcite determined by batch precipi-
tation experiments are only available for the temperature range
from 10 - 40°C. At most heat transfer surfaces the temperatures
are greater than 40°C. Such information can be conveniently
obtained by seeded crystallization experiments at controlled
solution temperatures greater than 40°C.

2. A study of the kinetics of calcium carbonate crystallization is
needed to investigate the effects of impurities commonly encoun-
tered in the surface waters. This will facilitate a more accu-
rate assessment to the scaling potential when waters are used as
cooling water. The effect of temperature and power input also
requires further study.

3. The mechanism of calcium carbonate crystallization has been generalized as surface-reaction controlled. The surfaces of the crystals produced from relatively low degrees of supersaturation show layering which indicates surface layer growth. However, it is not clear as to what type of surface reaction is the rate determining mechanism. Experiments can be designed to investigate the crystal product at different degrees of supersaturation by using scanning electron microscopy to observe the formation of the cyrstal surfaces. This is able to serve as the starting point to identify whether the surface reaction is nucleation controlled or screw dislocation.

4. The accuracy of the spontaneous precipitation method for general crystallization studies can be further improved by modification of the sampling method and also the crystals sizing methods. Further investigation is required to check the superiority for particle sizing of using fast scanning Coulter counter directly onto the final crystal suspensions as compared to the Microvideomat 2 image analyzer.

5. The spontaneous precipitation experiment at 25°C has special significance to power station cooling water systems. In power station cooling water systems when cooling towers are used as the cooling device, the cooling water is recirculated in a closed-loop pattern. The result of recirculation by pumps implies a constant increase of calcium carbonate nuclei in the system similar to secondary nucleation in relation to the power input studied by the batch spontaneous precipitation experiments. Because of the coexistence of bulk precipitation and wall crystallization in many calcium carbonate scaling situations, the role of bulk precipitation has to be described by secondary nucleation in the

cooling water system. Further study is required to relate the secondary nucleation of calcium carbonate to the cooling water systems. Such studies can be carried out on a test rig similar to the test rig described in Chapter 7 using various pumping speeds (r.p.m.) for a specified cooling water composition. The number of nuclei in the flow can be counted with respect to time to observe the transient increase/decrease of nuclei due to the power input. Two experiments can be carried out in parallel for each pumping speed, with heating and without heating, to determine the contribution of scaling due to bulk precipitation under similar test conditions.

6. The water chemical compostions calculated based on thermodynamic equilibria of the salts present can be improved by incorporating additional species such as silicate. The effect of magnesium on calcium carbonate precipitation has been investigated and reported (Möller and Rajagopalan, 1975; Reddy and Nancollas, 1976; Reddy and Wang, 1980; Watkinson, 1983). However, more work is still required to relate the effect of magnesium on calcium carbonate precipitation to calcium carbonate scaling in the heat exchangers. The effect of silicate can be significant, yet such information is very scarce. The presence of such foreign compounds will alter the rate of crystal growth as well as the tenacity of the scale.

7. The effect of heat transfer surface temperature on the formation of different crystallographic calcium carbonate crystals requires further investigation. This project has already indicated the significance of heat transfer surface temperature in predicting the scaling potential. Therefore, more information in this area will enable accurate predictions to be made.

8. The velocity shear stress of the cooling water plays a significant role in preventing or reducing the growth of calcium carbonate scale on the heat transfer surfaces. The precipitation experiments in Chapter 4 indicates that the formation of crystal habits are closely affected by the degree of mixing and temperature. Experiments PE18 and PE19 even suggested the possibility to encourage the formation of discrete acicular aragonite in the presence of magnesium by manipulating the degree of mixing. This implies that the formation of scale for certain velocities will be weak and easily removed due to the presence of the loosely formed aragonite. Further research is required to establish an optimal velocity related to a range of calcium carbonate deposits from pure calcium carbonate to mixtures of magnesium and calcium carbonates and silicates. The degree of tenacity of scale related to crystal composition and forms as the result of velocity (analogous to the degree of mixing in the stirred reactor experiments) can subsequently provide a more realistic estimate of the fouling factor due to calcium carbonate scaling for heat exchanger design.

9. The actual reaction or mass transfer surface area represented by the deposited crystal surface areas on the heat transfer surfaces have to be incorporated into either the overall growth rate model or the Hasson's diffusion model for accurate prediction of the rate of scaling.

NOTATION

a   Exponent

a_{sol} Activity of the solution

a_{sod} Activity of the solid

a'   Mean distance of closest approach

A   Surface area

A'   Cross sectional area of the flow stream

A_1 Constant

[Alk]   Total alkalinity in equivalents per litre

b   Slope of solubility curve

b'   Cooling rate

B   Adherence parameter

B_1 Constant

B^Q Nucleation rate

c   Concentration at any given time

c_o Incoming concentration

c_b Bulk concentration

c_i Interfacial concentration; molar concentration of ionic species with charge z_i

c_m Concentration greater than the saturated concentration but below which nucleation does not occur

c_r Concentration of material which undergoes the reaction

c_s Surface concentration; saturated concentration

c_{in} Initial concentration

c_{SE} Equilibrium concentration of surface adsorbed molecules at the given temperature

c_{t_1} Concentration of the liquid at temperature t_1

c'_{t_1} Hypothetical concentration of the liquid saturated with scaling component at temperature t_1

c_+	Concentration of the bulk cation
c_-	Concentration of the bulk anion
c'_+	Total concentration of the adsorbed cation
c'_-	Total concentration of the adsorbed anion
c_{+s}	Equilibrium concentration of the cation
c_{-s}	Equilibrium concentration of the anion
C	Impeller distance off vessel bottom
$C_1 - C_9$	Constants
C_p	Specific heat
C_T	Total carbon
C_{T_i}	Initial total carbon
Δc	Supersaturation
d	Particle diameter
d_m	Molecular diameter
d_o	Lattice parameter
d_p	Particle size
D	Molecular diffusivity; impeller diameter
D_e	Equivalent diameter of the annular flow passage
D_h	Hydraulic diameter
D_i	Inside diameter of the tube
D_o	Outside diameter of the tube
D_s	Surface diffusion coefficient
$\bar{D}_L$	Logarithmic mean diameter of the tube
Δd	Difference in lattice parameter between solid and nucleus
E	Activation energy of the reaction
E_{imp}	Impact energy
f	Blasius friction factor
f_m	Monovalent activity coefficient
f_d	Divalent activity coefficient

$f_{\pm}$	Mean activity coefficient
$f(C)$	Function of the precipitation solute concentration
$f(S)$	Function of the available surface area during crystallization
G	Linear growth rate
ΔG	Free energy change
ΔG^*	Critical free energy change
h	Step height
h_i	Film coefficient of the inside tube
h_o	Film coefficient of the outside tube
h_{d_i}	Fouling factor of the inside tube
h_{d_o}	Fouling factor of the outside tube
i	Exponent
I	Ionic strength
I_i	Chronomal of i order
J	Number nucleation rate
J'	Mass nucleation rate
J_G	Flux of solute on the surface of the crystal
J_K	Flux of solute away from the surface of the crystal
J_{c-c}	Contact nucleation rate due to crystal-crystal collision
J_{c-ms}	Contact nucleation rate due to collision of crystal-stirrer collision
k	Overall growth rate constant
k'	Factor defined in Equation (4-112)
K''	Gradient of overall growth rate equation with size consideration
k_f	Thermal conductivity of the deposit
k_m	Thermal conductivity of the tube wall
k_w	Thermal conductivity of the water
$k_1 - k_3$	First order rate constants in Equation (4-19)

k4   Rate constant in Equation (4-19)

K Boltzman constant

$K_{(eq. nos.)}$ Constant

K' Weight of the substance precipitated by cooling a unit volume

of saturated solution by 1°C

K_d Mass transfer coefficient

K_G Combined diffusion-reaction mass transfer coefficient

K_H Henry's constant

K_n Nucleation rate constant

K_r Surface reaction coefficient

K_T Constant in Equation (4-116)

K_w Dissociation constant of water

K_1 Dissociation constant of carbonic acid

K_2 Dissociation constant of bicarbonate

K_1' Dissociation constant of carbonic acid corrected for activity

coefficient

K_2' Dissociation constant of bicarbonate corrected for activity

coefficient

K_4 Dissociation constant of $CaCO_3^o$

K_5 Rate constant of the formation of $CaCO_3^o$/unit crystal surface

as defined in Equation (4-44)

K_{DJ} Constant of the Davies and Jones model

K_{sp} Solubility product of calcium carbonate

K_{sp}' Solubility product of calcium carbonate corrected for activity

coefficients

ℓ Exponent

1   Blade length of the impeller

L   Length; particle size

L_f	Final crystal size
L_{in}	Initial crystal size
$\overline{L}$	Mean crystal size
$\overline{L^3}$	Normalized third moment of size distribution
$\overline{L^3_f}$	Normalized third moment of size distribution of final size
m	Constant
m_4	4th moment about zero of population distribution
m_z	Mass of crystal of size z which do not redissolve into solution
M	Molecular weight
M_x	Total crystal mass above size d_x
M_T	Solids concentration
n	Exponent; particle population
n^o	Nuclei population density
n'	Number of molecule in a nucleus
n^*	Number of molecule in a critical nucleus
n_m	Number of the monomer
n_1	Number of impeller blade for condition 1
n_2	Number of impeller blade for condition 2
$\overline{n}$	Average population density in the size range $L_1 - L_2$
N	Impeller speed; number of nuclei generated by one collision; number of crystal per unit volume
N^o	Number of crystal of L→0
N_p	Power number
p	Wetted perimeter; constant
p'	Blade pitch of the impeller
P	Power input
P_1	Metastable zone width
P_d	Probability factor

$(Pr)_f$	Prandtl number based on average film temperature
Q	Volumetric flow rate
q	Heat flux
r	Radius of the nucleus
r^*	Radius of the critical nucleus
R	Standard gas constant
R'	Dissolution rate
R_c	Crystal growth rate perpendicular to the surface
R_f	Thermal resistance due to the fouling deposit
R_G	Overall growth rate
R_f^*	Asymptotic fouling resistance
Re	Reynolds number
$(Re)_f$	Reynolds number based on average film temperature
s	Supersaturation defined in Equation (6-41)
S	Degree of supersaturation
S'	Solute supersaturation in weight per unit volume
S_a	Degree of supersaturation based on activity
Sc	Schmidt number
Sh	Sherwood number
t	Temperature
t_b	Bulk temperature
t_w	Wall temperature
t_{in}	Inlet temperature
Δt_{max}	Maximum allowable undercooling
T	Absolute temperature; vessel diameter
T_G	Latency time
T_s	Surface temperature expressed in absolute temperature
T_{Ca}	Total molar calcium concentration
U	Overall heat transfer coefficient
U_K	Activation energy for the formation a kink
U_o	Overall heat transfer coefficient based on outside diameter

v	Velocity
v_∞	Velocity of a straight step of crystal growth
$\bar{v}_s$	Fluid velocity averaged over the cross section of the pipe; average speed of surface adsorbed
V	Volume
V_m	Molecular volume
V_o	Initial crystal growth velocity
w	Impeller blade width
w_{d_p}	Collision frequency of crystal with size d_p
W	Mass of the crystal or scale deposit
W_i	Dehydration energy of ions
W_K	Dehydration energy of kinks
W_T	Weight of total deposit (ionic diffusion and particulate)
x	Degree of precipitation
x_f	Thickness of the deposit
x_s	Mean diffusion distance on the surface in time θ
x_w	Thickness of the tube wall
Y_o	Step spacing
z	Exponent
z_1	Valencies or charges of cation
z_2	Valencies of charges of anion
Z	Liquid depth

Greek Symbol

α_1	Arbitrary constant characteristic of degree of precipitation when diffusion-controlled is valid
α_N	Gradient based on crystal number
α_t	Gradient based on induction period
α_a	Particle volume shape factor

α_v	Particle surface shape factor
β	Constant
β'	Geometry shape factor
β_r	Rate of removal of molecules from molecular cluster
δ	Length of diffusion path
δ'	Disregistry
ϵ	Dissipated energy per unit mass/volume
θ	Time
θ_1	Time scale
θ_c	Time constant characterizing the tenacity of deposit
θ_D	Induction period of scaling in heat exchanger
θ_m	Retention time
θ_{ind}	Induction period
θ_{lat}	Latent period
θ_o	Characteristic time constant defined in Equation (6-78)
θ_p	Retention time of plug flow system
ξ	Contact angle
ϕ	Factor
ϕ_d	Rate of deposition
ϕ_r	Rate of removal of scale
ρ	Density
ρ_c	Density of the crystal
ρ_f	Bulk density of deposit
ρ_w	Density of the fluid
η_r	Effective factor
σ	Solid-liquid surface energy
σ'	Degree of supersaturation defined as $S - 1$
τ	Fluid wall shear stress
ω	Apparent angular velocity of the spiral

ψ Potential difference between crystal and the bulk solution

ψ Function of the deposit structure

γ_o Kink retardation constant

μ_1 Chemical potential of the substance per molecule in the dissolved state

μ_2 Chemical potential of the substance per molcule in the solid state

μ_s Normalized s moment about the mean

Ω Degree of supersaturation as defined in Equation (4-33)

Ω Water characterization factor which is the function of Langelier Index

Σ Strain between nucleus and solid particle

ν Frequency of oscillations of the growth units in steps

Δ Amount of calcium carbonate remaining to be precipitated as defined in Equation (4-16)

APPENDIX A   RESULTS OF SPONTANEOUS CRYSTALLIZATION EXPERIMENT

TABLE A.1   Results of Experiment PE4

Temperature: 25°C

Initial Total Sodium: 0.001167 M

Initial Total Calcium: 0.001999 M

Initial Total Chloride: 0.003998 M

pH	Time (min)	$T_{Ca} \times 10^3$ M
8.86	0	1.999
8.85	16.1	1.989
8.84	18.4	1.958
8.83	19.3	1.937
8.82	19.9	1.917
8.81	20.7	1.897
8.80	21.2	1.877
8.79	21.5	1.857
8.78	22.1	1.837
8.77	22.5	1.817
8.76	23.0	1.798
8.75	23.7	1.778
8.72	24.5	1.730
8.71	25.1	1.711
8.70	25.5	1.702
8.69	25.8	1.683
8.68	26.2	1.664
8.66	26.8	1.636
8.65	27.1	1.626
8.64	27.4	1.608
8.63	27.6	1.599
8.62	28.0	1.581
8.61	28.3	1.572
8.60	28.7	1.563
8.59	28.9	1.545
8.57	29.7	1.518
8.56	29.9	1.509
8.54	30.5	1.491
8.53	31.0	1.482
8.52	31.2	1.465
8.51	31.6	1.456
8.50	31.8	1.447
8.49	32.1	1.439
8.48	32.8	1.430
8.47	33.0	1.422
8.46	33.3	1.414
8.44	33.5	1.397
8.43	33.9	1.389

TABLE A.1   (Cont'd)

8.42	34.5	1.372
8.41	35.0	1.364
8.40	35.4	1.356
8.38	36.2	1.340
8.37	36.7	1.332
8.36	36.9	1.324
8.34	37.8	1.308
8.33	38.2	1.300
8.32	38.6	1.293
8.30	39.5	1.285
8.29	40.4	1.277
8.28	40.9	1.259
8.27	41.4	1.262
8.26	41.9	1.255
8.25	42.4	1.247
8.24	43.2	1.240
8.23	43.6	1.232
8.21	45.1	1.225
8.20	45.7	1.218
8.19	46.7	1.210
8.18	47.1	1.203
8.17	48.6	1.196
8.16	49.1	1.189
8.15	50.7	1.183
8.14	51.1	1.176
8.13	52.7	1.169
8.12	54.0	1.163
8.11	54.9	1.156
8.10	58.4	1.149
8.09	59.3	1.137
8.08	61.6	1.130
8.07	64.4	1.124
8.06	66.9	1.117
7.95	equilibrated	

TABLE A.2   Results of Experiment PE5

Temperature: 25.0°C

Initial Total Sodium: 0.01167 M

Initial Total Calcium: 0.001999 M

Initial Total Chloride: 0.003998 M

pH	Time (min)	$T_{Ca} \times 10^3$ M
8.86	0	1.999
8.85	15.3	1.989
8.84	17.5	1.958
8.83	18.9	1.937
8.82	20.3	1.917
8.81	21.3	1.897
8.80	22.2	1.877
8.79	23.0	1.857
8.78	23.8	1.837
8.77	24.5	1.817
8.76	25.2	1.798
8.75	25.9	1.778
8.74	26.3	1.769
8.73	26.9	1.749
8.72	27.6	1.730
8.71	28.1	1.711
8.70	28.6	1.702
8.69	29.2	1.683
8.68	29.6	1.664
8.67	30.2	1.655
8.66	30.6	1.636
8.65	31.2	1.627
8.63	32.1	1.599
8.62	32.5	1.581
8.61	33.1	1.572
8.60	33.5	1.563
8.59	33.9	1.545
8.58	34.3	1.536
8.56	35.3	1.509
8.55	35.9	1.500
8.54	36.3	1.491
8.53	36.6	1.482
8.52	36.9	1.465
8.51	37.6	1.456
8.50	38.1	1.447
8.49	38.5	1.489
8.47	39.6	1.422

(Cont'd)

TABLE A.2   (Cont'd)

8.46	40.1	1.414
8.45	41.2	1.397
8.43	41.4	1.380
8.42	42.1	1.372
8.41	42.6	1.364
8.40	43.1	1.356
8.39	43.8	1.348
8.38	44.1	1.340
8.37	44.7	1.332
8.36	45.2	1.324
8.35	45.9	1.316
8.34	46.6	1.308
8.33	47.3	1.300
8.32	47.9	1.293
8.31	48.5	1.285
8.29	49.1	1.277
8.28	50.6	1.270
8.27	51.6	1.262
8.26	52.3	1.255
8.25	53.2	1.247
8.24	54.2	1.240
8.23	54.9	1.232
8.21	56.9	1.225
8.20	57.9	1.218
8.19	58.9	1.210
8.18	60.2	1.203
8.17	61.6	1.196
8.16	62.7	1.189
8.15	64.4	1.183
8.14	65.8	1.176
8.13	67.4	1.169
8.12	69.4	1.163
8.11	71.5	1.156
8.10	73.5	1.149
8.09	76.2	1.137
8.08	78.9	1.130
8.07	82.1	1.124
7.85		equilibrated

TABLE A.3 Results of Experiment PE6

Temperature: 25.0°C

Initial Total Sodium: 0.01167 M

Initial Total Calcium: 0.001999 M

Initial Total Chloride: 0.003998 M

pH	Time (min)	$T_{Ca} \times 10^3$ M
8.92	0	1.999
8.91	17.8	1.989
8.90	21.8	1.958
8.89	24.4	1.937
8.88	26.4	1.906
8.87	28.1	1.886
8.86	29.8	1.866
8.85	31.1	1.845
8.84	32.9	1.825
8.83	33.9	1.796
8.82	34.9	1.776
8.81	35.9	1.756
8.80	37.1	1.737
8.79	38.3	1.717
8.78	39.3	1.698
8.77	40.5	1.679
8.76	41.4	1.669
8.75	42.4	1.650
8.74	43.5	1.632
8.73	44.4	1.613
8.72	45.4	1.594
8.71	46.3	1.585
8.70	47.5	1.566
8.69	48.4	1.548
8.68	49.3	1.539
8.67	50.1	1.521
8.66	51.3	1.511
8.65	52.1	1.493
8.64	52.6	1.484
8.63	53.7	1.475
8.62	54.7	1.458
8.61	55.4	1.449
8.60	56.7	1.431
8.59	57.1	1.422
8.58	58.9	1.414
8.57	59.9	1.396
8.56	60.7	1.388
8.55	62.1	1.379
8.54	62.8	1.370
8.53	63.9	1.361

(cont'd)

TABLE A.3   (Cont'd)

8.52	64.8	1.353
8.51	65.9	1.336
8.50	66.3	1.328
8.49	67.8	1.319
8.48	69.2	1.311
8.47	70.3	1.303
8.46	71.1	1.295
8.45	72.1	1.286
8.44	73.5	1.278
8.43	74.3	1.270
8.42	75.4	1.262
8.41	76.9	1.254
8.40	77.8	1.246
8.39	79.1	1.238
8.38	80.8	1.230
8.37	82.1	1.223
8.36	83.2	1.215
8.35	84.6	1.207
8.34	85.7	1.199
8.33	87.5	1.192
8.32	89.1	1.184
8.31	89.4	1.177
8.30	91.1	1.169
8.29	93.2	1.162
8.28	94.6	1.154
8.26	98.4	1.149
8.25	100.8	1.139
8.24	102.9	1.132
8.23	104.6	1.125
8.22	107.2	1.117
8.20	111.4	1.110
7.85		equilibrated

TABLE A.4   Results of Experiment PE7

Temperature: 25.0°C

Initial Total Sodium: 0.01167 M

Initial Total Calcium: 0.001999 M

Initial Total Chloride: 0.003998 M

pH	Time (min)	$T_{Ca} \times 10^3$ M
8.87	0	1.999
8.86	12.5	1.989
8.85	13.9	1.968
8.84	15.1	1.937
8.83	16.2	1.917
8.82	17.1	1.897
8.81	17.9	1.877
8.80	18.6	1.856
8.79	19.4	1.836
8.78	19.9	1.817
8.77	20.7	1.797
8.76	21.4	1.778
8.75	21.8	1.758
8.74	22.5	1.739
8.73	25.9	1.729
8.72	23.5	1.710
8.71	24.0	1.691
8.70	24.4	1.682
8.69	25.0	1.663
8.67	26.0	1.635
8.66	26.5	1.616
8.65	27.2	1.607
8.64	27.9	1.589
8.62	28.6	1.562
8.61	28.9	1.552
8.60	29.4	1.544
8.59	29.8	1.526
8.58	30.4	1.517
8.57	30.8	1.499
8.56	31.4	1.490
8.55	31.8	1.481
8.54	32.4	1.472
8.53	32.8	1.463
8.52	33.5	1.446
8.51	33.9	1.437
8.50	34.4	1.429
8.49	34.8	1.420
8.48	35.3	1.412
8.47	36.0	1.403

(Cont'd)

TABLE A.4 (Cont'd)

8.45	37.2	1.387
8.44	37.4	1.378
8.43	38.2	1.362
8.42	38.6	1.354
8.41	39.2	1.345
8.40	39.8	1.337
8.39	40.4	1.329
8.38	41.2	1.321
8.37	41.5	1.313
8.36	42.3	1.306
8.35	42.9	1.298
8.34	43.9	1.290
8.33	44.3	1.282
8.32	45.3	1.274
8.30	45.7	1.267
8.29	47.5	1.259
8.28	48.3	1.252
8.27	49.2	1.244
8.26	50.0	1.237
8.25	51.2	1.229
8.24	52.2	1.221
8.22	53.2	1.214
8.21	55.5	1.207
8.20	56.8	1.199
8.19	57.8	1.192
8.18	59.4	1.185
8.17	61.0	1.178
8.15	62.8	1.171
8.14	64.6	1.165
8.13	66.6	1.158
8.12	68.6	1.151
8.11	73.7	1.138
8.10	76.4	1.132
8.09	80.0	1.125
8.08	83.9	1.119
8.07	87.9	1.106
8.05	98.9	1.099
8.04	106.4	1.092
8.03	115.9	1.086
8.01	126.8	1.079
7.88	equilibrated	

TABLE A.5   Results of Experiment PE8

Temperature: 25.0°C

Initial Total Sodium: 0.01167 M

Initial Total Calcium: 0.001999 M

Initial Total Chloride: 0.003998 M

pH	Time (min)	$T_{Ca} \times 10^3$ M
8.86	0	1.999
8.85	12.1	1.989
8.84	14.3	1.958
8.83	16.0	1.937
8.82	17.5	1.917
8.81	18.6	1.897
8.80	19.7	1.877
8.79	20.6	1.857
8.78	21.6	1.837
8.77	22.4	1.817
8.76	23.4	1.798
8.75	24.1	1.778
8.74	24.8	1.769
8.73	25.7	1.749
8.72	26.5	1.730
8.71	27.0	1.711
8.70	27.9	1.702
8.69	28.4	1.683
8.68	29.2	1.664
8.67	29.8	1.655
8.66	30.4	1.636
8.65	31.0	1.627
8.64	31.8	1.608
8.63	32.3	1.599
8.62	33.3	1.581
8.61	33.7	1.572
8.60	34.4	1.563
8.59	34.9	1.545
8.58	35.5	1.536
8.57	36.3	1.518
8.56	36.9	1.509
8.55	37.6	1.500
8.54	38.1	1.491
8.53	39.0	1.482
8.52	39.4	1.465
8.51	40.3	1.456
8.50	40.9	1.447
8.49	41.5	1.439
8.48	42.1	1.430
8.47	43.0	1.422

TABLE A.5   (Cont'd)

8.46	43.7	1.414
8.45	44.4	1.397
8.44	45.1	1.389
8.43	45.8	1.380
8.42	46.5	1.372
8.41	47.3	1.364
8.40	48.1	1.356
8.39	48.9	1.348
8.38	49.9	1.340
8.37	50.4	1.332
8.36	51.1	1.324
8.35	52.1	1.316
8.34	52.9	1.308
8.33	53.9	1.300
8.32	54.9	1.293
8.31	56.0	1.285
8.30	58.1	1.277
8.28	59.1	1.270
8.27	60.1	1.262
8.26	61.2	1.255
8.25	62.5	1.247
8.24	63.7	1.240
8.23	64.9	1.232
8.21	67.4	1.225
8.20	69.0	1.218
8.19	70.8	1.210
8.18	72.1	1.203
8.17	73.9	1.196
8.16	75.8	1.189
8.15	77.9	1.183
8.14	79.8	1.176
8.13	82.1	1.169
8.12	84.8	1.163
8.11	87.0	1.156
8.10	89.9	1.149
8.09	94.1	1.137
8.08	97.1	1.130
8.07	101.3	1.124
8.06	105.7	1.117
8.04	118.5	1.110
7.89		equilibrated

TABLE A.6 Results of Experiment PE9

Temperature: 25.0°C

Initial Total Sodium: 0.01401 M

Initial Total Calcium: 0.001999 M

Initial Total Chloride: 0.003998 M

pH	Time (min)	$T_{Ca} \times 10^3$ M
8.79	0	1.999
8.78	18.0	1.989
8.77	20.9	1.958
8.76	25.0	1.938
8.75	26.9	1.918
8.74	29.3	1.898
8.73	31.3	1.878
8.72	32.6	1.848
8.71	34.3	1.829
8.70	35.5	1.809
8.69	37.1	1.790
8.68	38.3	1.771
8.67	39.7	1.752
8.66	40.9	1.733
8.65	41.9	1.724
8.64	43.3	1.705
8.63	44.5	1.687
8.62	45.6	1.668
8.61	46.6	1.650
8.60	47.8	1.632
8.59	48.9	1.623
8.58	50.2	1.605
8.57	51.1	1.595
8.56	52.7	1.578
8.55	53.3	1.560
8.54	54.4	1.551
8.53	55.4	1.533
8.52	56.4	1.525
8.51	57.5	1.507
8.50	58.6	1.499
8.49	59.7	1.482
8.48	60.8	1.473
8.47	62.1	1.464
8.46	63.1	1.448
8.45	64.4	1.439
8.44	65.3	1.430
8.43	66.4	1.414
8.42	67.7	1.405

TABLE A.6   (Cont'd)

8.41	69.0	1.397
8.40	69.7	1.388
8.39	71.3	1.380
8.38	72.3	1.364
8.37	73.5	1.356
8.36	75.0	1.348
8.35	75.8	1.340
8.34	77.1	1.332
8.33	78.6	1.317
8.32	80.4	1.309
8.31	81.6	1.301
8.30	82.7	1.293
8.29	84.2	1.286
8.28	86.1	1.278
8.26	88.9	1.256
8.25	90.7	1.248
8.24	92.4	1.241
8.23	93.8	1.234
8.22	95.8	1.226
8.21	97.7	1.219
8.20	99.2	1.212
8.19	101.2	1.205
8.18	102.6	1.190
8.17	105.3	1.183
8.16	107.6	1.176
8.15	109.6	1.169
8.14	112,5	1.162
8.13	115.6	1.155
8.12	117.8	1.149
8.11	120.5	1.142
8.10	123.7	1.135
8.09	126.6	1.128
7.80	equilibrated	

TABLE A.7   Results of Experiment PE11

Temperature: 25.0°C

Initial Total Sodium: 0.005838 M

Initial Total Calcium: 0.001999 M

Initial Total Chloride: 0.003998 M

pH	Time (min)*	$T_{Ca} \times 10^3$ M
8.63	0	1.999
8.68	2.0	1.999
8.69	24.6	1.999
8.68	58.6	1.993
8.67	111.5	1.983
8.66	133.3	1.973
8.65	149.3	1.968
8.64	162.7	1.963
8.63	175.3	1.953
8.62	185.4	1.947
8.61	195.6	1.937
8.60	204.4	1.932
8.59	213.1	1.922
8.58	220.5	1.917
8.57	228.6	1.912
8.56	237.3	1.903
8.55	242.8	1.898
8.54	249.3	1.893
8.53	255.3	1.883
8.52	261.9	1.878
8.51	268.2	1.873
8.50	274.2	1.868
8.49	279.4	1.863
8.48	284.6	1.858
8.47	289.6	1.849
8.46	295.1	1.844
8.45	300.5	1.839
8.44	306.3	1.835

* The pH values occasionally rose to the previous values during the
  course of crystallization due to slight carbon dioxide transfer,
  therefore the times registered were the time of the corresponding
  pH values last recorded.

@ Equilibrated pH = 7.71

TABLE A.8   Results of Experiment PE13

Temperature: 25.0°C

Initial Total Sodium: 0.005838 M

Initial Total Calcium: 0.001999 M

Initial Total Chloride: 0.003998 M

pH	Time (min)*	$T_{Ca} \times 10^3$ M
8.64	0	1.999
8.68	2.0	1.999
8.69	12.4	1.999
8.68	109.4	1.993
8.67	176.4	1.983
8.66	209.4	1.973
8.65	245.5	1.968
8.64	273.8	1.963
8.63	297.2	1.953
8.62	322.4	1.947
8.61	344.8	1.937
8.60	367.7	1.932
8.22	equilibrated	

*   The pH values occassionally rose to the previous values during the
    course of crystallization due to slight carbon dioxide transfer,
    therefore the times registered were the time of the corresponding pH
    values last recorded.

TABLE A.9   Results of Experiment PE14

Temperature: 25.0°C

Initial Total Sodium: 0.009343 M

Initial Total Calcium: 0.001999 M

Initial Total Chloride: 0.003998 M

pH	Time (min)	$T_{Ca} \times 10^3$ M
8.72	0	1.999
8.73	6.8	1.999
8.72	45.9	1.989
8.71	55.6	1.979
8.70	62.7	1.958
8.69	67.7	1.948
8.68	72.1	1.928
8.67	75.4	1.919
8.66	79.2	1.909
8.65	82.4	1.899
8.64	84.9	1.879
8.63	87.9	1.869
8.62	90.2	1.859
8.61	92.9	1.849
8.60	95.9	1.839
8.59	97.2	1.830
8.58	99.7	1.820
8.57	101.6	1.811
8.56	103.9	1.801
8.55	105.4	1.783
8.54	107.5	1.773
8.53	109.1	1.764
8.52	110.9	1.755
8.51	112.6	1.746
8.50	114.3	1.736
8.48	115.9	1.727
8.47	119.3	1.718
8.46	120.4	1.709
8.45	122.9	1.700
8.44	123.9	1.691
8.43	126.0	1.683
8.42	127.9	1.674
8.41	129.3	1.665
8.39	132.3	1.656
8.38	133.9	1.647
8.37	135.4	1.639
8.36	137.3	1.630
8.34	140.3	1.622
8.33	142.2	1.614

(Cont'd)

TABLE A.9   (Cont'd)

8.32	143.9	1.605
8.31	145.2	1.597
8.29	148.6	1.589
8.28	150.4	1.581
8.27	151.9	1.573
8.25	155.2	1.565
8.24	157.1	1.557
8.23	158.8	1.549
8.21	163.1	1.542
8.20	164.8	1.534
8.19	167.1	1.527
8.17	169.8	1.519
8.16	172.6	1.512
8.15	174.5	1.504
8.13	180.3	1.497
8.12	182.4	1.490
8.11	184.9	1.483
8.09	190.2	1.476
7.79	equilibrated	

TABLE A.10   Results of Experiment PE15

Temperature: 25.0°C

Initial Total Sodium: 0.01185 M

Initial Total Calcium: 0.001999 M

Initial Total Chloride: 0.003998 M

pH	Time (min)	$T_{Ca} \times 10^3$ M
8.85	0	1.999
8.84	5.4	1.988
8.83	7.6	1.967
8.82	9.0	1.937
8.81	10.2	1.917
8.80	11.2	1.896
8.79	12.0	1.877
8.78	12.8	1.857
8.77	13.6	1.837
8.76	14.2	1.817
8.75	14.8	1.800
8.74	15.4	1.779
8.73	16.0	1.759
8.72	16.5	1.750
8.71	17.0	1.730
8.70	17.5	1.712
8.69	18.0	1.702
8.68	18.5	1.683
8.67	15.9	1.664
8.66	19.4	1.655
8.65	19.8	1.637
8.64	20.4	1.627
8.63	20.7	1.609
8.62	21.3	1.600
8.61	21.6	1.582
8.60	22.0	1.573
8.59	22.4	1.564
8.58	22.8	1.546
8.57	23.2	1.537
8.56	23.6	1.528
8.55	24.0	1.510
8.54	24.4	1.501
8.53	24.9	1.492
8.52	25.3	1.483
8.51	25.6	1.474
8.50	26.0	1.457
8.49	26.4	1.449
8.48	26.8	1.440
8.47	27.2	1.432
8.46	27.6	1.423

(Cont'd)

TABLE A.10   (Cont'd)

8.45	27.9	1.415
8.44	28.4	1.406
8.43	28.9	1.398
8.42	29.2	1.382
8.41	29.6	1.373
8.40	30.0	1.365
8.39	30.5	1.357
8.38	31.0	1.349
8.37	31.4	1.341
8.36	31.8	1.333
8.35	32.4	1.325
8.34	32.7	1.318
8.33	33.3	1.310
8.32	33.8	1.302
8.31	34.2	1.294
8.30	34.8	1.287
8.29	35.4	1.279
8.27	35.8	1.272
8.26	36.8	1.264
8.25	37.5	1.257
8.24	38.0	1.249
8.23	38.7	1.242
8.22	39.4	1.234
8.21	40.0	1.227
8.19	41.4	1.219
8.18	42.2	1.212
8.17	42.8	1.205
8.16	43.8	1.198
8.15	44.5	1.191
8.14	45.5	1.185
8.13	46.4	1.178
8.12	47.3	1.165
8.11	48.6	1.158
8.10	49.5	1.152
8.09	50.8	1.145
8.08	52.2	1.138
8.06	53.6	1.132
8.05	56.8	1.125
8.04	58.4	1.118
8.02	62.5	1.111
8.01	64.6	1.104
8.00	67.4	1.098
7.98	73.9	1.091
7.97	77.5	1.085
7.96	82.3	1.078
7.94	93.4	1.072
7.93	101.6	1.065
7.77		equilibrated

TABLE A.11   Results of Experiment PE16

Temperature: 25.0°C

Initial Total Sodium: 0.01231 M

Initial Total Calcium: 0.001999 M

Initial Total Chloride: 0.003998 M

pH	Time (min)	$T_{Ca} \times 10^3$ M
9.03	0	1.999
9.02	5.0	1.978
9.01	6.3	1.947
9.00	7.1	1.916
8.99	7.8	1.885
8.98	8.6	1.854
8.97	9.1	1.824
8.96	9.6	1.794
8.95	10.2	1.764
8.94	10.6	1.734
8.93	11.2	1.704
8.92	11.6	1.685
8.91	11.9	1.655
8.90	12.3	1.636
8.89	12.8	1.607
8.88	13.1	1.587
8.87	13.5	1.559
8.86	13.9	1.540
8.85	14.3	1.521
8.84	14.6	1.502
8.83	14.9	1.483
8.82	15.3	1.464
8.81	15.6	1.446
8.80	16.0	1.427
8.79	16.3	1.409
8.78	16.7	1.391
8.77	17.0	1.373
8.76	17.3	1.355
8.75	17.7	1.337
8.74	18.0	1.320
8.73	18.4	1.302
8.72	18.8	1.293
8.71	19.0	1.276
8.70	19.4	1.258
8.69	19.8	1.250
8.67	20.4	1.224
8.66	20.7	1.207
8.65	21.1	1.199
8.64	21.4	1.182
8.63	22.0	1.173
8.62	22.3	1.157

(Cont'd)

TABLE A.11   (Cont'd)

8.61	22.5	1.148
8.60	22.9	1.132
8.59	23.3	1.124
8.58	23.7	1.116
8.57	24.0	1.099
8.56	24.4	1.091
8.55	24.8	1.083
8.54	25.3	1.075
8.53	25.6	1.067
8.51	26.4	1.043
8.50	26.8	1.035
8.49	27.2	1.028
8.48	27.4	1.020
8.47	28.1	1.012
8.46	28.4	1.004
8.45	28.9	0.997
8.44	29.4	0.989
8.43	29.9	0.974
8.42	30.2	0.967
8.41	30.8	0.959
8.40	31.3	0.952
8.39	31.8	0.944
8.38	32.3	0.937
8.37	32.8	0.968
8.36	33.6	0.922
8.35	34.0	0.915
8.33	34.7	0.908
8.32	36.0	0.901
8.31	36.7	0.894
8.30	37.5	0.887
8.29	38.0	0.880
8.28	38.9	0.873
8.27	39.8	0.866
8.26	40.6	0.859
8.24	42.4	0.852
8.23	43.5	0.845
8.22	44.5	0.822
8.21	45.6	0.831
8.20	47.1	0.824
8.19	48.3	0.818
8.17	49.8	0.811
8.16	52.7	0.805
8.15	54.9	0.798
8.14	57.0	0.792
8.13	59.5	0.785
8.12	62.1	0.779
8.11	65.3	0.767
8.10	68.9	0.760
7.92	equilibrated	

TABLE A.12   Results of Experiment PE18

Temperature: 25.0°C

Initial Total Sodium: 0.01167 M

Initial Total Calcium: 0.001999 M

Initial Total Magnesium: 0.002001 M

Initial Total Chloride: 0.007998 M

pH	Time (min)	$T_{Ca} \times 10^3$ M
8.45	0	1.999
8.44	34.6	1.985
8.43	42.9	1.957
8.41	49.6	1.916
8.40	56.0	1.902
8.39	64.7	1.875
8.38	68.3	1.861
8.37	72.8	1.834
8.36	75.9	1.821
8.35	79.2	1.807
8.34	82.7	1.780
8.33	86.0	1.767
8.32	89.1	1.754
8.31	92.9	1.727
8.30	96.1	1.714
8.29	99.3	1.700
8.28	102.7	1.687
8.27	106.0	1.661
8.26	109.9	1.648
8.25	112.6	1.635
8.24	116.1	1.622
8.23	119.0	1.609
8.22	122.4	1.596
8.21	125.4	1.571
8.20	127.8	1.558
8.19	131.9	1.545
8.18	134.8	1.533
8.17	138.4	1.520
8.16	141.8	1.507
8.15	145.4	1.495
8.14	148.8	1.482
8.13	152.9	1.470
8.12	156.7	1.457
8.11	160.4	1.445
8.10	164.5	1.433
8.09	168.6	1.420

(Cont'd)

TABLE A.12   (Cont'd)

8.08	172.8	1.408
8.07	179.6	1.396
8.06	181.9	1.384
8.05	186.4	1.371
8.04	190.9	1.359
8.03	195.7	1.347
8.01	207.1	1.335
8.00	212.4	1.323
7.70	equilibrated	

TABLE A.13   Results of Experiment PE21

Temperature: 25.0°C

Initial Total Sodium: 0.01447 M

Initial Total Calcium: 0.001999 M

Initial Total Chloride: 0.003998 M

pH	Time (min)	$T_{Ca} \times 10^3$ M
8.70	0	1.999
8.72	4.8	1.999
8.71	8.0	1.988
8.70	9.7	1.968
8.69	12.8	1.948
8.68	13.7	1.919
8.67	14.9	1.900
8.66	15.5	1.880
8.65	16.5	1.861
8.64	17.1	1.842
8.63	17.7	1.823
8.62	18.5	1.813
8.61	19.1	1.795
8.60	19.9	1.776
8.59	20.4	1.757
8.58	21.0	1.739
8.57	21.4	1.730
8.56	22.0	1.711
8.55	22.6	1.693
8.54	23.1	1.684
8.53	23.5	1.666
8.52	24.1	1.648
8.51	24.7	1.639
8.50	25.4	1.622
8.49	26.0	1.613
8.48	26.8	1.595
8.47	27.2	1.587
8.46	27.5	1.569
8.45	27.8	1.561
8.44	28.8	1.552
8.43	29.4	1.535
8.42	29.8	1.527
8.41	30.4	1.518
8.40	30.9	1.501
8.39	31.7	1.492
8.38	32.1	1.484
8.37	32.9	1.476
8.36	33.4	1.467
8.35	34.0	1.451
8.34	34.9	1.443

(Cont'd)

TABLE A.13   (Cont'd)

8.33	35.3	1.435
8.32	35.8	1.427
8.31	36.5	1.411
8.30	37.1	1.404
8.29	37.4	1.396
8.28	38.5	1.388
8.27	39.1	1.373
8.26	39.8	1.365
8.25	40.9	1.357
8.24	41.7	1.350
8.23	42.4	1.342
8.22	43.4	1.335
8.21	44.4	1.320
8.20	45.8	1.313
8.19	46.4	1.306
8.18	47.4	1.298
8.17	48.4	1.291
8.16	49.5	1.284
8.15	50.8	1.270
8.14	51.9	1.263
8.13	53.5	1.256
8.12	54.9	1.249
8.11	56.7	1.242
8.10	59.1	1.235
8.09	60.4	1.228
8.08	62.4	1.214
8.07	63.9	1.208
8.06	66.2	1.201
8.05	68.4	1.194
8.04	70.9	1.187
8.03	74.5	1.181
8.02	79.8	1.168
8.01	82.4	1.156
8.00	88.5	1.149
7.99	95.8	1.137
7.98	100.1	1.119
7.97	105.1	1.112
7.96	111.9	1.100
7.81	equilibrated	

TABLE A.14   Results of Experiment E22

Temperature: 24.8°C

Initial Total Sodium: 0.01491 M

Initial Total Calcium: 0.001995 M

Initial Total Chloride: 0.003991 M

pH	Time (min)	$T_{Ca} \times 10^3$ M
8.82	0	1.995
8.81	8.3	1.985
8.80	10.9	1.955
8.79	12.8	1.925
8.78	14.3	1.905
8.77	15.5	1.875
8.76	16.5	1.855
8.75	17.7	1.856
8.74	18.6	1.806
8.73	19.6	1.787
8.72	20.5	1.767
8.71	21.3	1.738
8.70	22.2	1.719
8.69	23.0	1.700
8.68	23.8	1.681
8.67	24.5	1.663
8.66	25.3	1.644
8.65	26.1	1.626
8.64	26.8	1.608
8.53	34.2	1.431
8.52	34.7	1.422
8.51	35.4	1.414
8.50	36.0	1.397
8.49	36.6	1.388
8.48	37.3	1.372
8.47	37.9	1.363
8.46	38.5	1.347
8.45	39.2	1.339
8.44	39.9	1.332
8.43	40.4	1.314
8.42	41.0	1.306
8.41	41.6	1.290
8.40	42.3	1.281
8.39	43.0	1.273
8.38	43.6	1.265
8.37	44.3	1.257
8.36	44.9	1.241
8.35	45.5	1.233
8.34	46.3	1.226
8.33	46.9	1.218

TABLE A.14   (Cont'd)

8.32	47.6	1.203
8.31	48.4	1.195
8.30	49.0	1.188
8.29	49.7	1.180
8.28	50.5	1.165
8.27	51.2	1.158
8.26	52.0	1.151
8.25	52.7	1.143
8.24	53.4	1.136
7.50	equilibrated	

TABLE A.15   Results of Experiment E23

Temperature: 25.0°C

Initial Total Sodium: 0.01242 M

Initial Total Calcium: 0.001995 M

Initial Total Chloride: 0.003991 M

pH	Time (min)	$T_{Ca} \times 10^3$ M
8.98	0	1.995
8.96	9.3	1.958
8.95	10.5	1.938
8.94	11.7	1.907
8.93	12.5	1.877
8.92	13.6	1.847
8.91	14.4	1.827
8.90	15.2	1.797
8.89	15.8	1.768
8.88	16.5	1.748
8.87	17.2	1.719
8.86	17.9	1.700
8.85	18.5	1.680
8.84	19.1	1.651
8.83	19.5	1.632
8.82	20.3	1.612
8.81	20.8	1.593
8.80	21.4	1.565
8.79	22.0	1.556
8.78	22.5	1.528
8.77	23.0	1.519
8.76	23.5	1.500
8.75	24.1	1.482
8.73	25.3	1.446
8.72	25.8	1.428
8.71	26.4	1.410
8.70	26.8	1.401
8.69	27.4	1.383
8.68	27.9	1.366
8.67	28.5	1.348
8.66	29.0	1.340
8.65	29.5	1.322
8.64	30.1	1.314
8.63	30.5	1.296
8.60	32.3	1.254
8.59	32.8	1.246
8.58	33.3	1.237
8.57	33.8	1.229
8.56	34.4	1.213
8.55	34.9	1.204

TABLE A.15   (Cont'd)

8.54	35.5	1.196
8.53	36.1	1.180
8.52	36.6	1.171
8.51	37.3	1.163
8.50	37.9	1.155
8.49	38.4	1.147
8.47	39.8	1.123
8.46	40.3	1.115
8.45	40.9	1.108
8.44	41.7	1.100
8.43	42.3	1.092
8.41	43.5	1.077
8.40	44.2	1.069
8.39	45.0	1.062
8.38	45.8	1.054
8.37	46.5	1.046
8.36	47.1	1.039
8.35	48.0	1.031
8.27	54.9	0.974
8.26	55.9	0.967
8.25	56.9	0.960
8.24	47.8	0.953
8.23	58.9	0.946
8.22	59.9	0.939
8.21	61.4	0.932
8.19	63.8	0.925
8.18	64.9	0.918
8.17	66.3	0.911
8.16	67.9	0.904
8.15	69.3	0.898
8.14	70.8	0.891
8.13	72.2	0.885
8.11	75.7	0.872
8.09	79.8	0.859
8.08	82.1	0.853
8.07	83.9	0.846
8.05	89.0	0.840
8.04	91.5	0.833
8.03	94.4	0.827
8.01	100.8	0.820
8.00	104.4	0.814
7.99	107.9	0.808
7.97	115.6	0.801
7.96	119.9	0.795
7.95	124.8	0.789
7.93	135.8	0.783
7.70		equilibrated

TABLE A.16   Results of Experiment E24

Temperature: 24.8°C

Initial Total Sodium: 0.01277 M

Initial Total Calcium: 0.001997 M

Initial Total Chloride: 0.003993 M

pH	Time (min)	$T_{Ca} \times 10^3$ M
9.02	0	1.997
9.01	5.4	1.975
9.00	6.7	1.955
8.99	7.7	1.913
8.98	8.6	1.883
8.97	9.3	1.852
8.96	10.0	1.822
8.95	10.6	1.792
8.94	11.2	1.762
8.93	11.9	1.733
8.92	12.5	1.703
8.91	13.0	1.673
8.90	13.5	1.654
8.89	14.2	1.625
8.88	14.7	1.606
8.87	15.4	1.577
8.85	16.3	1.530
8.84	16.9	1.511
8.83	17.4	1.492
8.82	18.0	1.473
8.81	18.5	1.454
8.80	19.0	1.436
8.79	19.6	1.418
8.78	20.1	1.400
8.77	20.7	1.382
8.76	21.2	1.364
8.75	21.9	1.346
8.74	22.4	1.328
8.71	23.9	1.276
8.70	24.4	1.267
8.69	25.0	1.250
8.68	25.6	1.233
8.67	26.1	1.224
8.66	26.6	1.207
8.65	27.3	1.199
8.64	27.8	1.182
8.63	28.4	1.174
8.62	28.9	1.157
8.61	29.6	1.149
8.60	30.1	1.132

(Cont'd)

TABLE A.16   (Cont'd)

8.59	30.7	1.124
8.58	31.3	1.108
8.57	31.9	1.100
8.56	32.4	1.092
8.55	33.2	1.076
8.54	33.7	1.068
8.53	34.3	1.059
8.52	35.0	1.051
8.51	35.6	1.043
8.50	36.2	1.028
8.49	36.9	1.020
8.48	37.5	1.012
8.47	38.4	1.004
8.46	38.9	0.997
8.45	39.6	0.989
8.44	40.3	0.981
8.43	40.9	0.966
8.42	41.7	0.959
8.41	42.4	0.951
8.40	43.2	0.944
8.39	44.0	0.937
8.38	44.9	0.929
8.37	45.6	0.922
8.36	46.4	0.915
8.35	47.2	0.908
8.34	48.1	0.900
8.33	48.9	0.893
8.32	49.9	0.886
8.31	50.8	0.879
8.30	51.7	0.872
8.29	52.6	0.865
8.28	53.6	0.858
8.27	54.6	0.851
8.26	55.6	0.844
8.25	56.7	0.838
8.24	57.6	0.831
8.22	59.6	0.824
8.21	61.1	0.817
8.20	62.2	0.810
8.11	75.1	0.752
8.10	77.4	0.746
8.09	78.4	0.740
7.67	equilibrated	

APPENDIX B

PHOTOMICROGRAPHS OF CRYSTALS FROM
SPONTANEOUS CRYSTALLIZATION EXPERIMENTS

Some of the final crystal products from the spontaneous crystalli
zation experiments (Chapter 4) were photographed under light transmitt-
ing microscope (Zeiss Universal microscope, School of Mining) and scan-
ning electron microscope (ISI 100A, School of Textile Technology). Sam-
ples photographed under the scanning electron microscope were coated
with gold to form a conductive coating.

PLATE B1 PE8 (25°C, Geometry B, 400 r.p.m.) Vaterite and some calcite, 300x magnification.

PLATE B2 PE8 Vaterite and the very rare acicular aragonite entity found in this experiment, 1000x magnification.
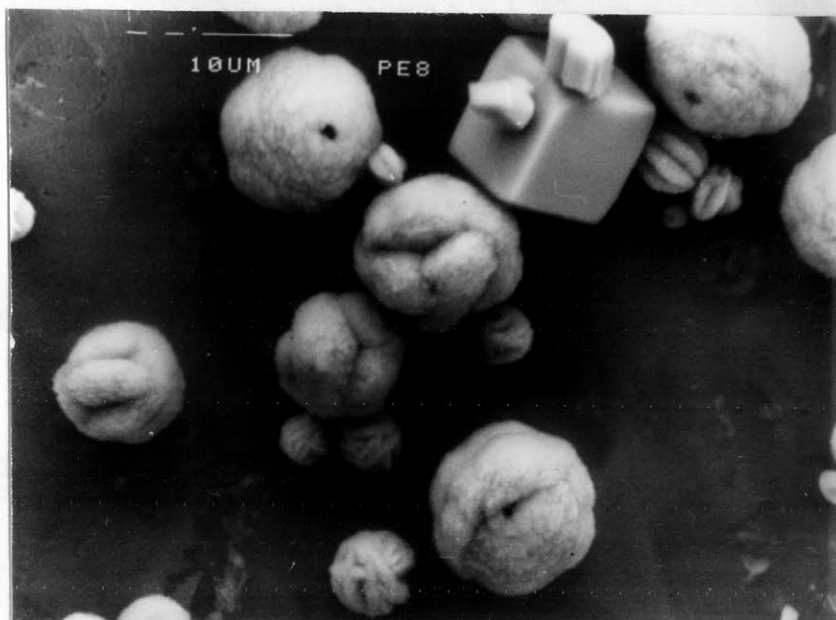
PLATE B3   PE8, Spherical vaterite and rhombohedral calcite,
           1200x magnification.
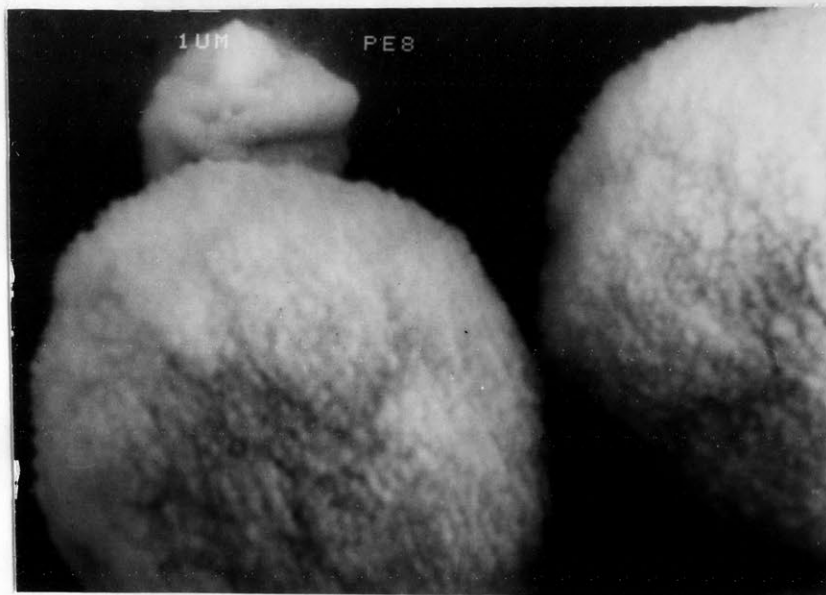
PLATE B4   PE8, Surface of spherical vaterite, 4200x
           magnification.
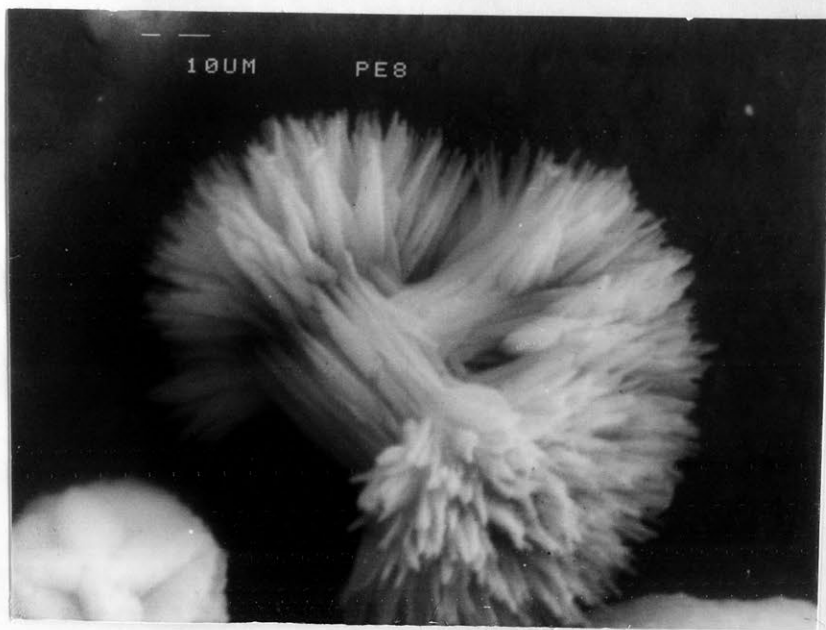
PLATE B5   PE8, An acicular aragonite entity resulted from
the continuing growth of aragonite aggregate,
4200x magnification.
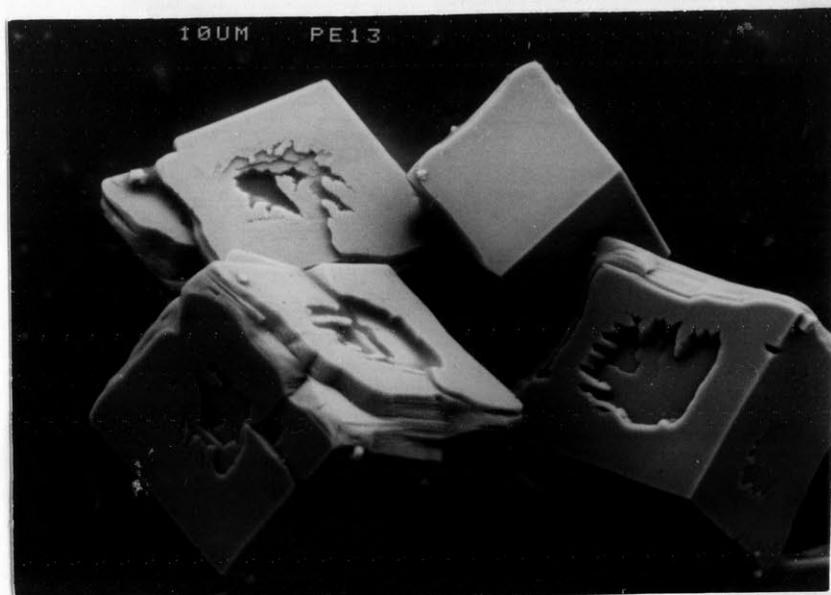
PLATE B6   PE13 (25°C, Geometry B, 400 r.p.m.) Rhombohedral
calcite crystals showing trail of surface layer
growth, 420x magnification.
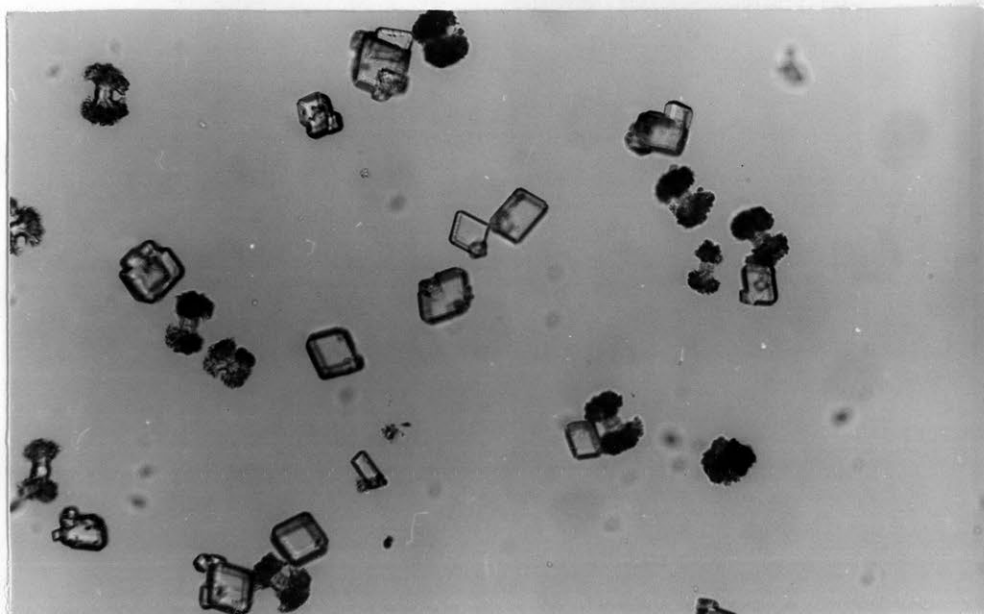
PLATE B7   E22 (24.8°C, Geometry A, 220 r.p.m.) Coexistence of
           calcite and aragonite entity resulted from the con-
           tinuing growth of aragonite aggregates, 250x magni-
           fication.
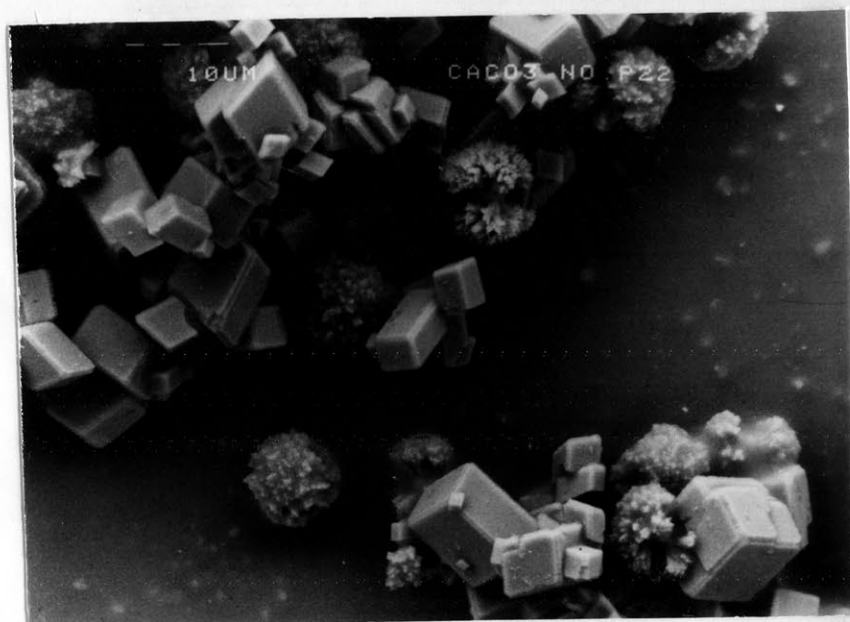
PLATE B8   E22, Coexistence of calcite and aragonite entity,
           420x magnification.
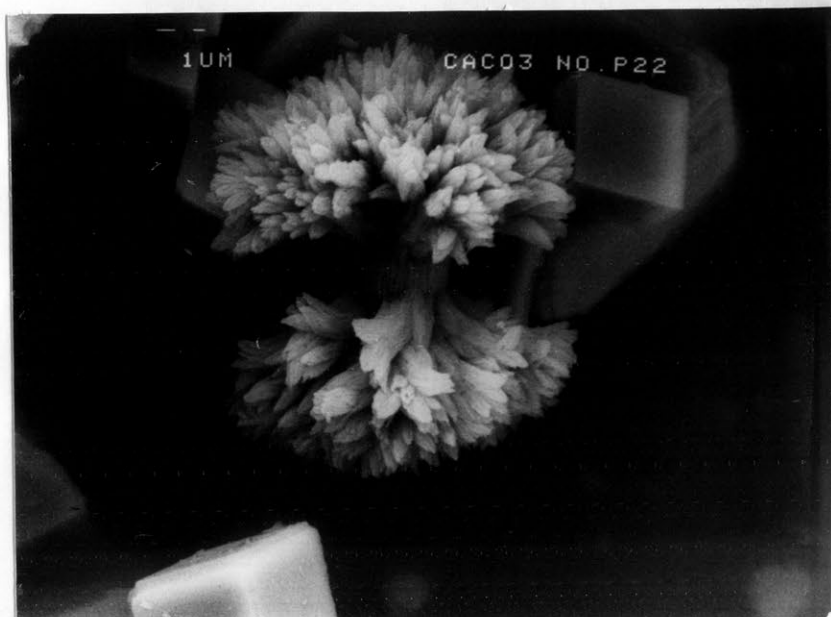
PLATE B9   E22, An aragonite entity resulted from the con-
            tinuing growth of centre aragonite aggregate to-
            ward the calcium carbonate rich surrounding,
            1500x magnification.
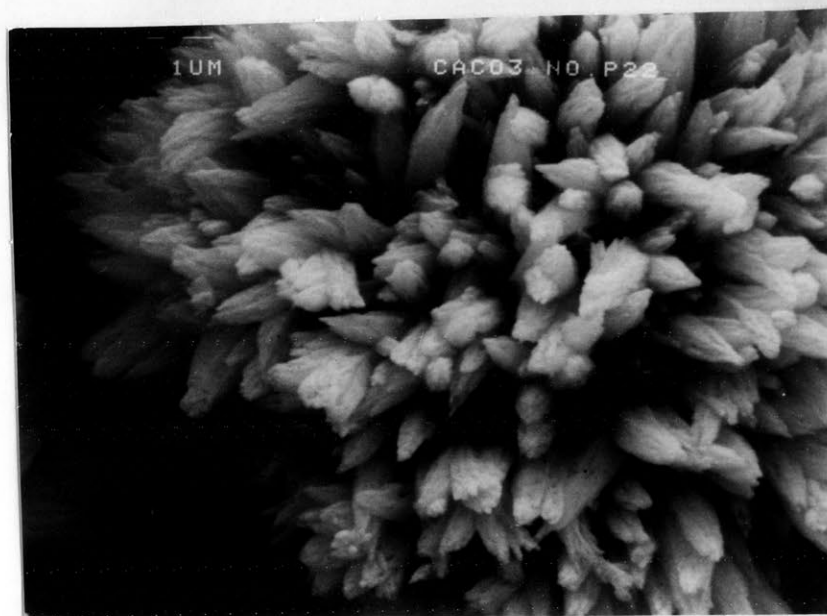
PLATE B10   E22, Surface of the acicular aragonite entity,
            4200x magnification.
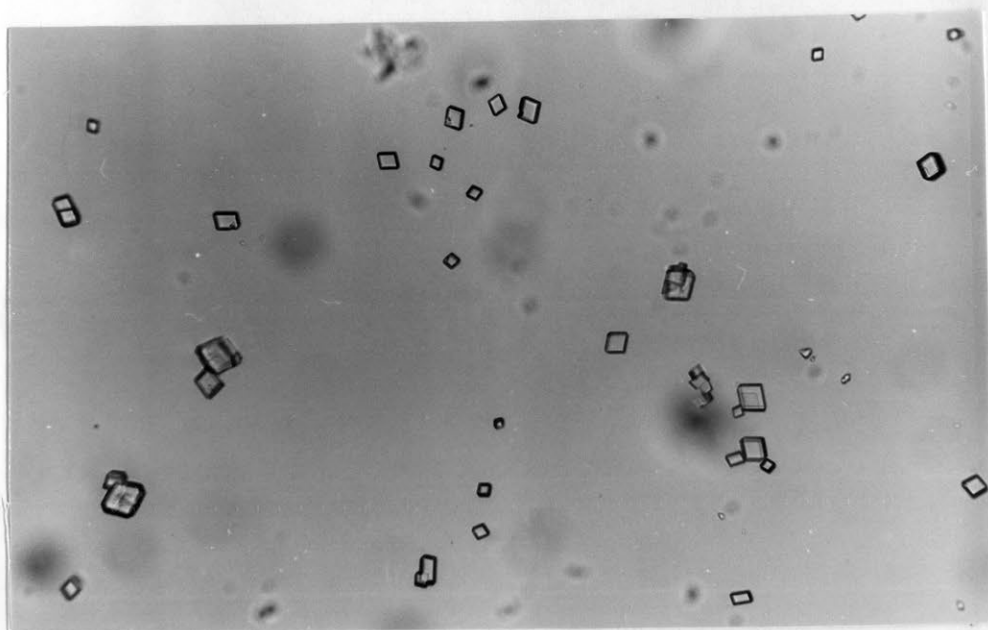
PLATE B11   E24 (24.8°C, Geometry A, 220 r.p.m.) rhombohedral calcite, 250x magnification.
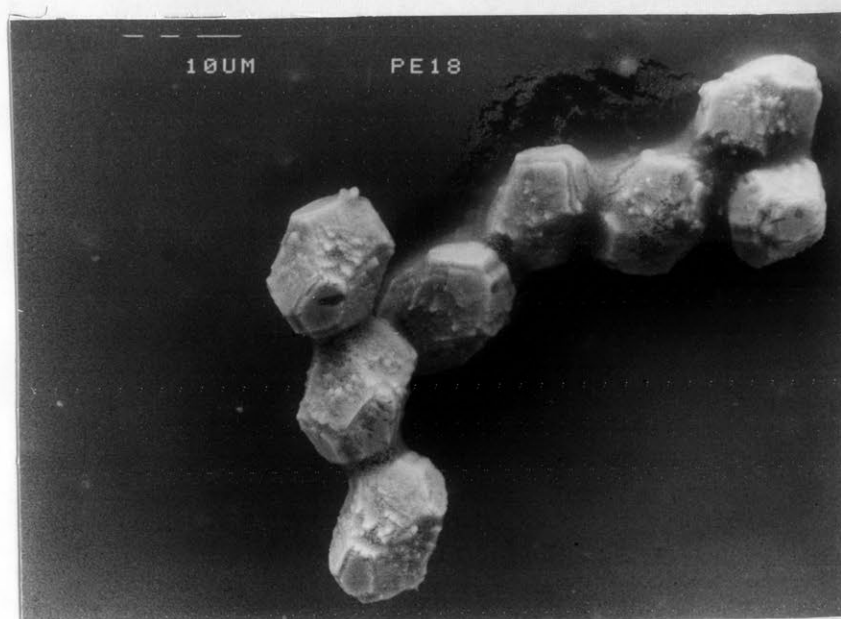
PLATE B12   PE18 (25°C, 1:1 Mg/Ca molar concentration, Geometry B, 700 r.p.m.) Calcite, the crystal habit is the result of the combination of rhombodedron and prism, 420x magnification.
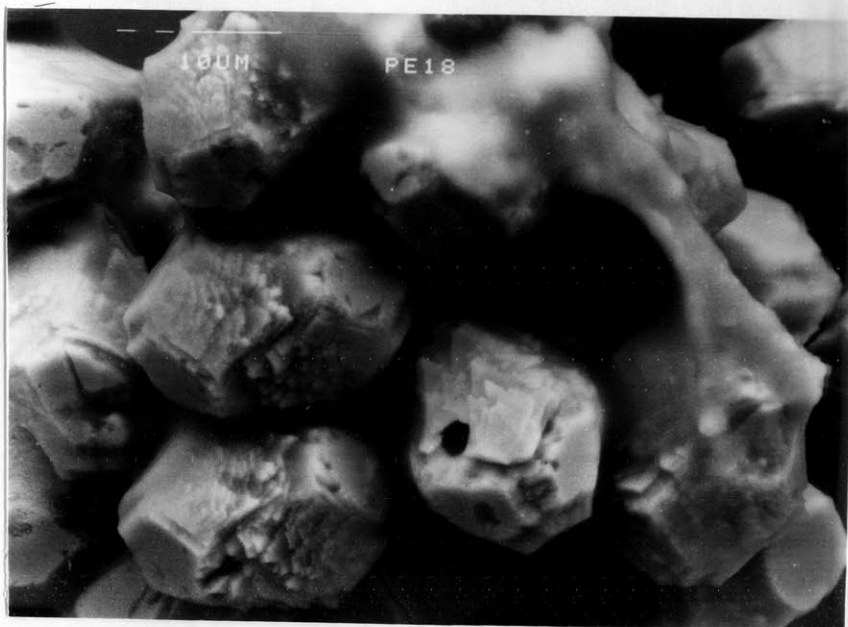
PLATE B13   PE18, calcite crystal surface showing trail of
surface layer growth, 1200x magnification.
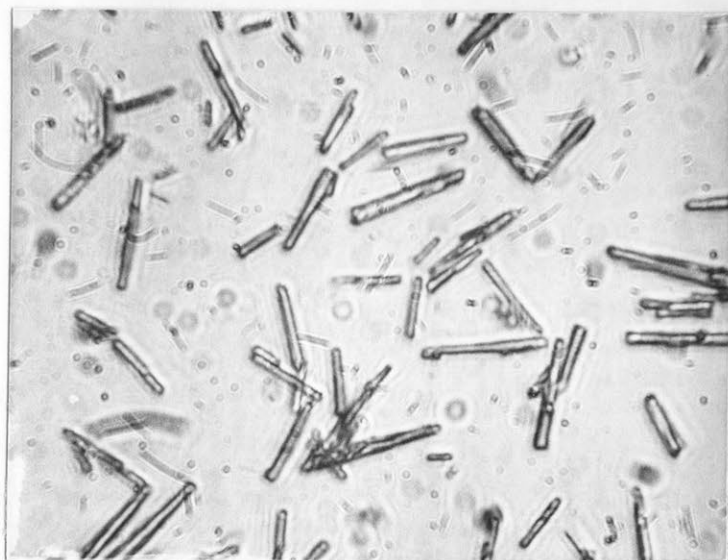
PLATE B14   E36 (55.8°C, Geometry A, 220 r.p.m.) Discrete
acicular aragonite crystals, 800x magnification
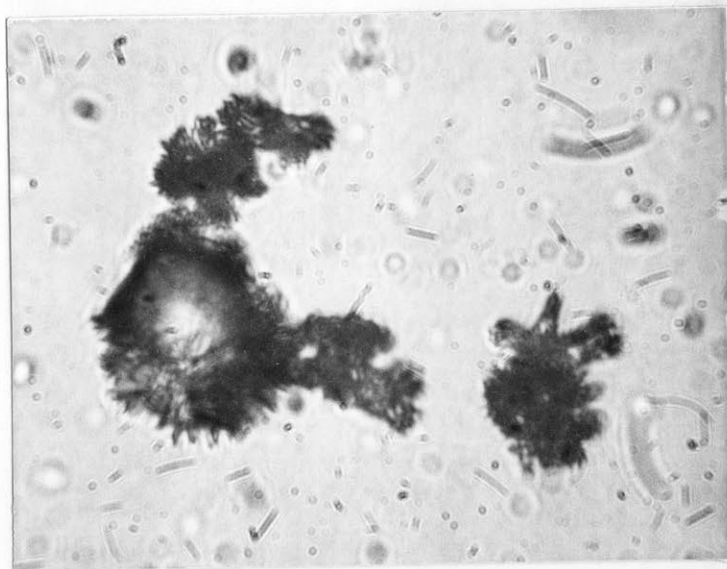
PLATE B15 PE19 (25°C, 1:1 Mg/Ca molar concentration, Geometry
B, 400 r.p.m.) Aragonite aggregates and a calcite
crystal showing sign of transformation to an ara-
gonite aggregate, 800x magnification

APPENDIX C

GRAPHS OF THE SPONTANEOUS CRYSTALLIZATION EXPERIMENTS -

THE CALCULATION OF THE OVERALL GROWTH RATE CONSTANTS

FIGURE C.1 Desupersaturation Curve of Expt. E22
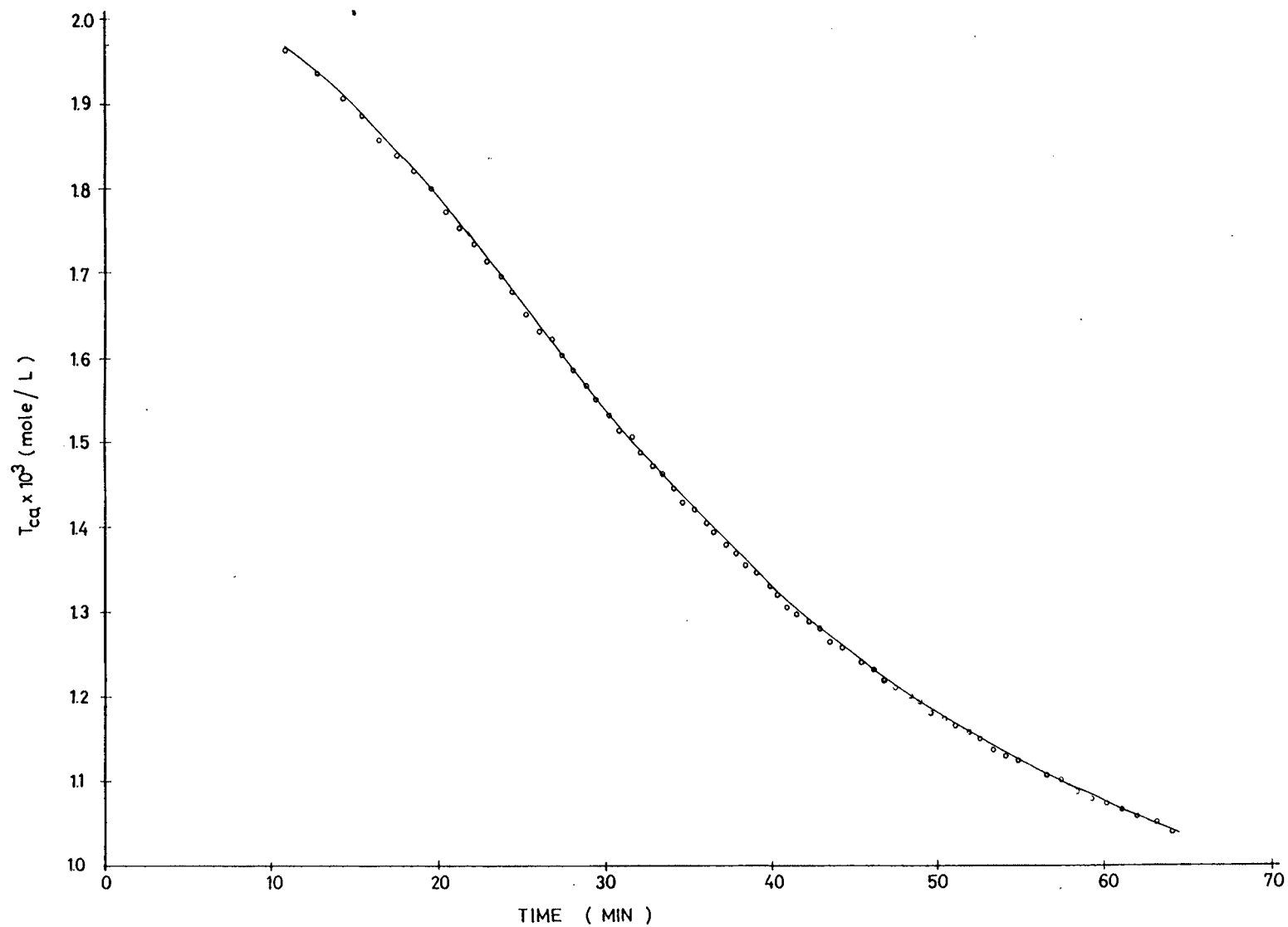
FIGURE C.2   Overall Growth Rate Constant of Expt. E22
Determined from Size Consideration

$k'' = 1.168$

$k_w = 34.7 \times 10^3$

y-axis: $\dfrac{1}{A} \dfrac{dT_{ca}}{do} \times 10^8$ (mole/L min cm^2)

x-axis: $f(C) \times 10^8$ (mole^2/L^2)
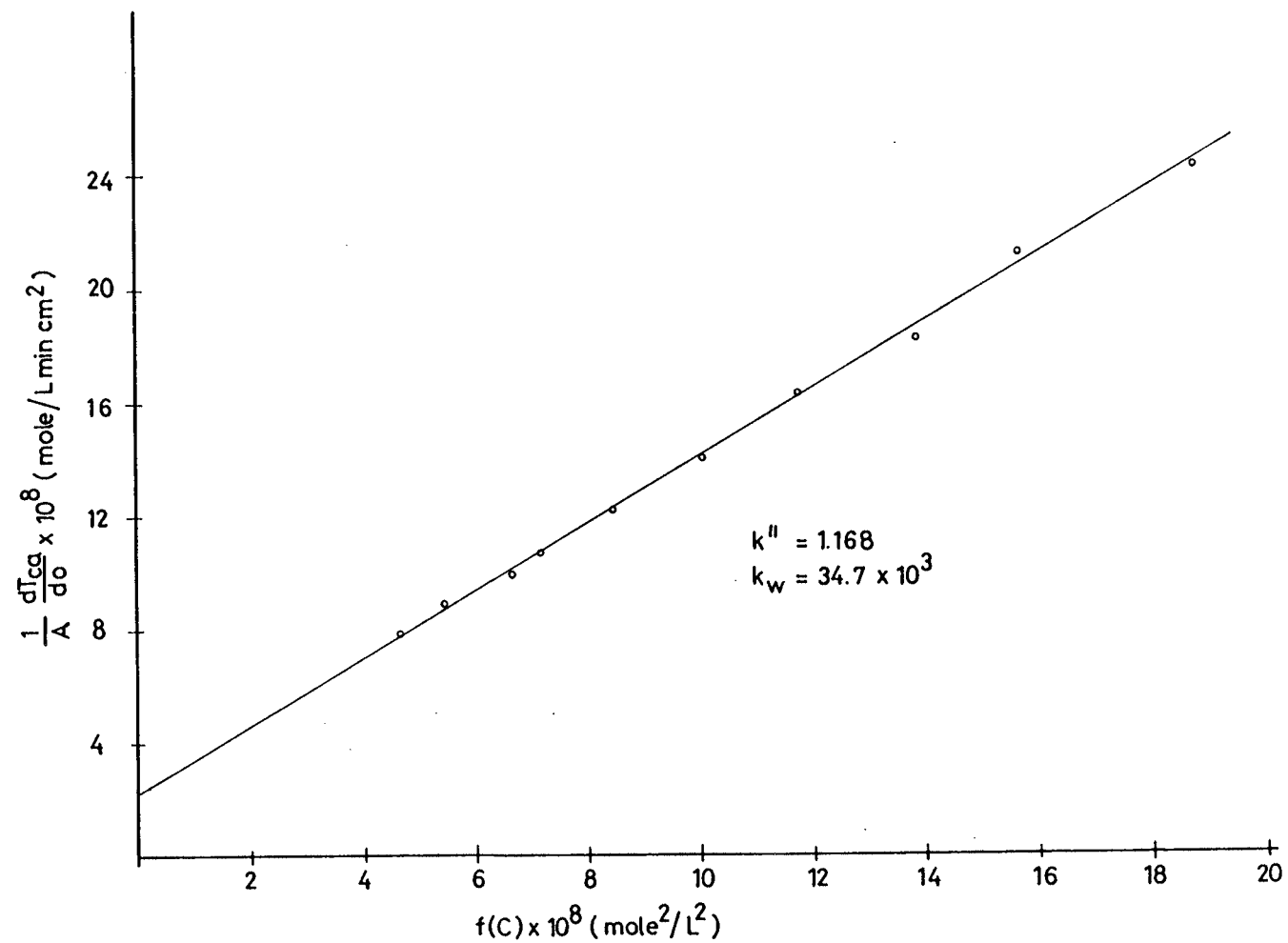
FIGURE C.3 Desupersaturation Curve of Expt. E23
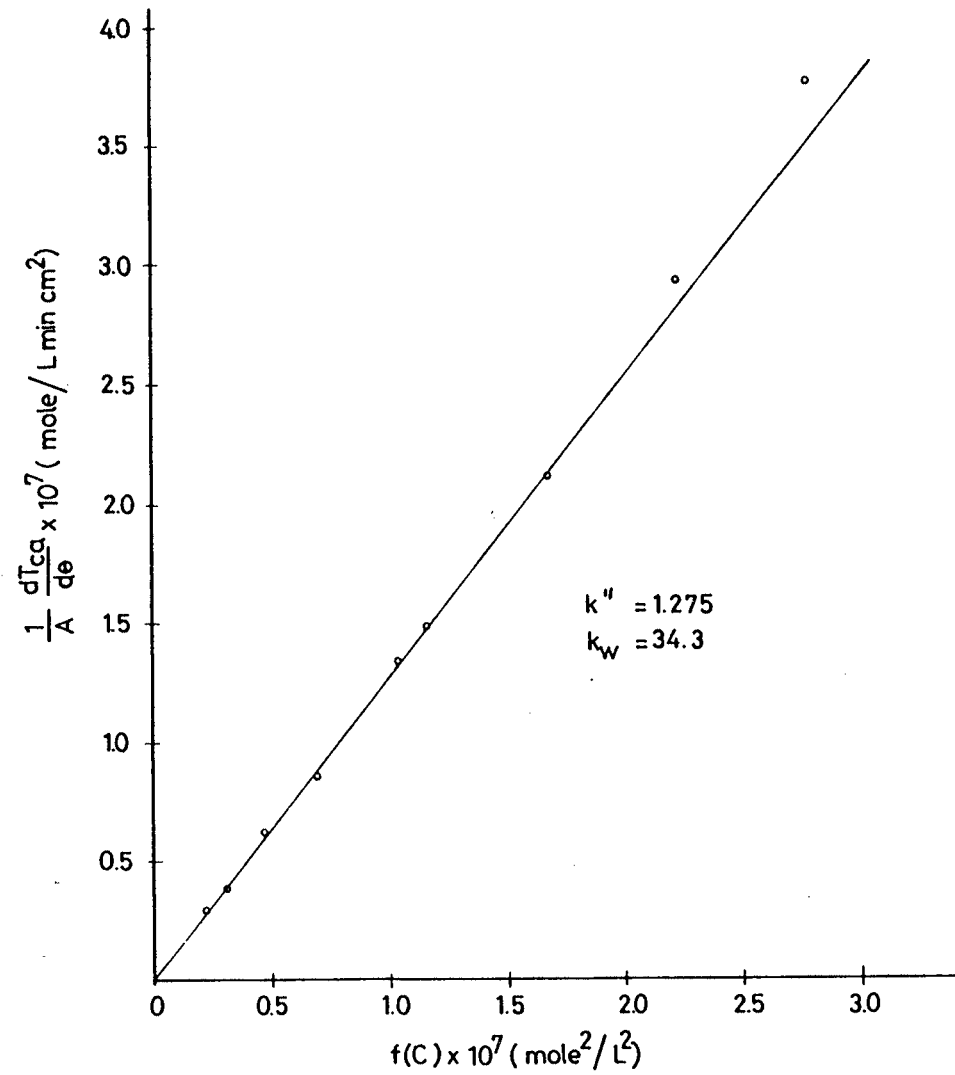
FIGURE C.5 Desupersaturation Curve of Expt. E24
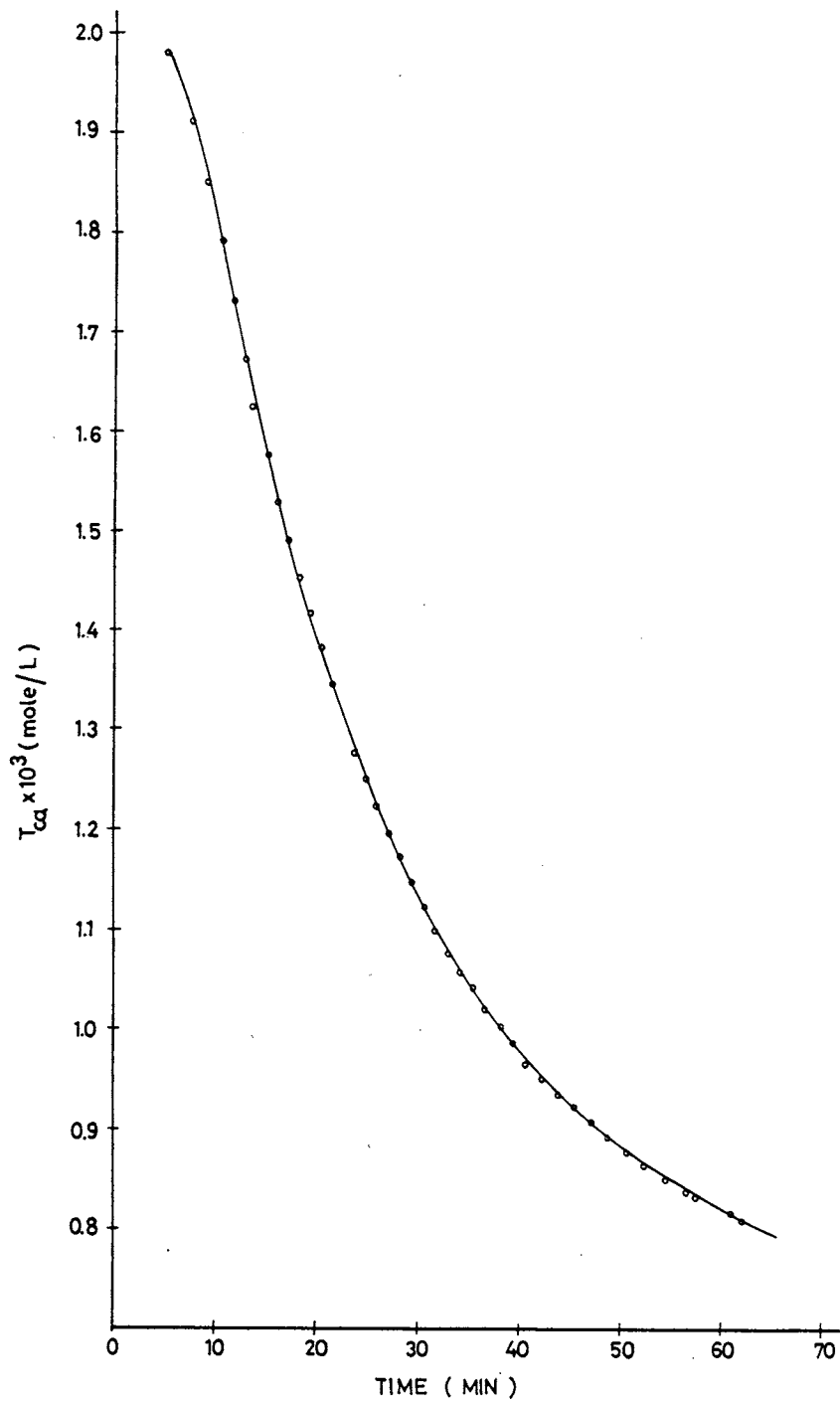
FIGURE C.6   Overall Growth Rate Constant of Expt. E24
Determined from Size Determination
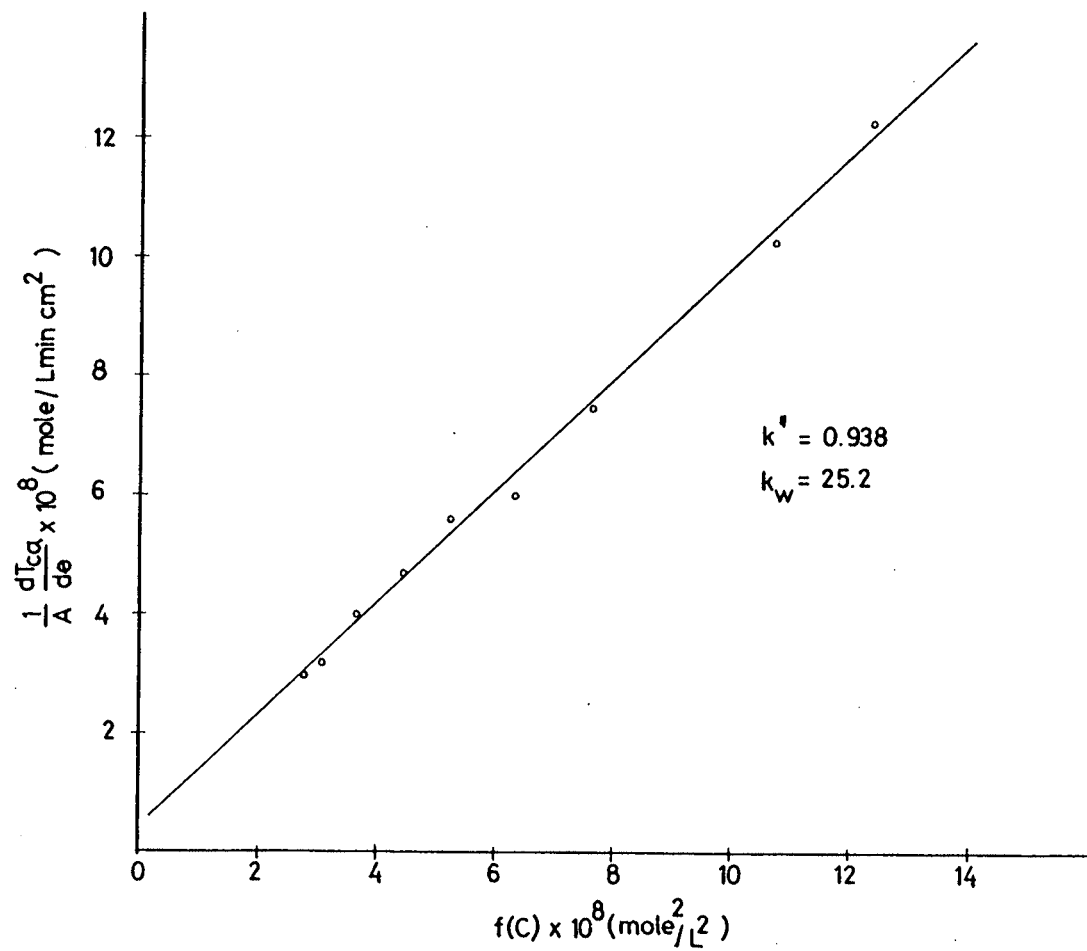
FIGURE C.7 Desupersaturation Curve of Expt. PE 4
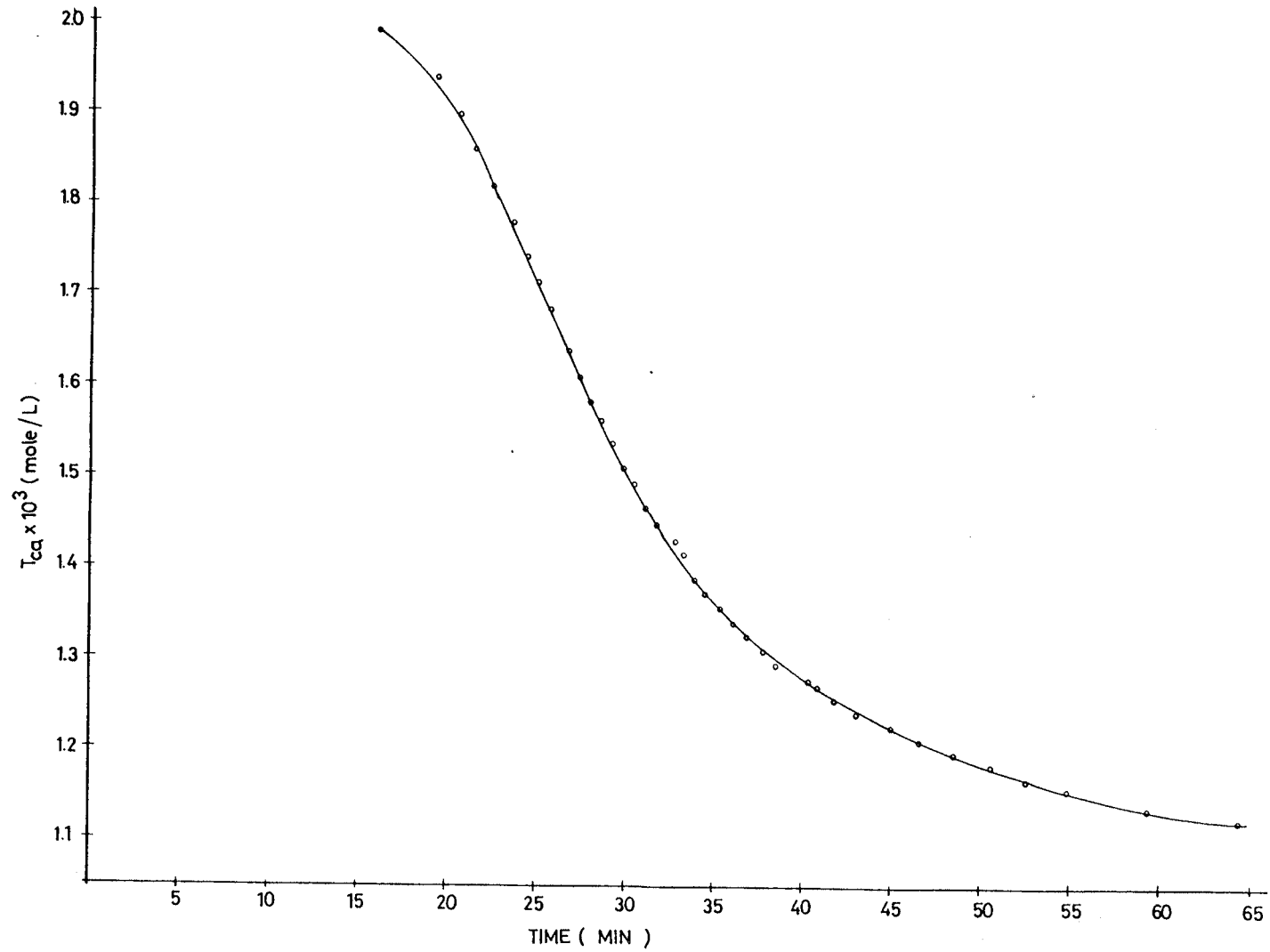
FIGURE C.8 Overall Growth Rate Constant of Expt. PE4
Determined by Simplified Method

$$k'N^{1/3} = 2.927 \times 10^4$$
$$N = 2.94 \times 10^8$$
$$k' = 44.32$$
$$k = 22.84$$

y-axis: $\frac{dT_{ca}}{d\theta} \times 10^3 / (T_{ca_{in}} - T_{ca})^{2/3} \ \frac{mole}{L \, min} / (\frac{mole}{L})^{2/3}$

x-axis: $f(C) \times 10^7 \ (mole^2/L^2)$
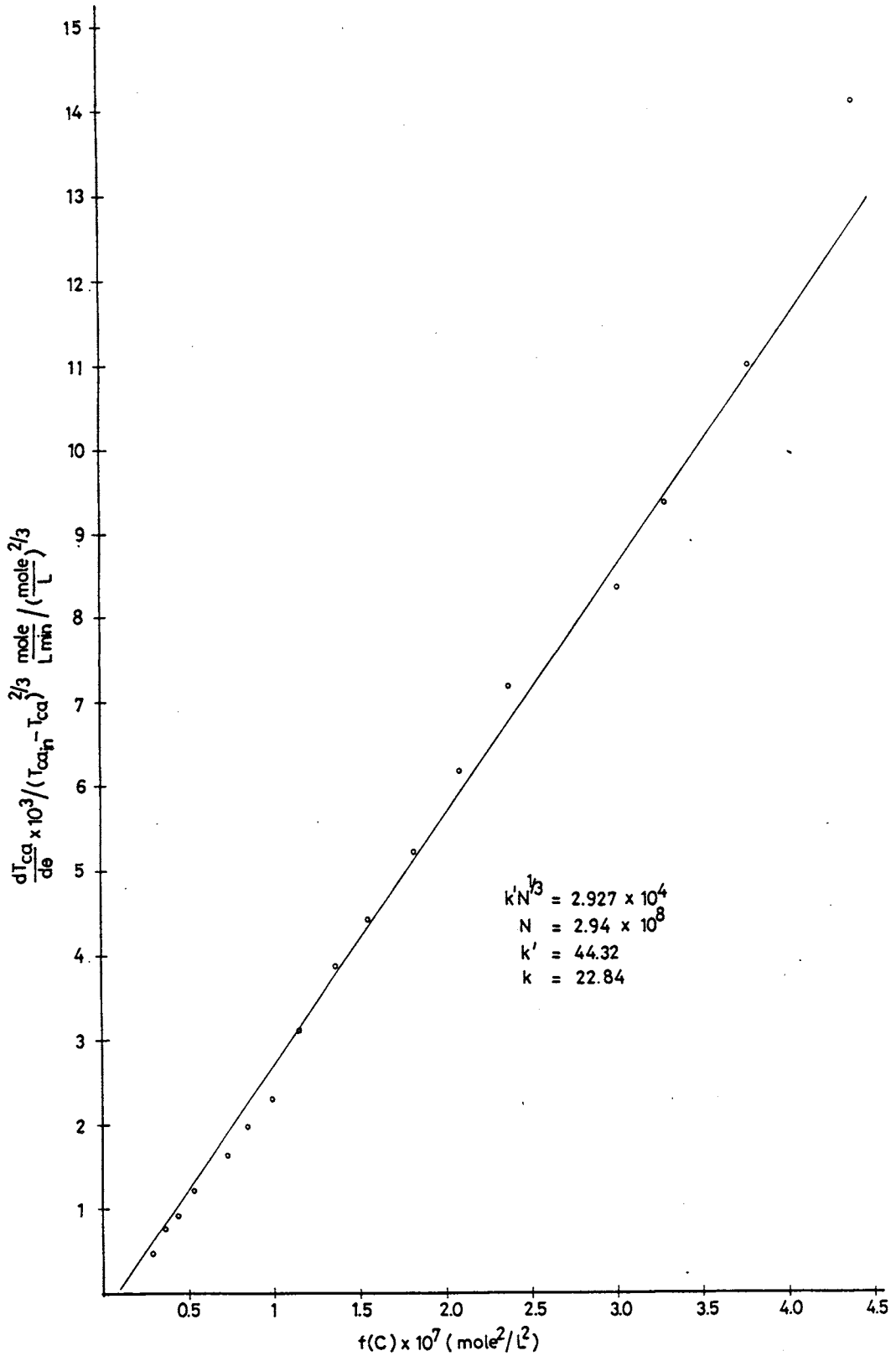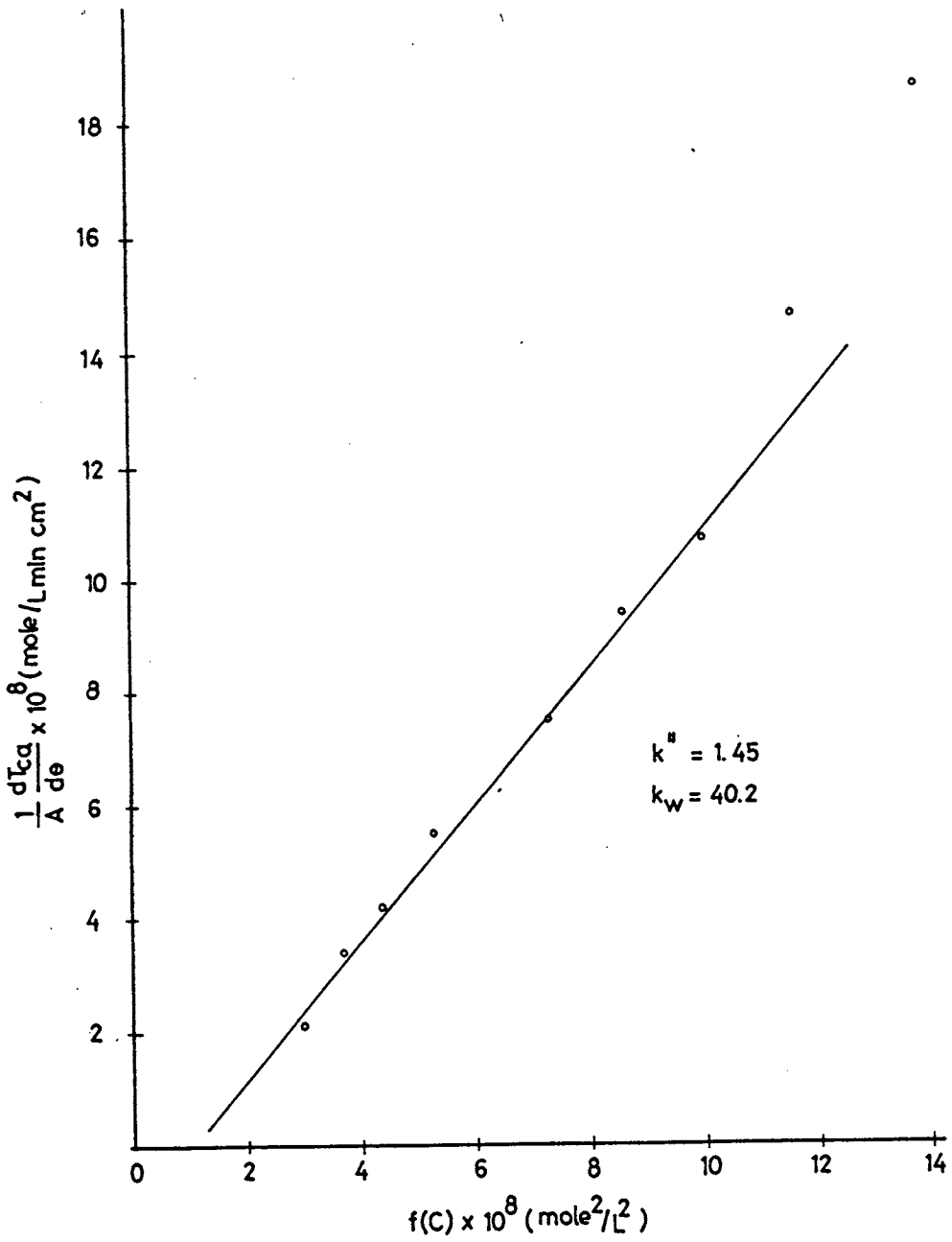
FIGURE C.9   Overall Growth Rate Constant of Expt. PE4
Determined by Size Consideration
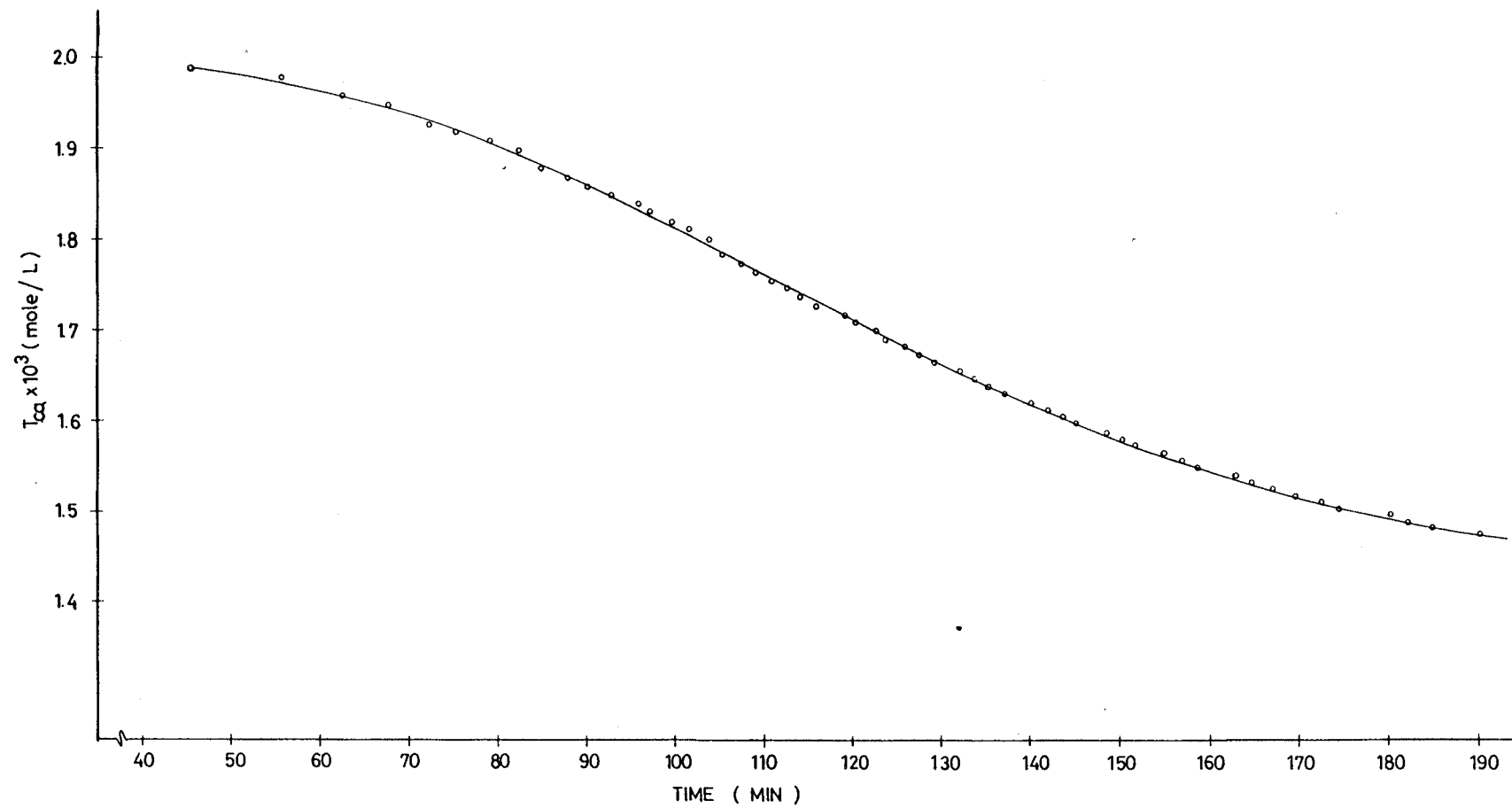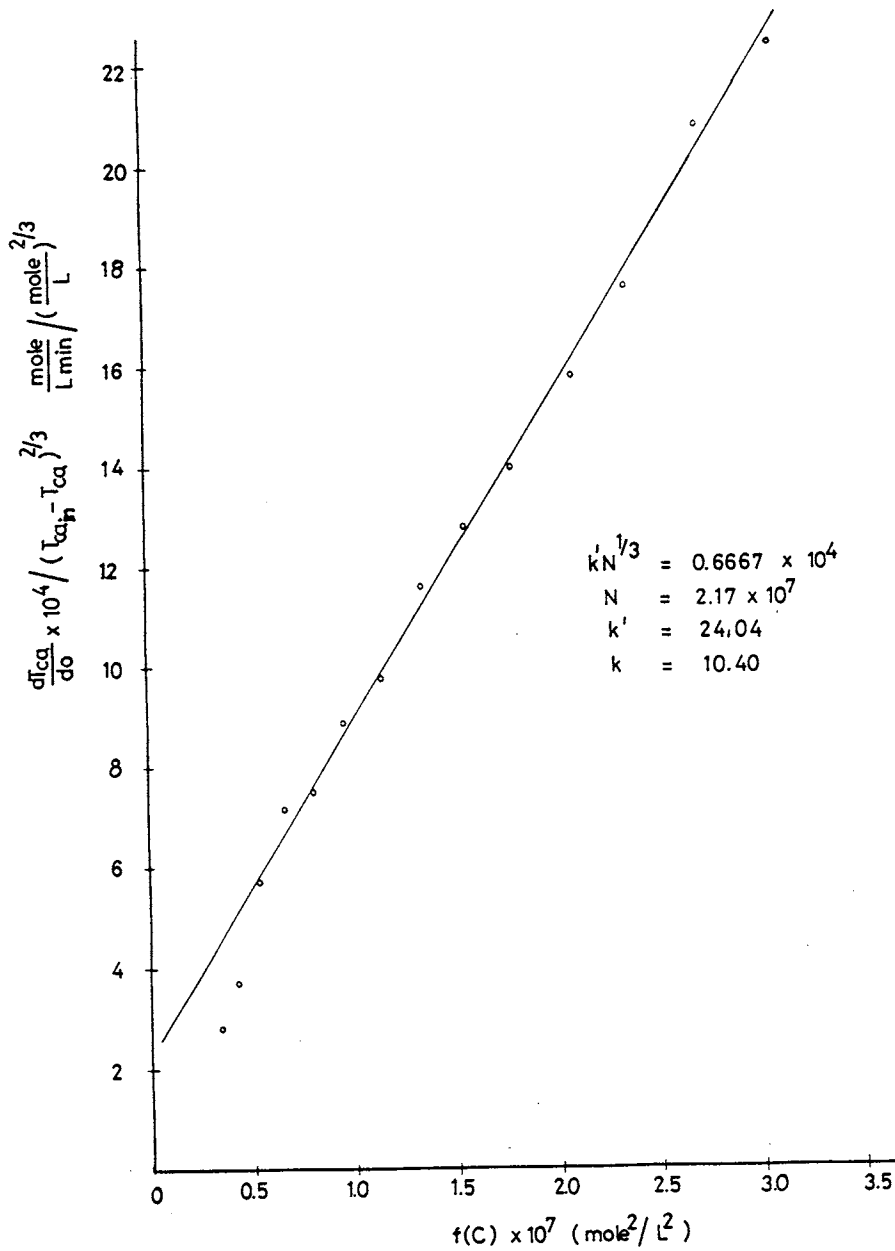
FIGURE C.10   Desupersaturation Curve of Expt. PE5
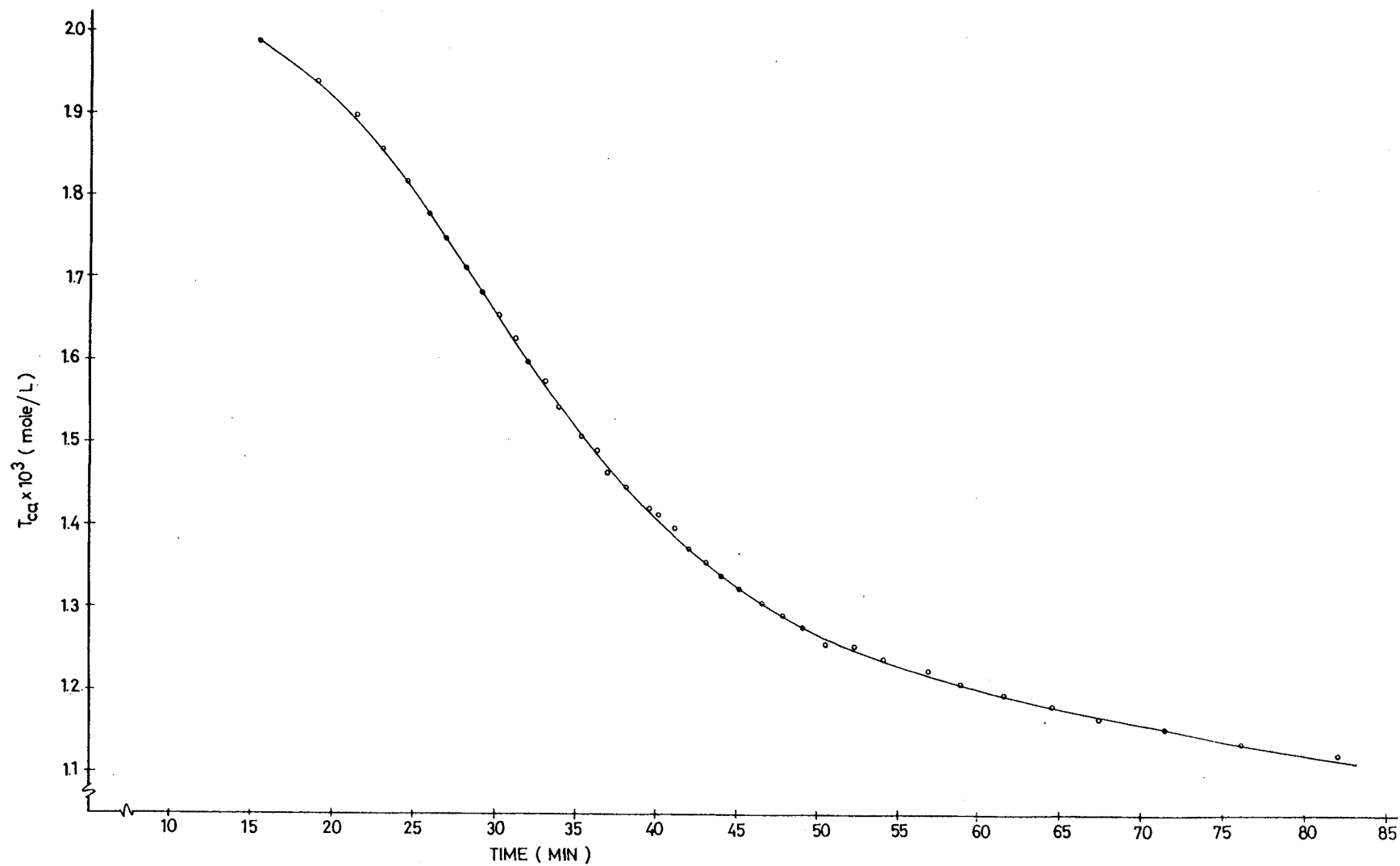
FIGURE C.11   Overall Growth Rate Constant of Expt. PE5
Determined by Simplified Method
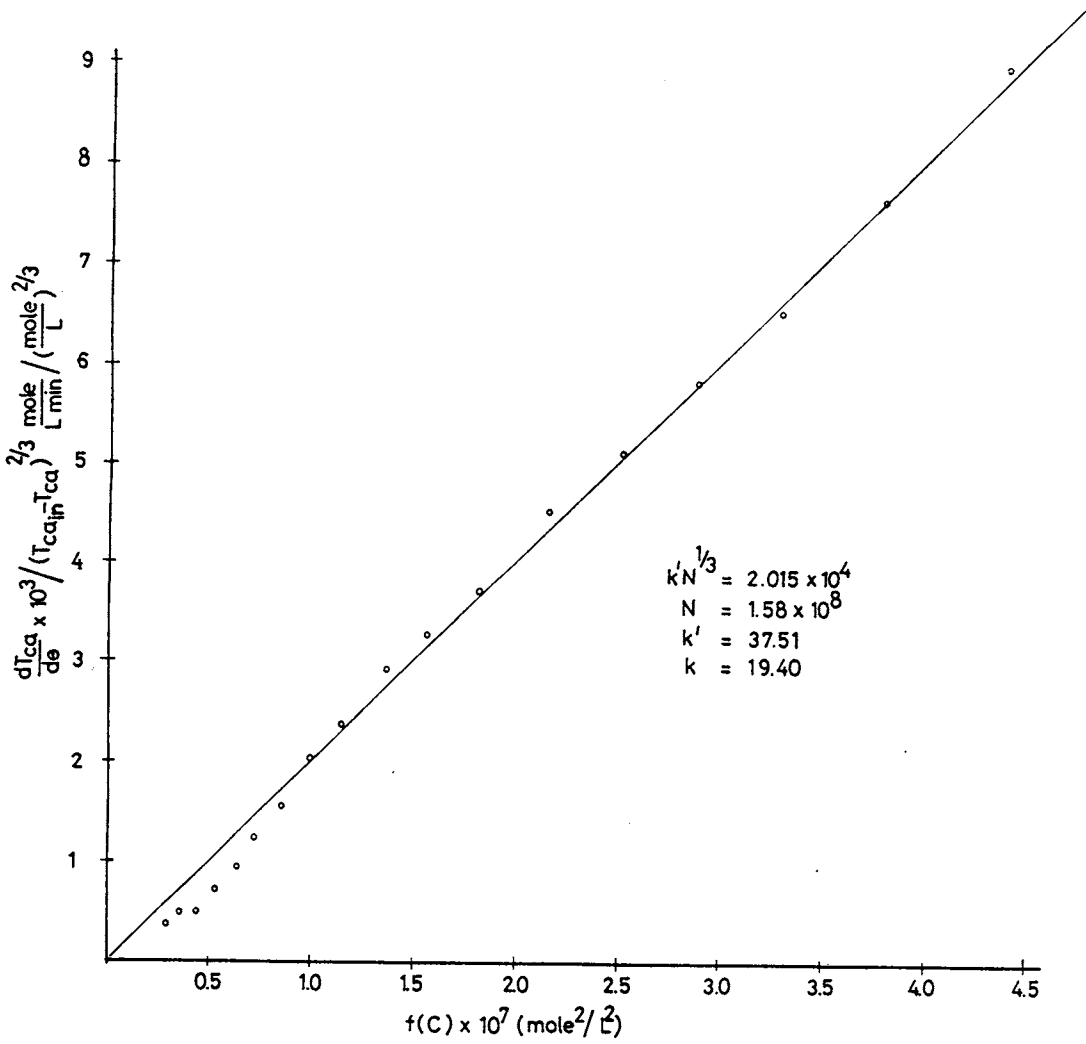
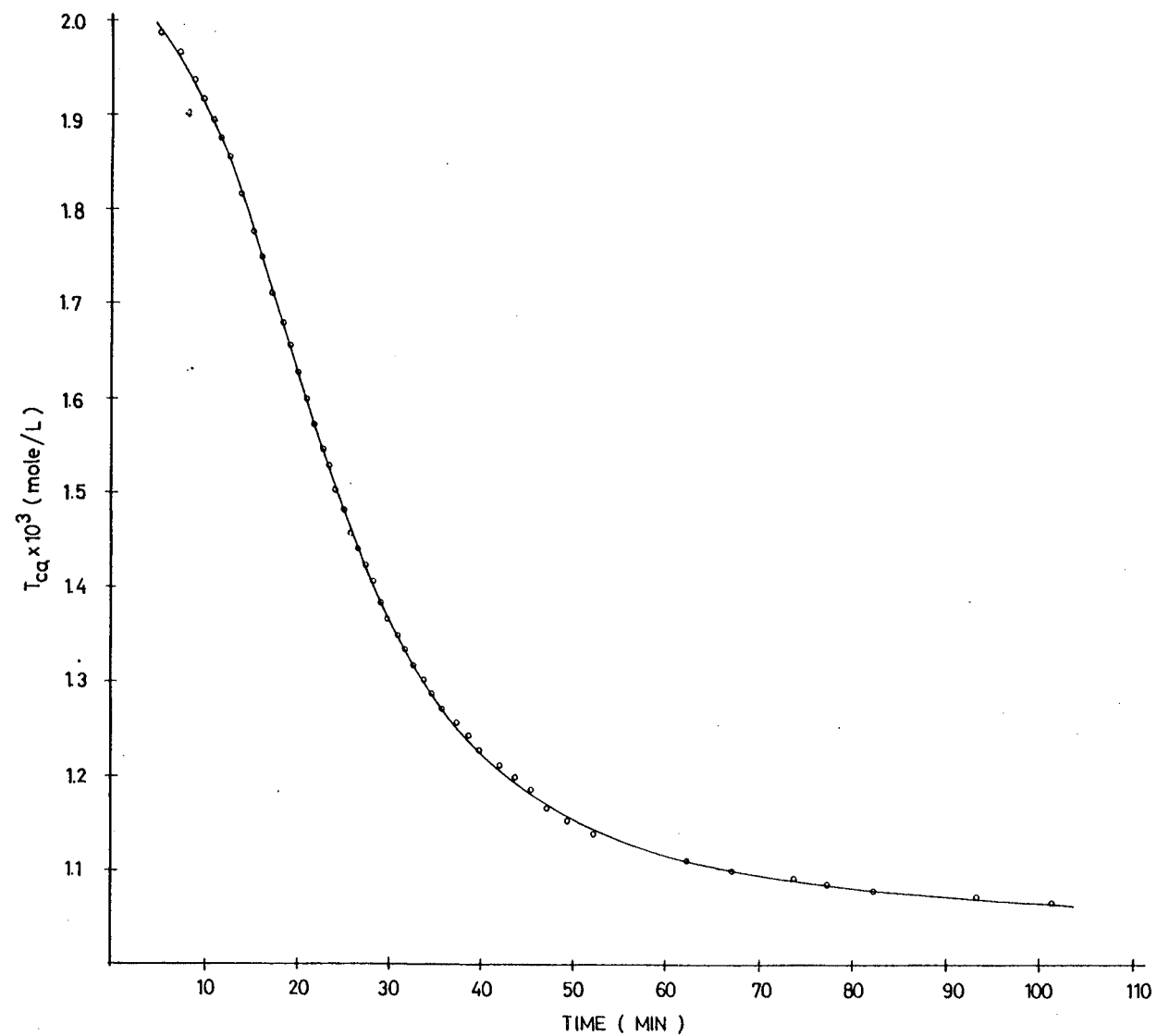FIGURE C.12 Desupersaturation Curve of Expt. PE6
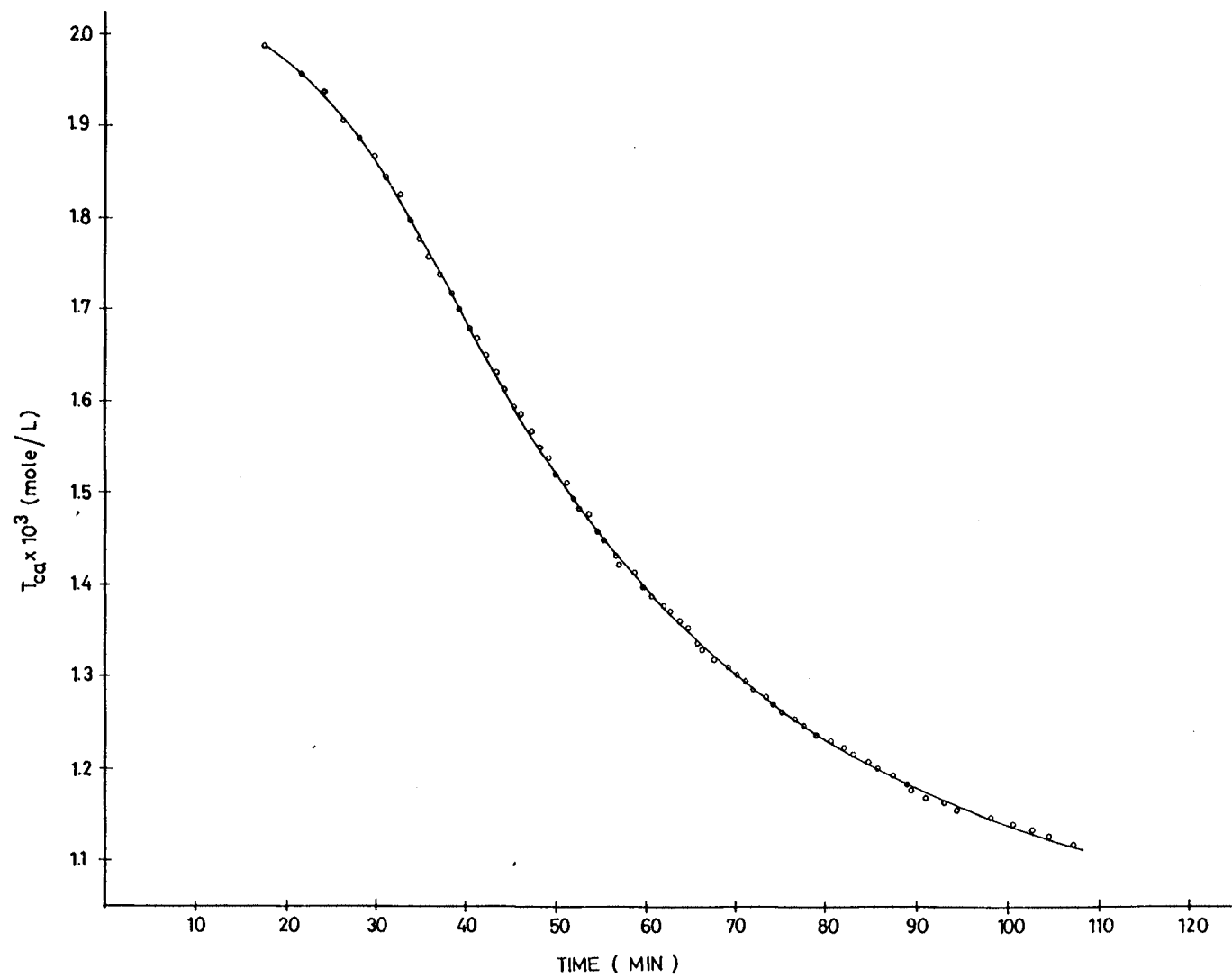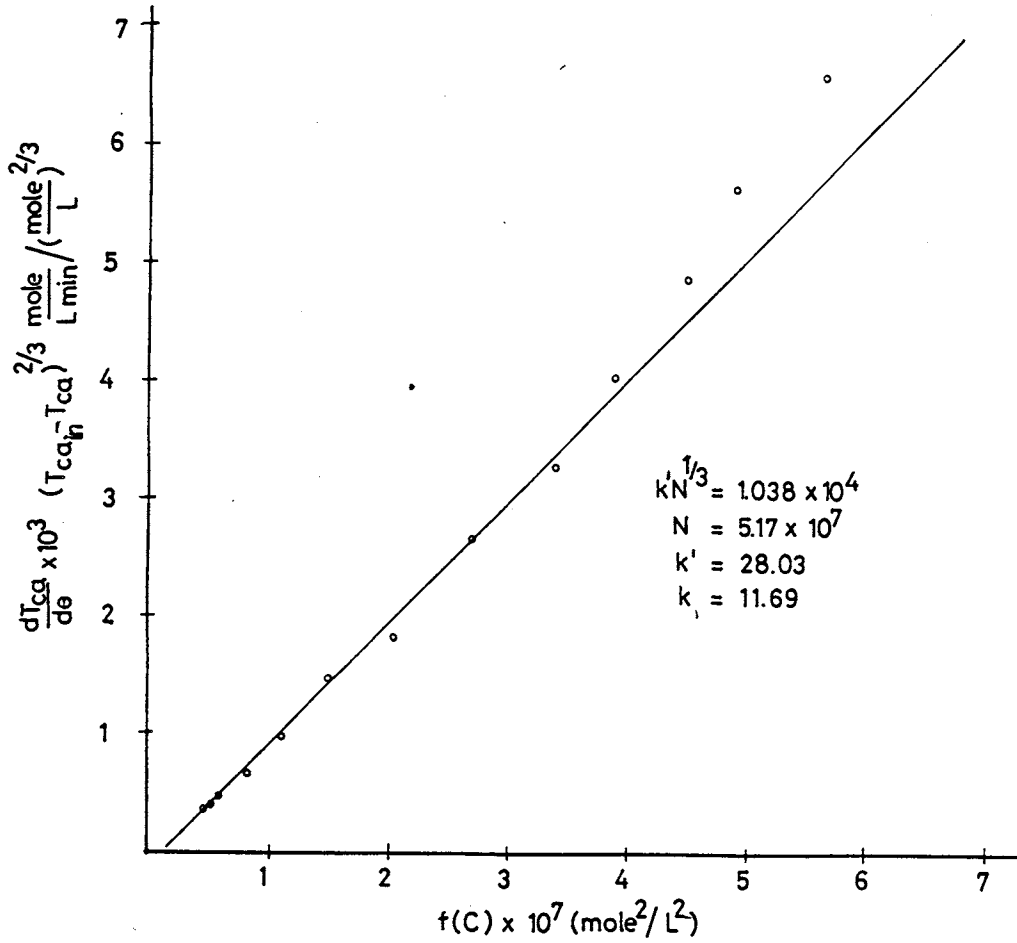
FIGURE C.13 Overall Growth Rate Constant of Expt. PE6
Determined by Simplified Method
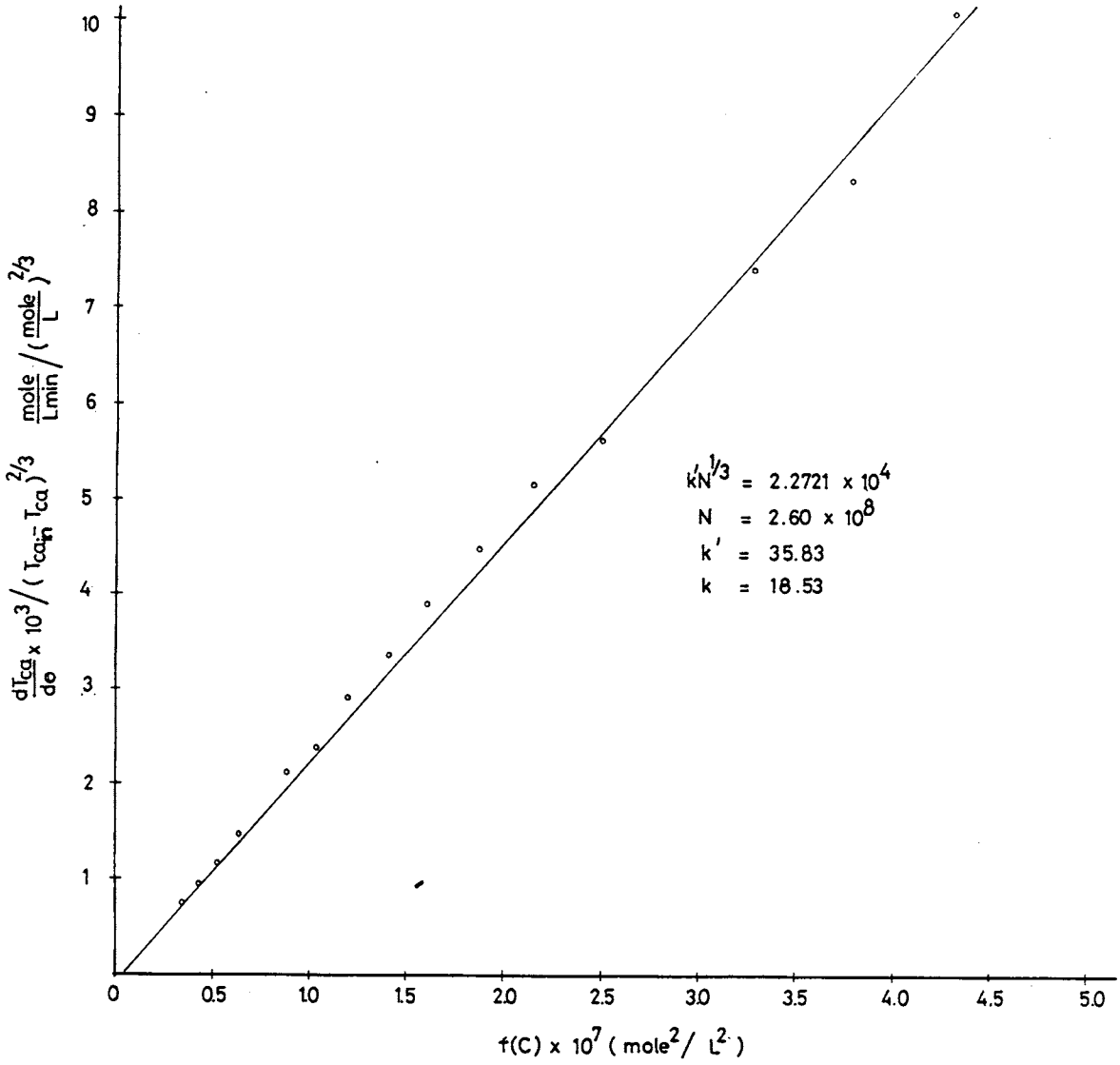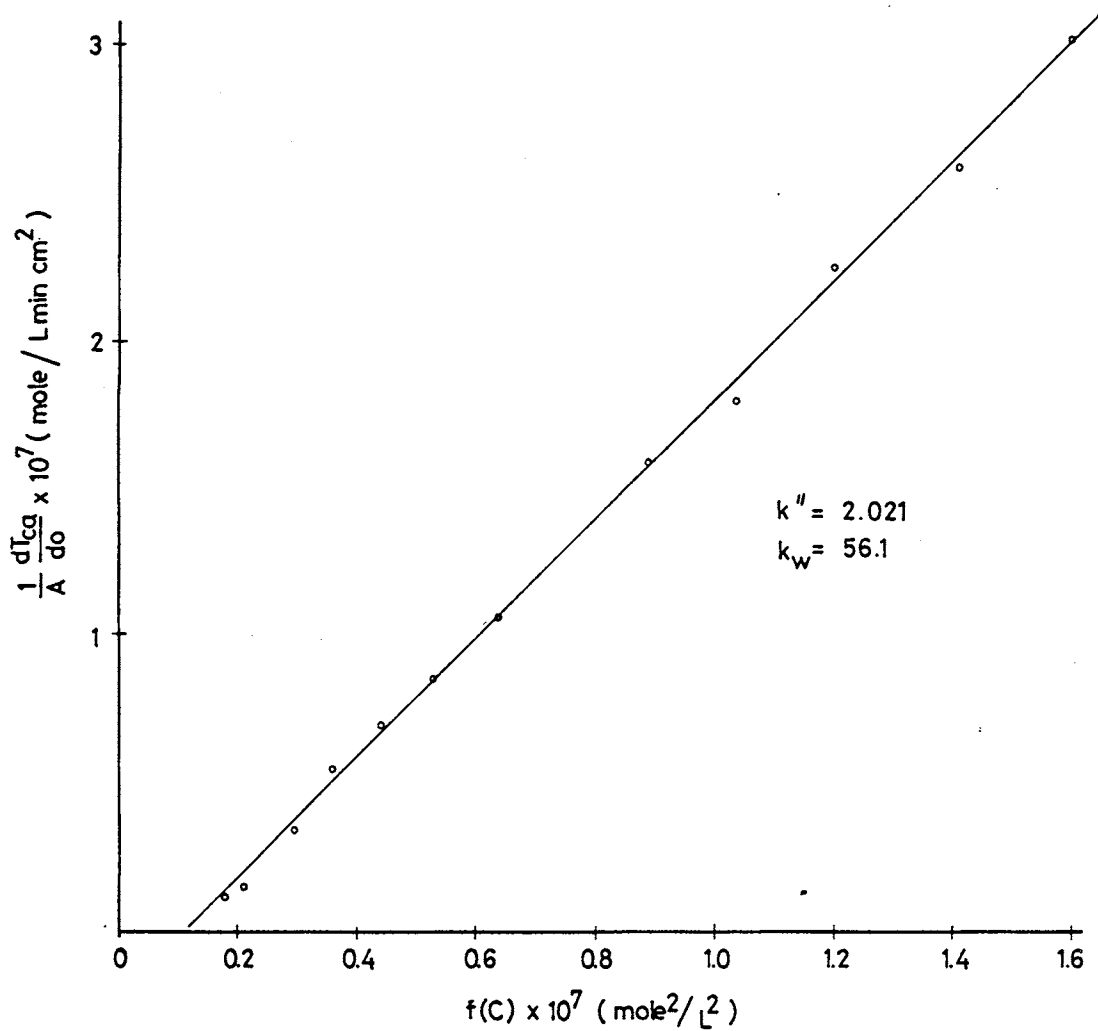
FIGURE C.14   Desupersaturation Curve of Expt. PE7
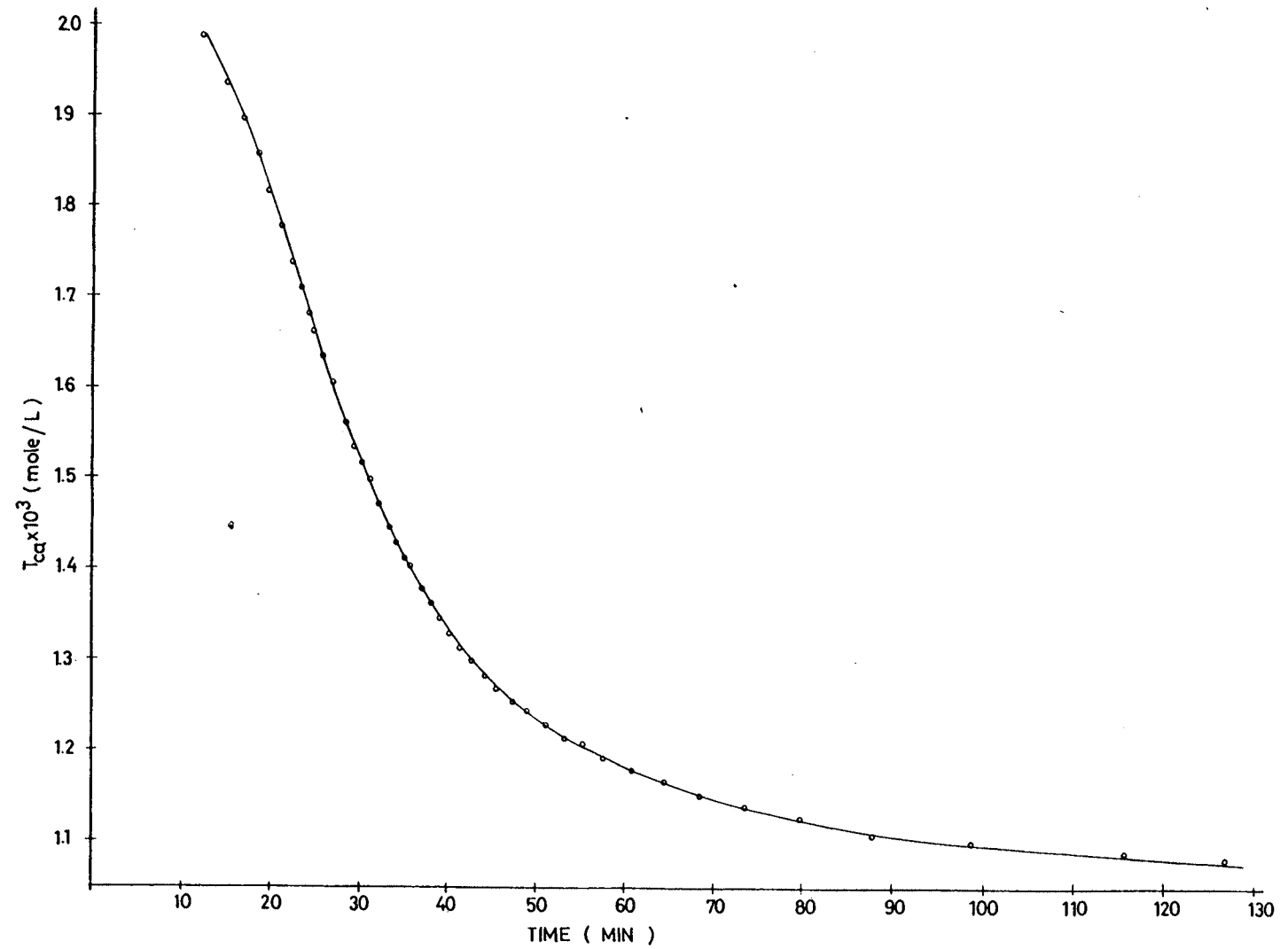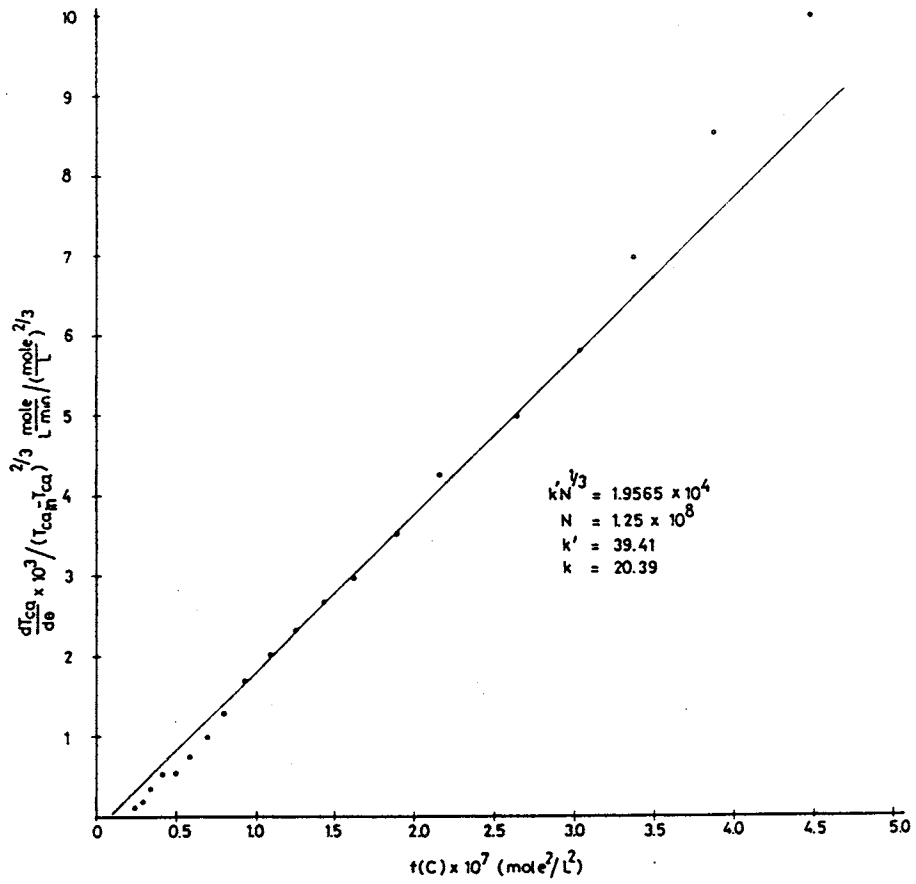
FIGURE C.15   Overall Growth Rate Constant of Expt. PE7
Determined by Simplified Method
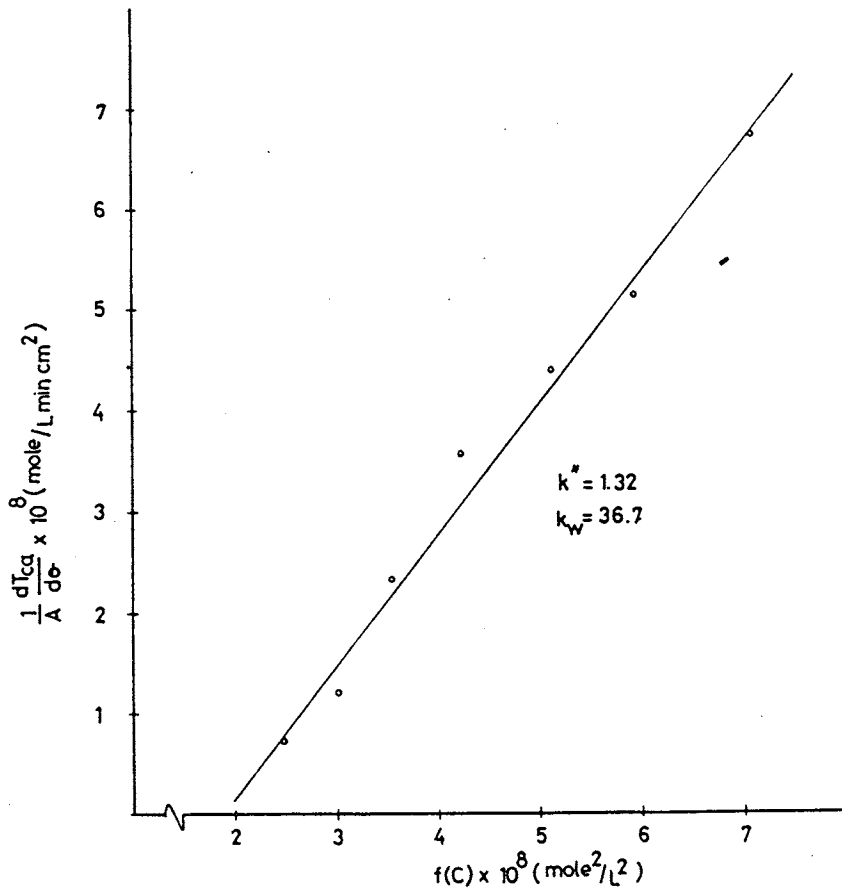
FIGURE C.16   Overall Growth Rate Constant of Expt. PE7
Determined by Size Consideration

FIGURE C.17   Desupersaturation Curve of Expt. PE8
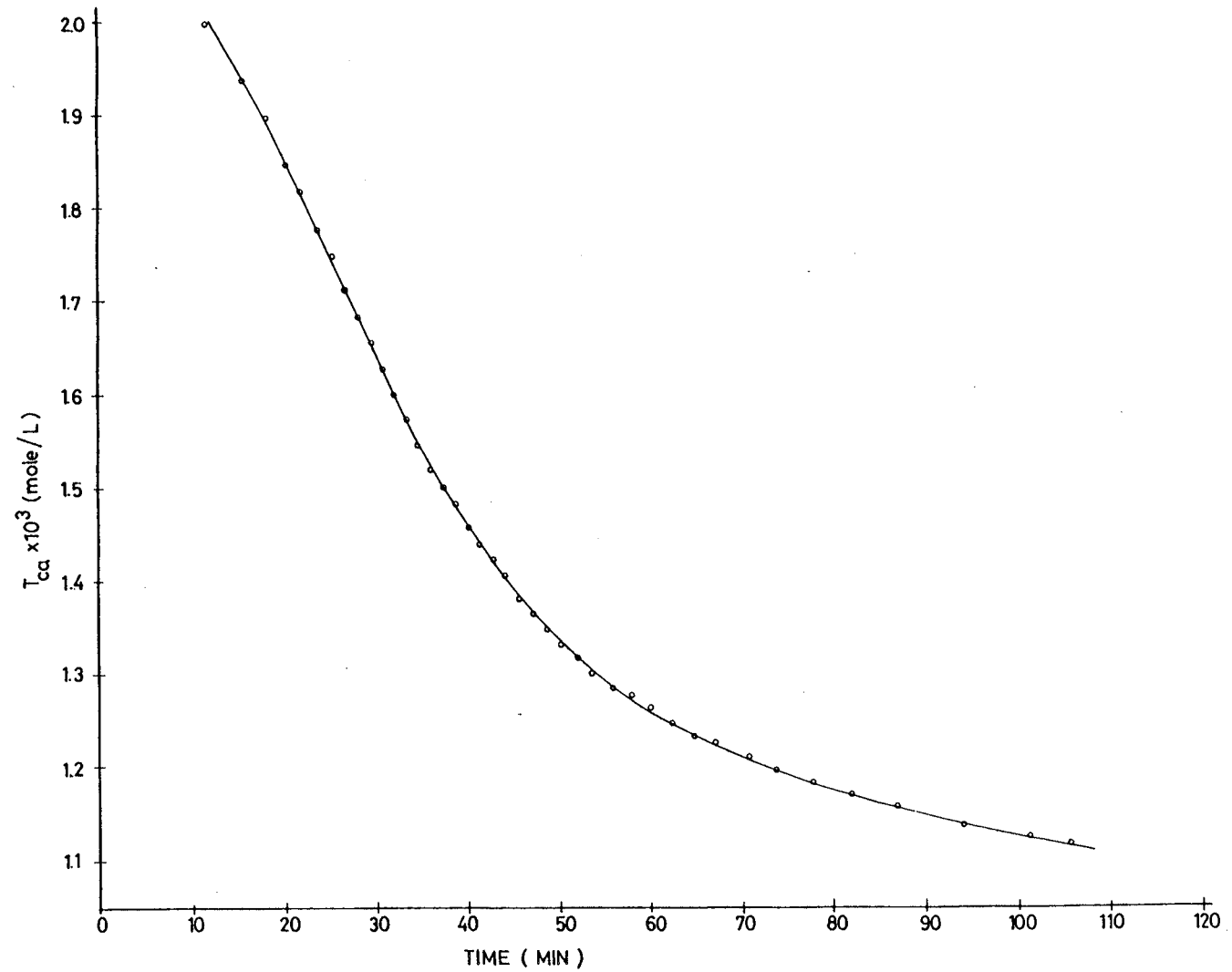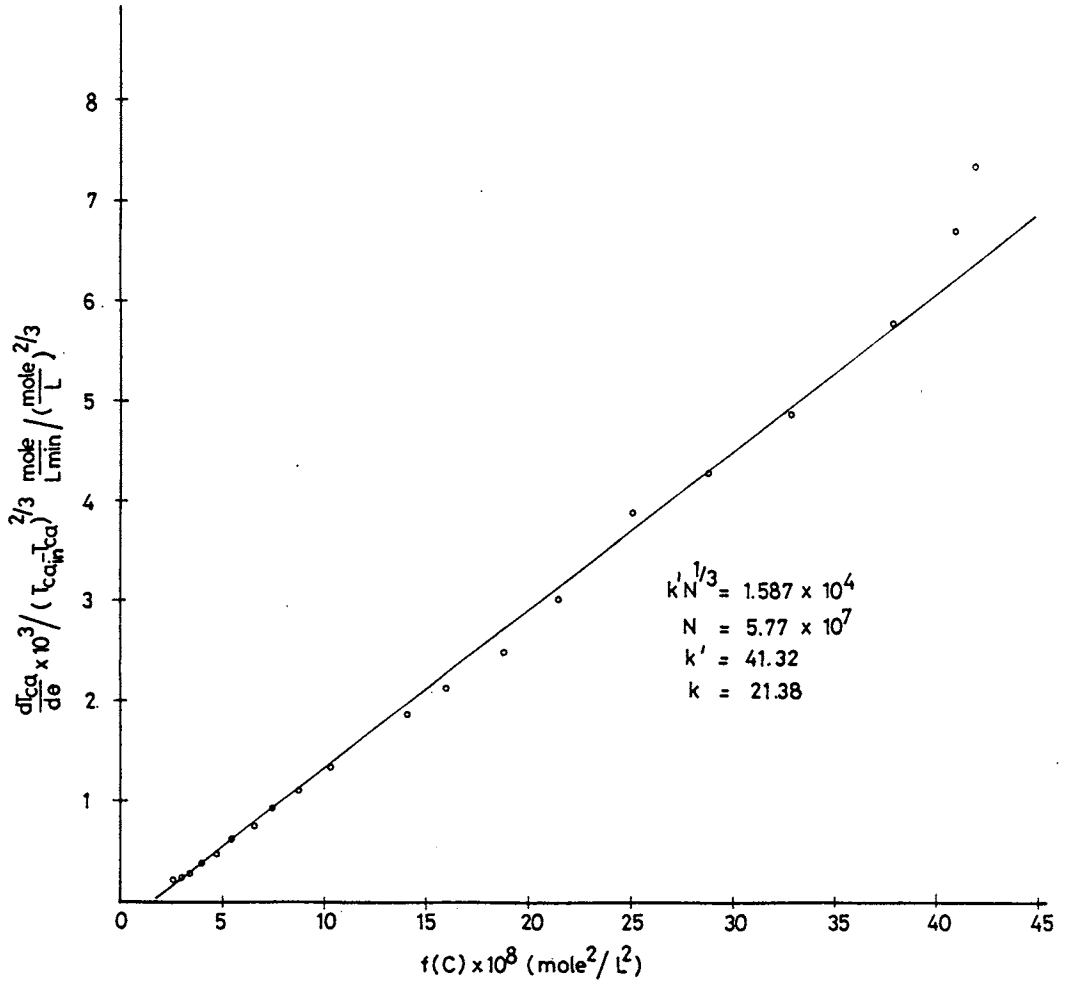
FIGURE C.18 Overall Growth Rate Constant of Expt. PE8
Determined by Simplified Method
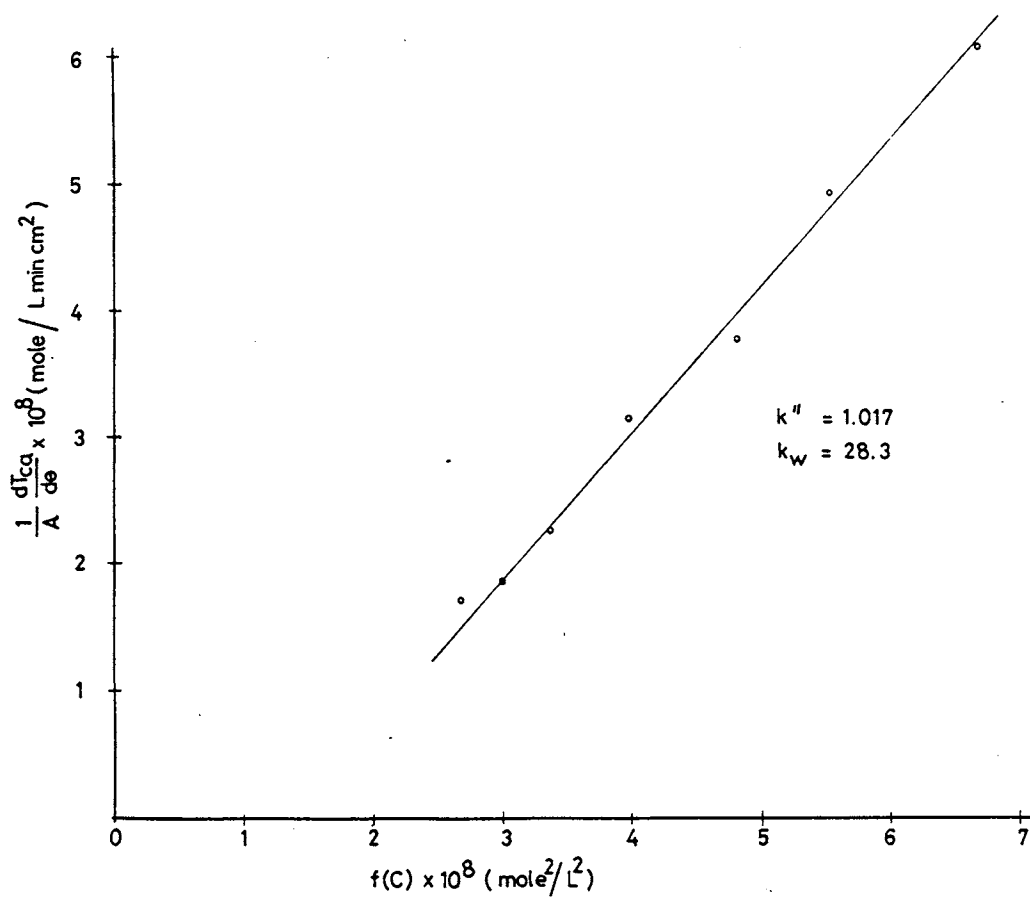
FIGURE C.19   Overall Growth Rate Constant of Expt. PE8
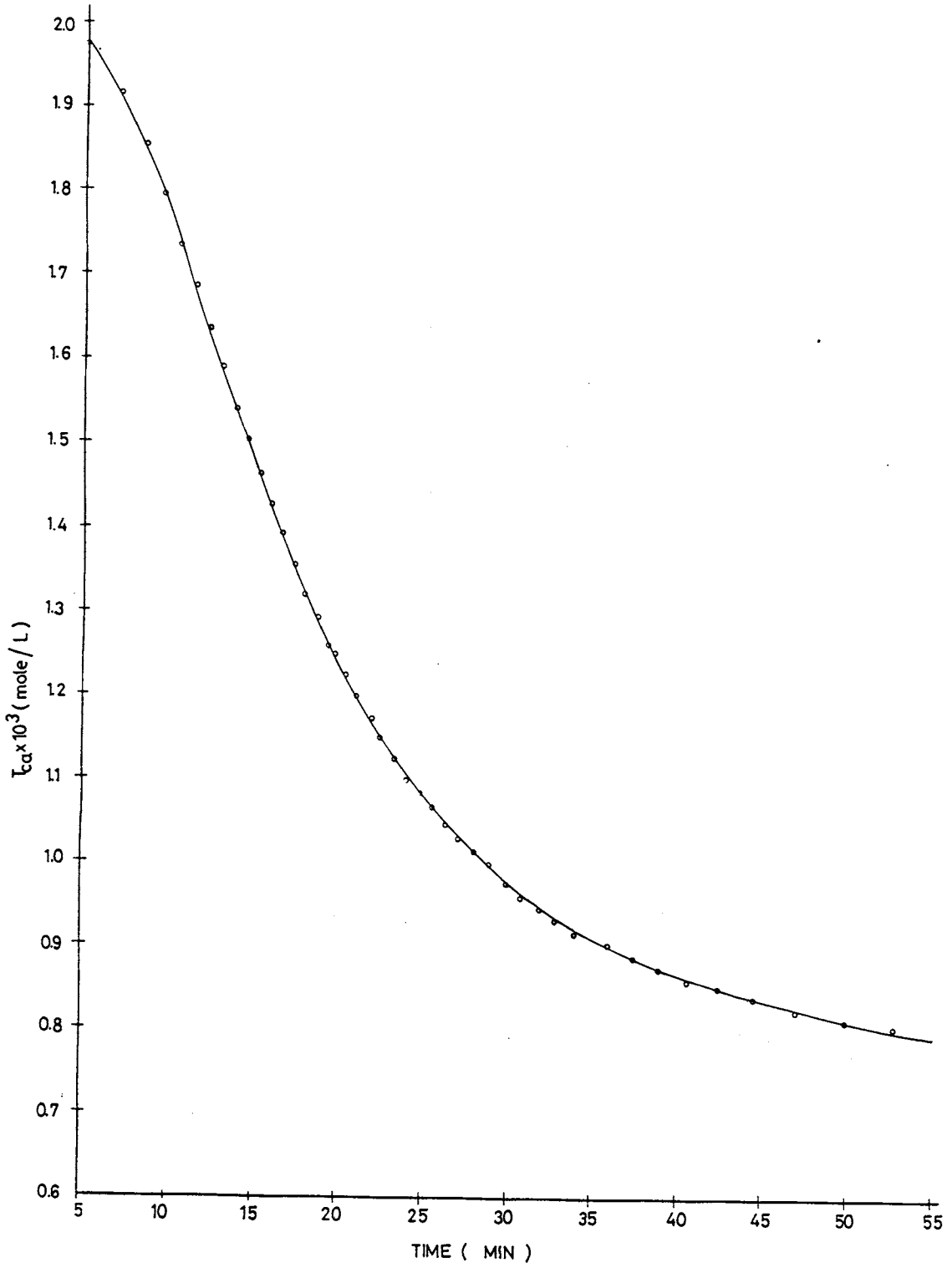Determined by Size Consideration

FIGURE C.20   Desupersaturation of Curve of Expt. PE9
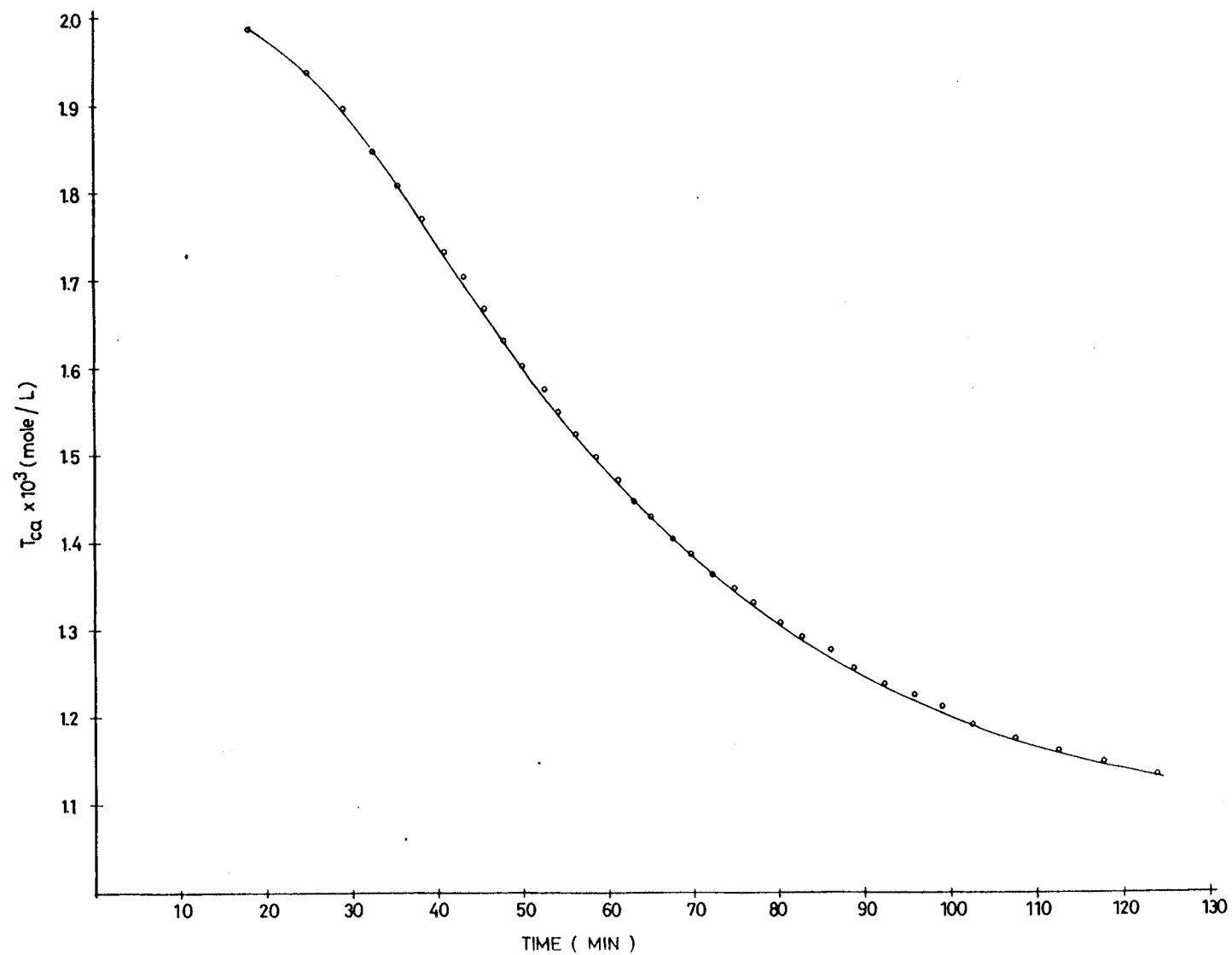
FIGURE C.21   Overall Growth Rate Constant of Expt. PE9
Determined by Simplified Method

$$k'N^{\frac{1}{3}} = 0.8909 \times 10^4$$
$$N = 3.00 \times 10^7$$
$$k' = 28.84$$
$$k = 12.44$$
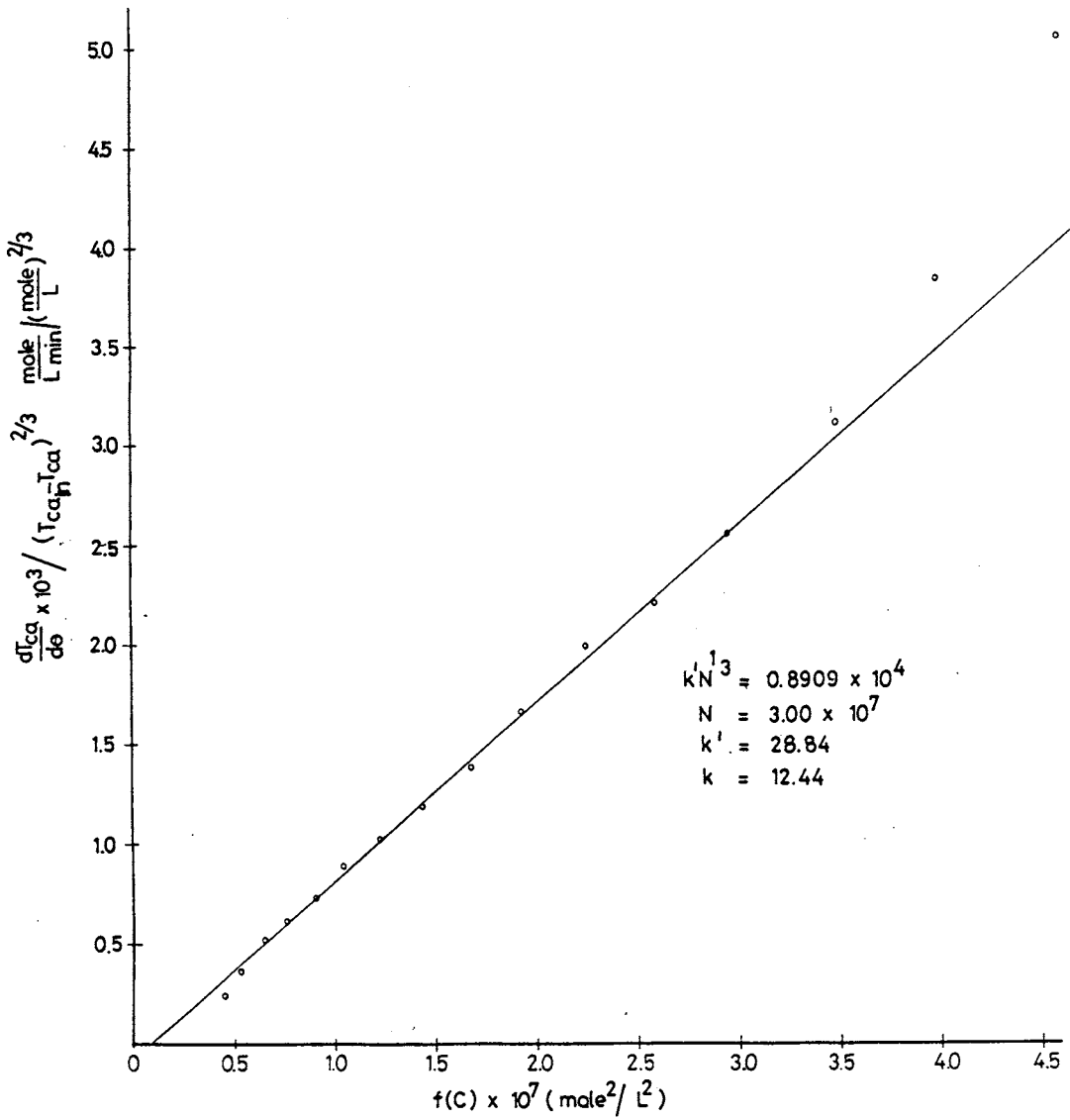
FIGURE C.22   Overall Growth Rate Constant of Expt. PE9
Determined by Size Consideration
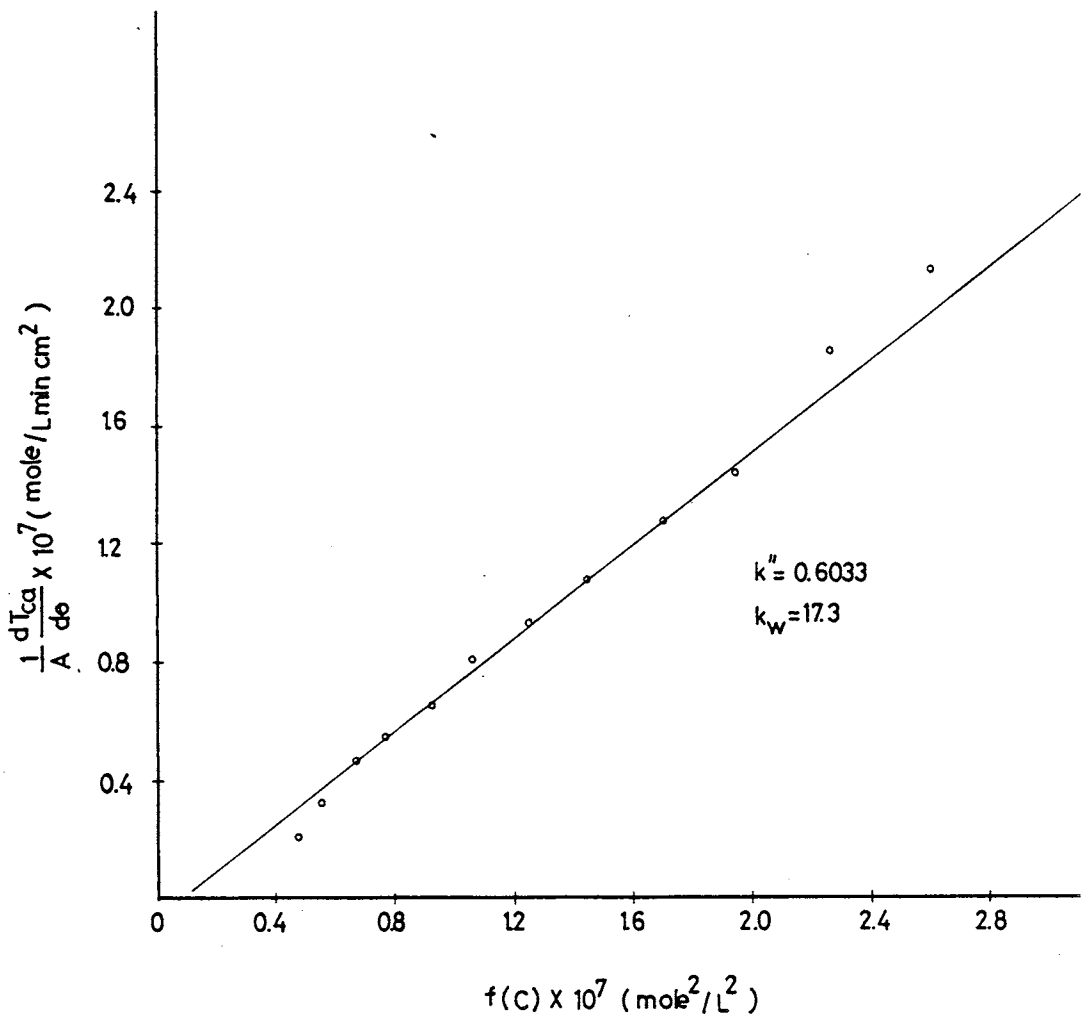
FIGURE C.23   Desupersaturation Curve of Expt. PE11
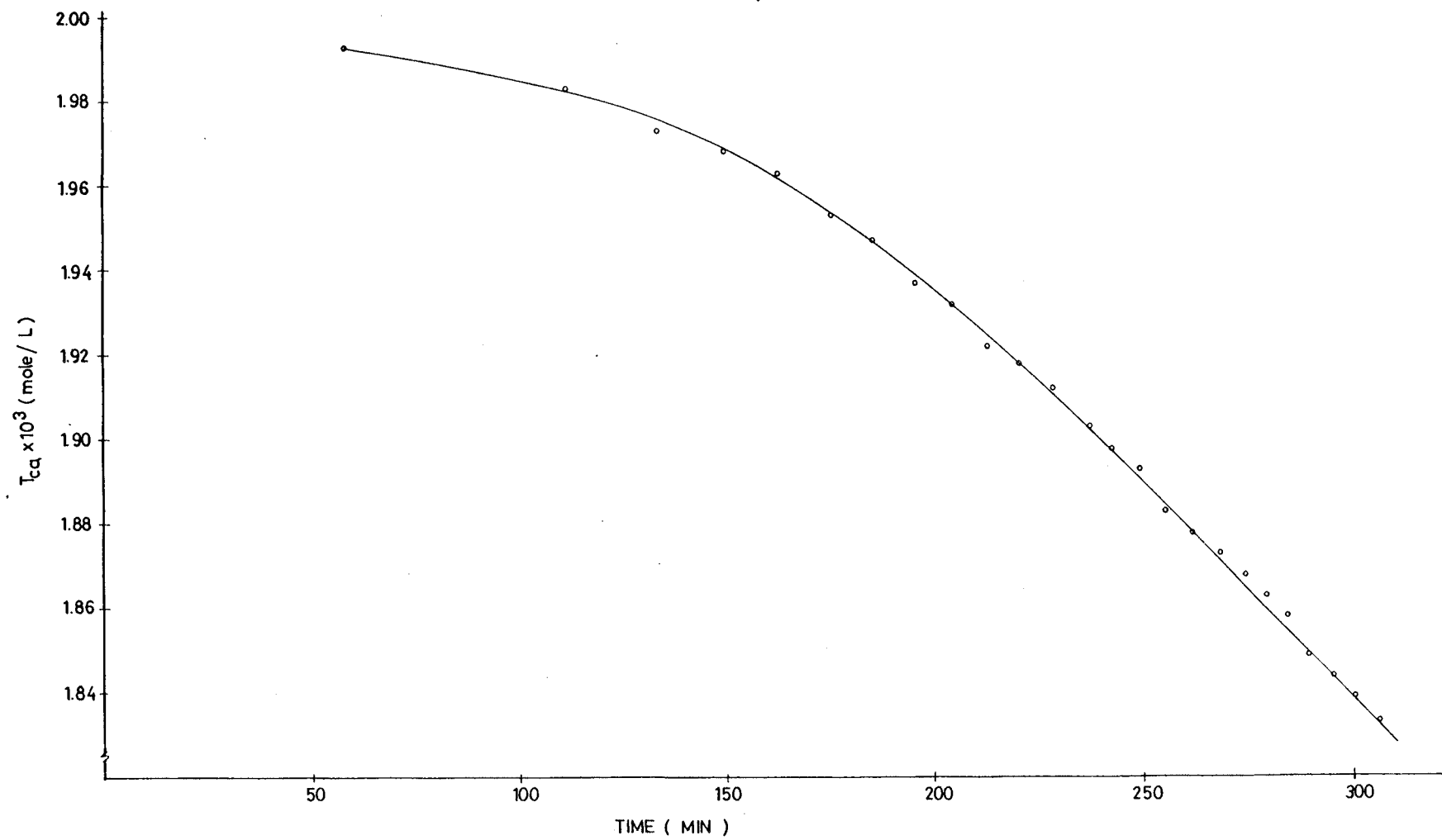
FIGURE C.24 Overall Growth Rate Constant of Expt. PE11
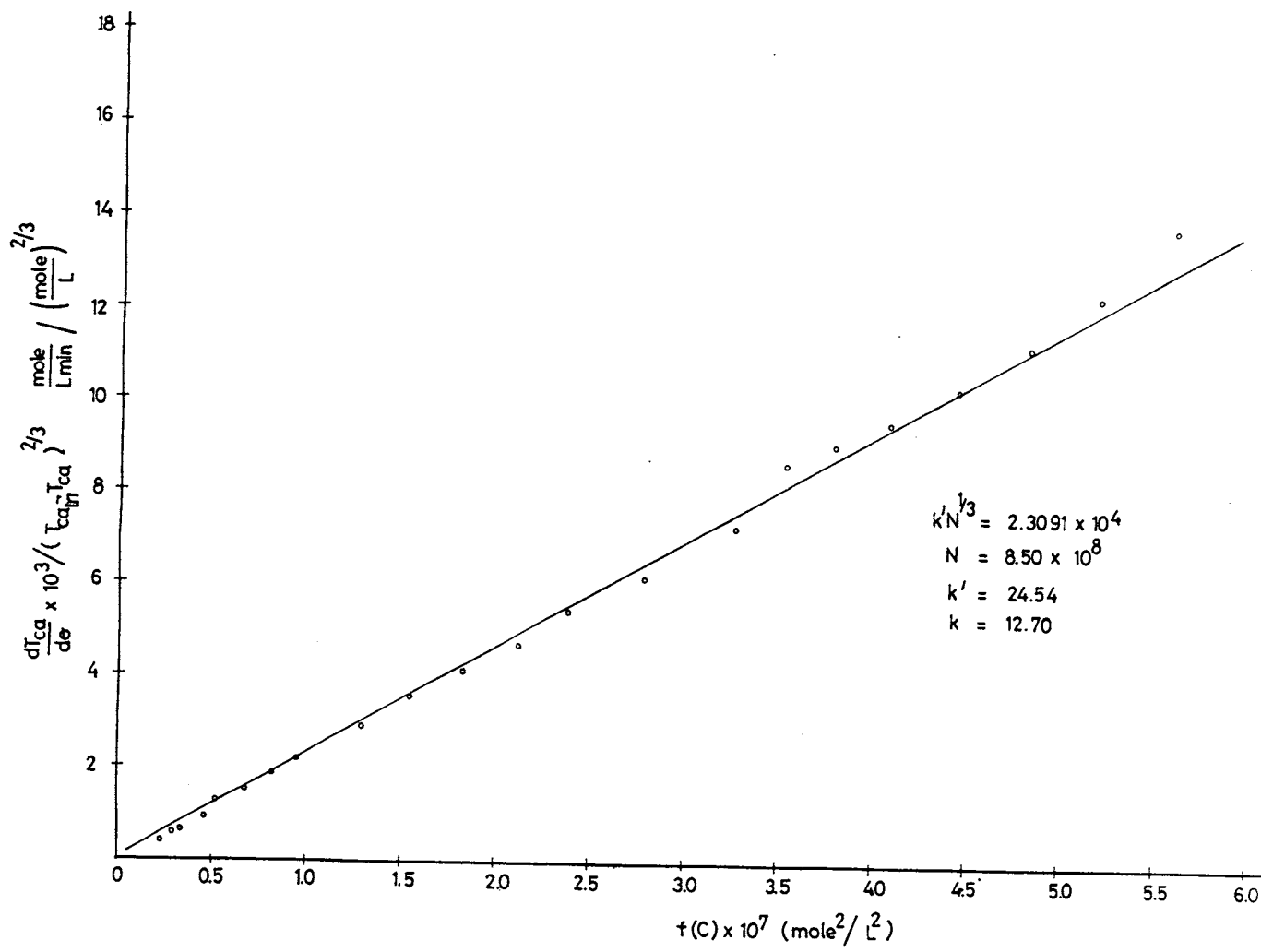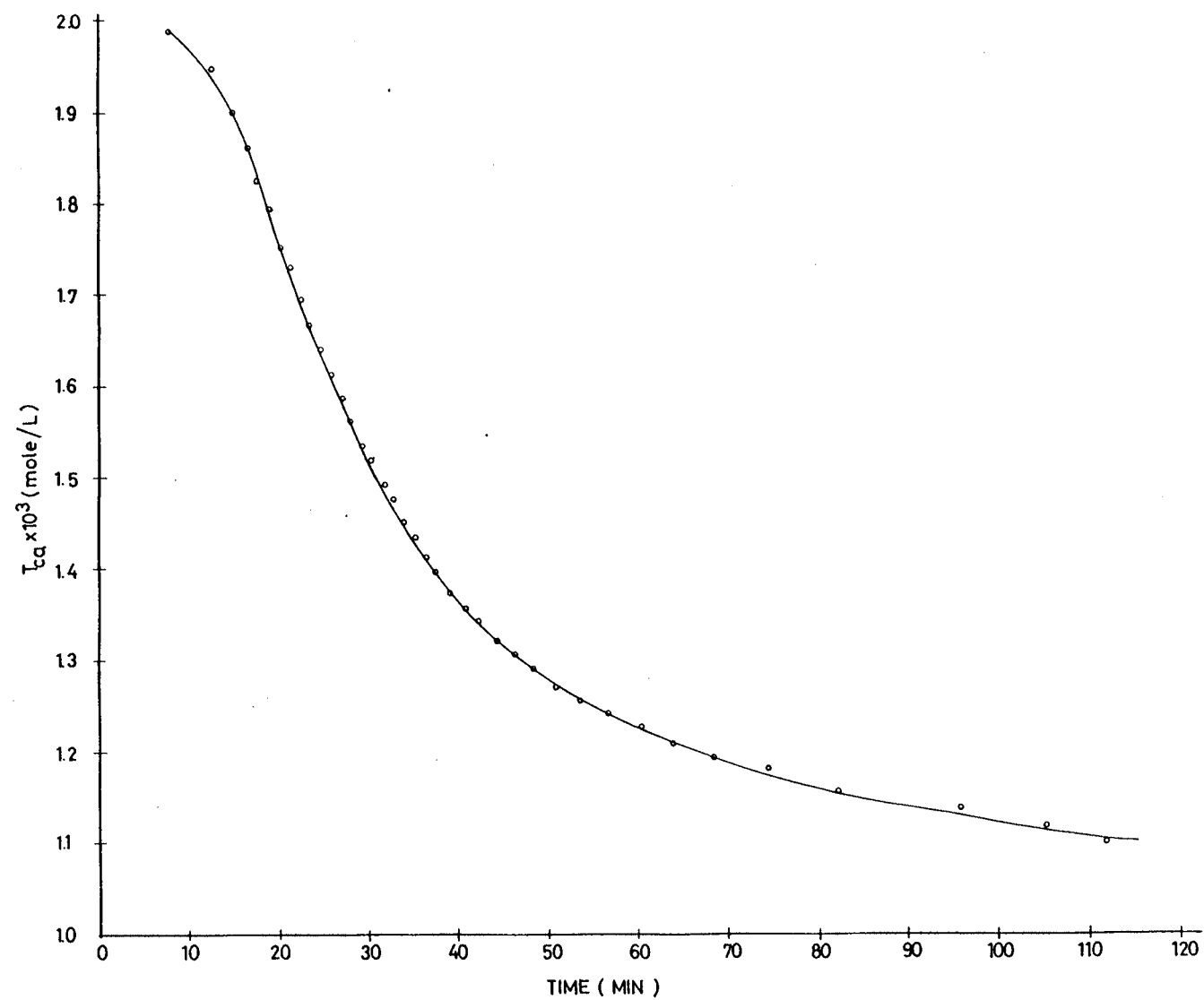Determined by Simplified Method
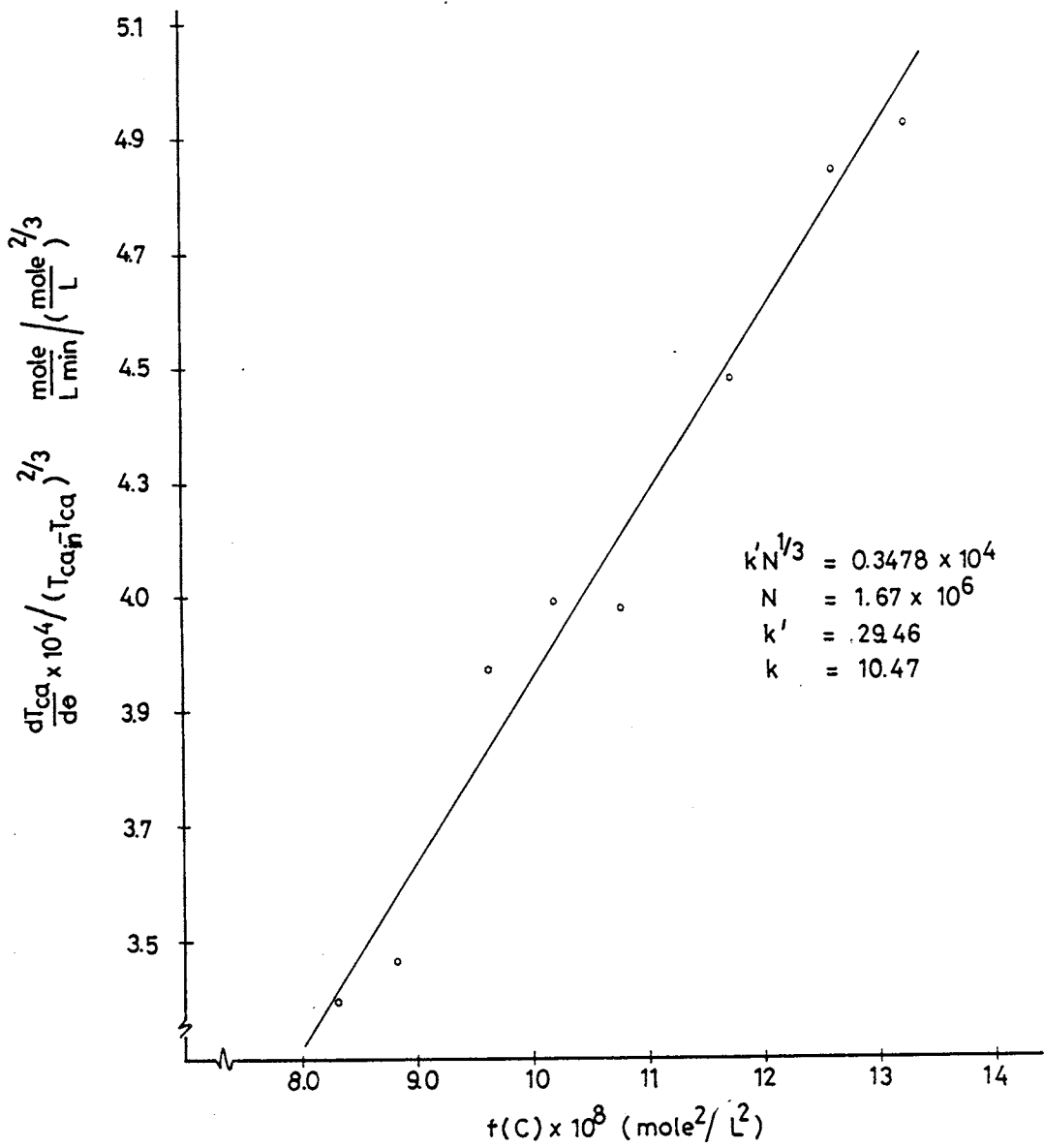
FIGURE C.25   Overall Growth Rate Constant of Expt. PE11
              Determined by Size Consideration
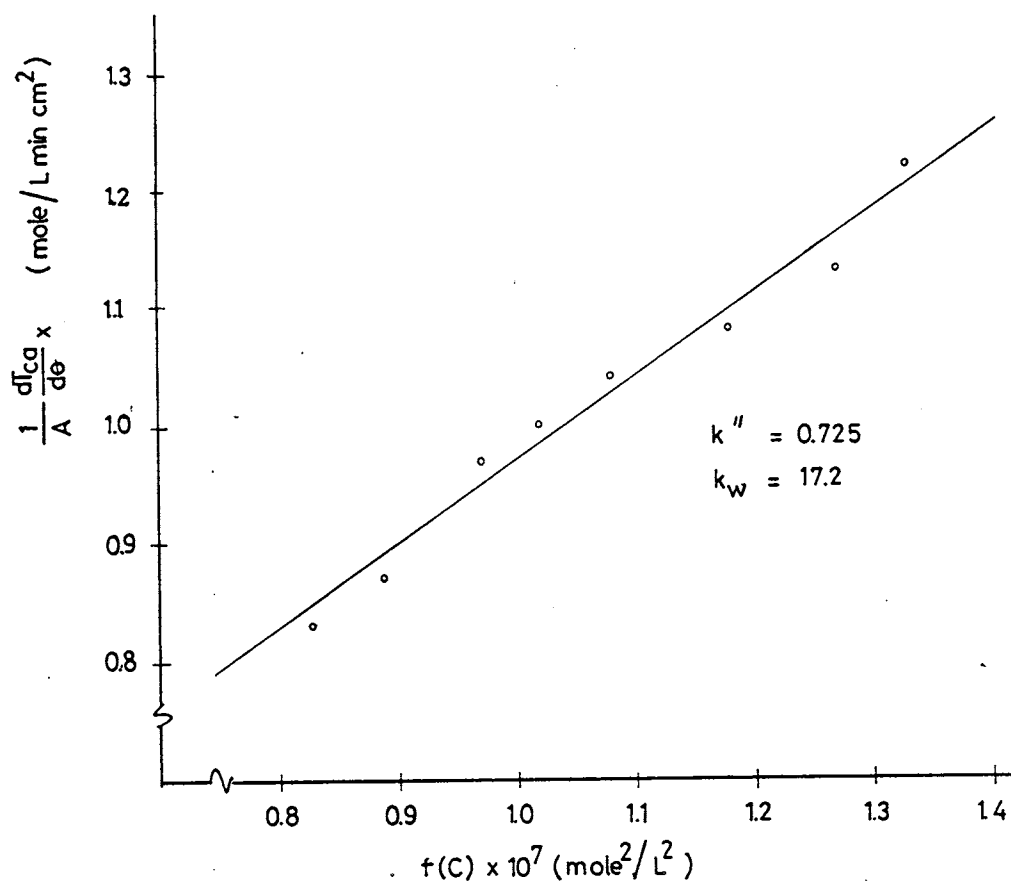
FIGURE C.26   Desupersaturation Curve of Expt. PE14
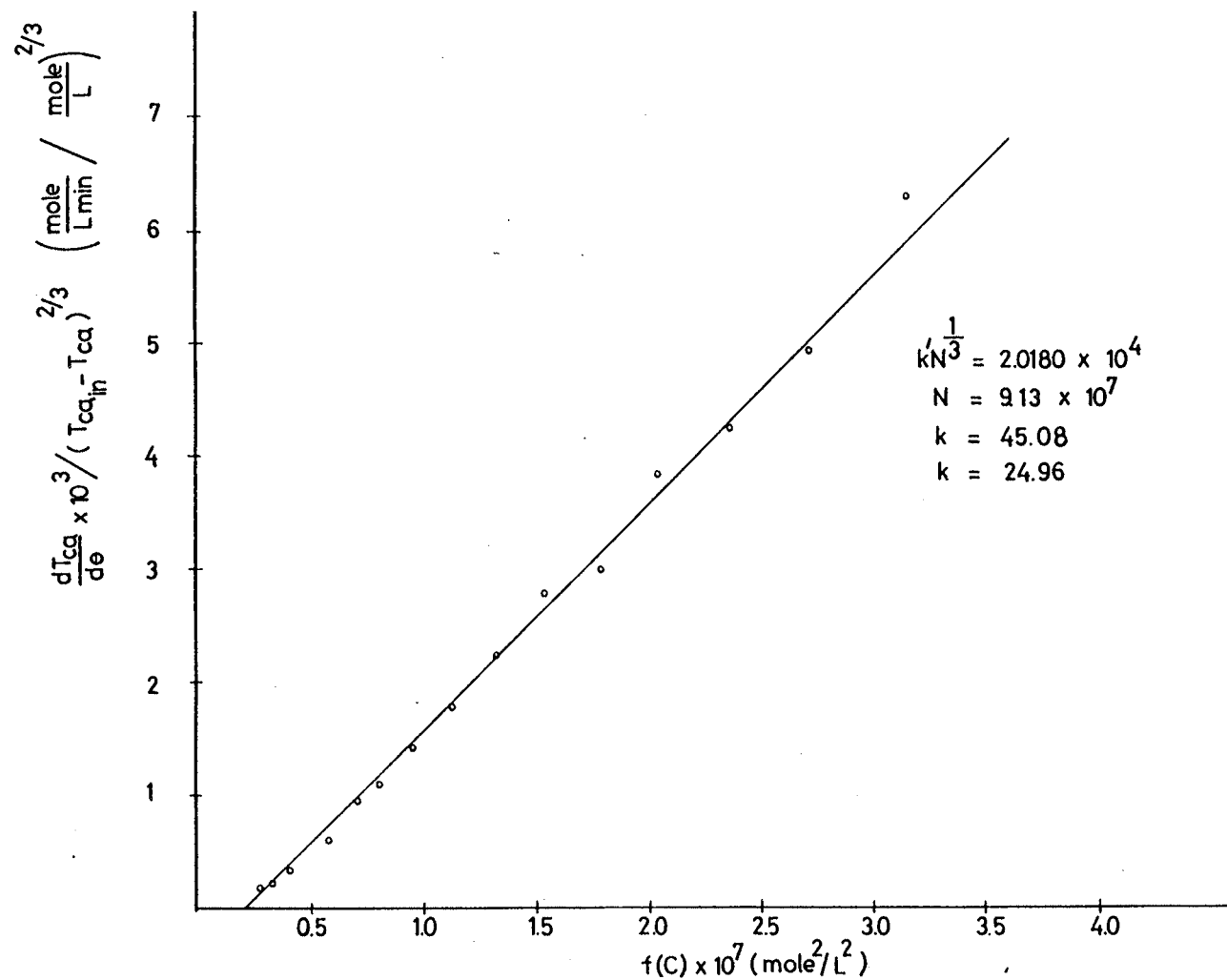
FIGURE C.27 Overall Growth Rate Constant of Expt. PE14
Determined by Simplified Method

$k'N^{1/3}$ = 0.6667 x 10^4
N = 2.17 x 10^7
k' = 24.04
k = 10.40

FIGURE C.28 Desupersaturation Curve of Expt. PE15

FIGURE C.29 Overall Growth Rate Constant of Expt. PE15
Determined by Simplified Method

FIGURE C.30 Overall Growth Rate Constant of Expt. PE15
Determined by Size Consideration

$k'' = 2.021$
$k_w = 56.1$

Axis label (y): $\frac{1}{A}\frac{dT_{ca}}{do} \times 10^7$ (mole / L min cm^2)

Axis label (x): $f(C) \times 10^7$ (mole^2/$_L^2$)

FIGURE C.31   Desupersaturation Curve of Expt. PE16

FIGURE C.32 Overall Growth Rate Constant of Expt. PE16
Determined by Simplified Method

$k'N^{1/3}$ = 2.3091 x 10^4

N = 8.50 x 10^8

k' = 24.54

k = 12.70

FIGURE C.33 Desupersaturation Curve of Expt. PE21

FIGURE C. 34 Overall Growth Rate Constant of Expt. PE21
Determined by Simplified Method

APPENDIX D   RESULTS OF FINAL CRYSTAL SIZE MEASUREMENT

   Some of the final crystal precipitates from the spontaneous crysta-
llization experiments were sampled and sized by the Micro-videomat 2 Ima-
ge Analyzer described in Section (4.4.3.3). This information is used
for crystal growth rate constant calculation using the Overall Growth
Rate with Size Consideration method described in Section (4.3.5). The
data of crystal size measurement are presented in number distribution.
They are tabulated in the following tables:

TABLE D1   DATA OF SIZE MEASUREMENT OF E22

Mean Chord Length (μm)	Number	Cummulative Percentage
5.0	74	0.7
7.0	1384	14.4
9.0	1507	29.3
10.9	1060	39.8
12.9	668	46.5
14.9	830	54.7
16.9	617	60.8
18.9	512	65.8
20.9	568	71.5
22.9	492	76.3
24.9	448	80.8
26.9	379	84.5
28.8	373	88.2
30.8	416	92.3
32.8	289	95.2
34.8	160	96.8
36.8	133	98.1
38.8	83	98.9
40.8	72	99.6
42.8	38	100.0

Mean chord length based on number distribution = 17.0μm

Total number of crystal counted = 10103

TABLE D2 DATA OF SIZE MEASUREMENT OF E23

Mean Chord Length (μm)	Number	Cummulative Percentage
4.0	9762	14.0
5.0	6516	23.4
6.0	3458	28.4
7.1	25.5	32.0
8.1	2680	35.8
9.1	3590	41.0
10.1	2916	45.2
11.2	3078	49.6
12.2	3130	54.1
13.2	2076	57.1
14.2	1995	60.0
15.3	2036	62.9
16.3	1937	65.7
17.3	1763	68.2
18.3	1752	70.8
19.4	1613	73.1
20.4	1450	75.2
21.4	1296	77.0
22.4	1301	78.9
23.5	1317	80.8
24.5	1207	82.5
25.5	1297	84.4
26.5	1067	85.9
27.6	1112	87.5
28.6	915	88.8
29.6	843	90.0
30.6	876	91.3
31.7	770	92.4
32.7	788	93.5
33.7	712	94.6
34.8	639	95.5
35.8	666	96.4
36.8	597	97.3
37.8	512	98.0
38.9	403	98.6
39.9	371	99.2
40.9	304	99.6
41.9	285	100.0

Mean chord length based on number distribution = 14.6μm

Total number of crystal counted = 69535

TABLE D3   DATA OF SIZE MEASUREMENT OF E24

Mean Chord Length (μm)	Number	Cummulative Percentage
3.2	557	5.8
3.6	389	9.9
4.1	518	15.3
4.5	377	19.3
5.0	395	23.4
5.5	325	26.8
5.9	301	30.0
6.4	434	34.5
6.8	283	37.5
7.3	354	41.2
7.7	375	45.1
8.2	364	48.9
8.6	395	53.1
9.1	267	55.9
9.6	242	58.4
10.0	259	61.1
10.5	144	62.6
10.9	137	64.1
11.4	162	65.8
11.8	155	67.4
12.3	130	68.8
12.7	118	70.0
13.2	85	70.9
13.6	105	72.0
14.1	113	73.2
14.6	83	74.0
15.0	130	75.4
15.5	86	76.3
15.9	97	77.3
16.4	82	78.2
16.8	57	78.8
17.3	79	79.6
17.7	81	80.4
18.2	71	81.2
18.7	23	81.4
19.1	56	82.0
19.6	100	83.1
20.0	39	83.5
20.5	118	84.7
20.9	40	85.1
21.4	86	86.0
21.8	73	86.8
22.3	62	87.4
22.7	56	88.0
23.2	96	89.0
23.7	74	89.8
24.1	62	90.5
24.6	85	91.3

(cont'd)

TABLE D3   (Cont'd)

25.0	80	92.2
25.5	54	92.8
25.9	77	93.6
26.4	66	94.3
26.8	88	95.2
27.3	81	96.0
27.8	69	96.7
28.2	73	97.5
28.7	55	98.1
29.1	61	98.7
29.6	33	99.1
30.0	57	99.7
30.5	32	100.0

Mean chord length based on number distribution = 11.2μm

Total number of crystal counted = 9546

TABLE D4   DATA OF SIZE MEASUREMENT OF PE4

Mean chord length (μm)	Number	Cummulative Percentage
0.5	3303	15.9
1.4	4148	35.8
2.4	2831	49.4
3.3	1895	58.5
4.3	1642	66.4
5.2	1330	72.7
6.1	1314	79.1
7.1	1116	84.4
8.0	823	88.4
9.0	743	91.9
9.9	496	94.3
10.9	384	96.2
11.8	184	97.0
12.8	233	98.2
13.7	77	98.5
14.7	75	98.9
15.6	88	99.3
16.5	42	99.5
17.5	26	99.6
18.4	27	99.8
19.4	35	99.9
20.3	14	100.0

Mean chord length based on number distribution = 4.0μm

Total number of crystal counted = 20826

TABLE D5   DATA OF SIZE MEASUREMENT OF PE7

Mean Chord Length (μm)	Number	Cummulative Percentage
0.5	2056	12.1
1.4	2196	24.9
2.4	2206	37.9
3.3	972	43.6
4.3	1269	51.0
5.2	677	55.0
6.1	602	58.5
7.1	581	62.0
8.0	632	65.7
9.0	601	69.2
9.9	688	73.2
10.9	600	76.7
11.8	747	81.1
12.8	671	85.1
13.7	755	89.5
14.7	521	92.5
15.6	391	94.8
16.6	249	96.3
17.5	129	97.1
18.4	82	97.5
19.4	61	97.9
20.3	46	98.2
21.3	48	98.5
22.2	53	98.8
23.2	34	99.0
24.1	28	99.1
25.1	40	99.4
26.0	24	99.5
27.0	18	99.6
27.9	24	99.7
28.8	21	99.9
29.8	22	100.0

Mean chord length based on number distribution = 6.6μm

Total number of crystal counted = 17044

TABLE D6   DATA OF SIZE MEASUREMENT OF PE8

Mean Chord Length (µm)	Number	Cummulative Percentage
1.5	36	0.6
2.6	310	5.9
3.6	623	16.6
4.6	684	28.3
5.6	494	36.8
6.7	362	43.0
7.7	321	48.5
8.7	372	54.9
9.7	317	60.3
10.8	291	65.3
11.8	267	69.9
12.8	241	74.0
13.8	176	77.0
14.8	148	79.5
15.9	172	82.5
16.9	86	84.0
17.9	158	86.7
18.9	107	88.5
20.0	120	90.6
21.0	115	92.5
22.0	85	94.0
23.0	87	95.5
24.1	71	96.7
25.1	58	97.7
26.1	24	98.1
27.1	15	98.4
28.2	19	98.7
29.2	3	98.8
30.2	6	100.0

Mean chord length based on number distribution = 9.9µm

Total number of crystal counted = 5768

TABLE D7   DATA OF SIZE MEASUREMENT OF PE9

Mean Chord Length (µm)	Number	Cummulative Percentage
1.0	93	6.7
3.1	133	16.2
5.1	84	22.3
7.2	62	26.7
9.2	128	35.9
11.3	59	40.2
13.3	94	46.9
15.3	53	50.7
17.4	59	55.0
19.4	88	61.3
21.5	81	67.1
23.5	80	72.8
25.6	81	78.7
27.6	74	84.0
29.7	82	89.9
31.7	71	95.0
33.8	46	98.3
35.8	24	100.0

Mean chord length based on number distribution = 16.4µm

Total number of crystal counted = 1392

TABLE D8   DATA OF SIZE MEASUREMENT OF PE11

Mean Chord Length (µm)	Number	Cummulative Percentage
20.8	3	0.6
22.5	8	2.3
24.3	5	3.3
26.0	21	7.6
27.7	1	7.8
29.4	21	12.2
31.1	0	12.2
32.8	16	15.5
34.5	1	15.7
36.2	10	17.7
38.0	15	20.8
39.7	0	20.8
41.4	26	26.2
43.1	9	28.0
44.8	21	32.4
46.5	18	36.1
48.2	17	39.6
49.9	25	44.7
51.6	32	51.3
53.4	54	62.5
55.1	76	78.1
56.8	106	100.0

Mean chord length based on number distribution = 47.6µm

Total number of crystal counted = 485

APPENDIX E: COMPOSITION OF SCALE

The scale samples of the Lake Liddell water experiments (Chapter 7) were taken from the condenser tube. They were sent to the Central Laboratories of the Electricity Commission of New South Wales for analysis. The samples were sectioned, mounted, polished and presented to the electron microscope in order to measure scale depth on the insides of the condenser tube walls. Scrapings of the deposits were examined under the electron microscope using energy dispersive X-ray microanalysis to determine the minerals present and the elemental analysis.

Plates of both the spectra and electron microscope scans are presented. The data can be summarised:

Run	Distance From Outlet	Composition	Depth
4	0 m	monohydrocalcite	40µm with growths to 100µm
4	1 m	monohydrocalcite	80µm with growths to 200µm
4	2 m	monohydrocalcite	80µm with growths to 200µm
4	3 m	monohydrocalcite	100µm with growths to 300µm
4	3.5 m	monohydrocalcite	190µm with growths to 300µm
5	1 m	clay, iron oxide, copper carbonate, copper chloride hydroxide (green) zinc, copper chloride hydroxide and traces of calcium carbonate.	N/A
6	3 m	copper carbonate, copper zinc chloride hydroxide, traces of clay and calcium carbonate	N/A
7	3.5 m	silica, clay, traces of calcium carbonate, iron oxide	N/A
8	0 m	copper zinc chloride hydroxide traces of silica, clay and calcium carbonate.	N/A
8	3.5 m	copper carbonate, copper zinc chloride hydroxide, traces of silica and calcium carbonate.	N/A
10	0 m	copper zinc chloride hydroxide	2-5µm sparce
10	1 m	copper carbonate, traces of calcium carbonate	5-10µm sparce
10	2 m	copper carbonate, copper zinc chloride hydroxide	2-5µm even

Run	Distance From Outlet	Composition	Depth
10	3 m	copper zinc chloride hydroxide copper carbonate	2-5µm even
10	3.5 m	copper carbonate, copper chloride hydroxide	5-15µm even
11	0 m	monohydrocalcite	40µm with growths to 200µm
11	1 m	monohydrocalcite	40µm with growths to 200µm
11	2 m	monohydrocalcite	40µm with growths to 200µm
11	3 m	monohydrocalcite	50µm sparce
11	3.5 m	monohydrocalcite	50µm sparce with growths to 100µm

Samples were coated with gold to form a conductive coating, thus two gold peaks appear at 2.1 KeV and 9.7 KeV on the elemental spectra should be disregarded.

The major peaks of the elements detected occur as follows:

Element	Energy (KeV)
Sodium (Na)	1.05
Potassium (K)	3.30, 3.59
Magnesium (Mg)	1.25
Aluminium (Al)	1.49, 1.55
Silicon (Si)	1.74, 1.82
Chloride (Cl)	2.60, 2.80
Calcium (Ca)	3.70, 4.00
Iron (Fe)	6.40, 7.05
Copper (Cu)	8.05, 8.90
Zinc (Zn)	8.61, 9.59

Energy dispersive X-ray micro-analysis will not detect elements with atomic numbers less than that of Sodium (11) thus Hydrogen, Helium, Lithium, Beryillium, Boron, Carbon, Nitrogen, Oxygen and Fluorine will not be shown on the spectra though any of them may be present.
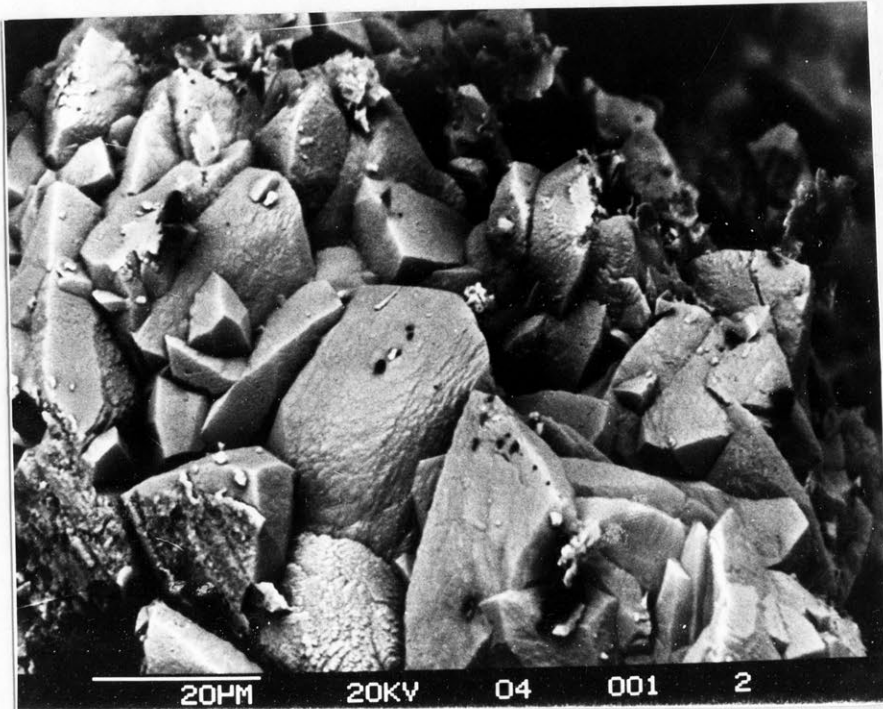
PLATE E1   Run 4, 0 m scale, 1000x magnification, H.F.W.
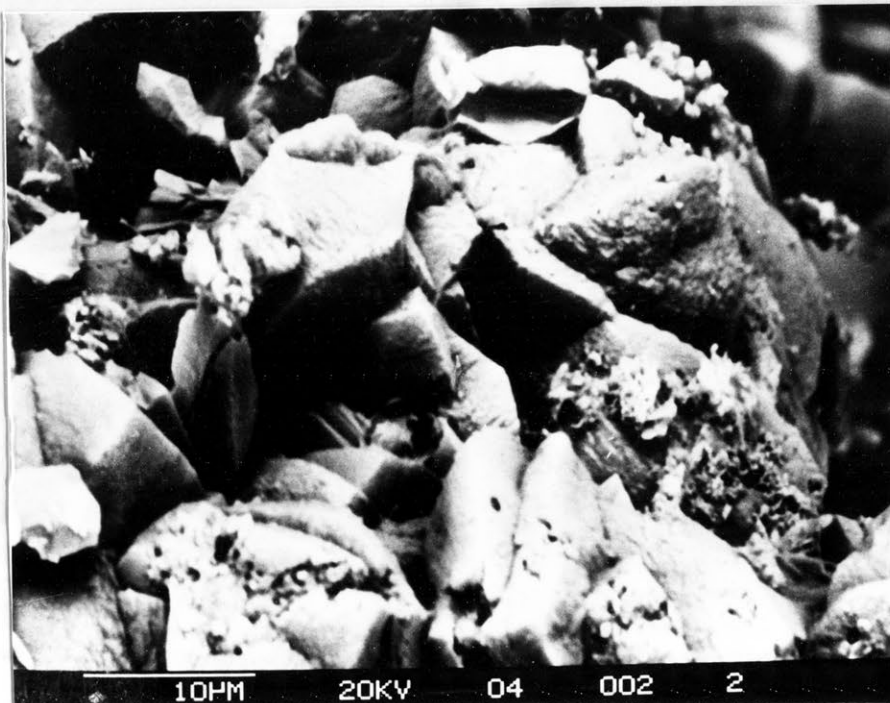   0.25mm.

PLATE E2   Run 4, 1 m scale, 2100x magfication, H.F.W.
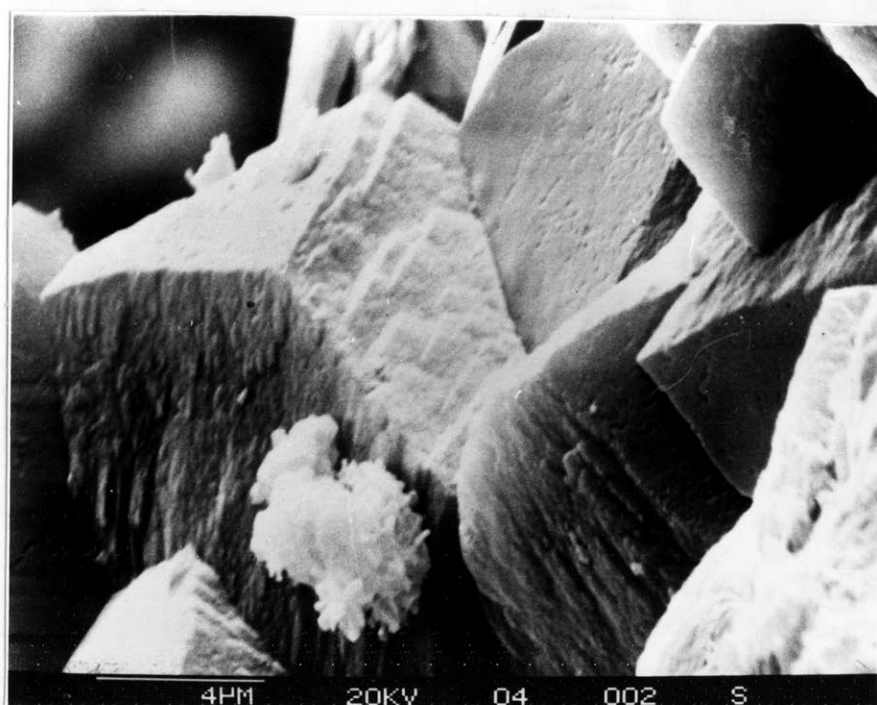   0.05mm

PLATE E3 Run 4, 1 m scale, 5259x magnification, H.F.W.
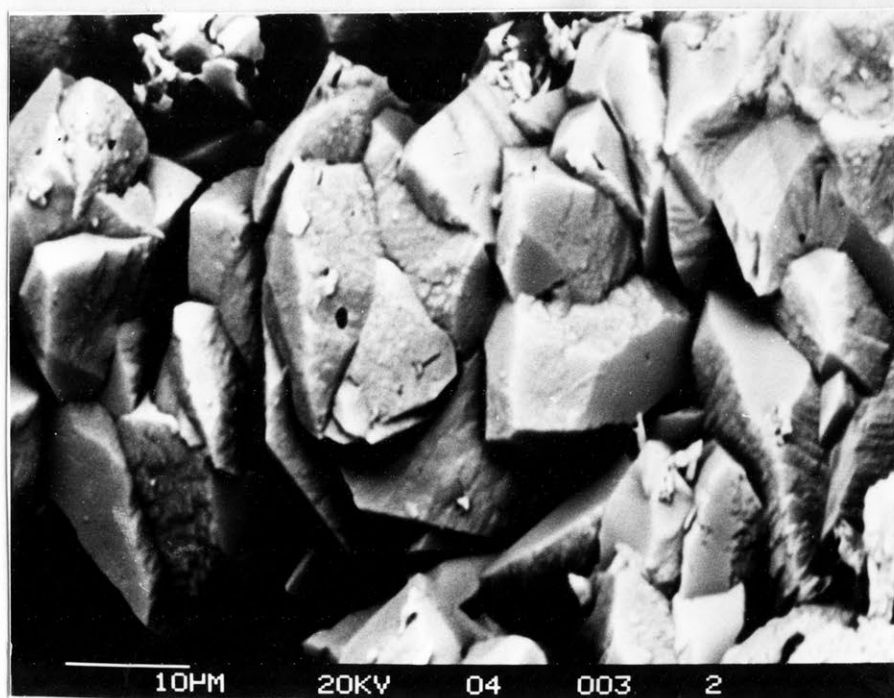0.02mm

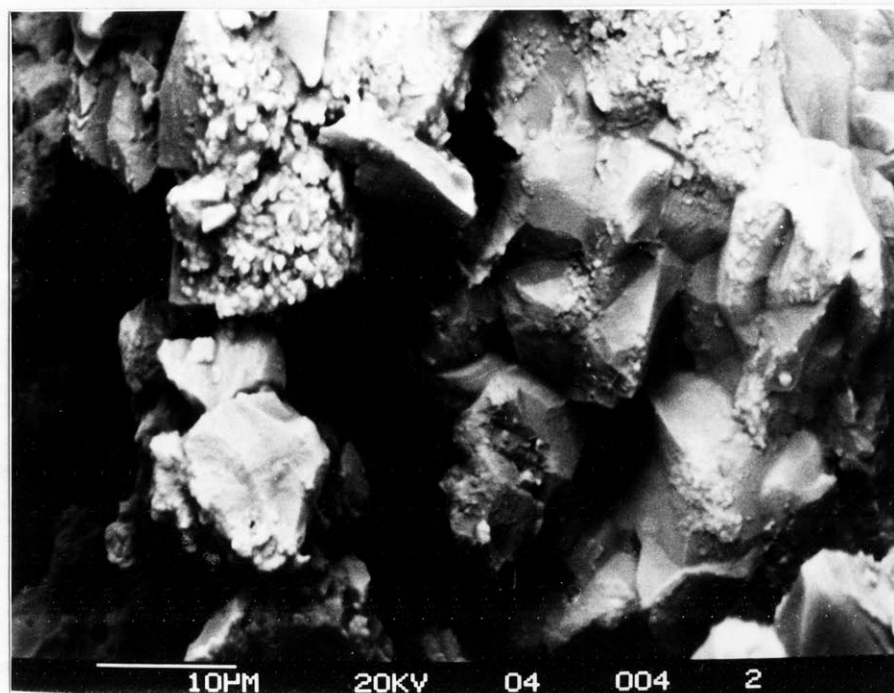PLATE E4 Run 4, 2 m scale, 1500x magnification, H.F.W.
0.83mm.

PLATE E5 Run 4, 3 m scale, 1700x magnification, H.F.W.
0.73mm.

PLATE E6 Run 4, 3.5 m scale, 1300x magnification,
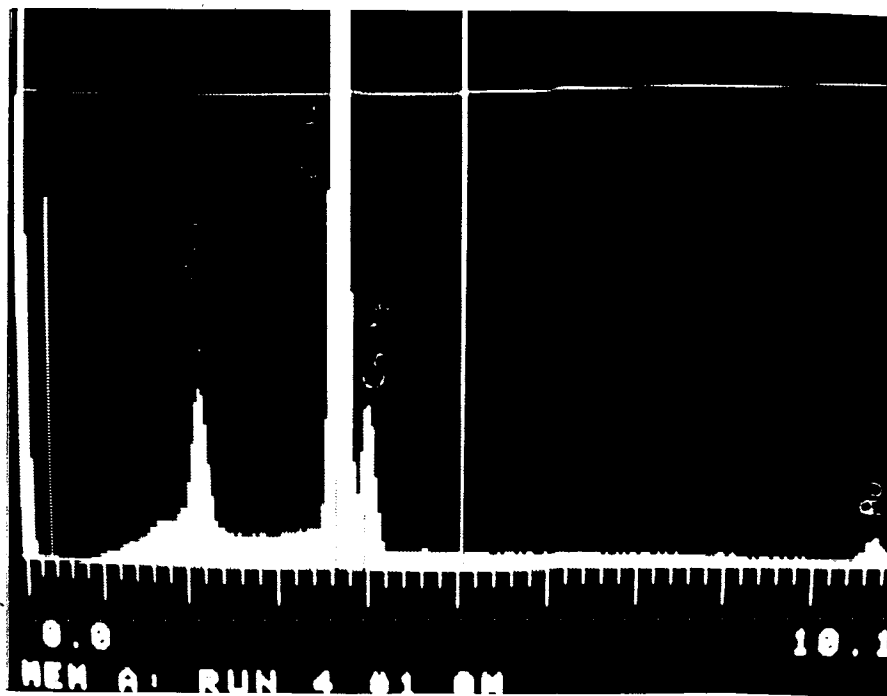H.F.W. 0.96mm.
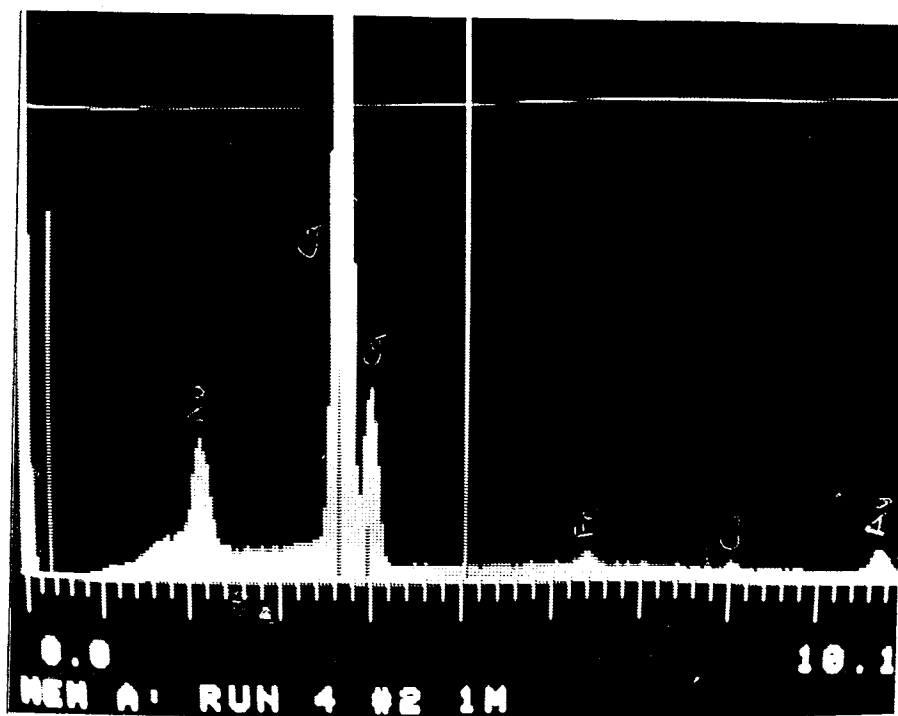
PLATE E7   Spectra run 4, 0 m, monohydrocalcite.

PLATE E8   Spectra run 4, 1.o m, monohydrocalcite.
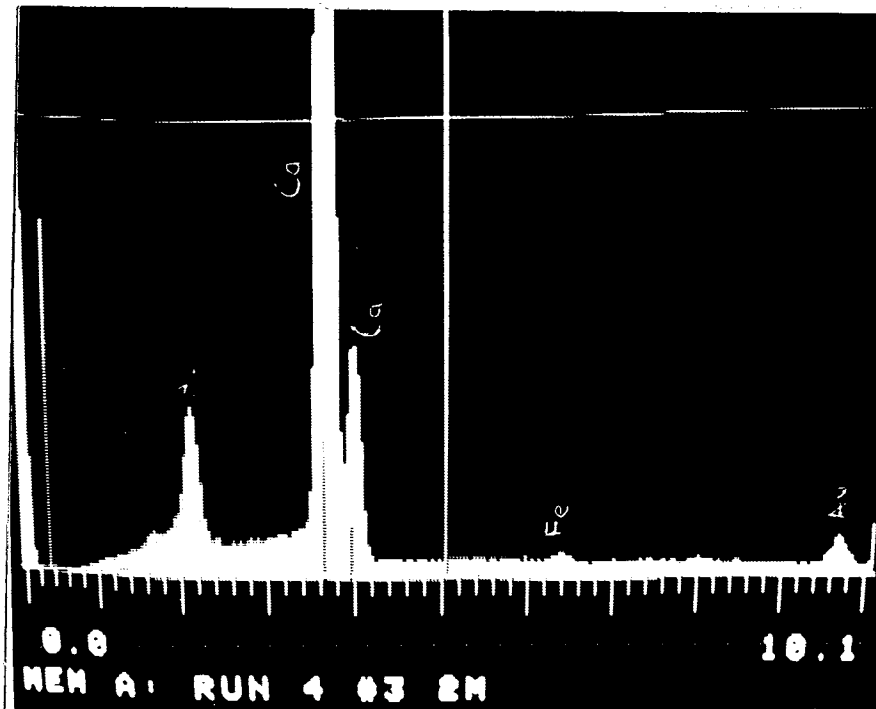
PLATE E9   Spectra run 4, 2.0 m, monohydrocalcite and
            traces of iron.
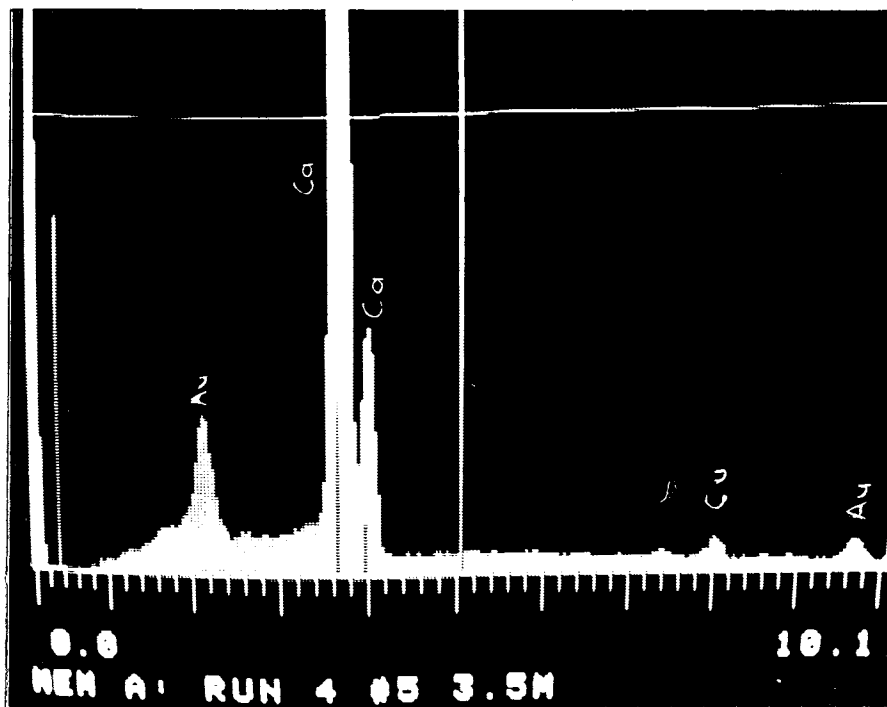

PLATE E10   Spectra run 4, 3.5 m, monohydrocalcite
            and traces of copper.
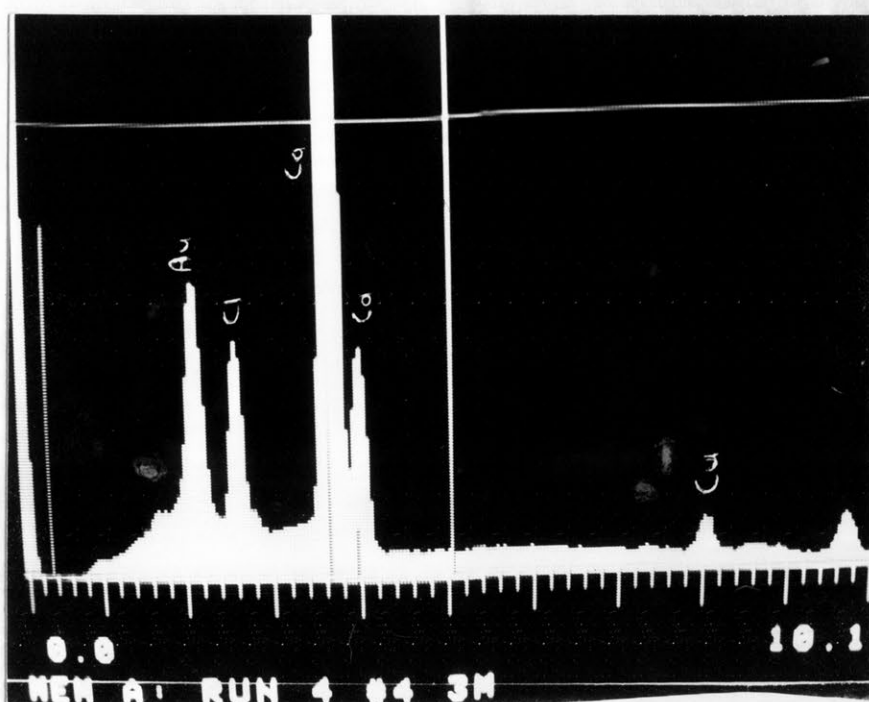
PLATE E11   Spectra run 4, 3 m, calcium (monohydrocalcite)
            chlorine and copper, chlorine is possibly
            present as copper chloride hydroxide.

PLATE E12   Run 5, 1 m scale, 1300x magnification,
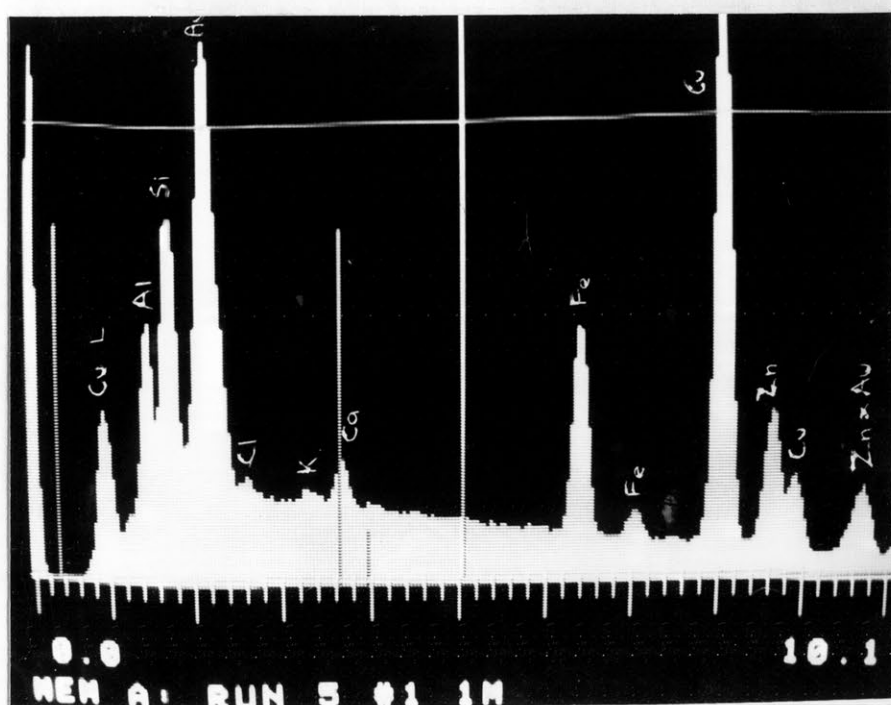   H.F.W. 0.96mm.

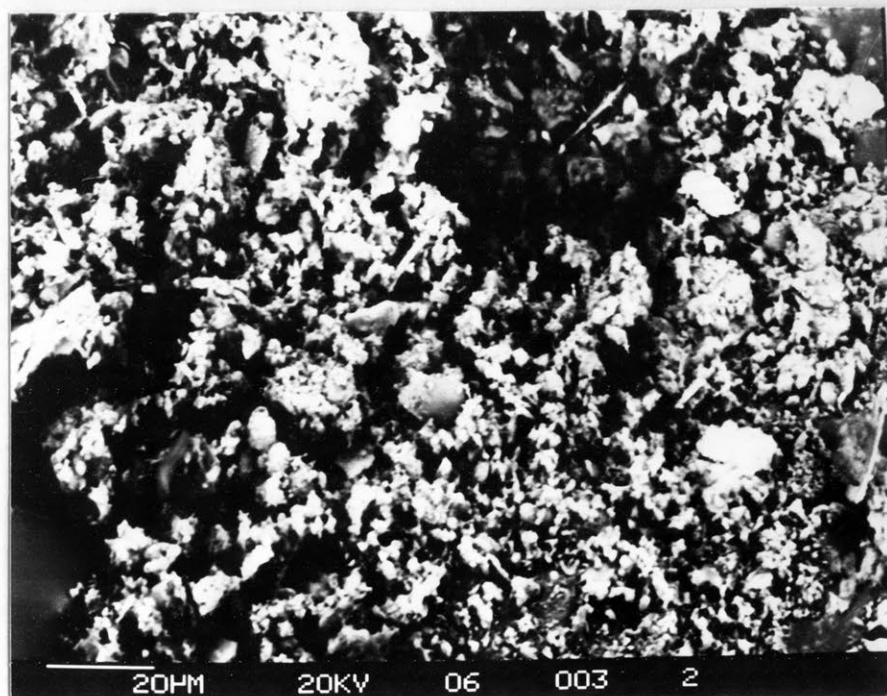PLATE E13   Spectra run 5, 1 m

PLATE E14   Run 6, 3 m scale, 650x magnification,
H.F.W. 0.92mm.

PLATE E15   Spectra run 6, 3 m.
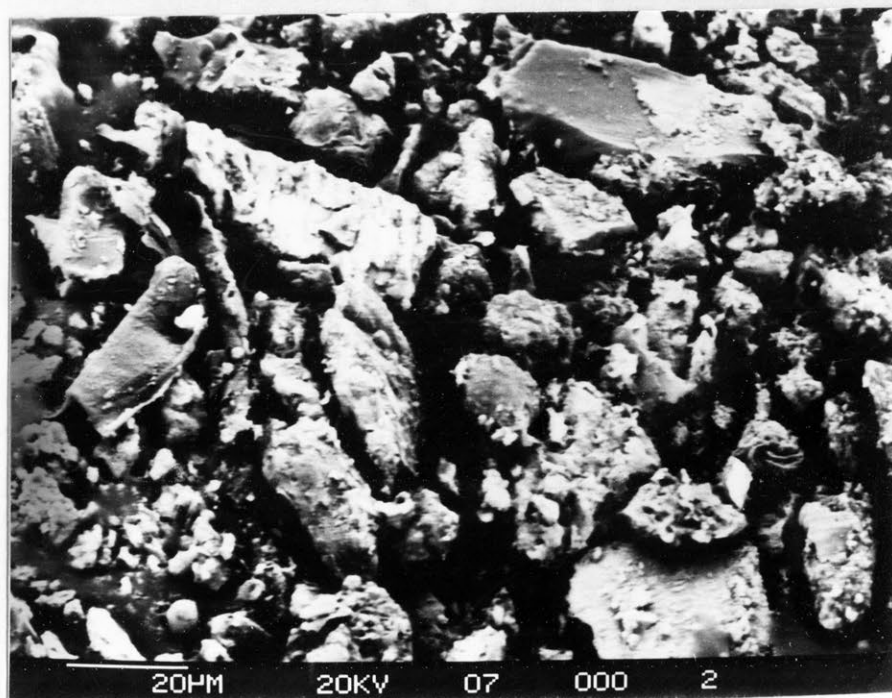
PLATE E16   Run 7, 3.5 m scale, 650x magnification,
H.F.W. 0.67mm, note angular grain of silica
in top right.
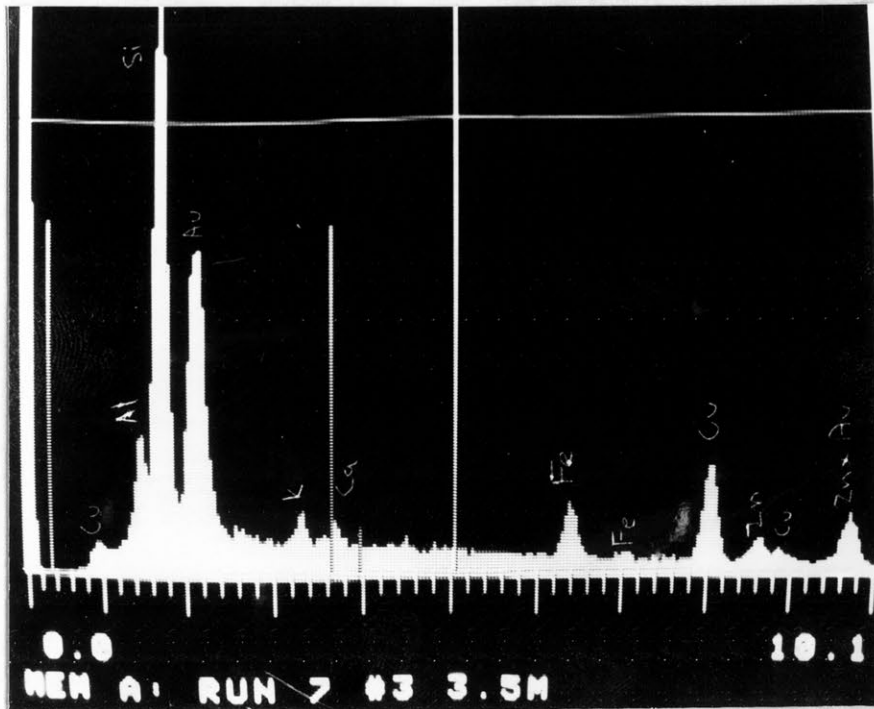
PLATE E17 Spectra run 7, 3.5 m.
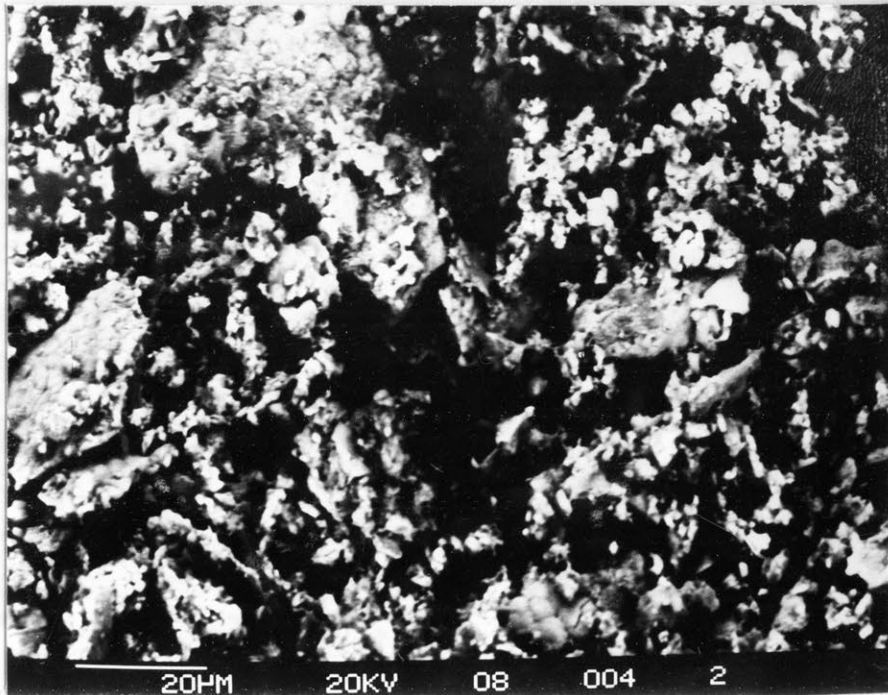
PLATE E18 Run 8, 0m scale, 800x magnification,
H.F.W. 0.156mm.
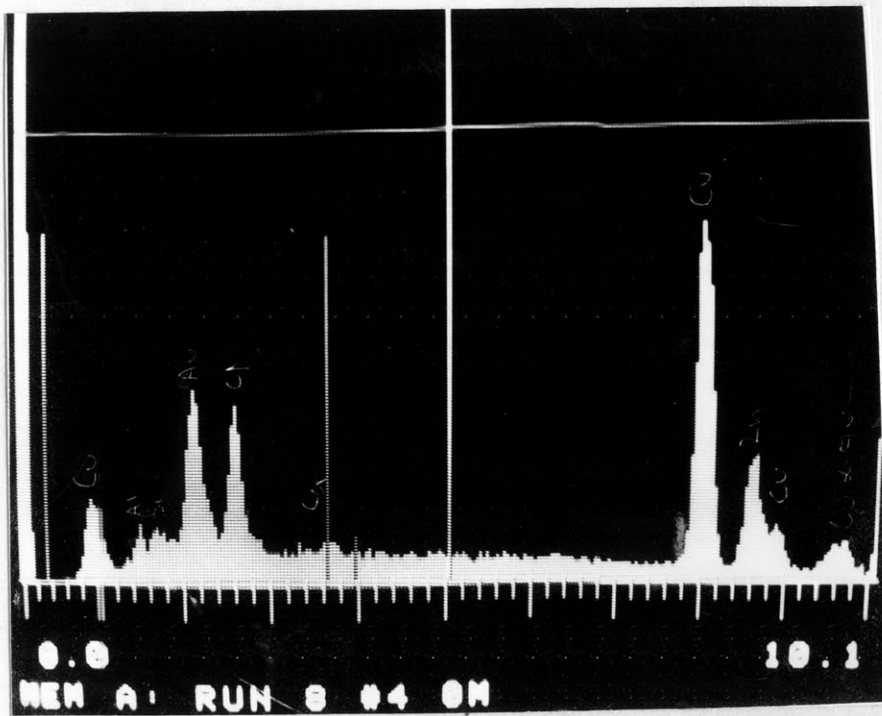
PLATE E19   Spectra run 8, 0 m.

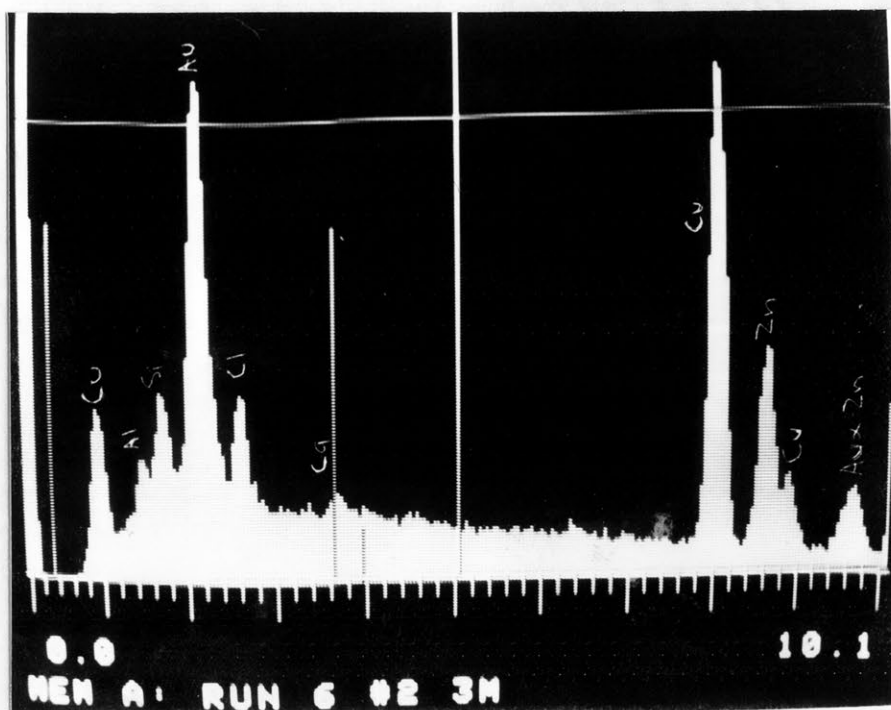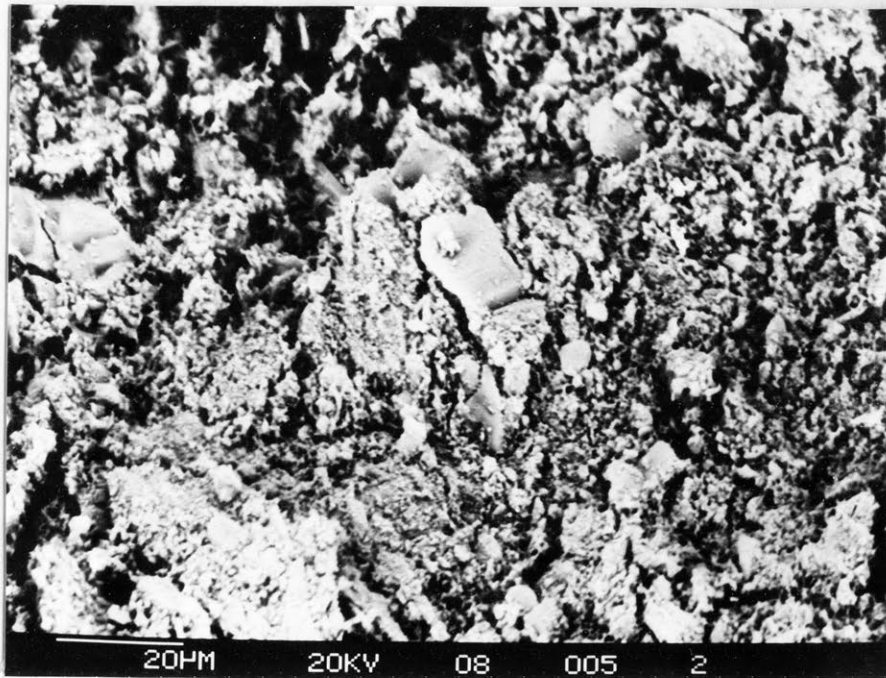PLATE E20   Run 8, 3.5 m scale, 750x magnification,
H.F.W. 0.167mm.
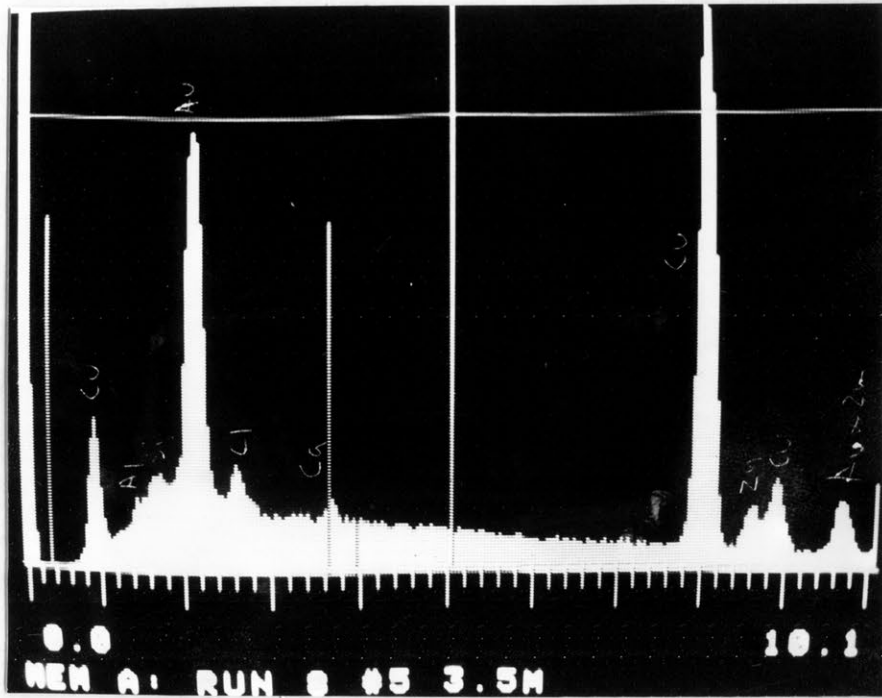
PLATE E21   Spectra run 8, 3.5 m.

PLATE E22   Run 10, 0 m scale, 1100x magnification
H.F.W. 0.113mm.

PLATE E23   Run 10, 1 m scale, 1150x magnification,
            H.F.W. 0.109mm.
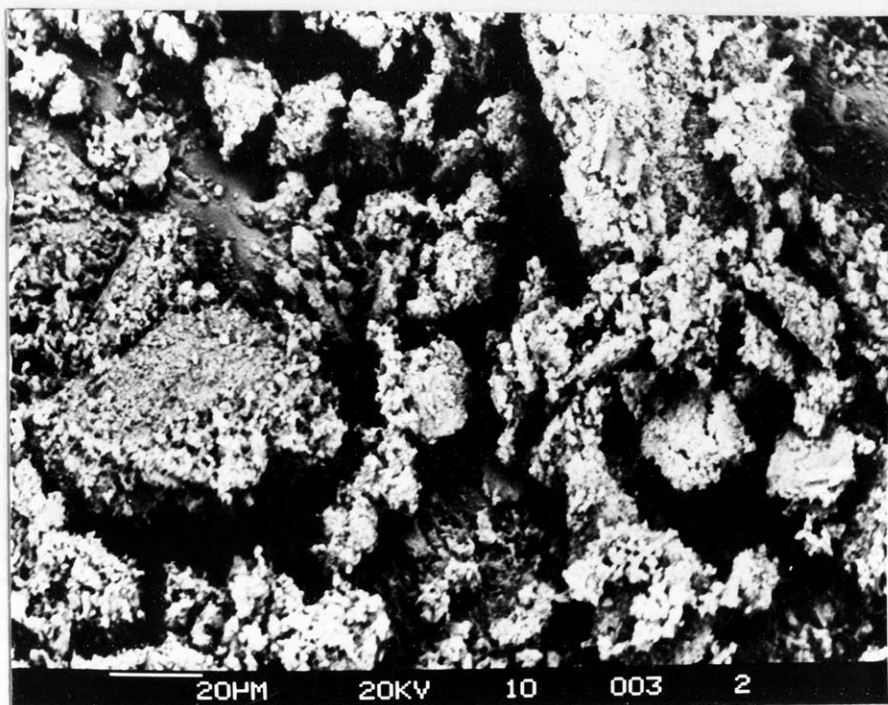
PLATE E24   Run 10, 2 m scale, 575x magnification,
            H.F.W. 0.217mm.

PLATE E25   Run 10, 3 m scale, 1100x magnification, H.F.W. 0.114mm.

PLATE E26   Run 10, 3.5 m scale, 575x magnification, H.F.W. 0.217mm.

PLATE E27   Spectra run 10, 0 m.

PLATE E28   Spectra run 10, 1 m.

PLATE E29 Spectra run 10, 2 m.
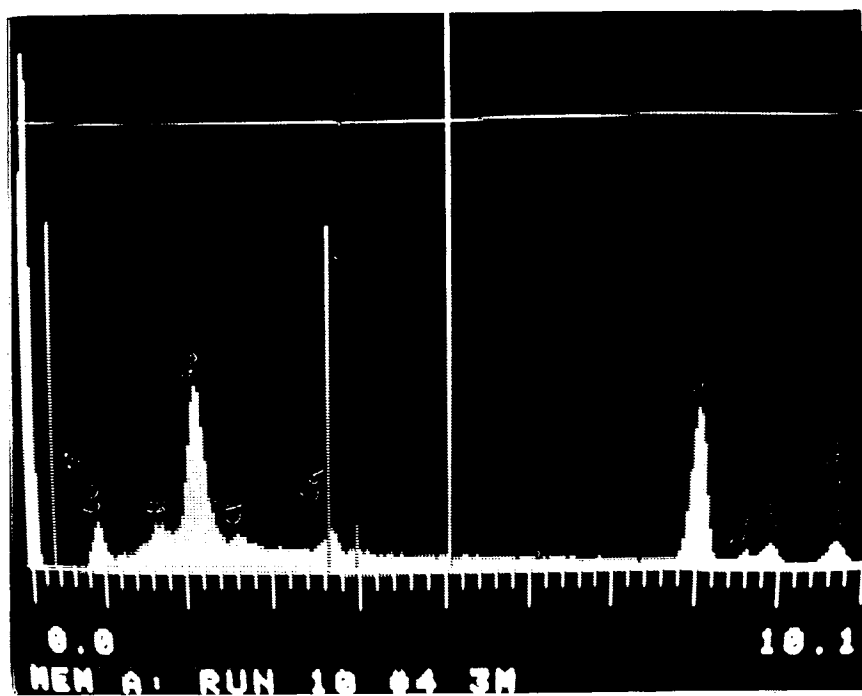
PLATE E30 Spectra run 10, 3 m.
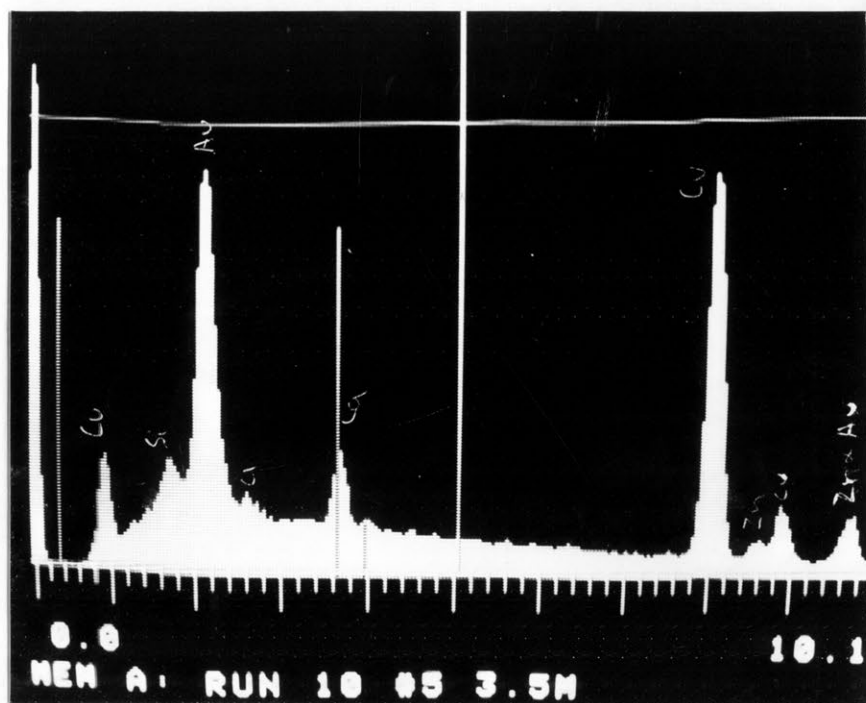
PLATE E31   Spectra run 10, 3.5 m.
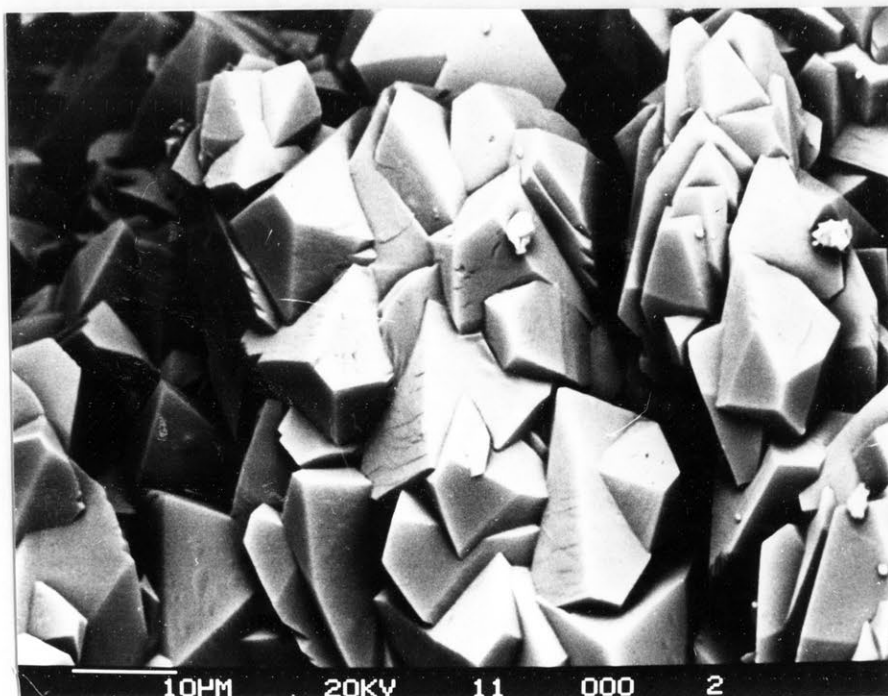
PLATE E32   Run 11, 1 m scale, 1250x magnification,
H.F.W. 0.1mm.
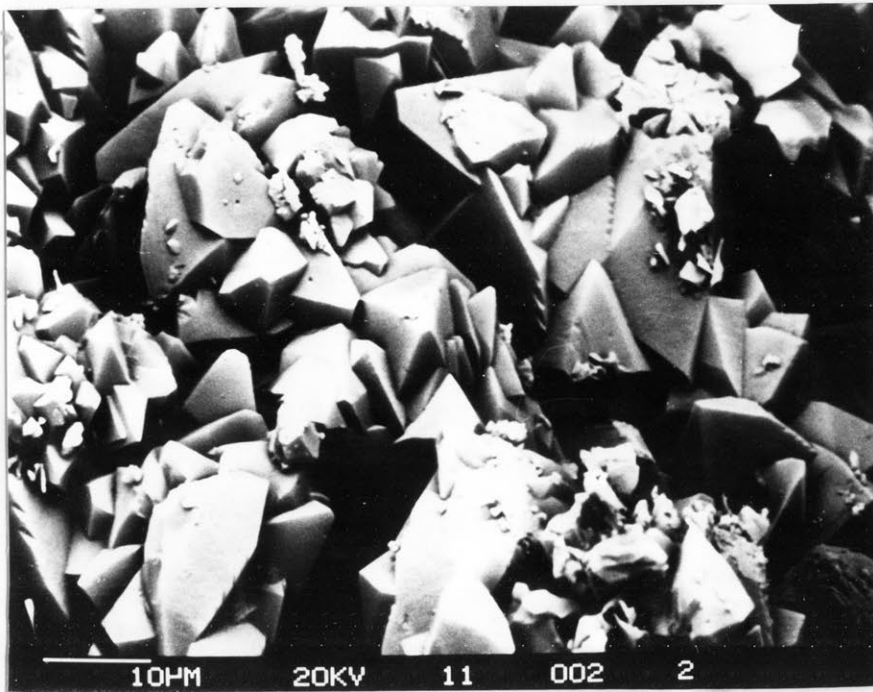
PLATE E33   Run 11, 1 m scale, 1300x magnification,
            H.F.W. 0.096mm.
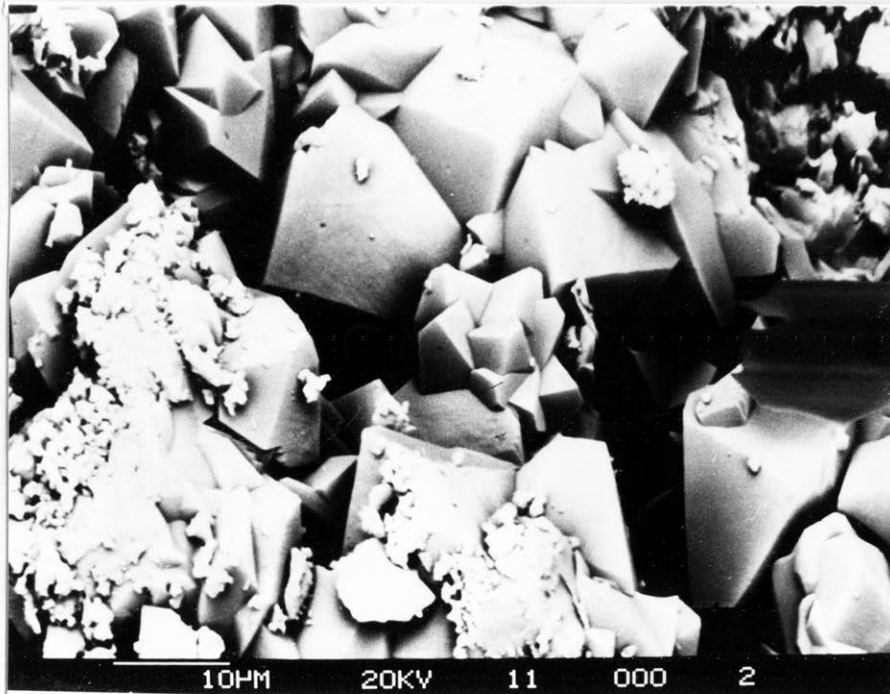
PLATE E34   Run 11, 2 m scale, 1400x magnification,
            H.F.W. 0.089mm.
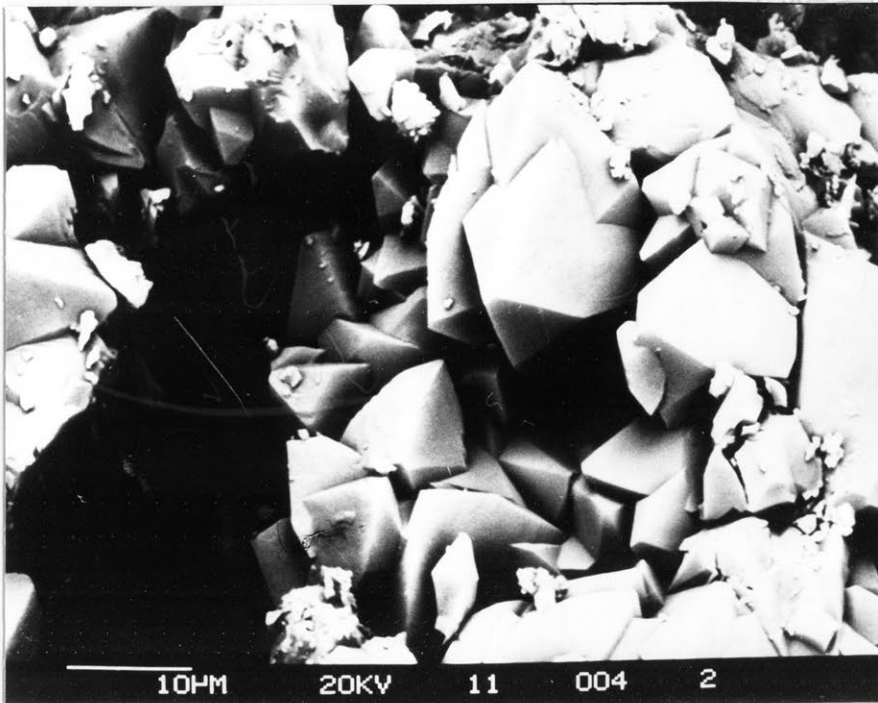
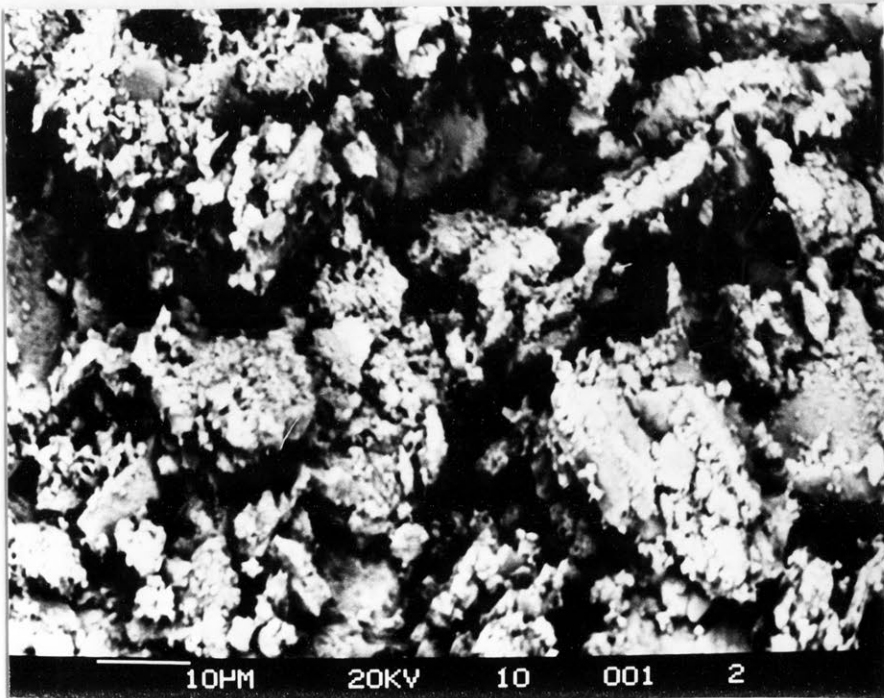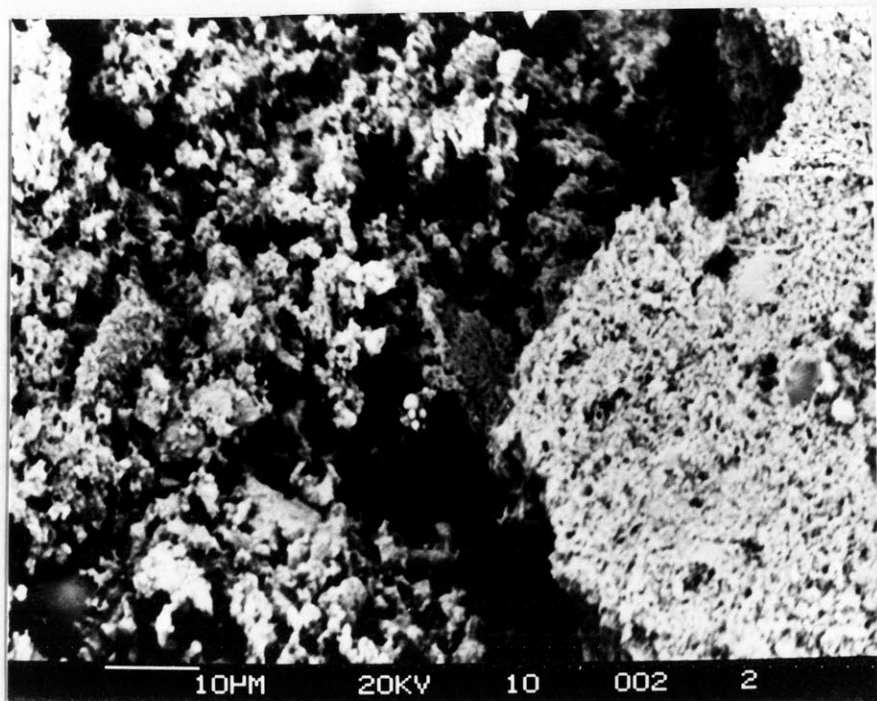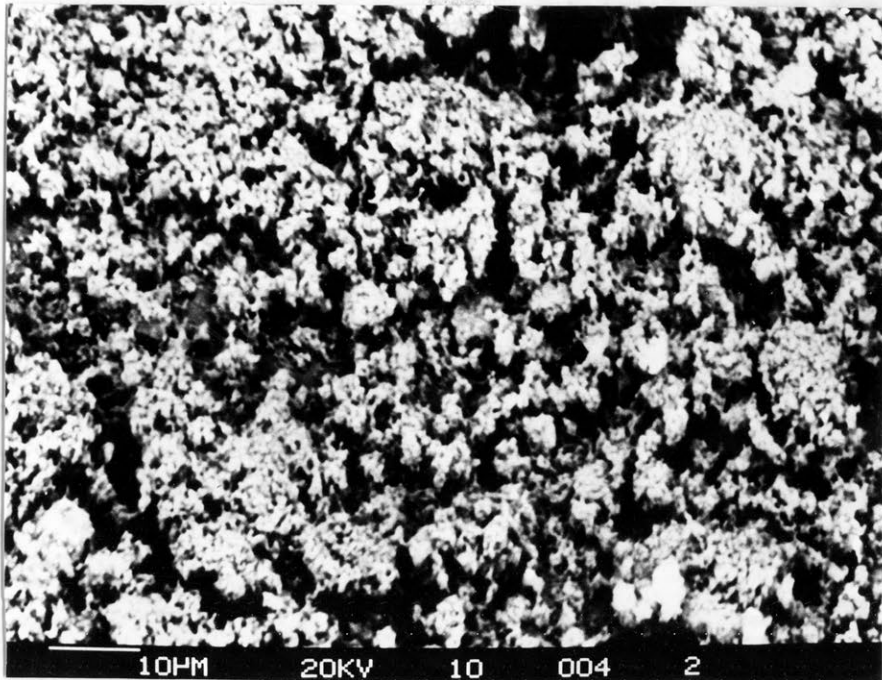PLATE E35   Run 11, 3 m scale, 1500x magnification,
            H.F.W. 0.083mm.
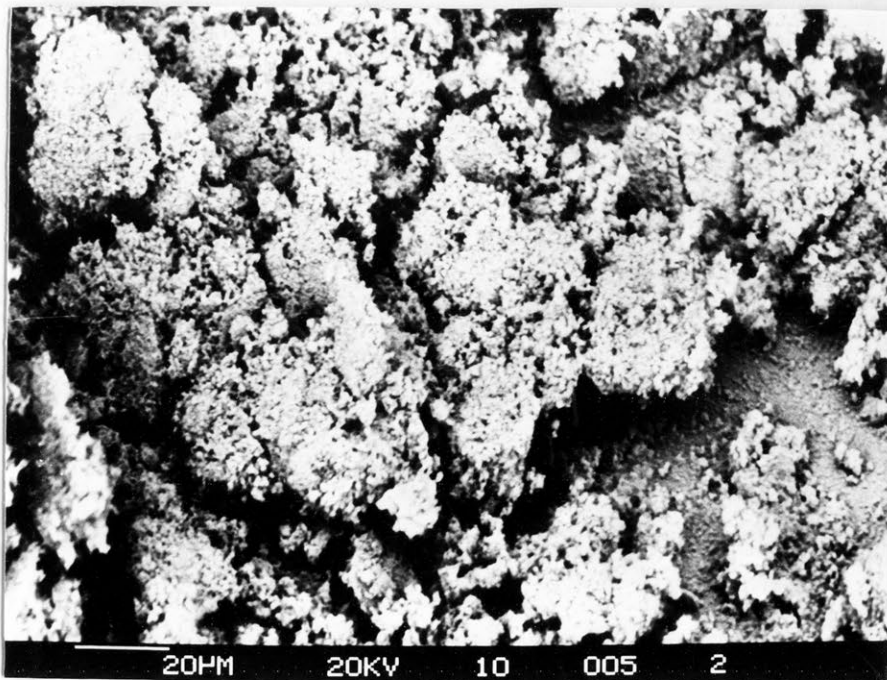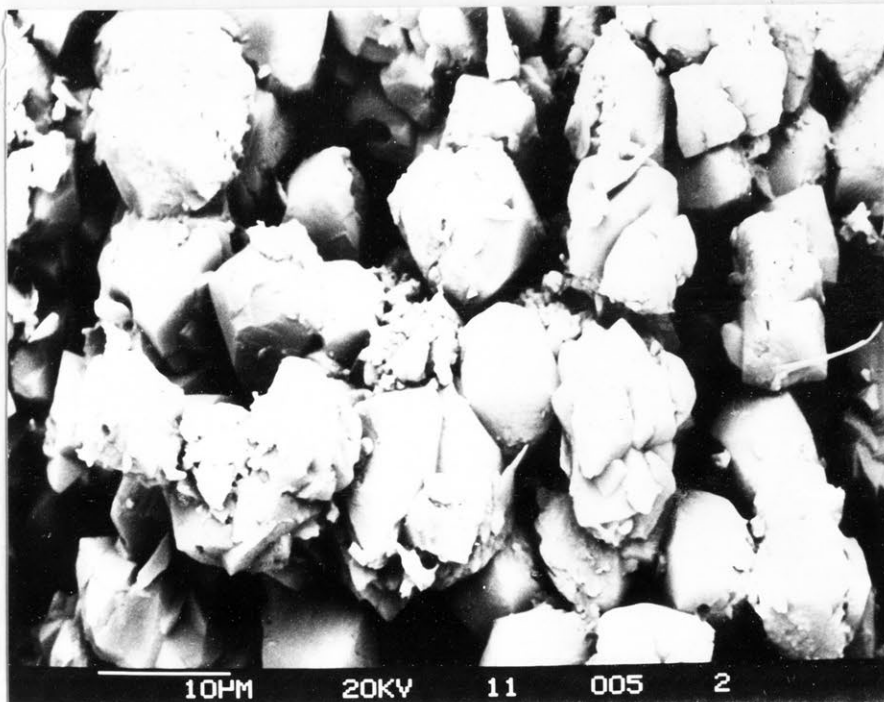

PLATE E36   Run 11, 3.5 m scale, 1700x magnification,
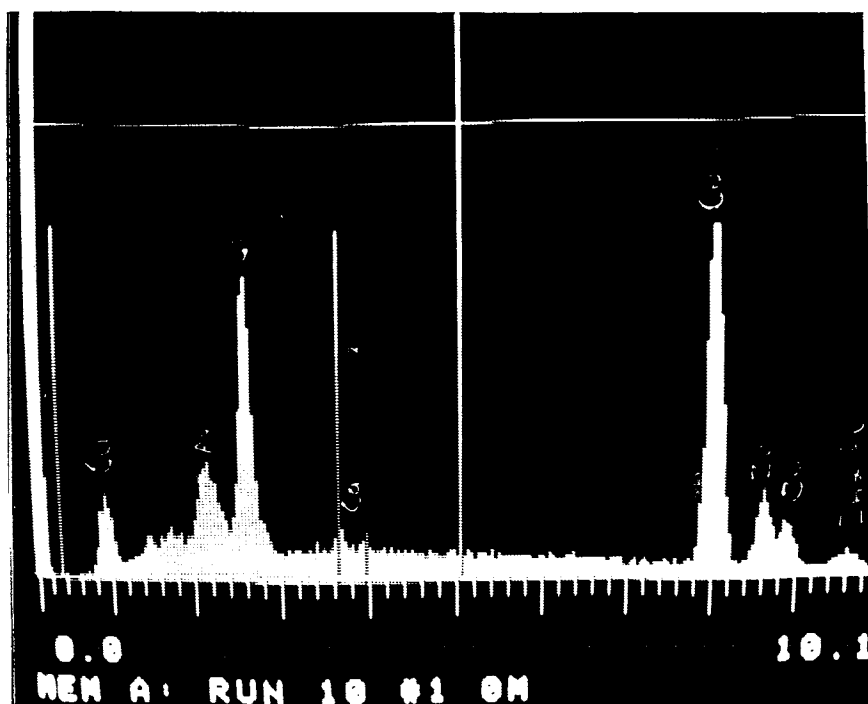   H.F.W. 0.075mm.
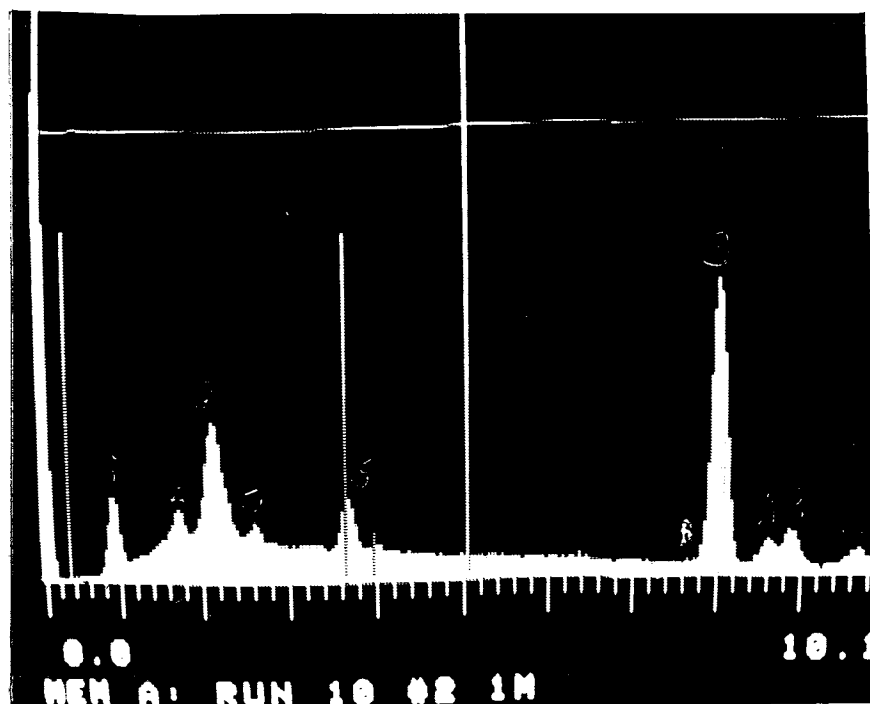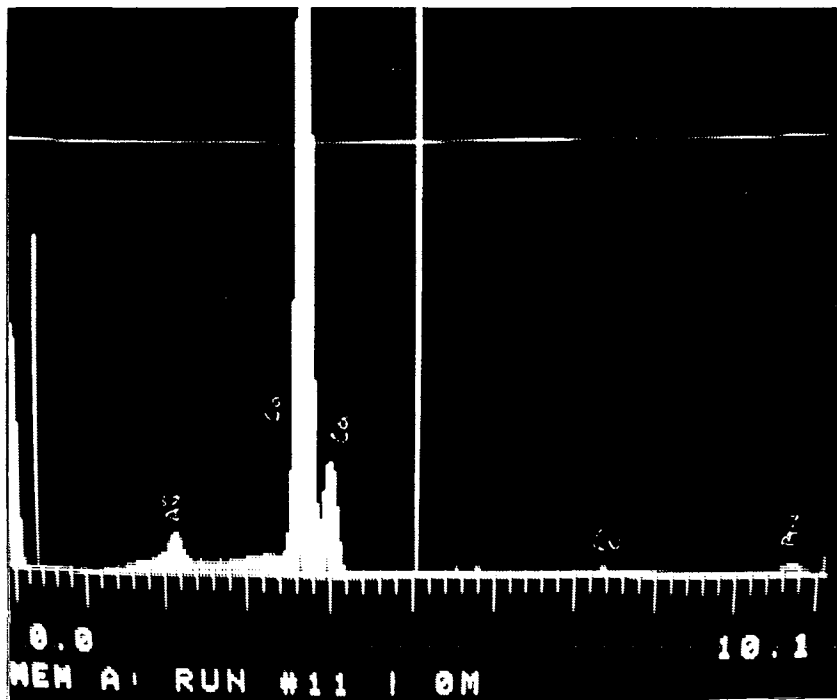
PLATE E37 Spectra run 11, 0 m.
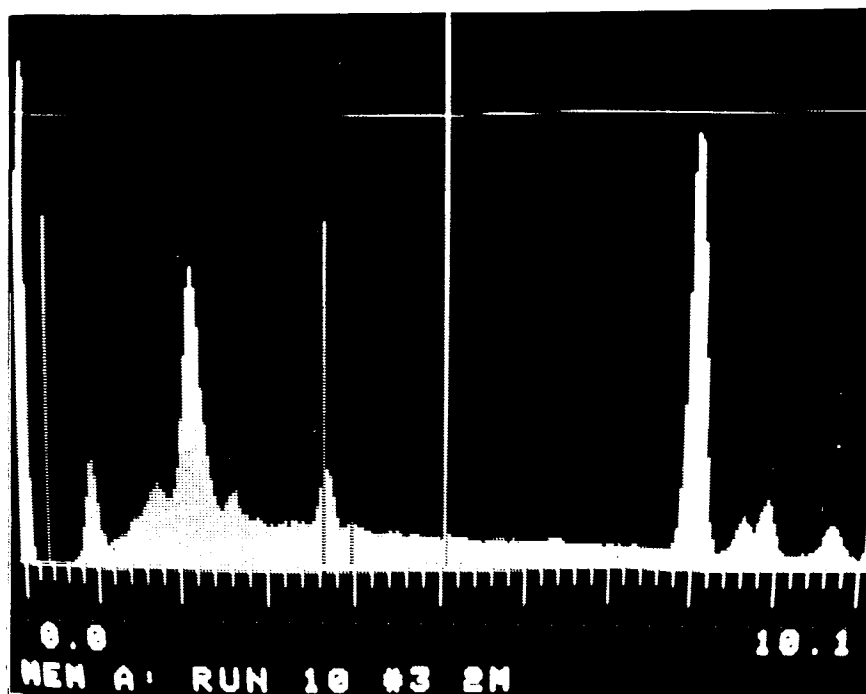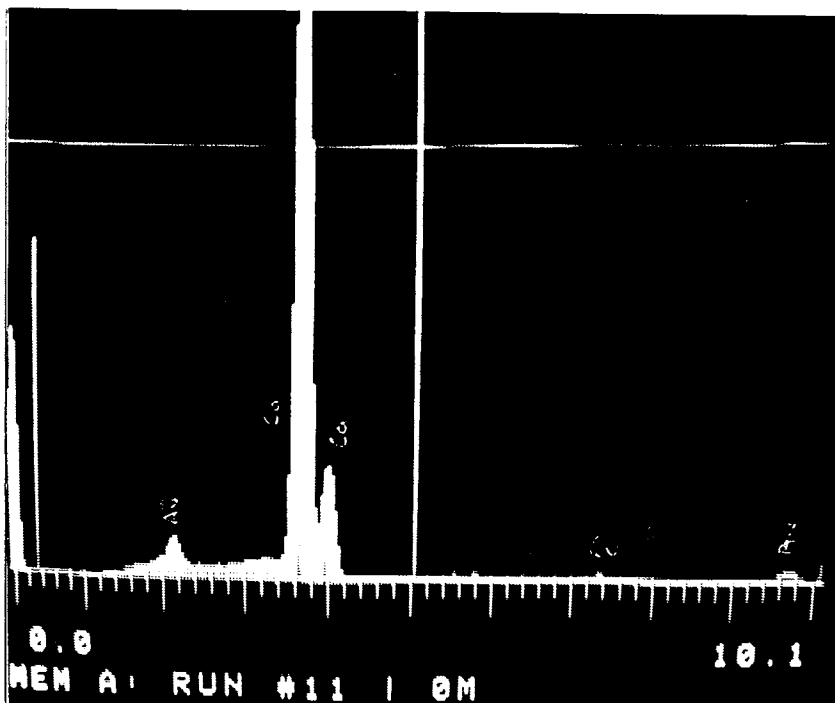

PLATE E38 Spectra run 11, 1 m.
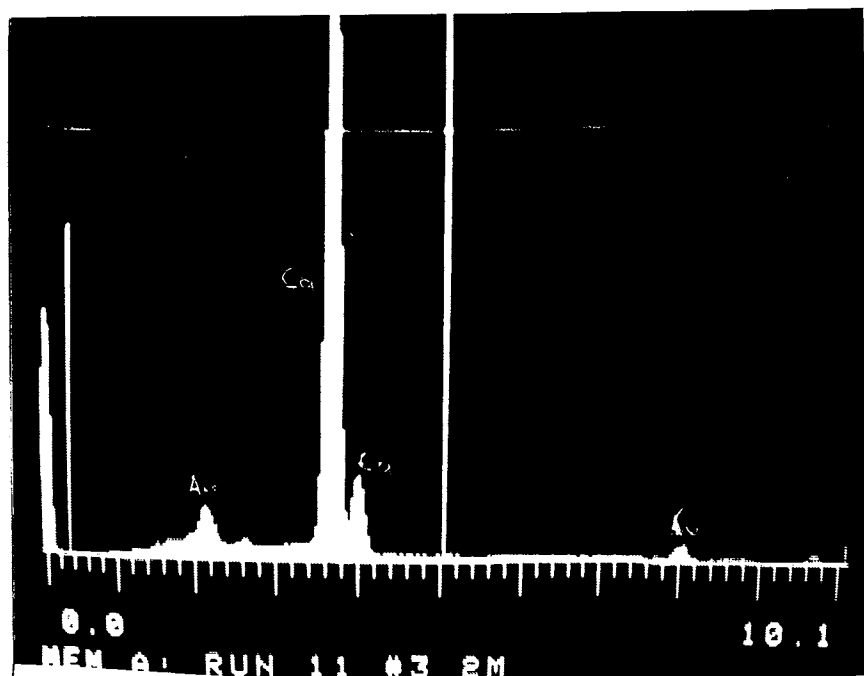
PLATE E39 Spectra run 11, 2 m.
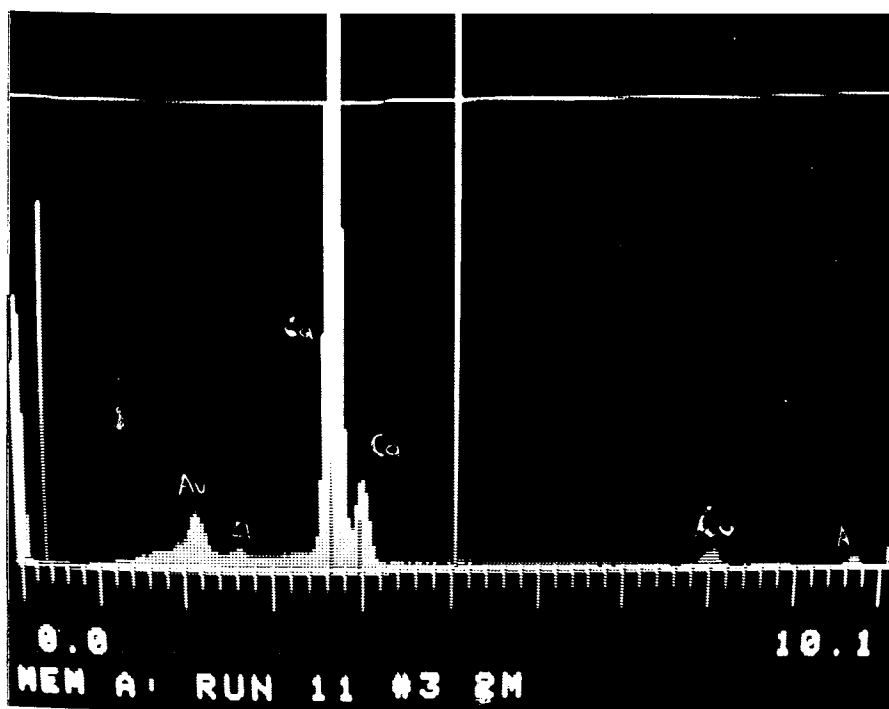
PLATE E40 Spectra run 11, 3 m.
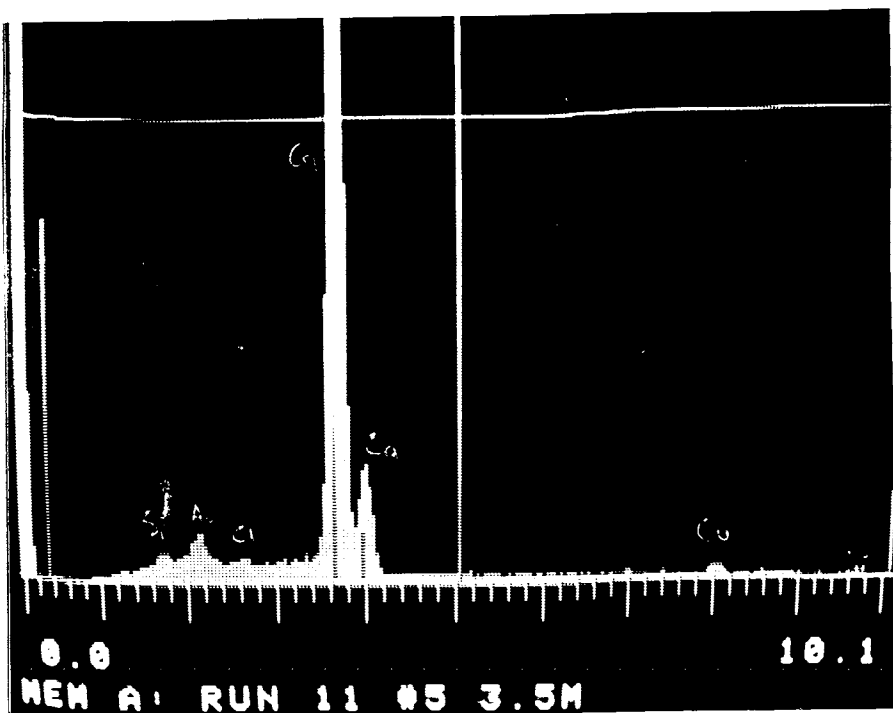
PLATE E41   Spectra run 11, 3.5 m.

APPENDIX F LISTINGS OF PROGRAMMES

```
]LIST
]LIST 1,560
```

```
1    REM    PROG-CS
5    REM    THIS IS THE PROGRAM TO CALCULATE THE CHEMICAL COMPOSITIO
N OF SOLUTION
6    REM    AFTER MIXING SODIUM BICARBONATE AND CALCIUM CHORIDE
7    REM    BY THERMAL DYNAMIC EQUILIBRIA
11   READ T1,PH,C1BT,C,N1
12   REM    T1 IS THE TEMP
13   REM    C1BT IS THE TOTAL CALCIUM
14   REM    M1 IS THE TOTAL MAGNESIUM
15   REM    A3 IS THE TOTAL ALKANITY
16   REM    N1 S THE SODIUM ION
17   REM    GSO4 IS THE SULPHATE ION
18   REM    C IS THE CHLORIDE ION
20 TA = T1 + 273
25 P1 = 17052 / TA + 215.21 *  LOG (TA) / 2.303 - 0.12675 * TA -
 545.56
28 K1 = 1 / (10 ^ P1)
30 P2 = 2902.39 / TA + 0.02379 * TA - 6.498
33 K2 = 1 / (10 ^ P2)
35 PKW = 4787.3 / TA + 7.1321 *  LOG (TA) / 2.303 + 0.01037 * TA
 - 22.801
38 KW = 1 / (10 ^ PKW)
40 SPKSP = 0.01183 * T1 + 8.03
43 S1 = 1 / (10 ^ SPKSP)
45 P3 =  - 27.393 + 4114 / TA + 0.05617 * TA
47 K3 = 1 / (10 ^ P3)
50 P4 =  - 2.95 + 0.0133 * TA
53 K4 = 1 / (10 ^ P4)
55 K5 = 0.00450: REM   K5 IS KCASO40
56 K6 = 0.004365: REM   K6 IS KMGSO40
57 K7 = 0.000398: REM   K7 IS KMGCO30
60   DATA   24.8,8.77,0.001986,0.003972,0.01233
70   PRINT "ABS TEMP=      ";TA
71   PRINT "K1        =      ";K1
72   PRINT "K2        =      ";K2
73   PRINT "KW        =      ";KW
74   PRINT "KSP       =      ";S1
75   PRINT "KCACO30 =      ";K3
76   PRINT "KCAHCO3+=      ";K4
77   PRINT "KCASO40 =      ";K5
80   INPUT "HCO3-";A
85   INPUT "FM";F1
90   INPUT "FD";F2
95 J =  - PH -  LOG (F1) / 2.303
100 H = 10 ^ J
102 OH = KW / (H * F1 ^ 2)
103 A3 = A * (1 + (2 * K2) / (H * F2)) + OH - H
105 ICA2 = C1BT / (1 + (A * F2) / K4 + (K2 * F2 * A) / (K3 * H)
+ (E * F2 ^ 2) / 0.00450): REM       ICA2 IS CALCIUM I
ON
110 LH2CO3 = (H * A * F1 ^ 2) / K1: REM   LH2CO3 IS CONCENTRATION
 OF H2CO3
115 MCO3 = (A3 - OH + H) / ((H * F2 / K2) + 2)
120 NCAHCO3 = (ICA2 * A * F2) / K4: REM   NCAHCO3 IS THE CONCENTR
ATION OF CAHCO3+
130 QCACO30 = ICA2 * MCO3 * (F2 ^ 2) / K3: REM      QCACO3 I
     S                    THE CONCENTRAT                    ION OF CACO30
```

```
139 S = 0.5 * (N1 + H + 4 * ICA2 + NCAHCO3 + C + OH + A + 4 * MC
O3)
140 U = ( SQR (S) / (1 +  SQR (S))) - 0.3 * S
145 F1 = 10 ^ ( - 0.5 * U)
150 F2 = 10 ^ ( - 2.0 * U)
157 C2 = LH2CO3 + A + MCO3 + QCACO3 + NCAHCO3
370 A1 = N1 + 2 * ICA2 + H + NCAHCO3 - C - OH - 2 * MCO3
375  IF A1 > (A) THEN  GOTO 400
380  IF  ABS (A - A1) < (0.001 * A) THEN  GOTO 500
385 A = A - 0.01 * A
390  PRINT "A TOO BIG";A
395  GOTO 95
400  IF (0.99 * A1) < (A) THEN  GOTO 450
405 A = A + 0.01 * A
410  PRINT "A TOO SMALL";A
415  GOTO 95
450 A = A + 0.0001 * A
455  PRINT "A LITTLE TOO SMALL";A
460  GOTO 95
500 S3 = ICA2 * MCO3 * (F2 ^ 2) / S1
510  PRINT "TOTAL CARBON=";C2
515  PRINT "HCO3=";A
520  PRINT "CO3=";MCO3
525  PRINT "H2CO3=";LH2CO3
530  PRINT "CACO30=";QCACO3
535  PRINT "CAHCO3+=";NCAHCO3
540  PRINT "CA+=";ICA2
550  PRINT "DEGREE OF SUPERSATURATION=";S3
552  PRINT "FM=";F1
554  PRINT "FD=";F2
560  STOP
```

```
]SVVV
]LIST 1,560

I    REM   PROG-CMS
2    REM   THIS IS THE PROGRAM TO CALCULATE THE CHEMCIAL COMPOSITIO
N OF SOLUTION
3    REM   AFTER MIXING SODIUM BICARBONATE AND CALCIUM CHLORIDE INT
O
4    REM   THE SOLUTION OF MAGNESIUM CHLORIDE
5    REM   BY THERMODYNAMIC EQUILIBRIA
11   READ T1,PH,C1BT,C,N1,M1
12   REM   T1 IS THE TEMP
13   REM   C1BT IS THE TOTAL CALCIUM
14   REM   M1 IS THE TOTAL MAGNESIUM
15   REM   A3 IS THE TOTAL ALKANITY
16   REM   N1 S THE SODIUM ION
17   REM   GSO4 IS THE SULPHATE ION
18   REM   C IS THE CHLORIDE ION
20   TA = T1 + 273
25   P1 = 17052 / TA + 215.21 *  LOG (TA) / 2.303 - 0.12675 * TA -
  545.56
28   K1 = 1 / (10 ^ P1)
30   P2 = 2902.39 / TA + 0.02379 * TA - 6.498
33   K2 = 1 / (10 ^ P2)
35   PKW = 4787.3 / TA + 7.1321 *  LOG (TA) / 2.303 + 0.01037 * TA
  - 22.801
38   KW = 1 / (10 ^ PKW)
40   SPKSP = 0.01183 * T1 + 8.03
43   S1 = 1 / (10 ^ SPKSP)
45   P3 =  - 27.393 + 4114 / TA + 0.05617 * TA
47   K3 = 1 / (10 ^ P3)
50   P4 =  - 2.95 + 0.0133 * TA
53   K4 = 1 / (10 ^ P4)
55   K5 = 0.00450: REM   K5 IS KCASO40
56   K6 = 0.004365: REM   K6 IS KMGSO40
57   K7 = 0.000398: REM   K7 IS KMGCO30
58   K8 = 0.06918
60   DATA     25,8.45,0.001999,0.007998                    ,0.
01167,0.00           2000
70   PRINT "ABS TEMP=     ";TA
71   PRINT "K1        =   ";K1
72   PRINT "K2        =   ";K2
73   PRINT "KW        =   ";KW
74   PRINT "KSP       =   ";S1
75   PRINT "KCACO30 =    ";K3
76   PRINT "KCAHCO3+=    ";K4
77   PRINT "KCASO40 =    ";K5
78   PRINT "KMGCO30";K7
79   PRINT "KMGHCOI3+=   ";K8
80   INPUT "HCO3-";A
85   INPUT "FM";F1
90   INPUT "FD";F2
95 J =  - PH -  LOG (F1) / 2.303
100 H = 10 ^ J
102 OH = KW / (H * F1 ^ 2)
103 A3 = A * (1 + (2 * K2) / (H * F2)) + OH - H
105 ICA2 = C1BT / (1 + (A * F2) / K4 + (K2 * F2 * A) / (K3 * H)
 + (E * F2 ^ 2) / 0.00450): REM     ICA2 IS CALCIUM I
ON
110 LH2CO3 = (H * A * F1 ^ 2) / K1: REM   LH2CO3 IS CONCENTRATION
```

368 - 368 -

```
OF H2CO3
115 MCO3 = (A3 - OH + H) / ((H * F2 / K2) + 2)
120 NCAHCO3 = (ICA2 * A * F2) / K4: REM  NCAHCO3 IS THE CONCENTR
ATION OF CAHCO3+
130 QCACO30 = ICA2 * MCO3 * (F2 ^ 2) / K3: REM    QCACO3 I
      S            THE CONCENTRAT            ION OF CACO30

135 M2 = M1 / (1 + (MCO3 * (F2 ^ 2)) / K7 + (A * F2) / K8): REM
M2 IS MG2+
136 M5 = M2 * A * F2 / K8: REM  M5 IS MGHCO3+
137 M4 = M1 - M2 - M5: REM  M4 IS MGCO30
139 S = 0.5 * (N1 + H + 4 * ICA2 + NCAHCO3 + C + OH + A + 4 * MC
O3 + 4 * M2 + M5)
140 U = ( SQR (S) / (1 +  SQR (S))) - 0.3 * S
145 F1 = 10 ^ ( - 0.5 * U)
150 F2 = 10 ^ ( - 2.0 * U)
157 C2 = LH2CO3 + A + MCO3 + QCACO3 + NCAHCO3 + M4 + M5
370 A1 = N1 + 2 * ICA2 + H + NCAHCO3 - C - OH - 2 * MCO3 + 2 * M
2 + M5
375  IF A1 > (A) THEN  GOTO 400
380  IF  ABS (A - A1) < (0.001 * A) THEN  GOTO 500
385 A = A - 0.01 * A
390  PRINT "A TOO BIG";A
395  GOTO 95
400  IF (0.99 * A1) < (A) THEN  GOTO 450
405 A = A + 0.01 * A
410  PRINT "A TOO SMALL";A
415  GOTO 95
450 A = A + 0.0001 * A
455  PRINT "A LITTLE TOO SMALL";A
460  GOTO 95
500 S3 = ICA2 * MCO3 * (F2 ^ 2) / S1
510  PRINT "TOTAL CARBON=";C2
515  PRINT "HCO3=";A
520  PRINT "CO3=";MCO3
525  PRINT "H2CO3=";LH2CO3
530  PRINT "CACO30=";QCACO3
535  PRINT "CAHCO3+=";NCAHCO3
540  PRINT "CA+=";ICA2
543  PRINT "MG++";M2
545  PRINT "MGCO30";M4
546  PRINT "MGHCO3+=";M5
550  PRINT "DEGREE OF SUPERSATURATION=";S3
552  PRINT "FM=";F1
554  PRINT "FD=";F2
560  STOP
```

```
]LIST 1,1760

1   REM  PROG-CMSS
2   REM   THIS IS THE PROGRAM TO CALCULATE THE CHEMICAL COMPOSITIO
N OF THE WATER
3   REM   CONTAINING NA, MG, CA, CL SO4 AND CARBONIC SPECIES
4   REM   BASED ON THE PH AND THE TEMPERATURE OF THE WATER MEASURE
D
5   REM   THE CALCULATEION IS ITERATIVE
10   REM   CAL FOR THERMODYNAMIC DISSOCIATION CONSTANT  WITH RESPE
CT TO TEMPERATURE
11   READ T1,PH,C1BT,M1,A3,GSO4,C
12   REM   T1 IS THE TEMP
13   REM   C1BT IS THE TOTAL CALCIUM
14   REM   M1 IS THE TOTAL MAGNESIUM
15   REM    A3 IS THE TOTAL ALKANITY
16   REM   N1 S THE SODIUM ION
17   REM   GSO4 IS THE SULPHATE ION
18   REM   C IS THE CHLORIDE ION
20 TA = T1 + 273
25 P1 = 17052 / TA + 215.21 *  LOG (TA) / 2.303 - 0.12675 * TA -
 545.56
28 K1 = 1 / (10 ^ P1)
30 P2 = 2902.39 / TA + 0.02379 * TA - 6.498
33 K2 = 1 / (10 ^ P2)
35 PKW = 4787.3 / TA + 7.1321 *  LOG (TA) / 2.303 + 0.01037 * TA
 - 22.801
38 KW = 1 / (10 ^ PKW)
40 SPKSP = 0.01183 * T1 + 8.03
43 S1 = 1 / (10 ^ SPKSP)
45 P3 =  - 27.393 + 4114 / TA + 0.05617 * TA
47 K3 = 1 / (10 ^ P3)
50 P4 =  - 2.95 + 0.0133 * TA
53 K4 = 1 / (10 ^ P4)
55 K5 = 0.00450: REM  K5 IS KCASO40
56 K6 = 0.004365: REM  K6 IS KMGSO40
57 K7 = 0.000398: REM  K7 IS KMGCO30
60  DATA   25.5,7.15,3.31E-3,3.44E-       3,7.24E-3,6.91E-3,
9.25E-3
70   PRINT "ABS TEMP=      ";TA
71   PRINT "K1        =     ";K1
72   PRINT "K2        =     ";K2
73   PRINT "KW        =     ";KW
74   PRINT "KSP       =     ";S1
75   PRINT "KCACO30 =      ";K3
76   PRINT "KCAHCO3+=      ";K4
77   PRINT "KCASO40 =      ";K5
80   INPUT "SO4--";E
85   INPUT "FM";F1
90   INPUT "FD";F2
92   INPUT "NA+";N1
95 J =  - PH -  LOG (F1) / 2.303
100 H = 10 ^ J
102 OH = KW / (H * F1 ^ 2)
103 A = (A3 - OH + H) / (1 + (2 * K2) / (H * F2))
105 ICA2 = C1BT / (1 + (A * F2) / K4 + (K2 * F2 * A) / (K3 * H)
+ (E * F2 ^ 2) / 0.00450): REM    ICA2 IS CALCIUM I
ON
110 LH2CO3 = (H * A * F1 ^ 2) / K1: REM  LH2CO3 IS CONCENTRATION
```

```
    OF H2CO3
115 MCO3 = (A3 - OH + H) / ((H * F2 / K2) + 2)
120 NCAHCO3 = (ICA2 * A * F2) / K4: REM  NCAHCO3 IS THE CONCENTR
ATION OF CAHCO3+
130 QCACO30 = ICA2 * MCO3 * (F2 ^ 2) / K3: REM     QCACO3 I
       S              THE CONCENTRAT              ION OF CACO30

131 M2 = M1 / (1 + (E * (F2 ^ 2)) / K6 + MCO3 * (F2 ^ 2) / K7)
133 M3 = M2 * E * (F2 ^ 2) / K6: REM  M3 IS MGSO40
135 M4 = M2 * MCO3 * (F2 ^ 2) / K7: REM  M4 IS MGCO30
137 E1 = ICA2 * E * (F2 ^ 2) / K5: REM  E1 IS CASO40
139 S = 0.5 * (N1 + H + 4 * ICA2 + NCAHCO3 + C + OH + A + 4 * MC
OI3 + 4 * E + 4 * M2)
140 U = ( SQR (S) / (1 +  SQR (S))) - 0.3 * S
145 F1 = 10 ^ ( - 0.5 * U)
150 F2 = 10 ^ ( - 2.0 * U)
157 C2 = LH2CO3 + A + MCO3 + QCACO3 + NCAHCO3 + M4
159 E2 = GSO4 - M3 - E1
160  IF E2 > E THEN  GOTO 200
165  IF  ABS (E - E2) < (0.001 * E) THEN  GOTO 370
170 E = E - 0.01 * E
175  GOTO 95
200  IF (0.99 * E2) < E THEN  GOTO 250
205 E = E + 0.01 * E: GOTO 95
250 E = E + 0.0001 * E: GOTO 95
370 N2 = A - (2 * ICA2) - H - NCAHCO3 + C + OH + (2 * MCO3) + (2
 * E2) - (2 * M2)
380  IF N2 > N1 THEN  GOTO 500
385  IF  ABS (N1 - N2) < (0.001 * N1) THEN  GOTO 1000
390 N1 = N1 - 0.01 * N1
395  GOTO 95
500  IF (0.99 * N2) < N1 THEN  GOTO 550
505 N1 = N1 + 0.01 * N1: GOTO 95
550 N1 = N1 + 0.0001 * N1: GOTO 95
1000 L1 = PH - (P2 +  LOG (F2) / 2.303 - SPKSP - 2 *  LOG (F2) /
 2.303 -  LOG (ICA2) / 2.303 -  LOG (A3) / 2.303 -  LOG (F1) / 2
.303)
1001 T5 = PH - L1
1002 S3 = ICA2 * MCO3 * (F2 ^ 2) / S1
1003 X1 = ((S3 ^ (1 / 2) - 1) ^ 2) * (S1 / F2 ^ 2)
1010 T9PHS = P2 - SPKSP -  LOG (C1BT) / 2.303 -  LOG (A3) / 2.30
3 - 5 *  LOG (F1) / 2.303
1012 M5PHS = P2 - SPKSP -  LOG (C1BT) / 2.303 -  LOG (A3) / 2.30
3 -  LOG ((F1 ^ 5) / (1 + (K5 * (F1 ^ 8) * GSO4))) / 2.303
1015 L2 = PH - T9PHS
1016 L3 = PH - M5PHS
1017 R4 = 2 * T9PHS - PH
1018 R5 = 2 * T5 - PH
1019  PRINT X7 = S1 / (F2 ^ 2)
1020  PRINT  TAB( 2);"TEMP=";T1; TAB( 10);"PH=";PH; TAB( 30);"TC
A=";C1BT
1022  PRINT  TAB( 2);"TMG=";M1; TAB( 10);"ALK=";A3
1023  PRINT  TAB( 2);"TSO4=";GSO4; TAB( 12);"CL=";C
1030  PRINT "LANGELIER INDEX WITH ION PAIR CONSIDERATION";L1
1031  PRINT "LARSON AND BUSWELL LI";L2
1034  PRINT "LARSON AND BUSWELL PHS=";T9PHS
1036  PRINT "PHS WITH ION PAIR CONSIDERATION";T5
1040  PRINT "DEG OF SUP=";S3
1042  PRINT "SQUARE OF DIFF S=";X1
1044  PRINT "H2CO3*=";LH2CO3
```

```
1045   PRINT "CA2+ =   ";ICA2
1050   PRINT "HCO3- = ";A
1055   PRINT "CO3-- = ";MCO3
1080   PRINT "NA+    =";N1
1611   PRINT "MG2+= ";M2
1612   PRINT "SO4--= ";E2
1740   PRINT "FM=";F1
1745   PRINT "FD=";F2
1750   PRINT "SQ OF KSP/FD^2=";X7
1760   STOP
```

```
]]]]]
]LIST 1,590

1    REM    PROG-PCS
2    REM    THIS PROGRAM IS CALCULATING THE CHEMICAL COMPOSITION
3    REM    DURING PRECIPITATION WITH THE SOLUTION CONTAINING
4    REM    NA, CA, CL AND CARBONIC SPECIES
5    DIM CA(200),LH2CO3(200),A(200),MCO3(200),NCAHCO3(200),QCACO3(
200),F1(200),F2(200),C2(200)
6    DIM H(200),OH(200),PH(200)
10   REM    CAL OF SPECIES CONCENTRATION IN THE PROCESS OF CRYSTALL
IZATION
11   READ T1,CA(0),LH2CO3(0),A(0),C,N1,MCO3(0),F1(0),F2(0)
12   REM    T1 IS THE TEMP
13   REM    C1BT IS THE TOTAL CALCIUM
14   REM    M1 IS THE TOTAL MAGNESIUM
15   REM      A3 IS THE TOTAL ALKANITY
16   REM    N1 S THE SODIUM ION
17   REM    GSO4 IS THE SULPHATE ION
18   REM    C IS THE CHLORIDE ION
20   TA = T1 + 273
21   INPUT "INITIAL TOTAL CA= ";C1BT
22   INPUT "VOLUME (L)= ";V
23   INPUT "INITIAL SUPSAT=";S9
25   P1 = 17052 / TA + 215.21 *  LOG (TA) / 2.303 - 0.12675 * TA -
 545.56
28   K1 = 1 / (10 ^ P1)
30   P2 = 2902.39 / TA + 0.02379 * TA - 6.498
33   K2 = 1 / (10 ^ P2)
35   PKW = 4787.3 / TA + 7.1321 *  LOG (TA) / 2.303 + 0.01037 * TA
 - 22.801
38   KW = 1 / (10 ^ PKW)
40   SPKSP = 0.01183 * T1 + 8.03
43   S1 = 1 / (10 ^ SPKSP)
45   P3 =  - 27.393 + 4114 / TA + 0.05617 * TA
47   K3 = 1 / (10 ^ P3)
50   P4 =  - 2.95 + 0.0133 * TA
53   K4 = 1 / (10 ^ P4)
55   K5 = 0.00450: REM   K5 IS KCASO40
56   K6 = 0.004365: REM   K6 IS KMGSO40
57   K7 = 0.000398: REM   K7 IS KMGCO30
60   DATA  25.0,0.00176718387,0.0000174552857,0.00510815611,0.003
998,0.005838,0.000160938057,0.898551089,0.651885168
70   PRINT "ABS TEMP=        ";TA
71   PRINT "K1       =       ";K1
72   PRINT "K2       =       ";K2
73   PRINT "KW       =       ";KW
74   PRINT "KSP      =       ";S1
75   PRINT "KCACO30 =        ";K3
76   PRINT "KCAHCO3+=        ";K4
77   PRINT "KCASO40 =        ";K5
79   INPUT "I";I
80   INPUT "DECREASE IN CALCIUM";Y
91   FOR I = 1 TO 200
92   CA(I) = CA(I - 1) - Y
93   MCO3(I) = MCO3(I - 1):LH2CO3(I) = LH2CO3(I - 1)
94   F1(I) = F1(I - 1):F2(I) = F2(I - 1)
95   X7 = LH2CO3(I - 1) + A(I - 1) + MCO3(I - 1) + CA(I)
96   X8 = CA(I - 1) + LH2CO3(I) + MCO3(I)
97   A(I) = X7 - X8
```

```
100 H(I) = K2 * A(I) / (MCO3(I) * F2(I))
102 LH2CO3(I) = H(I) * A(I) * (F1(I) ^ 2) / K1
105 OH(I) = KW / (H(I) * (F1(I) ^ 2))
110 PH(I) =  - LOG (H(I) * F1(I)) / 2.303
115 QCACO3(I) = CA(I) * MCO3(I) * (F2(I) ^ 2) / K3
120 NCAHCO3(I) = (CA(I) * A(I) * F2(I)) / K4
139 S = 0.5 * (N1 + H(I) + 4 * CA(I) + NCAHCO3(I) + C + OH(I) +
A(I) + 4 * MCO3(I))
140 U = ( SQR (S) / (1 +  SQR (S))) - 0.3 * S
145 F1(I) = 10 ^ ( - 0.5 * U)
150 F2(I) = 10 ^ ( - 2.0 * U)
370 M3CO3 = 0.5 * (2 * CA(I) + NCAHCO3(I) + N1 + H(I) - C - OH(I
) - A(I))
375  IF M3CO3 > MCO3(I) THEN  GOTO 400
380  IF  ABS (MCO3(I) - M3CO3) < (0.001 * MCO3(I)) THEN  GOTO 50
0
385 MCO3(I) = MCO3(I) - 0.01 * MCO3(I)
395  GOTO 95
400  IF (0.99 * M3CO3) < MCO3(I) THEN  GOTO 450
405 MCO3(I) = MCO3(I) + 0.01 * MCO3(I)
415  GOTO 95
450 MCO3(I) = MCO3(I) + 0.0001 * MCO3(I)
460  GOTO 95
500 S3 = CA(I) * MCO3(I) * (F2(I) ^ 2) / S1
502 C5 = CA(I) + QCACO3(I) + NCAHCO3(I)
503 X1 = ((S3 ^ (1 / 2) - 1) ^ 2) * (S1 / F2(I) ^ 2)
504 X2 = (S3 - 1) * (S1 / F2(I) ^ 2)
505 C2(I) = LH2CO3(I) + A(I) + MCO3(I) + QCACO3(I) + NCAHCO3(I)
506 X3 = (C1BT - C5) * V * 100
507  PRINT "NUMBER OF CA DECREMENT=  ";I: PRINT : PRINT
510  PRINT "TOTAL CARBON=";C2(I)
512  PRINT "TOTAL CA=";C5
515  PRINT "HCO3=";A(I)
518  PRINT "PH=   ";PH(I)
520  PRINT "CO3=";MCO3(I)
525  PRINT "H2CO3=";LH2CO3(I)
530  PRINT "CACO30=";QCACO3(I)
535  PRINT "CAHCO3+=";NCAHCO3(I)
540  PRINT "CA+";CA(I)
550  PRINT "DEGREE OF SUPERSATURATION=";S3
552  PRINT "FM=";F1(I)
553 D1 = (S3 - 1) / (S9 - 1): PRINT "FRACTION TO INI S=";D1
554  PRINT "FD=";F2(I)
555  PRINT "SQUARE OF DIF IN SUPERSATURATION= ";X1
556  PRINT "NACALLOS DIF INSUPERSATURATION= ";X2
557  PRINT "WEIGHT OF CACO3 PPTED= ";X3
560 Z1 = (0.001999 - C5) ^ (2 / 3)
562 Z2 = (CA(I) * MCO3(I)) ^ (0.5)
563 Z3 = (S1 / (F2(0) ^ 2)) ^ (0.5)
564 Z4 = Z2 - Z3
565 Z5 =  LOG (Z4) / 2.303
570  PRINT "(TCAI-TCA)^(2/3)=";Z1
575  PRINT "DELTA C=";Z4
577  PRINT "LOG DELTA C=";Z5
580  NEXT I
590  STOP
```

```
]LIST 1,590

1  REM   PROG-PCMS
2  REM   THIS PROGRAM IS CACLULATING THE CHEMICAL COMPOSITION WIT
H MG AS IMPURITY
3  REM   THIS PROGRAME USES THE DECREMENT OF TOTAL CA TO SIMULATE
 THE DECLINE IN THE PH REGISTED
5  DIM CA(200),LH2CO3(200),A(200),MCO3(200),NCAHCO3(200),QCACO3(
200),F1(200),F2(200),C2(200)
6  DIM H(200),OH(200),PH(200),M2(200),M4(200),M5(200)
10  REM  CAL OF SPECIES CONCENTRATION IN THE PROCESS OF CRYSTALL
IZATION
11  READ T1,CA(0),LH2CO3(0),A(0),C,N1,MCO3(0),M1,F1(0),F2(0)
12  REM   T1 IS THE TEMP
13  REM   C1BT IS THE TOTAL CALCIUM
14  REM   M1 IS THE TOTAL MAGNESIUM
15  REM    A3 IS THE TOTAL ALKANITY
16  REM   N1 S THE SODIUM ION
17  REM   GSO4 IS THE SULPHATE ION
18  REM   C IS THE CHLORIDE ION
20 TA = T1 + 273
21  INPUT "INITIAL TOTAL CA= ";C1BT
22  INPUT "VOLUME (L)= ";V
23  INPUT "INITIAL SUPSAT=";S9
25 P1 = 17052 / TA + 215.21 *  LOG (TA) / 2.303 - 0.12675 * TA -
 545.56
28 K1 = 1 / (10 ^ P1)
30 P2 = 2902.39 / TA + 0.02379 * TA - 6.498
33 K2 = 1 / (10 ^ P2)
35 PKW = 4787.3 / TA + 7.1321 *  LOG (TA) / 2.303 + 0.01037 * TA
 - 22.801
38 KW = 1 / (10 ^ PKW)
40 SPKSP = 0.01183 * T1 + 8.03
43 S1 = 1 / (10 ^ SPKSP)
45 P3 =  - 27.393 + 4114 / TA + 0.05617 * TA
47 K3 = 1 / (10 ^ P3)
50 P4 =  - 2.95 + 0.0133 * TA
53 K4 = 1 / (10 ^ P4)
55 K5 = 0.00450: REM  K5 IS KCASO40
56 K6 = 0.004365: REM  K6 IS KMGSO40
57 K7 = 0.000398: REM  K7 IS KMGCO30
58 K8 = 0.06918: REM  K8 IS KMGHCO3+
60  DATA  25.0,0.00165434997,0.0000793352991,0.0138218581,0.0039
98,0.01167,0.000277487955,0.002001,0.868525105,0.569022585
70  PRINT "ABS TEMP=     ";TA
71  PRINT "K1      =     ";K1
72  PRINT "K2      =     ";K2
73  PRINT "KW      =     ";KW
74  PRINT "KSP     =     ";S1
75  PRINT "KCACO30 =     ";K3
76  PRINT "KCAHCO3+=     ";K4
77  PRINT "KCASO40 =     ";K5
79  INPUT "I";I
80  INPUT "DECREASE IN CALCIUM";Y
91  FOR I = 1 TO 200
92 CA(I) = CA(I - 1) - Y
93 MCO3(I) = MCO3(I - 1):LH2CO3(I) = LH2CO3(I - 1)
94 F1(I) = F1(I - 1):F2(I) = F2(I - 1)
95 X7 = LH2CO3(I - 1) + A(I - 1) + MCO3(I - 1) + CA(I)
```

```
96 X8 = CA(I - 1) + LH2CO3(I) + MCO3(I)
97 A(I) = X7 - X8
100 H(I) = K2 * A(I) / (MCO3(I) * F2(I))
102 LH2CO3(I) = H(I) * A(I) * (F1(I) ^ 2) / K1
105 OH(I) = KW / (H(I) * (F1(I) ^ 2))
110 PH(I) =  -  LOG (H(I) * F1(I)) / 2.303
115 QCACO3(I) = CA(I) * MCO3(I) * (F2(I) ^ 2) / K3
120 NCAHCO3(I) = (CA(I) * A(I) * F2(I)) / K4
122 M2(I) = M1 / (1 + (MCO3(I) * (F2(I) ^ 2)) / K7 + (A(I) * F2(
I)) / K8): REM  M2(I) IS MG2+
123 M5(I) = M2(I) * A(I) * F2(I) / K8: REM  M5(I) IS MGHCO3+
125 M4(I) = M1 - M2(I) - M5(I): REM  M4(I) IS MGCO30
139 S = 0.5 * (N1 + H(I) + 4 * CA(I) + NCAHCO3(I) + C + OH(I) +
A(I) + 4 * MCO3(I) + 4 * M2(I) + M5(I))
140 U = ( SQR (S) / (1 +  SQR (S))) - 0.3 * S
145 F1(I) = 10 ^ ( - 0.5 * U)
150 F2(I) = 10 ^ ( - 2.0 * U)
370 M3CO3 = 0.5 * (2 * CA(I) + NCAHCO3(I) + N1 + H(I) - C - OH(I
) - A(I) + 2 * M2(I) + M5(I))
375  IF M3CO3 > MCO3(I) THEN  GOTO 400
380  IF  ABS (MCO3(I) - M3CO3) < (0.001 * MCO3(I)) THEN  GOTO 50
0
385 MCO3(I) = MCO3(I) - 0.01 * MCO3(I)
395  GOTO 95
400  IF (0.90 * M3CO3) < MCO3(I) THEN  GOTO 450
405 MCO3(I) = MCO3(I) + 0.01 * MCO3(I)
415  GOTO 95
450 MCO3(I) = MCO3(I) + 0.0001 * MCO3(I)
460  GOTO 95
500 S3 = CA(I) * MCO3(I) * (F2(I) ^ 2) / S1
502 C5 = CA(I) + QCACO3(I) + NCAHCO3(I)
503 X1 = ((S3 ^ (1 / 2) - 1) ^ 2) * (S1 / F2(I) ^ 2)
504 X2 = (S3 - 1) * (S1 / F2(I) ^ 2)
505 C2(I) = LH2CO3(I) + A(I) + MCO3(I) + QCACO3(I) + NCAHCO3(I)
+ M4(I)
506 X3 = (C1BT - C5) * V * 100
507  PRINT "NUMBER OF CA DECREMENT=  ";I: PRINT : PRINT
510  PRINT "TOTAL CARBON=";C2(I)
512  PRINT "TOTAL CA=";C5
515  PRINT "HCO3=";A(I)
518  PRINT "PH=  ";PH(I)
520  PRINT "CO3=";MCO3(I)
525  PRINT "H2CO3=";LH2CO3(I)
530  PRINT "CACO30=";QCACO3(I)
535  PRINT "CAHCO3+=";NCAHCO3(I)
540  PRINT "CA+";CA(I)
550  PRINT "DEGREE OF SUPERSATURATION=";S3
552  PRINT "FM=";F1(I)
553 D1 = (S3 - 1) / (S9 - 1): PRINT "FRACTION TO INI S=";D1
554  PRINT "FD=";F2(I)
555  PRINT "SQUARE OF DIF IN SUPERSATURATION= ";X1
556  PRINT "NACALLOS DIF INSUPERSATURATION= ";X2
557  PRINT "WEIGHT OF CACO3 PPTED= ";X3
558  PRINT "MG2+";M2(I)
559  PRINT "MGCO30";M4(I)
560 Z1 = (0.001999 - C5) ^ (2 / 3)
562 Z2 = (CA(I) * MCO3(I)) ^ (0.5)
563 Z3 = (S1 / (F2(0) ^ 2)) ^ (0.5)
564 Z4 = Z2 - Z3
565 Z5 =  LOG (Z4) / 2.303
```

```
570   PRINT "(TCAI-TCA)^(2/3)=";Z1
575   PRINT "DELTA C=";Z4
577   PRINT "LOG DELTA C=";Z5
580   NEXT I
590   STOP
```

```
]]]]]
]LIST

1   REM   PROG-SIZE
10  REM   THIS IS THE PROGRAM TO CALCULATE THE SURFACE AREA OF CA
CO3 BASED
20  REM   ON NUMBER DISTRIBUTION BY DECREMENTAL SIZE REDUCTION FR
OM THE FINAL CRYSTAL SIZE REDUCTION FROM THE FINAL CRYSTAL NUMBE
R DISTRIBUTION
30  REM   THE SURFACE AREA AND THE WEIGHT OF CRYSTALS DURING CRYS
TALLIZATION ARE ALSO CALCULATED
40  REM   BACKWARD TO ENABLE RATE OF CRYSTALLIZATION CALCULATION
60  DIM N(100),D(100)
61  DIM A(100),W(100)
62  DIM E(100)
65  INPUT "SURFACE SHAPE FACTOR ";F1
66  INPUT "VOLUME SHAPE FACTOR ";F2
70  INPUT "SIZE DECREMENT ";X
75  M = 18: REM   M IS THE NUMBER OF DATA PAIR
76  INPUT "WEIGHT FACTOR";W1
77  PRINT   TAB( 1);"TOTAL SURF AREA"; TAB( 25);"TOTAL WEIGHT"; T
AB( 40);"TOTAL NUMBER"; TAB( 54);"MEAN SIZE"
78  PRINT   TAB( 7);"(SQ CM)"; TAB( 29);"(GM)"; TAB( 50);"BASED O
N NUMBER": PRINT
80  FOR I = 1 TO M
85  READ N(I),D(I)
93  DATA   93,1
94  DATA   133,3.1
95  DATA   84,5.1
96  DATA   62,7.2
97  DATA   128,9.2
98  DATA   59,11.3
99  DATA   94,13.3
100  DATA   53,15.3
101  DATA   59,17.4
102  DATA   88,19.4
103  DATA   81,21.5
104  DATA   80,23.5
105  DATA   81,25.6
106  DATA   74,27.6
107  DATA   82,29.7
108  DATA   71,31.7
109  DATA   46,33.8
110  DATA   24,35.8
200  NEXT I
205 SUMA = 0
206 WSUM = 0
208 GSUM = 0
209 QSUM = 0
211  FOR I = 1 TO M
212  IF D(I) < 0 THEN  GOTO 226
215 A(I) = F1 * N(I) * (D(I) ^ 2)
216 W(I) = F2 * 2.71 * N(I) * (D(I) ^ 3)
217 E(I) = D(I) * N(I)
220 SUMA = SUMA + A(I)
221 WSUM = WSUM + W(I)
222 GSUM = GSUM + N(I)
223 QSUM = QSUM + E(I)
226  NEXT I
230 SUMA = SUMA * (10 ^ ( - 8)) * W1
```

```
232 WSUM = WSUM * (10 ^ ( - 12)) * W1
233 Z1 = SUMA:Z2 = WSUM
234 L1 = QSUM / GSUM
237  PRINT  TAB( 1);Z1; TAB( 25);Z2; TAB( 44);GSUM; TAB( 52);L1
256  PRINT : PRINT
257  FOR I = 1 TO M
258 D( I ) = D( I ) - X
260  NEXT I
265  IF SUMA = 0 THEN  GOTO 500
270  GOTO 205
500  STOP
```

LIST OF REFERENCES

ANG, H-M. and MULLIN, J.W. (1979) "Crystal Growth Rate Determinations from Desuperaturation Measurements: Nickel Ammonium Sulphate Hexahydrate", Trans. Inst. Chem. Engr., 57, 237

A.P.H.A.-A.W.W.A.-W.P.C.F. (1980) Standard Methods for the Examination of Water and Wastewater, 15th edition.

ATTARIAN, C. BAKER, C.G.J. and SURCEK, W.Y. (1976) "pH Control of a Continuous Precipitator", Can. J. Chem. Eng., 54, 606.

A.W.W.A. (1977) "A.W.W.A. Standard for Asbestos-Cement Transmission Pipe, 18 in. Through 42 in., for Water and Other Liquids", A.W.W. A. Standard C402-77, Denver, Colo.

BATES, R.L., FONDY, P.L. and CORPSTEIN, R.R. (1963) "An Examination of Some Geometric Parameters of Impeller Power", I & EC Proc. Des. & Develop., 2, 311.

BAUER, L.G., LARSON, M.A. and DALLONS, V.J. (1974) "Contact Nucleation of $MgSO_4 \cdot 7H_2O$ in a Continuous MSMPR Crystallizer", Chem. Eng. Sci., 29, 1253.

BENNETT, R.C., FIEDELMAN, H. and RANDOLPH, A.D. (1973) "Crystallizer In-flunced Nucleation", Chem. Eng. Progr., 69, 86.

BECKER, R.VON and DÖRING, W. (1935) "Kinetische Behandlung der Keimbil-dung in übersättigen Dämpfen", Annln. Phys., 24, 719.

BERGLUND, K.A. (1981) "Formation and Growth of Contact Nuclei", Univ. Microfilms Int., Order No. DA8209097. From Diss. Abstr. Int. B 1982, 42(11), 4496.

BERTHOND, A., (1912) "Theorie de la Formation des Faces dun Crystal", J. Chim. Phys., 10, 624.

BOWEN, B.D., LEVINE, S. and EPSTEIN, N. (1976) "Fine Particle Deposition in Laminar Flow Through Parallel-Plate and Cylindrical Channels", J. Colloid & Interf. Sci., 54, 375.

BROOKS, R., CLARK, L.M. and THURSTON, E.R. (1950) "$CaCO_3$ and its Hydrates", Trans. Roy. Soc. London, A243, 145.

BUCKLEY, H.E. (1951) Crystal Growth, John Wiley and Sons Ltd.

BURTON, W.K., CABRERA, N. and FRANK, F.C. (1951) "The Growth of Crystals and the Equilibrium Structure of their Surfaces", Phil. Trans., A243, 299.

CABLE, M. and EVANS, D.J. (1967) "Spherically Symmetrical Diffusion-Controlled Growth or Dissolution of a Sphere", J. App. Phys., 38, 2899.

CARDEW, D.T. (1982) "Crystal Growth Rates from Batch Experiments", J. Cryst. Growth, 57, 391.

CHANDLER, J.L. (1964) "The Effect of Supersaturation and Flow Conditions on the Initiation of Scale Formation", Trans. Inst. Chem. Engr., 42, 724.

CHERNOV, A.A. (1961) "The Spiral Growth of Crystals", Soviet Phys. Usp., 4, 116.

CHRISTIANSEN, J.A. and NIELSEN, A.E. (1951) "Kinetic Determination of the Size of Crystal Germs", Acta Chem. Scand., 5, 674.

CHRISTIANSEN, J.A. (1954) "On Attainment of the Stationary (Steady) State in Nucleation", Acta Chem. Scand., 8, 909.

CISE, M.D. and RANDOLPH, A.D. (1972) "Secondary Nucleation of Potassium Sulphate in a Continuous Flow Seeded Crystallizer", A.I.Ch.E. Symp. Ser., 68(121), 42.

CLONTZ, N.A. and McCabe, W.L. (1971) "Contact Nucleation of Magnesium Sulphate Heptahydrate", A.I.Ch.E. Symp. Ser., 67(110), 6.

COATES, K.E. and KNUDSEN, J.G. (1980) "Calcium Carbonate Scaling Characteristic of Cooling Tower Water". ASHRAE Trans., 86, part 2, 68.

DAHNEKE, B. (1973) "Measurements of Bouncing of Small Latex Spheres", J. Colloid & Interf. Sci., 45, 584.

DAVIES, C.W. and JONES, A.L. (1955) "The Precipitation of Silver
     Chloride from Aqueous Solutions", Trans. Faraday Soc., 51, 812.

DAVIES, C.W. (1967) Electrochemistry, George Newnes Ltd., London.

DE BOER, J.H. (1968) The Dynamical Character of Adsorption, Clanen-
     don Press, Oxford.

DIEHL, H., GOETZ, C. and HACH, C. (1950) "Determination of Calcium and
     Determination of the Total Hardness of Water", J. Am. Wat. Wks.
     Assoc., 42, 40.

DOREMUS, R.H. (1958) "Precipitation Kinetics of Ionic Salts from Solu-
     tions", J. Phys. Chem., 62, 1068.

DOREMUS, R.H. (1970) "Crystallization of Slightly Soluble Salts from
     Solutions", J. Phys. Chem., 74, 1405.

DYE, J.F. (1952) "Calculations of the Effect of Temperature on pH, Free
     Carbon Dioxide and the Three Forms of Alkalinity", J. Am. Wat.
     Wks. Assoc., 44, 356.

ENCYLOPEDIA BRITANNICA (1984) Encyclopedia Britannica, William Benton
     Publisher, 3, p.833.

FEITLER, H. (1972) "Cooling Water Scale Control: The Scale Meter and
     the Critical pH of Scaling", Mat. Prot. & Perf., 11, 29.

FEITLER, H. (1974) "The Effect of Scaling Indexes on Cooling Water Treat-
     ment Practice", 35th Annual Meeting, International Water Confer-
     ence, Paper No. IWC74-21, October, Pittsburgh, Pa.

FEITLER, H. (1975) "Critical pH Scaling Indexes", Mat. Prot. & Perf.,
     14, 33.

FISCHER, P., SUITOR, J.W. and RITTER, R.B. (1975) "Fouling Measurement
     Techniques", Chem. Eng. Progr., 77, 66.

FRANK, F.C. (1949) "The Influence of Dislocations on Crystal Growth",
     Symposium on Crystal Growth, Discuss. Faraday Soc., No. 5, 48.

FRISCH, H.L. and COLLINS, F.C. (1952) "Diffusional Processes in the
     Growth of Aerosol Particles", J. Chem. Phys., 20, 1797.

FRISCH, H.L. and COLLINS, F.C. (1953) "Diffusional Processes in the Growth of Aerosol Particles", J. Chem. Phys., 21, 2158.

GARRELS, R.M. and THOMPSON, M.E. (1962) "A Chemical Model for Sea Water at 25°C and One Atmospheric Total Pressure", Am. J. Sci., 260, 57.

GARSIDE, J. (1971) " The Concept of Effectiveness Factors in Crystal Growth", Chem. Eng. Sci., 26, 1425.

GARSIDE, J. and LARSON, M.A. (1978) "Direct Observation of Secondary Nuclei Production", J. Cryst. Growth, 43, 694.

GARSIDE, J., RUSLI, I.T. and LARSON, M.A. (1979) "Origin and Size Distribution of Secondary Nuclei", A.I.Ch.E. J., 25, 57.

GAZIT, E. and HASSON, D. (1975) "Scale Deposition from an Evaporating Falling Film", Desalination, 17, 339.

GIBBS, J.W. (1928) "On the Equilibrium of Heterogeneous Substances", Vol. 1, Collected Works, Longmans.

GOLDSTEIN, M. (1968) "Interparticle Interference Effects in Diffusion Controlled Growth", J. Cryst. Growth, 3/4, 594.

GOUJON, G, and MUTAFTSCHIEV, B. (1976) "On Some Energetic and Chemical Properties of the Calcite Surface. A. Heat of Immersion in Water", J. Chim. Physique, 73, 351.

HAM, F.S. (1958) "Theory of Diffusion-limited Precipitation", Phys. Chem. Solids, 6, 335.

HARNED, H.S. and HAMER, W.J. (1933) "Ionization Constant of Water and the Dissociation of Water in Potassium Chloride Solutions from Electromotive Forces of Cells Without Liquid Junctions", J. Am. Chem. Soc., 55, 2194.

HARNED, H.S. and DAVIS, R. (1943) "The Ionization Constant of Carbonic Acid in Water and the Solubility of Carbon Dioxide in Water and Aqueous Salt Solution from 0 to 50°C", J. Am. Chem. Soc., 65, 2030.

HARNED, H.S. and SCHOLES, S.R. (1943) "The Ionization Constant of HCO_3^- from 0 to 50°C", J. Am. Chem. Soc., 63,1706.

HASSON, D (1962) "Rate of Decrease of Heat Transfer due to Scale Deposition", Dechema-Monographien, 47, 233.

HASSON, D., AVRIEL, M., RESNICK, W., ROZENMAN, T. and WINDREICH, S. (1968) "Mechanism of Calcium Carbonate Scale Deposition on Heat Transfer Surfaces", I & EC Fundam., 7, 59.

HASSON, D., SHERMAN, H. and BITON, M. (1978) "Prediction of Calcium Carbonate Scaling Rates", 6th Intern. Symp. Fresh Water from the Sea, 193.

HAWTHORN, D. and PERRY, D.J. (1980) "The Fouling of Power Station Condenser Tubes by Tricalcium Phosphate", Eff. & Water Treat. J., 20, 77.

HEAT EXCHANGER INSTITUTE (1978) Standards for Steam Surface Condensers, p.6, 7th Edition.

HILTON, H. (1903) Mathematical Crystallography, Oxford.

HOUSE, W.A. and TUTTON, J.A. (1982) "An Investigation of the Heterogeneous Nucleation of Calcite", J. Cryst. Growth, 56, 699.

HOUSE, W.A. (1981) "Kinetics of Crystallization of Calcite from Calcium Bicarbonate Solutions", J. Chem. Soc. Faraday Trans. I, 77, 341.

HULBURT, H.M. and KATZ, S. (1964) "Some Problems in Particle Technology: a Statistical Mechanical Formation", Chem. Eng. Sci., 19, 555.

JACOBSON, R.L. and LANGNUIR, D. (1974) "Dissociation Constants of Calcite and $CaHCO_3^+$ from 0 to 50°C", Geochim. Cosmochim. Acta, 38, 301.

JOHNSON, G.W. (1950) "Some Observations on the Epitaxy of Sodium Chloride on Silver", J. App. Phys., 21, 1057.

JOHNSON, G.W. (1951) "The Epitaxy of Alkali Chlorides on Metals", J. App. Phys., 22, 797.

JOHNSON, R.T., ROUSSEAU, R.W. and McCABE, W.L. (1972) "Factors Affecting Cantact Nucleation". A.I.Ch.E. Sym. Ser., 68(121), 31.

JOHNSTONE, R.E. and THRING, M.W. (1957) Pilot Plants, Models and Scale-up Methods in Chemical Engineering, McGraw-Hill, New York.

KAHLWEIT, M. (1960) "Kinetics of Phase Formation in Condensed Systems. (Precipitation of Difficulty Soluble Electrolytes from Aqueous Solutions). ", Z. Physik. Chem. N. F., 25, 125.

KAZMIERCZAK, T.F. (1979) Ph.D. Thesis, State University of New York, Buffalo.

KAZMLERCZAK, T.F., TOMSON, M.B. and NANCOLLAS, G.H. (1982) "Crystal Growth of Calcium Carbonate. A Controlled Composition Kinetic Study", J. Phys. Chem., 86, 103.

KERN, D.Q. and SEATON, R.E. (1959) "A Theoretical Analysis of Thermal Surface Fouling", Br. Chem. Eng., 4, 258.

KHAMSKII, E.V. (1969) Crystallization from Solutions, Consultants Bureau, New York, London.

KHARIN, V.M. (1974) "Kinetics of the Crystallization of Polymorphic Modifications of Calcium Carbonate", Zh. Fiz. Khim., 48, 1724.

KHARIN, V.M., KOSOVTSEVA, A.V. and DOBROMIROVA, V.F. (1980) "Analysis of the Kinetics of Crystal Nucleation and Growth in Solutions", Translated from Teore. Osn. Khim. Tekhnologii, 14, 364.

KITANO, Y. (1962) "Calcium Carbonate Crystals Forms formed from Sea Water by Inorganic Processes", J. Oceanogr. Soc. Japan, 18, 35.

KITANO, Y. and HOOD, D.W. (1965) "The Influence of Organic Material on the Polymorphic Crystallization of Calcium Carbonate", Geochim. Cosmochim. Acta, 29, 29.

KITANO, Y. (1966) "Synthesis of Magnesian Calcite at Low Temperatures and Pressures", Geochim. J. (Nagoya), 1, 1.

KNUDSEN, J.G. and STORY, M. (1975) "The Effect of Heat Transfer Surface
Temperature on the Scaling Behavior of Simulated Cooling Tower
Water", A.I.Ch.E. Sym. Ser., 74(174), 26.

KONAK, A.R. (1971) "The Crystallization and Dissolution of Gypsum", Ph.D.
Thesis, The University of Birmingham.

KONAK, A.R. (1974) "A New Model for Surface Reaction-controlled Growth of
Crystals from Solution", Chem. Eng. Sci., 29, 1537.

KOSSEL, W. (1934) "Zur Energetik von Oberflächenvorgängen", Annln. Phys.,
21, 457.

LAL, D.P., MASON, R.E.A. and STRICKLAND-CONSTABLE, R.F. (1969) "Collision
Breeding of Nuclei", J. Cryst. Growth, 5, 1.

LANGMUIR, D. (1968) "Stability of Calcite Based on Aqueous Solubility
Measurements", Geochim. Cosmochim. Acta, 32, 835.

LARSON, M.A. (1982) "Secondary Nucleation: An Analysis", in Industrial
Crystallization 81, edited by Jancic, S.J. and De Jong, E.J., North-
Holland Publishing Company, 55.

LARSON, T.E. and BUSWELL, A.M. (1942) "Calcium Carbonate Saturation In-
dex and Alkalinity Interpretation", J. Am. Wat. Wks. Assoc., 34, 1667.

LEE, S.H. and KNUDSEN, J.G. (1978) "Scaling Characteristics of Cooling
Tower Water", ASHRAE Trans., 85, part I.

LIESER, K.H. (1969) "Steps in Precipitation Reactions", Angew. Chem. In-
ternat. Edit., 8, 188.

LINTON, W.H. and SHERWOOD, T.K. (1950) "Mass Transfer from Solid Shapes
to Water in Streamline and Turbulent Flow", Chem. Eng. Progr., 46,
258.

LITTLE, S. (1984) Personal Communication, Electricity Commission of New
South Wales.

LOEWENTHALL, R.E. and MARAIS, G.v.R. (1976) Carbonate Chemistry of Aquatic
Systems: Theory and Application, Ann Arbor Publishers, Ann Arbor.

McCABE, W.L. and ROBINSON, C.S. (1924) "Evaporator Scale Formation", Ind. Eng. Chem., 16, 478.

McCABE, W.L. and SMITH, J.C. (1967) Unit Operations of Chemical Engineering, p.336, McGraws-Hill Book Co., Inc., N.Y.

MARC, R. (1908) "Über die Kristallisation aus wasserigen Losurgen", Z. Phys. Chem., 61, 385.

MARUSCAK, A, BAKER, C.G.J. and BERGOUGNOU, M.A. (1971) "Calcium Carbonate Precipitation in a Continuous Stirred Tank Reactor", Cand. J. Chem. Eng., 49, 819.

MASON, R.E.A. and STRICKLAND-CONSTABLE, R.F. (1966) "Breeding of Crystal Nuclei", Trans. Faraday Soc., 62, 455.

MELIA, T.P. and MOFFITT, W.P. (1964) "Secondary Nucleation from Aqueous Solution", I & EC Fundam., 3, 313.

MELIA, T.P. (1965) "Crystal Nucleation from Aqueous Solution", J. App. Chem., 15, 345.

MERRILL, D.T. (1976) "Chemical Conditioning for Water Treatment and Corrosion Control", Water Treatment Plant Design, edited by Sanks, R. L,, Ann Arbor Science Publ., Ann Arbor, Mich.

MERRILL, D.T. and Sanks, R.L. (1977a) "Corrosion Control by Deposition of $CaCO_3$ Films: A Practical Approach for Plant Operators", J. Am. Wat. Wks. Assoc., 69, 592.

MERRILL, D.T. and SANKS, R.L. (1977b) "Corrosion Control By Deposition of $CaCO_3$ Films: A Practical Approach for Plant Operators", J. Am. Wat. Wks. Assoc., 69, 634.

MERRILL, D.T. and SANKS, R.L. (1978) "Corrosion Control by Deposition of $CaCO_3$ Films: A Practical Approach for Plant Operators", J. Am. Wat. Wks. Assoc., 70, 12.

MIERS, H.A. and ISAAC, F. (1906) "Refractive Indices of Crystallizing Solutions", J. Chem. Soc., 89, 413.

MÖLLER, P. and RAJAGOPALAN, G. (1975) "Precipitation Kinetics of $CaCO_3$ in Presence of Mg^{2+} Ions", Zeit. für Phys. Chem. Neue Folge, Bd. 94, S.297.

MÖLLER, P. and RAJAGOPALAN, G. (1976) "Changes of Excess Free Energies in the Crystal Growth Processes of Calcite and Aragonite due to the Presence of Mg^{2+} Ions in Solution", Zeit. für Phys. Chem. Neue Folge, Bd.99, S.187.

MORSE, R.W. and KNUDSEN, J.G. (1977) "Effect of Alkalinity on the Scaling of Simulated Cooling Tower Water", Can. J. Chem. Eng., 55, 272.

MULLIN, J.W. and RAVEN, K.D. (1961) "Nucleation in Agitated Solutions", Nature, 4772, 251.

MULLIN, J.W. (1972) Crystallization, Butterworths, London.

MULLIN, J.W. and OSMAN, M.M. (1973) "Nucleation and Precipitation of Nickel Ammonium Sulphate Crystals from Aqueous Solution", Krist. Tech., 8, 471.

MULLIN, H.W. and ANG, H-M. (1977) "Nucleation Characteristics of Aqueous Nickel Ammonium Sulphate Solutions", Krist. Tech., 12, 105.

NANCOLLAS, G.H. and REDDY, M.M. (1971) "The Crystallization of Calcium Carbonate II. Calcite Growth Mechanism", J. Colloid Interf. Sci., 37, 824.

NERNST, W. (1904) "Theorie der Reaktions Geschwindigkeit in Heterogenen Systemen", Z. Phys. Chem., 47, 52.

NEWKIRK, and TURNBULL, D. (1955) "Nucleation of Ammonium Iodide Crystals from Aqueous Solutions", J. App. Phys., 26, 579.

NIELSEN, A.E. (1955) "The Kinetics of Electrolyte Precipitation", J. Colloid Sci., 10, 576.

NIELSEN, A.E. (1964) Kinetics of Precipitation, Pergamon Press, London.

NIELSEN, A.E. (1967) "Nucleation in Aqueous Solution", Crystal Growth,

Edited by Peiser, Pergamon, Oxford.

NIELSEN, A.E. (1969) "Nucleation and Growth of Crystals at High Super-

saturation", Krist. Teck., 4, 17.

NIELSEN, A.E. (1982) "Theory of Electrolytic Crystal Growth" in Indus-

trial Crystallization 81, edited by Jancic, S.J. and De Jong, E.

J., North-Hallard Publishing Company, 35.

NIELSEN, A.E. and SÖHNEL, O. (1971) "Interfacial Tensions Electrolyte

Crystal-Aqueous Solution from Nucleation Data", J. Cryst. Growth,

11, 233.

NOYES, A.A. and WHITNEY, W.R. (1897a) "Rate of Solution of Solid Subs-

tances in their Own Solution", J. Am. Chem. Soc., 19, 930.

NOYES, A.A. and WHITNEY, W.R. (1897b) "Rate of Solution of Solid Subs-

tances in their Own Solution", Z. Phys. Chem., 23, 689.

NYVLT, J. (1968) "Kinetics of Nucleation in Solutions", J. Cryst. Gro-

wth, 3/4, 377.

O'ROURKE, J.D. and JOHNSON, R.A. (1955) "Kinetics and Mechamism in For-

mation of Slightly Soluble Ionic Precipitates", Anal. Chem., 27,

1699.

OHARA, M. and REID, R.C. (1973) Modeling Crystal Growth Rates from So-

lution, Prentice-Hall, Inc., N.J.

OLSON, R.M. (1973) Essentials of Engineering Fluid Mechanics, pp.356-357

Intext Educational Publishers, N.Y.

OTTENS, E.P.K., JANSE, A.E. and DE JONG, E.J. (1972) "Secondary Nuclea-

tion in a Stirred Vessel Cooling Crystallizer", J. Cryst. Growth,

13/14, 500.

PINCUS, L.I. (1962) Practical Boiler Water Treatment, P.227, McGraw-

Hill Book Co., Inc., New York.

PLUMMER, L.N. and WIGLEY, T.M.L. (1976) "The Dissolution of Calcite in CO_2-saturated Solution at 25°C and 1 Atmosphere Total Pressure", Geochim. Cosmochim. Acta, 40, 191.

PLUMMER, L.N., WIGLEY, T.M.L. and PARKHURST, D.L. (1978) "The Kinetics of Calcite Dissolution in CO_2-water Systems at 5° to 60°C and 0.0 to 1.0 Atm. CO_2", Am. J. Sci., 278, 179.

PLUMMER, L.N., PARKHURST, D.L. and WIGLEY, T.M.L. (1979) "Critical Review of the Kinetics of Calcite Dissolution and Precipitation", in Chemical Modeling in Aqueous Systems, edited by Jenne, E.A. (American Chemical Society Symposium Series), 93, 537.

POUND, G.M. and LA MER, V.K. (1952) "Kinetics of Crystalline Nucleus Formation in Supercooled Liquid Tin", J. Am. Chem. Soc., 74, 2323.

PYTKOWICA, R.M. (1965) "Rates of Inorganic Calcium Carbonate Nucleation", J. Goel., 73, 196.

RANDOLPH, A.D. (1964) "A Population Balance for Countable Entities", Can. J. Chem. Eng., 42, 280.

RANDOLPH, A.D. and CISE, M.D. (1972) "Nucleation Kinetics of the Potassium Sulphate-Water System", A.I.Ch.E. J., 18, 798..

RANDOLPH, A.D. and LARSON, M.A. (1971) Theory of Particulate Process - Analysis and Techniques of Continuous Crystallization, Academic Press, N.Y.

RANDOLPH, A.D. and SIKDAR, S.K. (1976) "Creation and Survival of Secondary Crystal Nuclei. The Postassium Sulphate-Water System", I & EC Fundam., 15, 64.

REARDON, E.J. and LANGMUIR, D. (1974) "Thermodynamic Properties of the Ion Pairs $MgCO_3^o$ and $CaCO_3^o$ from 10 to 50°C", Am. J. Sc., 274, 599.

REDDY, M.M. (1977) "Crystallization of Calcium Carbonate in the Presence of Trace Concentrations of Phosphorus-containing Anions", J. Cryst.

Growth, <u>41</u>, 287.

REDDY, M.M. and GAILLARD, W.D. (1981) "Kinetics of Calcium Carbonate
(Calcite)-seeded Crystallization: Influence of Solide/Solution
Ratio on the Reaction Rate Constant", <u>J. Colloid Interf. Sci.</u>,
<u>81</u>, 171.

REDDY, M.M. and NANCOLLAS, G.H. (1971) "The Crystallization Calcium
Carbonate I. Isotopic Exchange and Kinetics", <u>J. Colloid Interf.
Sci.</u>, 36, 166.

REDDY, M.M. and NANCOLLAS, G.H. (1973) "Calcite Crystal Growth Inhibi-
tion by Phosphonates", <u>Desalination</u>, <u>12</u>, 61.

REDDY, M.A. and NANCOLLAS, G.H. (1976) "The Crystallization of Calcium
Carbonate IV. The Effect of Magnesium, Strotium and Sulphate Ions",
<u>J. Cryst. Growth</u>, <u>35</u>, 33.

REDDYM M.M., PLUMMER, L.N. and BUSENBERG, E. (1981) "Crystal Growth of
Calcite from Calcium Bicarbonate Solutions at Constant P_{CO_2} and
25°C: A Test of a Calcite Dissolution Model", <u>Geochim. Cosmochim.
Acta</u>, <u>45</u>, 1281.

REDDY, M.M. and WANG, K.K. (1980) "Crystallization of Calcium Carbonate
in the Presence of Metal Ions. I. Inhibition by Magnesium Ions at
pH 8.8 and 25°C", <u>J. Cryst. Growth</u>, <u>50</u>, 470.

REITZER, B.J. (1964) "Rate of Scale Formation in Tubular Heat Exchanger",
<u>I & EC Proc. Des. & Develop.</u>, <u>3</u>, 345.

ROQUES, H. and GIROU, A. (1974) "Kinetics of the Formation Conditions of
Carbonate Tartars", <u>Wat. Res.</u>, <u>8</u>, 907.

ROSSUM, J.R. and MERRILL, D.T. (1983) "An Evaluation of the Calcium Car-
bonate Saturation Indexes", <u>J. Am. Wat. Wks. Assoc.</u>, <u>72</u>, 95.

RUCKENSTEIN, E. and PRIEVE, D.C. (1973) "Rate of Deposition of Brownian
Particles under the Action of London and Double-layer Forces",
<u>J. Chem. Soc. Faraday II</u>, <u>69</u>, 1522.

RUSLI, I.T., LARSON, M.A. and GARSIDE, J. (1980) "Crystallization. Initial Growth of Secondary Nuclei Produced by Contact Nucleation", CEP Sym. Ser., 76(193), 52.

RUSHTON, J.H., COSTICH, E.W. and EVERETT, H.J. (1950a) "Power Characteristics of Mixing Impellers, Part I", Chem. Eng. Progr., 46, 395.

RUSHTON, J.H., COSTICH, E.W. and EVERETT, H.J. (1950b) "Power Characteristics of Mixing Impellers, Part II", Chem. Eng. Progr., 46, 467.

RYZNAR, J.W. (1944) "A New Index for Determining Amount of Calcium Carbonate Scale Formed by a Water", J. Am. Wat. Wks. Assoc., 36, 472.

SCHIERHOLZ, P. and STEVENS, J.D. (1975) "Determination of the Kinetics of Precipitation in a Dilute System", A.I.Ch.E. Sym. Ser., 71(151), 249.

SNOEYINK, V.L. and JENKINS, D. (1980) Water Chemistry, John Wiley and Sons, New York.

SOHNEL, O and MULLIN, J.W. (1978) "A Method for the Determination of Precipitation Induction Periods", J. Cryst. Growth, 44, 377.

SOHNEL, O. and MULLIN, J.W. (1982) "Precipitation of Calcium Carbonate", J. Cryst. Growth, 60, 239.

SOMERSCALES, E.F.C. (1979) "Introduction and Summary: The Fouling of Heat Transfer Equipments", Int. Conf. on the Fouling of Heat Transfer Equipment, Troy, New York.

SPIELMAN, L.A. and FRIEDLANDER, S.K. (1974) "Role of the Electrical Double Layer in Particle Deposition by Convective Diffusion", J. Colloid Interf. Sci., 46, 22.

STEINBERG, S. and HASSON, D. (1979) "Analysis of the Effect of Brine Retention Time on the Scaling Potential", Desalination, 31, 267.

STRANSKI, I.N. (1928) "Zur Theorie des Kristallwachstums", Z. Phys. Chem., 136, 259.

STRANSKI, I.N. (1930) "Growth and Solution of Nonpolar Crystals", Z. Physik. Chem., 11B, 342.

STRANSKI, I.N. (1939) "Growth Phenomena in Cadmium Single Crystals and Their Importance for the Investigation of the Forces Active Between Lattice Atoms", Ber., 72A, 141.

STRANSKI, I.N. and KAISKEV, R. (1939) "Theory of Crystal Growth and the Formation of Crystal Nuclei", Uspekhi Fiz. Nauk., 21, 408.

STRICKLAND-CONSTABLE, R.F. (1968) Kinetics and Mechanism of Crystallization, Academic Press.

STUMM, W. and MORGAN, J.J. (1970) Aquatic Chemistry, Wiley-Interscience, New York.

SUITOR, J.W., MARNER, W.J. and RITTER, R.B. (1977) "The History and Status of Research in Fouling of the Exchangers in Cooling Water Service", Can. J. Chem. Eng., 55, 374.

SUNG, C.Y., YOUNGQUIST, G.R. and ESTRIN, J. (1973) "Secondary Nucleation of Magnesium Sulphate by Fluid Shear", A.I.Ch.E. J., 19, 957.

SWINNEY, L.D., STEVENS, J.D. and PETERS, R.W. (1982) "Calcium Carbonate Crystallization Kinetics", I & EC Fundam., 21, 31.

T.E.M.A., Inc. (1968) Standards of the Tubular Exchanger Manufacturers Association, 5th Edition, New York.

TABOREK, J., AOKI, T., RITTER, R.B., PALEN, J.W. and KNUDSEN, J.G. (1972a) "Fouling: The Major Unresolved Problem in Heat Transfer", Chem. Eng. Progr., 68, 59.

TABOREK, J., AOKI, T., RITTER, R.B., PALEN, J.W. and KNUDSEN, J.G. (1972b) "Heat Transfer - Predictive Methods for Fouling Behaviour", Chem. Eng., 68, 69.

TAFT, W.H. (1967) Developments in Sedimentology, Vol. 9B, pp151-167, Ed. Chilingar, G.V., Bissel, H.J. and Fairbridge, R.W., Elsevier, New York.

TRAPNELL, B.M.W. and HAYWARD, D.O. (1964) Chemisorption, Butterworths.

TURNBULL, D. (1952) "Kinetics of Solidification of Supercooled Mercu-
ry Droplets", J. Chem. Phys., 20, 411.

TURNBULL, D. (1953) "The Kinetics of Precipitation of Barium Sulphate
from Aqueous Solution", Acta Metall., 1, 684.

TURNBULL, D. and VONNEGUT, B. (1952) "Nucleation Catalysis", Ind. Eng.
Chem., 44, 1292.

VALETON, J.J.P. (1923) "Wachstum und Auflösung der Kristalle", Z. Kris-
tallogr., 59, 135.

VALETON, J.J.P. (1924) "Wachstum und Auflösung der Kristalle", Z. Kris-
tallogr., 60, 1.

VAN HOOK, A. (1961) Crystallization: Theory and Practice, Reinhold Pub.
Co., Chapman and Hall Ltd., London.

VOLMER, M. (1939) Kinetik der Phasenbildung, Dresden and Leipzig, Stein-
kopff.

VOLMER, M. (1945) Kinetik der Phasenbildung, Ann Arbor, Michigan, Edwards
Bros.

VOLMER, M. and WEBER, A. (1922) "Zum Problem des Kristallwachstums", Z.
Phys. Chem., 102, 267.

VOLMER, M. and WEBER, A. (1929) "Zum Problem des Kristallwachstums", Z.
Phys. Chem., 35, 555.

VON LANE, M. (1943) "Der Wulffsche Satz fur die Gleichgewichtsform von
Kristallen", Z. Kristallogr., 105, 124.

VONNEGUT, B. (1948) "Variation with Temperature of the Nucleation Rate
of Supercooled Liquid Tin and Water Drops", J. Colloid Sci., 3,
563.

WALTON, A.G. (1963) "A Theory of Surface Reaction Controlled Growth"
J. Phys. Chem., 67, 1920.

WALTON, A.G. (1967) The Formation and Properties of Precipitates, Interscience, New York.

WATKINSON, A.P. and MARTINEZ, O. (1975) "Scaling of Heat Exchanger Tubes by Calcium Carbonate", Trans. Am. Soc. Mech. Engr., 97, 504.

WATKINSON, A.P. (1983) "Water Quality Effects on Fouling from Hard Waters", Heat Exchangers Theory and Practice, 853, edited by Taborek, J. Hewitt, G.F. and Afgan, N., Hemisphere Publishing Corp.

WEYL, P.K. (1958) "The Solution Kinetics of Calcite", J. Geol., 66, 163.

WHITE, M.L. and FROST, A.A. (1957) "The Rate of Nucleation of Supersaturated KNO_3 Solutions", J. Colloid Sci., 14, 247.

WIECHERS, H.N.S., STURROCK, P. and MARAIS, G.v.R. (1975) "Calcium Carbonate Crystallization Kinetics", Wat. Res., 9, 835.

WRAY, J.L. and DANIELS, F. (1957) "Precipitation of Calcite and Aragonite", J. Am. Chem. Soc., 79, 2031.

WULFF, G. (1901) "Zur Frage der Geschwindigkit des Wachsthums und der Auflosung der Krystallflachen", Z. Kristallogr., 34, 449.

YOUNGQUIST, G.R. and RANDOLPH, A.D. (1972) "Secondary Nucleation in a Class II System: Ammonium Sulphate-Water", A.I.Ch.E. J., 18, 421.

ZEISS, C. (1978) Micro-Videomat 2. Basic Instrument with Structure Analyzer, (G.41-494-e). Carl Zeiss, Okerkochen, w. Germany.

ZEISS, C. (1980) Micro-Videomat 2: Semi-automatic and Automatic Configurations; Software Stereology 1, (400865). Carl Zeiss, Oberkochen, W. Germany.